Phinichkusolchit, Narisa (2021) *ROCK1-mediated apoptotic blebbing in genetic models of tissue homeostasis and tumourigenesis.* PhD thesis.

https://theses.gla.ac.uk/81903/

Copyright and moral rights for this work are retained by the author

A copy can be downloaded for personal non-commercial research or study, without prior permission or charge

This work cannot be reproduced or quoted extensively from without first obtaining permission from the author

The content must not be changed in any way or sold commercially in any format or medium without the formal permission of the author

When referring to this work, full bibliographic details including the author, title, awarding institution and date of the thesis must be given

Enlighten: Theses
https://theses.gla.ac.uk/
research-enlighten@glasgow.ac.uk

ROCK1-mediated apoptotic blebbing in genetic models of tissue homeostasis and tumourigenesis

Narisa Phinichkusolchit
MPharmacol (Hons)

Submitted in fulfilment of the requirements for the
Degree of Doctor of Philosophy

Beatson Institute for Cancer Research
College of Medical, Veterinary and Life Scenes
University of Glasgow

September 2020

Abstract

Apoptosis is a controlled form of cell death that contributes to the removal of unwanted cells to maintain tissue homeostasis. Cells undergoing apoptosis display characteristic morphological changes including apoptotic membrane blebbing and apoptotic body formation. The Rho associated coiled-coiled containing kinase (ROCK) 1 is cleaved upon the activation of caspase-3 during apoptosis, resulting in a hyper-activated truncated form of the protein. This drives actin-myosin contractions to form dynamic apoptotic membrane blebs. In order to dissect the specific functionality of ROCK1-mediated apoptotic membrane blebbing, the Olson lab generated a mouse model of a mutant, non-cleavable form of ROCK1 (ROCK1nc). This unique model has been studied under conditions of tissue homeostasis focusing on thymic development and apoptotic cell clearance within the thymus.

The ROCK1nc mutation did not affect the anatomical and cellular properties of the thymus under physiological conditions, nor when challenged with apoptosis-inducing agent dexamethasone. However adoptive transfer experiments did reveal that injection of apoptotic thymocytes into ROCK1nc recipients yielded greater immune cell infiltrations in comparison to ROCK1wt recipients. As no differences were observed between the genotypes during apoptotic conditions. These results suggest that apoptotic membrane blebbing is likely dispensable in maintaining homeostasis in the thymus.

The importance of apoptotic membrane blebbing was also investigated in a genetic mouse model of lung adenocarcinoma Here the addition of the ROCK1nc mutation accelerated tumourigenesis with animals succumbing to lung tumours at a significantly earlier time. Interestingly while this particular model of lung adenocarcinoma is characterised by increased immunogenicity, the acceleration with ROCK1nc was not attributed to immune cell infiltration. These results suggest that defective apoptotic membrane blebbing is important in facilitating tumourigenesis in lung adenocarcinomas. Taken together, the results shown here indicate that apoptotic morphology alters tumourigenesis to a greater extent than homeostasis itself. These studies allow for a better understanding of the functions of apoptotic membrane blebbing and shed light on whether ROCK inhibitors could be used for the treatment of different cancers.

Table of Contents

List of Tables

List of Figures

Author's Declaration

I am the sole author of this thesis. The work presented in this thesis is the result of my own work, unless otherwise stated, and has not been submitted for any other degree at the University of Glasgow or any other institution.

Narisa Phinichkusolchit

September 2020

Acknowledgements

My PhD journey has been both a challenging and rewarding experience; one that has only been possible with the help and support from my supervisors, colleagues, friends and family. I would like to thank my first supervisor, Professor Michael Olson, for the opportunity to start a research project in his lab at the Beatson Institute and for his guidance during my PhD.

I would like to extend a special thank you to Professor Karen Blyth for adopting me as her PhD student. Your incredible guidance and scientific expertise has helped me in so many ways. I am so grateful for the opportunity to work in your lab, for the fact that you took on projects that were different and for your continued support. Your kindness, encouragement and passion has really kept me going.

I would also like to thank my second supervisor Dr. Seth Coffelt, and panel member Dr. Leo Carlin for their helpful discussions, and a special thanks to Professor Daniel Murphy for the opportunity to collaborate on an exciting project. My sincere thanks also goes to Professor Owen Sansom for the chance to embark on a new project with the help of Dr. Tam Jamieson.

I would also like to extend my gratitude to Cancer Research UK for funding my project, and to all the staff and research services, particularly histology and the BSU/BRU team, for their exceptional support during my time here at the Beatson Institute.

I have been lucky to have been part of two amazing labs, R17 and Y35. I would like to thank the members of R17 for their tremendous support, friendship and great memories - in particular, Steven, Gregory, David, June and Dominika for their mentorship and encouragement. I would also like to thank past and present members of Y35 for making it so easy to join a new group. A special thanks to Dimitris for helping me with all the animal work and to Kirsteen for your invaluable discussions. My time at the Beatson has been that much better because of the individuals in both of these labs – for that I thank you.

I would not have been able to go through my PhD journey without the support of my friends. Thanks to my friends in Glasgow, especially Natasha and Ilaria, and the bhangra crew. A big thank you to Alba - you have been such a big part of my time here and I couldn't have done it without your support and friendship! Thanks to Mona for always being there for me and encouraging me. Thanks to my cousins Rameet and Harleen for always having my back. Thanks to Rajpal for your creative illustrations and constant support. I would also like to say a big thanks to the pharmacolols and Bath University friends, as well as my friends from Bangkok for keeping me sane – you know who you are!

Finally, a huge thank to you everyone in my family. Your love and support means everything to me. My parents especially, have been my rocks through this time and I can't thank them enough. Thank you for helping me throughout, for encouraging me and for helping me get to where I am today.

Abbreviations and definitions

Abbreviations	Definition
AA	Arachidonic acid
AD	Alzheimer's disease
AICD	Activated (antigen)-induced cell death
AIF	Apoptosis inducing factor
APAF-1	Apoptotic protease activating factor 1
APC	Antigen presenting cells
ATM	Ataxia-telangiectasia mutated
ATP	Adenosine triphosphate
ATR	Ataxia telangiectasia and Rad3 related
Aß	Amyloid- ß
BAK	BCL-2 homologous antagonist killer
BAX	BCL-2 associated X protein
BCA	Bicinchoninic acid
BCL-2	B-cell lymphoma 2
BCL-XL	B-cell lymphoma-extra-large
BCR	B-cell receptors
BH	BCL-2 homology
BID	BCL-2 associated agonist of cell death
BIM	BCL-2 like protein 11
BOK	BCL-2 related ovarian killer
BrdU	5-bromo-2'-deoxyuridine
CAD	Caspase activated DNAse
CAF	Cancer associated fibroblasts
CD	Cluster of differentiation
CDC	Classical dendritic cells
CDK1	cyclin dependent kinase inhibitors
CHK	Checkpoint kinase
Cl. Casp3	Cleaved caspase-3
CLL	Chronic lymphocytic leukaemia
COP-1	Constitutive photomorphogenesis protein 1
COPD	Chronic pulmonary disease
CRD	Cysteine rich zinc finger like domain
CTL	Cytotoxic T-cells
DAB	3,3′-Diaminobenzidine
DAMPs	Damage associated molecular patterns
Daxx	Death domain-associated protein
DCs	Dendritic cells
DEN	Diethylnitrosamine
Dex	Dexamethasone
DISC	Death inducing signalling complex
DMEM	Dulbecco's Modified Eagle Medium
DMPK	Dystrophia myotonica protein kinase
DMSO	Dimethyl sulfoxide
DN	Double negative
DNA	Deoxyribonucleic acid
DNA	Deoxyribonucleic acid
DP	Double positive
EMT	Epithelial-to mesenchymal transition
Enz1	Enzyme 1

ER	Endoplasmic reticulum
ER2	Epitope retrieval 2
ERM	Ezrin, radixin, moesin
FACS	Fluorescence activated cell sorting
FADD	Fas-associated death domain protein
FAK	Focal adhesion kinase
FasL	Fas ligand
FBS	Fetal bovine serum
FFPE	Formalin fixed paraffin embedded
FHOD1	Formin homology 2 domain containing 1
Fli-1	Fli-1 Proto-Oncogene
GAP	GTPases-activating proteins
GC	Glucocorticoids
GDI	Guanine nucleotide dissociation inhibitors
GDP	Guanine diphosphate
GEF	Guanine exchange factor
GEM	Genetically engineered model
GEM1	Mitochondrial Rho GTPase-1
GFP	Green fluorescent protein
GM	Genetically modified
GMCSF	Granulocyte macrophage stimulating factor
GPCR	G-protein coupled receptors
GR	Glucocorticoids receptor
GRE	Glucocorticoid response elements
GTP	Guanine triphosphate
H&E	Haematoxylin and eosin
HAUSP	Herpesvirus-associated ubiquitin-specific protease
HCC	Hepatocellular carcinoma
Hemi	Hemizygous
HET	Heterozygous
HOM	Homozygous
IAP	Inhibitor of apoptosis
ICD	Immunogenic cell death
IDEXX	IDEXX ProCyte Dx*
Ig	Immunoglobulin
IHC	Immunohistochemistry
IL-2	Interleukin-2
IP	Intraperitoneal
IRF4	Interferon regulatory factor 4
IκB	Inhibitor of NFκB
KO	Knockout
LDH	Lactate dehydrogenase
LIM	MLC phosphatase and LIM domain
LoxP	Locus of X-over P1
LPC	Lysophosphatidylcholine
LPS	Lipopolysaccharide
LRP-1/CD91	Low density lipoprotein receptor related protein
LSL	Lox-stop-lox
LuAD	Lung adenocarcinomas
MAPK	Mitogen-activated protein kinases
MCL	Myosin light chain
MCL-1	Myloid cell leukemia
MCL-P	MLC phosphatase

MDM	Murine double minute
MEF	Mouse embryonic fibroblast
MEM	Minimal essential media
MES	2-ethanesulfonic acid
MFG-E8	Milk fat globule epidermal growth factor 8
MFI	Mean fluorescence intensity
MHC	Major histocompatibility complex
MLC	Myosin II light chain
MLN	Mesenteric lymph node
MOMP	Mitochondrial outer membrane permeabilisation
MOPS	mM 3-(N-morpholino) propane sulfonic acid
MRCK	Myotonic dystrophy kinase related-Cdc42 related kinases
mRNA	Messenger RNA
MYPT1	Myosin phosphatase target subunit1
NBF	Neutral buffered formalin
NES	Nuclear export signal
NFκB	Nuclear factor kappa light chain enhancer of activated B cells
NK	Natural killer
NLS	Nuclear localisation sequence
NoLS	Nucleolar localisation signal
NOXA	Phorbol-12-myristate-13-acetate-induced protein 1
NSCLC	Non-small cell lung cancer
OMI	Omi stress-regulated endoprotease
PAGE	Polyacrylamide gel electrophoresis
PAMPs	Pattern associated molecular patterns
PBS	Phosphate buffered saline
PCID	Phagocytosis induced dead
PDC	Plasmacytoid dendritic cells
PDK-1	Phosphoinositide dependent kinase 1
PFA	Paraformaldehyde
PFU	Plaque forming unit
PH	Pleckstrin homology
PI	Propidium iodide
Pirh2	p53-induced RING-H2 protein
PKB	Protein kinase B
PKC	Protein kinase C
PLK	Polo-like 1 kinase
PRR	Pattern recognition receptors
PRR	Proline rich region
PS	Phosphatidylserine
PTEN	Phosphatase and tensin homolog
RA	Rheumatoid arthritis
RAC1	Ras-related botulinum toxin substrate 1
RBC	Red blood cells
RBD	Rho binding domain
RhoE	Rho related GTP binding protein E
RING	Really interesting gene
RNA	Ribonucleic acid
RNAseq	RNA sequencing
ROCK1	Rho-associated coiled-coiled containing kinase 1
ROCK1nc	Non cleavable ROCK1
ROS	Reactive oxygen species
rpm	Revolutions per minute

RT	Room temperature
S1P	Sphingosine 1-phosphate
SCLC	Small cell lung cancer
SD	Standard deviation
SDS	Sodium dodecyl suflate
SEM	Scanning electron microscopy
SEM	Standard error of mean
SIRP1α	Signal regulatory protein alpha
SLE	Systemic lupus erythematous
SMAC	Second mitochondria-derived activator of caspase/diablo IAP-binding mitochondrial protein
SPC	Sphingosylphosphorylcholeine
Sp-C	Surfactant protein C
TAD	Transactivation domain
TCR	T-cell receptor
TEM	Transendothelial migration
TGFß	Transforming growth factor ß
T_H17	T-helper 17
TIGAR	TP53-induced glycolysis and apoptosis regulator gene
TiGER	Tissue-specific gene expression and regulation
TNF	Tumour necrosis factor
TNFR-1	Tumour necrosis factor receptor 1
TRADD	TNF-receptor associated death domain protein
TRAIL	TNF-related apoptosis inducing ligand
Treg	Regulatory T-cells
TUNEL	Terminal deoxynucleotidyl transferase dUTP nick end labeling
UTP	Uridine triphosphate
UV	Ultraviolet
WIP1	Wild-type p53-induced phosphatase
WT	Wild-type

1 Introduction

1.1 Cell death

Cell death is a physiological process that aids in maintaining homeostatic balance between proliferating cells and removal of unwanted cells (D'Arcy, 2019). The death of a cell can be regulated or unregulated, depending on the stimuli. At first, cell death was divided into three subtypes – apoptosis, autophagy and necrosis (Green and Llambi, 2015). However, more recently cell death is classified more broadly in two categories –non-programmed and programmed cell death (Galluzzi et al., 2018). Necrosis is a form of non-programmed cell death that results in cytoplasmic swelling, random degradation of DNA, and plasma membrane ruptures (Weerasinghe and Buja, 2012). This results in the release of intracellular content, often resulting in an inflammatory response (Vanlangenakker et al., 2012).

Majority of cell death modalities, including but not limited to apoptosis, autophagy, pyroptosis and ferroptosis are classed as programmed cell death. The most widely studied is apoptosis (discussed in detail below) (Kerr et al., 1972). Autophagy, a process involved in recycling and removing intracellular components, can result in programmed cell death upon the occurrence of an irreversible cellular stresses (Bialik et al., 2018). During autophagy induced cell death, cells display large intracellular vesicles, enlarged organelles and plasma membrane blebbing (Liu and Levine, 2015). Another form of programmed cell death, pyroptosis, is known as an inflammatory form. Upon the recognition of pathogenic stimuli in immune cells, intracellular signalling cascades cause the formation of pores on the plasma membrane (Liu et al., 2016a). Thus, these cells present with swelling, plasma membrane rupture and DNA fragmentation (Ryter and Choi, 2014). On the other hand, ferroptosis is known as an iron dependent form cell death resulting in an accumulation of lipid reactive oxygen species induced by small molecules and drugs (Dixon et al., 2012, Manz et al., 2016). Cells undergoing ferroptosis do not exhibit the morphological features of apoptosis or autophagy. Rather, ferroptotic cells display smaller and denser mitochondria with reduced cristae (Dixon et al., 2012). The different modes of programmed cell death is determined by their stimuli, molecular mechanism and morphological features.

1.2 Apoptosis

Apoptosis is a form of programmed cell death that results in the efficient removal of damaged or unwanted cells (Kerr et al., 1972). As a naturally occurring process, apoptosis can occur in both physiological and pathological conditions. In physiological settings, programmed cell death is important for a number of reasons including the developmental process, the maintenance of homeostasis, as well as a defence mechanism against foreign bodies. Apoptosis is then seen as a requirement to maintain the balance in multicellular organisms, offsetting mitotic events. As such, it is estimated that the human body has an apoptotic turnover rate of ~150 billion cells per day (Bianconi et al., 2013, Devitt and Marshall, 2011). When apoptosis is triggered in a cell past a certain stage, an irreversible process ensues. A variety of controlled morphological and intracellular disassembling changes occur, ultimately breaking the cell up into fragments allowing for its clearance (Wickman et al., 2012).

Equally as important as cell death itself, is efferocytosis, or the clearance of apoptotic cells and debris by phagocytic cells (Devitt and Marshall, 2011). While cells undergo apoptosis, signals are released and recognised by phagocytic cells to allow cellular uptake. Apoptosis is a clever, immunologically silent self-destruct design that leads a cell to its death and its clearance. Together, both apoptosis and apoptotic cell clearance play vital roles in the management of cell numbers, immunity, responses to injury and development. Defects in either cell death or cell clearance mechanisms can trigger detrimental consequences including immune cell activation and cellular accumulation. This could potentially lead to pathological states including autoimmunity and cancer (Green et al., 2016).

1.3 Apoptotic process

1.3.1 Triggering apoptosis

The apoptotic process can be triggered from both internal and external stimuli on a cell. This gives rise to two main pathways for apoptosis induction – the intrinsic pathway and the extrinsic pathway (Figure 1-1). Regardless of which

pathway is activated, the apoptotic process yields the same defining biochemical and morphological hallmark changes (Fulda and Debatin, 2006).

1.3.1.1 Intrinsic pathway

The intrinsic pathway is triggered by a variety of non-receptor mediated stimuli arising from within the cell. These stimuli can be classed as positive or negative. Positive stimuli include, but are not limited to, damage to the cell inflicted by radiation or chemotherapy, oxidative stress, hypoxia, and increased intracellular calcium. Negative stimuli refer to the lack of suppression of apoptosis which results in the induction of the intrinsic apoptotic pathway. These negative stimuli include a lack of growth factors, hormones or cytokine survival signals. An important sensor of intracellular stresses is p53 that can trigger cell death via the intrinsic pathway (discussed in a later section) (Haupt et al., 2003). Once triggered, a variety of intracellular signalling cascades leads to a series of mitochondrial initiated events (Elmore, 2007). The mitochondria are double membraned organelles which lose their membrane integrities, resulting in the release of mitochondrial content and ultimately, cell death (Figure 1-1).

This process is tightly controlled by the larger B-cell lymphoma (BCL-2) family of proteins(Adams and Cory, 2007). The Bcl-2 family of proteins is classified into three main groups based on their structure of the Bcl-2 homology (BH) domain that function as either pro-apoptotic or anti-apoptotic proteins. The pro-apoptotic proteins can be further subdivided into two groups – the effector proteins and BH3 only proteins (Shamas-Din et al., 2013). The effector proteins contain multiple BH domains and members of this family include BCL-2 associated X protein (BAX), BCL-2 homologus antagonist killer (BAK) and BCL-2 related ovarian killer (BOK). Members of the BH3 only proteins contains only the BH3 motif and these include, but are not limited to, BCL-2 like protein 11 (BIM), BCL-2 associated agonist of cell death (BAD), BH3-interacting domain death agonist (BID), Phorbol-12-myristate-13-acetate-induced protein 1 (NOXA) and p53 upregulated modulator of apoptosis (PUMA) (Letai et al., 2002). The anti-apoptotic protein family include BCL-2, myeloid cell leukaemia 1 (MCL-1) and B-cell lymphoma-extra-large (BCL-XL), all of which contain multiple BH domains (Campbell and Tait, 2018). Interactions between pro and anti- apoptotic proteins can bind and sequester the effects of each other, either prohibiting the release

of mitochondrial content or promoting it. A delicate balance exists between these three groups of proteins, whereby the dominant subgroup determines the fate of the cell (Kale et al., 2018).

The induction of apoptosis via the intrinsic pathway activates the pro-apoptotic BCL-2 proteins, namely BAX or BAK. BAX and BAK both have the ability to oligomerise once activated and form pores in the outer mitochondrial membrane. Mitochondrial outer membrane permeabilisation (MOMP) causes the release of mitochondrial contents, committing a cell to death (Brunet et al., 1998, Marsden et al., 2002, Singh et al., 2019). These contents include cytochrome C, Second mitochondria-derived activator of caspase/diablo IAP-binding mitochondrial protein (SMAC), and Omi stress-regulated endoprotease (OMI) as the primary group and apoptosis inducing factor (AIF), endonuclease G and caspase activated DNAse (CAD) as the secondary group. All these activate downstream caspases either directly or indirectly. In a direct manner, cytosolic cytochrome C binds to apoptotic-protease-activating factor 1 (APAF-1) forming an apoptosome with caspase-9, leading to the activation of caspase-3. Indirectly, SMAC and OMI inhibit the inhibitor of apoptosis (IAP) proteins in order to free caspase-3 and -9 for activation and execution of downstream pathways (Kroemer et al., 2007, LaCasse et al., 2008). The secondary group of protein release occurs after the release of the primary proteins. Following the release of AIF, endonuclease G and CAD from the mitochondria, these proteins translocate to the nucleus to facilitate DNA fragmentation and chromatin condensation (Elmore, 2007).

The initiation of MOMP is considered the key event for the commitment to apoptosis (Chipuk et al., 2006). MOMP is the common denominator between the different initiators of cell death, intrinsic or extrinsic, and occurs irrespective of caspase activation (Chipuk and Green, 2005). Upon commencement of MOMP, mitochondrial function is disrupted, DNA fragmentation and chromatin condensation occur, and a decline in energy production ensures the destruction of a cell (Ricci et al., 2003).

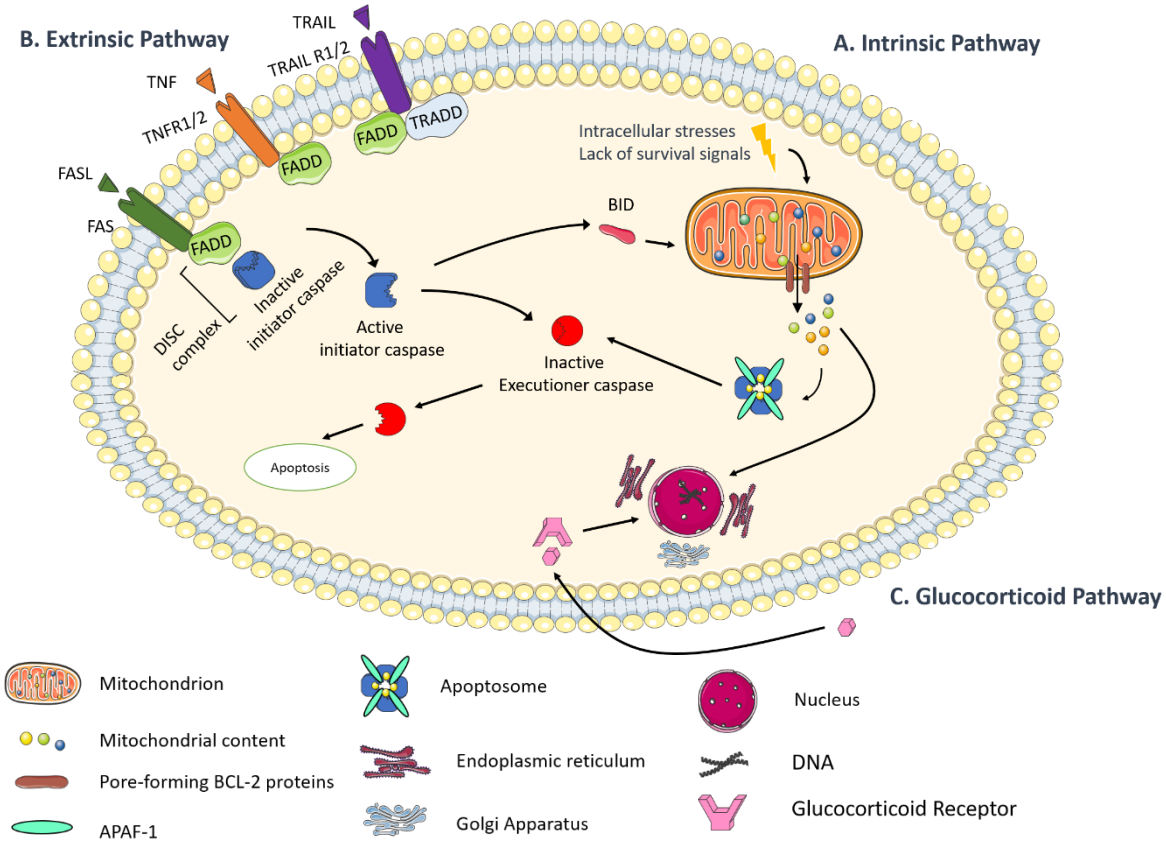

Figure 1-1 Overview of the apoptotic pathways. Apoptosis can be triggered in a variety of ways including the intrinsic pathway (A), extrinsic pathway (B) and glucocorticoid pathway (C). The intrinsic pathway is triggered by a variety of intracellular stresses including DNA damage or a lack of survival signals. Once sensed, pro-apoptotic proteins in the BCL-2 family ultimately form pores on the outer mitochondrial membrane. Mitochondrial content, including cytochrome C, SMAC, OMI, endonuclease G, AIF and CAD, are released into the cytoplasm in two phases. The first is where cytochrome C forms a complex with initiator caspase 9 and APAF-1 to activate downstream executioner caspase -3, 6 and 7. In the second phase, endonuclease G, AIF and CAD translocate to the nucleus to facilitate chromatin condensation and DNA fragmentation. With the extrinsic pathway, death ligands bind to death receptors which recruit adaptor proteins and initiator procaspases such as caspase-8. Once activated, caspase-8 further activates executioner caspases as well as cleave BID, a BH3 pro-apoptotic BCL-2 protein, to cause mitochondrial outer membrane permeabilisation. Glucocorticoids bind to intracellular receptors which translocate into the nucleus to initiate gene activation and repression. An upregulation of BIM feeds back to the intrinsic apoptotic pathway. This figure was made using contents from Servier Medical Art, under the Creative Commons Attribution 3.0 Unported License https://smart.servier.com/

1.3.1.2 Extrinsic pathway

The extrinsic apoptotic pathway involves the induction of apoptosis through transmembrane receptors known as death receptors. These death receptors are part of the tumour necrosis factor (TNF) gene superfamily (Locksley et al., 2001). Each individual death receptor binds to its own corresponding death ligand. For example, TNF receptor 1 (TNFR1) binds to its ligand TNF, CD95 (FAS) binds to CD95-ligand (FAS ligand; FasL) and TNF-related apoptosis inducing ligand (TRAIL) receptor 1 and 2 binds to TRAIL (Wajant, 2002, Hsu et al., 1995c). The expression of death receptors, FAS and TRAIL, can be induced by p53 when

exposed to cellular insults (Haupt et al., 2003). The death receptor is made up of a cysteine-rich extracellular portion and a cytoplasmic portion of about 80 amino acids. This intracellular portion contains a death domain, where upon ligand binding causes the recruitment of adaptor proteins with a corresponding death domain (Kischkel et al., 1995). Adaptor proteins such as Fas-associated death domain protein (FADD) and TNF-receptor associated death domain protein (TRADD) mediate downstream signalling.

The receptor, adaptor proteins and monomeric pro-caspase-8 form a death inducing signalling complex (DISC) to assemble dimers of procaspase-8, allowing auto-proteolytic cleavage and subsequent activation (Galluzzi et al., 2018). Depending on the type of cell, caspase-8 drives the activation of caspase-3 and successive signalling cascades in Type I cells (such as thymocytes and lymphocytes); in Type II cells (such as hepatocytes, pancreatic β cells and cancer cells), activated caspase-8 cleaves BH3 pro-apoptotic protein BID to its truncated form tBID, causing MOMP to occur and activation of caspase-3 (Huang et al., 2016). Once the caspases are activated, the same cascade of events occur as in the intrinsic pathway (Figure 1-1).

1.3.1.3 Glucocorticoid-mediated apoptosis

Apart from the main extrinsic and intrinsic triggers of apoptosis, apoptosis can also be triggered by glucocorticoids (GC). GCs are steroid hormones known for their ability to modulate the immune system (Ashwell et al., 2000). Some cell types are sensitive to GC-induced apoptosis, most notable are T-lymphocytes. GCs bind to glucocorticoid receptors (GR), which are found in a complex in the cytoplasm (Howard et al., 1990). Once bound, the GC-GR complex translocate into the nucleus and bind to glucocorticoid response elements (GRE) of target gene promoter regions, either repressing or activating the transcription of target genes (Bamberger et al., 1996). Importantly, there is an upregulation in BIM, a BH3 pro-apoptotic protein that facilitates the reorganisation of BAX and BAK to cause MOMP. At this point, mechanisms similar to the intrinsic pathway are triggered (Figure 1-1). Additionally, GC-induced apoptosis can also mediate the transcriptional activation of inhibitor of NFκB (IκB). IκB inhibits the pro-survival effects of nuclear factor kappa light chain enhancer of activated B cells (NFκB), including increased expression of IAP (Schmidt et al., 2004).

1.3.1.4 Caspase activation

Regardless of which pathway apoptosis is induced, a crucial aspect and common denominator of triggering apoptosis is the activation of caspases. Caspases are essential and broken down into two classes - the initiators and executioner (also called effector). In mammalian cells, the initiators include caspase-2, -8, -9, and -10, while caspase-3, -6, and -7 are part of the executioner caspases. These proteolytic enzymes exist initially as procaspases that need to be activated either by dimerization, auto-activation, or cleavage, for the initiators or effectors respectively (Muzio et al., 1998, Chang et al., 2003). Once activated, initiator caspases are recruited into complexes, initiating a cascade activation and cleavage of effector caspases and downstream proteins. Executioner caspases are then capable of cleaving a plethora of downstream targets and other effector caspases, creating a positive feedback loop (McIlwain et al., 2013). Inherently, the proteolytic ability of caspases targets cleavage after aspartate residues on proteins, whilst the specificity of each individual caspase is determined by amino acid residues nearby the aspartate residue (Riedl and Shi, 2004). It is evident that caspases are key to the apoptotic process. In particular, caspase-3 is considered one of the more important executioner caspases that is activated. The activation of caspases mediates a number of characteristic morphological, structural and biochemical changes that occur during apoptosis. This allows the appropriate dismantling of a cell, preparing it for clearance.

1.3.1.5 Non apoptotic roles of caspases

Although caspases are widely known for their roles in apoptosis, a variety of non-apoptotic functions have been discovered as well. Caspases have been shown to play a role in inflammation, development and proliferation (Shalini et al., 2015). Several caspases have been identified as important in inflammation including caspase-1. Caspase-1 was shown to aid the maturation process of IL-1β and IL-18 by cleaving the cytokines (Thornberry et al., 1992, Cerretti et al., 1992). The processing of these cytokines are mediated through inflammasome activation of caspases (Martinon et al., 2002). This cascade is initiated through a variety of stimuli including DAMPs, such as reactive oxygen species, and PAMPs, such as RNA (Shalini et al., 2015). Inflammasome-caspase mediated processing of IL-1β

can result pyroptosis, a type of cell death considered to promote an immune response (Miao et al., 2011). Similar to caspase-1, caspase-8 has also been shown to form a complex with RIG-1 following a viral infection, resulting in the inhibition IFN production (Rajput et al., 2011).

In addition to inflammation, caspases have been involved in cell differentiation (Shalini et al., 2015). Caspase-3 was revealed to be important in the differentiation of different cell types including lens fibre formation, osteoblasts, neuronal differentiation and macrophage formation (Ishizaki et al., 1998, Mogi and Togari, 2003, Yan et al., 2001, Sordet et al., 2002). All of these caspase-3 mediated functions were carried out in the absence of apoptosis. Furthermore, there has been evidence showing that in macrophages, non-apoptotic caspase-3 can cleave downstream rho-associated coiled-coiled containing kinase (ROCK) 1 protein to alter cell polarity (Liu et al., 2016b). Furthermore, both caspase-11 and caspase-8 have also been implicated in altering cytoskeleton dynamics during cell migration (Nakajima and Kuranaga, 2017, Helfer et al., 2006, Li et al., 2007). These are several emerging pieces of evidence that shed light on the various non-apoptotic functions of caspases.

1.3.2 Cellular changes during apoptosis.

1.3.2.1 Morphological changes

The apoptotic process sees a number of hallmark morphological changes occur to a cell. During the early phases of apoptosis, an apoptotic cell rounds up, shrinks and detaches from neighbouring cells and the extracellular matrix (Kerr et al., 1972). The detachment of cells from its environment is only true for adherent cells, as this phenomenon is not observed with suspension cells (Lane et al., 2005). Following this, several key features are observed – the condensation of chromatin; nuclear and DNA fragmentation; the formation of dynamic membrane blebs; and ultimately, the pinching off of these blebs into apoptotic bodies. Fragments of DNA and other intracellular contents, including organelles are packaged into these enclosed apoptotic bodies (Kerr et al., 1972, Elmore, 2007). This allows apoptotic bodies to be engulfed by phagocytic cells and cleared efficiently (Figure 1-2). These morphological features are unique to apoptosis, which is in contrast to the uncontrolled form of cell death, necrosis (Wyllie et

al., 1980). During necrosis, cells lose their membrane integrity rapidly, releasing its intracellular contents to promote an immune response. This renders apoptosis as an immunologically silent process.

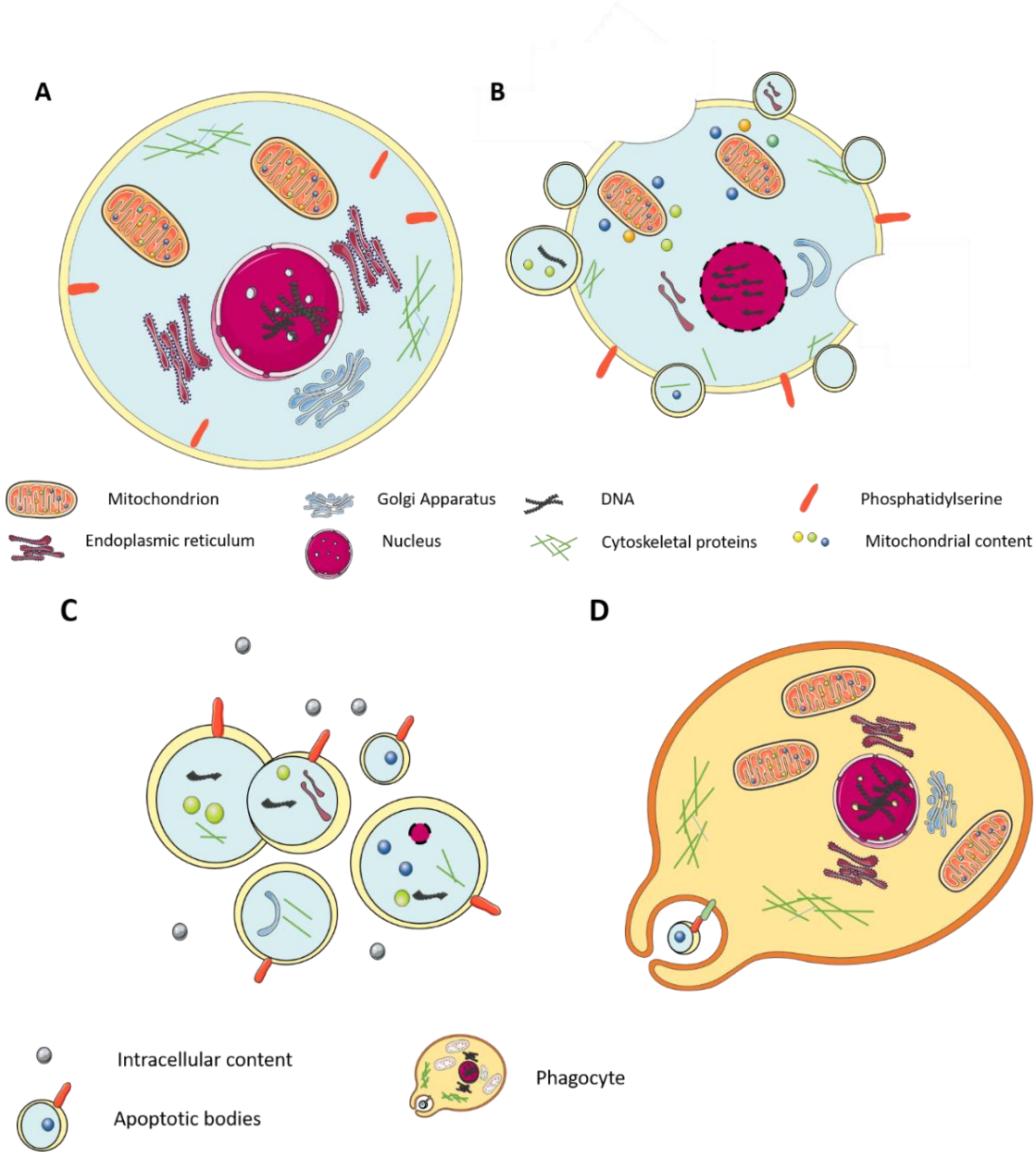

Figure 1-2 Apoptotic process involves morphological, structural and biochemical changes. When a healthy cell undergoes apoptosis, it rounds up, shrinks and detaches from neighbouring cells (A). The cell then undergoes a number of changes including chromatin condensation, fragmentation of the DNA and nucleus, disruption of the actin cytoskeleton, dynamic membrane blebbing and externalisation of phosphatidylserine (B). Apoptotic bodies are formed by the pinching off of the membrane blebs packaged with disintegrated cellular content (C). Phagocytes are recruited by 'find-me' signals sent out of dying cells culminating in phagocytosis of the dead cell upon 'eat-me' signal recognition (D). This figure was made using contents from Servier Medical Art, under the Creative Commons Attribution 3.0 Unported License. https://smart.servier.com/

1.3.2.2 Structural changes and mechanisms during apoptosis

The structural integrity of a cell is one of the first aspects targeted by caspases. Cytoskeletal components, microtubular proteins and intermediate filament proteins are downstream targets of caspases (Taylor et al., 2008). The cytoskeletal targets include actin, myosin and filamin; the microtubulular proteins include tubulins, tau, and cytoplasmic dynein intermediate chain; and lastly the intermediate filament proteins include vimentin, keratins and nuclear laminins (Communal et al., 2002, Thiede et al., 2005, Taylor et al., 2008). Furthermore, the dismantling of focal adhesion sites and cell-cell adherens junctions by cleavage of focal adhesion kinase (FAK), $p130^{cas}$, tensin, as well as catenins required for adhesion sites, have been shown to trigger the detachment of apoptotic cells. Caspase-mediated cleavage of these cytoskeletal components and focal adhesion sites leads to the morphological changes seen during early apoptosis – rounding up, shrinking and detachment.

A key substrate of caspase that mediates the dynamic membrane blebbing of apoptotic cells is the Rho effector kinase, rho-associated coiled-coiled containing kinase 1 (ROCK1) (discussed later). The c-terminus of ROCK1 is cleaved by caspase-3 during apoptosis which results in a constitutively active kinase. This causes downstream phosphorylation of ROCK1 targets including myosin light chain (MLC), MLC phosphatase and LIM domain (LIM) kinase, leading to the contraction of actin and stabilisation of actin (Figure 1-3). This process initiates the formation of membrane apoptotic blebs, and subsequently apoptotic bodies. Membrane blebs are formed due to the hydrostatic pressure that builds up following actomyosin contraction mediated by ROCK1 (Wickman et al., 2012). The formation of apoptotic bodies depends on the presence of actin at the base of membrane blebs, the degradation of the stress fibres and microtubule disruption (Mills et al., 1998). All of these play an important part in compartmentalising intracellular content and concentrating phagocytic signals for efficient removal (Coleman et al., 2001, Sebbagh et al., 2001).

Another characteristic morphological change during apoptosis is nuclear and DNA fragmentation. The weakening of the nuclear lamina is mediated by the proteolytic cleavage of laminin A, B and C. Additionally, ROCK1 also plays a crucial role in the dismantling of the nuclear envelope. The reorganisation of the

actin-cytoskeleton by ROCK1 and the weakening of the nuclear lamina, results in tearing the nuclear envelope during apoptosis (Croft et al., 2005, Coleman et al., 2001, Sebbagh et al., 2001). Once the nucleus is dismantled, the intracellular nuclear fragments and organelles are dispersed into the apoptotic blebs (Moss et al., 2006).

The organelles within a cell are also subject to degradation and fragmentation. Although at first, these organelles are intact during early apoptosis, during late stage apoptosis, they are cleaved, dismantled and disseminated into apoptotic blebs and bodies. The golgi apparatus and endoplasmic reticulum are cleaved in a caspase-mediated manner. Caspases are also important in shutting down mitochondrial function through cleavage of components in complex I. The fragmentation of the mitochondria itself is attributed to the function of pro-apoptotic BCL-2 proteins (Ricci et al., 2004).

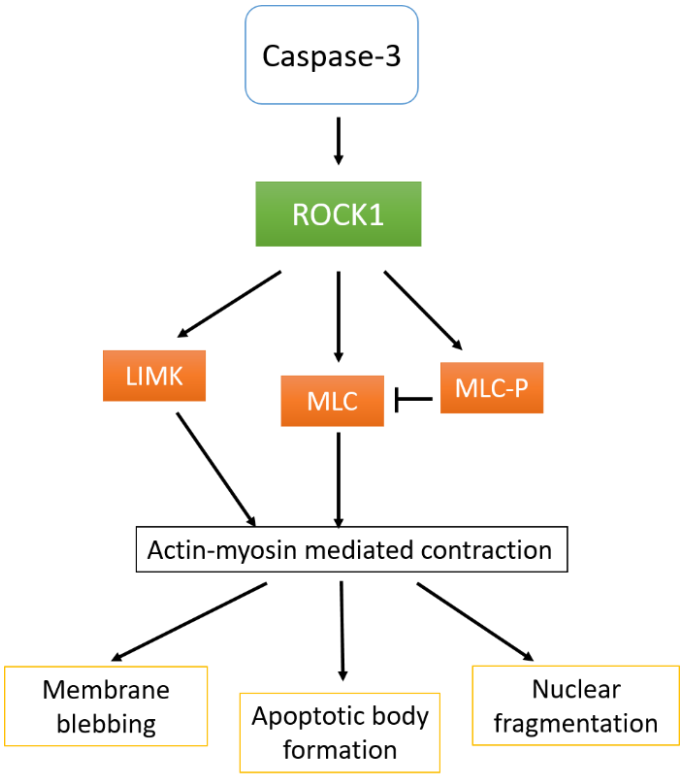

Figure 1-3 ROCK1 signalling during apoptosis. ROCK1 is cleaved by the executioner caspase-3. The truncated kinase is hyperactive, phosphorylating downstream signals such as LIM domain kinase (LIMK), myosin light chain (MLC), and MLC phosphatase (MLC-P). Phosphorylation of MLC-P disinhibits MLC activity. The phosphorylation of these downstream proteins mediates actin-myosin contraction which contribute to apoptotic membrane blebbing and apoptotic body formation. Changes in the cytoskeleton also assist in nuclear fragmentation during apoptosis.

1.3.2.3 Biochemical changes

The activation of the proteolytic caspase cascade is a key biochemical feature during apoptosis. Caspase activation is often known as the point of no return, committing a cell to death. In addition to the activation of caspases and cleavage of proteins, widespread protein cross-linking is also another feature observed during apoptosis. The expression and activation of transglutaminase allow extensive protein cross-linking to occur (Nemes et al., 1996).

Moreover, another characteristic biochemical feature is the fragmentation of DNA and condensation of chromatin. Both DNA fragmentation and further chromatin condensation is dependent on CAD, a protein released from the mitochondria upon MOMP induction. Chromatin condensation is observed in two stages. During early apoptosis, the chromatin is tightly packed within the nucleus in stage 1. In stage 2, CAD leads to more distinct chromatin condensation (Enari et al., 1998). CAD also initiates the fragmentation of DNA at internucleosomal sites into smaller portions (Samejima et al., 2001). It is speculated that both DNA fragmentation and chromatin condensation are required to avoid the activation of immune cells, as apoptosis-associated DNA fragments released extracellularly could cause an immune response (Napirei et al., 2000).

In addition to changes at the nuclear level, alterations at the membrane level also occur. The externalisation of phosphatidylserine (PS) is an important process during apoptosis. PS functions as a phagocytic ligand which, under normal, physiological circumstances, remains on the intracellular plasma membrane leaflet (Fadok et al., 1992). During apoptosis however, PS is translocated to the external leaflet of the plasma membrane to promote phagocytosis. The lipid transporter proteins, flippases, floppases and scramblases are responsible for maintaining the lipid integrity of plasma membranes and subsequently, the externalisation of PS upon an apoptotic stimuli (Hankins et al., 2015). These changes facilitate a dying cell into dismantling itself in a controlled manner, while enabling the exposure of certain phagocytic markers to promote engulfment by phagocytic cells, a process known as efferocytosis (Figure 1-2).

1.3.3 Apoptotic cell clearance

1.3.3.1 Release of 'find-me' signals

The process of apoptotic cell clearance begins with the release of signals, known as 'find-me' signals from the apoptotic cell itself. This begins before the cell has actually died in order to recruit phagocytes and promote the clearance of dead cells rapidly (Ravichandran, 2003). A variety of 'find-me' signals have been discovered, including fractalkine, nucleotides, lysophosphatidylcholine (LPC) and sphingosine 1-phosphate (S1P). In *in vivo* scenarios however, only fractalkine and nucleotides have been able to attract monocytes to apoptotic cells (Elliott et al., 2009, Truman et al., 2008).

Fractalkine, a chemokine that is known to attract macrophages, is processed and released during the early stages of apoptosis through small membraned vesicles known as micro-particles (Truman et al., 2008). Nucleotides adenosine triphosphate (ATP) and uridine triphosphate (UTP) on the other hand are released through pore-opening channel receptors known as pannexin channels, in particular the P2γ2 receptor (Chekeni et al., 2010). The role of nucleotides as in apoptotic cell clearance was clearly demonstrated in the thymus, whereby interference with the signalling axis resulted in impairment in thymocyte clearance *in vivo* (Elliott et al., 2009). LPC and S1P recruit macrophages by binding to G-protein coupled receptors (GPCRs) and S1P receptor respectively (Gude et al., 2008, Peter et al., 2008). The release of these find me signals are caspase-mediated events aimed at inducing phagocyte migration to the source site. Cells can be phagocytosed by professional phagocytes, such as macrophages and dendritic cells, as well as neighbouring cells that have engulfment capabilities, such as epithelial cells (Medina and Ravichandran, 2016).

1.3.3.2 Recognition of 'eat-me' signals

'Find-me' signals act as a beacon for phagocytic cells towards apoptotic cells. 'Eat-me' signals are then exposed on the surface of apoptotic cells, inviting phagocytes in to engulf the apoptotic debris. The most well characterised 'eat-me' signal is PS. PS externalisation is a characteristic biochemical change that occurs during apoptosis. It is speculated that the engulfment of apoptotic cells occurs if the levels of PS are above a certain threshold (Fadeel, 2004). PS can be

recognised by macrophages in two ways. The first is through the receptors including Ba1, Tim5 and Stablin2 (Wickman et al., 2012). The second is through bridging molecules such as milk fat globule epidermal growth factor 8 (MFG-E8). The molecule MFG-E8, is secreted by macrophages and anchors itself and PS to $\alpha_v\beta_3$ integrins on the phagocyte (Hanayama et al., 2002). It has been speculated that PS focalises on apoptotic membrane blebs as externalised phospholipids accumulate on blebs (Pace et al., 1999).

In addition to PS, the externalisation of proteins and molecules such as calreticulin plays an important part in efferocytosis. Calreticulin is normally maintained intracellularly, however, during apoptosis it is translocated to the plasma membrane (Panaretakis et al., 2009). Extracellular calreticulin is recognised by the low density lipoprotein receptor related protein (LRP-1/CD91) that is expressed on phagocytes. More recently, calreticulin has been shown to bind to PS itself and aid in efferocytosis (Wijeyesakere et al., 2016). CD91 seems to have additional roles at apoptotic membrane blebs binding to complement component C1q, acting as bridging molecules, particularly in human endothelial cells (Wickman et al., 2012).

As apoptotic cells express ‘eat-me’ signals to initiate phagocytosis, they also reduce their expression of ‘don’t eat-me’ signals. Two main ‘don’t eat-me’ signals are CD47 and CD31, both of which are expressed in abundance in healthy cells. The interaction between CD47 on healthy cells and signal regulatory protein alpha (SIRP1α) suppresses the actin-cytoskeletal arrangement required for phagocytosis. Thus, apoptotic and damaged cells reduce their expression of, or alter the distribution of CD47, allowing efferocytosis (Gardai et al., 2005, Lv et al., 2015). Similarly, the expression of CD31 induces repulsion of healthy cells when interacting with CD31 on phagocytic cells. This homotypic interaction is not carried out due to a reduction of CD31 on apoptotic cells. Altogether, the exposure of ‘eat-me’ signals and the reduction of ‘don’t eat-me’ signals serve important processes to ensure the clearance of apoptotic cells.

1.3.3.3 Engulfment of apoptotic cells

The entire apoptotic process culminates in the clearance of damaged or unwanted cells. The uptake of apoptotic debris is carried out by professional

phagocytes or in some cases, neighbouring cells that have phagocytic capabilities. Macrophages are regarded as the main professional phagocyte population responsible for most of the apoptotic cell removal. Alongside macrophages, dendritic cells (DCs) and monocytes are also classed as professional phagocytes (Henson, 2017). It is important to note that tissue specificity for phagocytosis is determined by the presence of different PS receptors. For example, TIM-1 is important in the kidneys, whereas BAI-1 provides tissue specificity towards the spleen, brain and bone marrow (Hochreiter-Hufford and Ravichandran, 2013).

Once a phagocyte engages with the apoptotic cell, reorganisations in its cytoskeleton are required to internalise the debris and degrade it (Doran et al., 2020). Similar in how Rho effector kinases, such as ROCK, are important in altering the cytoskeletal structure of apoptotic cells, ROCK and Ras-related botulinum toxin substrate 1 (Rac1) play further roles in disrupting the membrane of phagocytes to allow for engulfment of dead cells (Nakaya et al., 2006, Erwig et al., 2006). The uptake of apoptotic bodies through reduced stress fibre formation and changes in cellular shape utilises a large amount of plasma membrane for internalisation that needs to be replenished (Doran et al., 2020). Once internalised, the phagocytic cell must process the highly metabolic cargo load, containing lipids, nucleic acids and amino acids. Phagolysosomes are formed to degrade the cargo, and metabolic pathways are upregulated to process the metabolic load (Martinez et al., 2011). Ultimately efferocytosis aims to achieve 3 goals – the prevention of secondary necrosis; suppression of inflammatory responses; and promotion of self-tolerance (Doran et al., 2020). If either the apoptotic process or the clearance of apoptotic cells are disrupted, there can be dramatic consequences in the onset of certain diseases.

1.4 Apoptosis in physiology and disease

As previously discussed, apoptosis is an important process for the removal of unwanted or damaged cells. It is imperative for the developmental process, the maintenance of normal tissue functions and the immune system (Henson and Hume, 2006).

1.4.1 Development

During the developmental process, apoptosis acts a quality control measure, repairing any developmental errors that arise (Meier et al., 2000). Three model systems: the *Caenorhabditis elegans*, *Drosophila melanogaster,* and the mouse (*Mus musculus)*, have greatly increased our understanding of how apoptosis is key for development. Unlike in *C. elegans* and *D. melanogaster*, the developmental process does not stop at birth or metamorphosis in vertebrates. In vertebrates, development is a continual process (Rich et al., 2000, Meier et al., 2000). Tissue development is based on three principles – proliferation, differentiation and death. One of the most well characterised roles of apoptosis in organ development and morphogenesis is the development of limbs in digit individualisation models (Zakeri et al., 1994). Aberrations in the cell death process caused malformations in limb formation (Hernandez-Martinez and Covarrubias, 2011, Zakeri et al., 1994).

Not only is apoptosis important in the development of limbs, but also in the formation of hollow structures such as vessels and neural tubes (Weil et al., 1997, Coucouvanis and Martin, 1995). Additionally, another process important for development is anoikis – apoptosis resulting from detachment of cells from neighbouring cells (Frisch and Francis, 1994). Anoikis is essential for preventing the translocation of lone cells to inappropriate locations, a process cancer cells become resistant to (Malagobadan and Nagoor, 2019). Other processes in the body that rely on apoptosis include the turnover of photoreceptors, spermatogenic differentiation, heart development and neural development (Finnemann et al., 1997, Nakagawa et al., 2005, Abdelwahid et al., 2002, Awasaki et al., 2006).

Multiple genetic studies have argued that apoptosis is not entirely essential in development. Strasser *et. al.* have shown that although the majority of mice lacking the pro-apoptotic BCL-2 proteins BAX, BAK and BOK, do display developmental defects and do die, majority of the organs were developed normally in the foetus and in rare cases, some mice survived until adulthood (Ke et al., 2018). Furthermore, some caspase-3 deficient mice on a C57/Bl6 background alone can survive until adulthood with limited defects in the central nervous sytem (Zheng et al., 1999). Simiarly, although the majority of mice

lacking APAF-1 or caspase-9 suffer from neuronal defects and die prior to birth, a small percentage of mice survive and develop normally into adulthood (Cecconi et al., 1998, Hakem et al., 1998). If even a small number of mice can develop without key components of the apoptotic cascade, then the absolute requirement of apoptosis during development is questioned.

1.4.2 Tissue homeostasis

Tissue homeostasis is achieved by maintaining a delicate balance between the renewal of and demise of cells in the body (Biteau et al., 2011). The majority of cells in the body have a limited life span, which indicates that cells are constantly being turned over. Despite high levels of apoptotic activity, evidence of apoptosis is rarely seen in organs when analysed by immunohistochemistry (Nakanishi et al., 2011, Platt et al., 2000). Individual organs have different rates of turnover. For example, the intestinal epithelium is replaced every 5 days, while the lung epithelium is replaced every 6 months (Blanpain et al., 2007). Tissue remodelling is also reliant on cell death and regeneration, particularly evident in the mammary gland during the ovarian cycle, pregnancy and weaning (Hennighausen and Robinson, 2005). Cell turnover is also important for certain tissue-specific functions. The skin is an important barrier from external insults, a function depending on the renewal and death of epithelial cells (Pellettieri and Sanchez Alvarado, 2007). It is not surprising then that the balance between cell death and renewal is imperative for human health. Augmentation of cell death or impediment of regeneration underpin these phenomena (Sharpless and DePinho, 2004). On the contrary, increased cell proliferation and evasion of cell death mechanisms underlie cancer (Green and Evan, 2002, Pardal et al., 2003).

1.4.3 Apoptosis and the immune system

The immune system is required to protect the body from foreign pathogens, such as microbes, viruses, and damaged cells (Nicholson, 2016). Structural, chemical and cellular barriers are three fundamental requirements of a functioning immunity (Marshall et al., 2018). The cellular barriers are categorised into two central arms that mediate immunity – the innate and the adaptive immunity (Janeway, 2001). Both of which contribute to eliminating threats to the body and mediating self-tolerance. Further understanding of the immune system has

shed light on how important apoptosis is for the regulation of the immune system. Apoptosis has been shown to be important in, activation (antigen) induced cell death, B-cell maturation, T-cell development and cytotoxicity mechanisms (Feig and Peter, 2007).

1.4.3.1 Activated (antigen)-induced cell death (AICD)

A variety of immune cells once activated experience proliferation. However, to keep the number of immune cells in check, they must undergo apoptosis once a threat is resolved (Feig and Peter, 2007). Neutrophils are part of the innate immune system and are known as the first responders to a site of inflammation (Jenne et al., 2018, Fox et al., 2010). Neutrophils have short life spans of 24-36 hours, undergoing spontaneous apoptosis regulated by MCL-1 (Moulding et al., 2001, Edwards et al., 2004). Integrin engagement, pro-inflammatory cytokines and growth hormones such as interleukin-2 (IL-2) and granulocyte macrophage stimulating factor (GMCSF), and hypoxic conditions, typically found at sites of inflammation, can extend the lifespan of neutrophils in order to fulfil their function effectively (Edwards et al., 2004).

Key executioners of adaptive immunity come in the form of T-lymphocytes. IL-2 is required for successful T-cell activation and clonal expansion. Simultaneously however, IL-2 can signal MYC, condemning the cell to die (Lenardo, 1991, Shi et al., 1992). The extrinsic pathway, through CD95, plays an important role in regulating T-cell apoptosis. One hypothesis stipulates that activated T-cells upregulate CD95L, and appear to have more efficient intracellular signalling when compared to resting T-cells (Zhang et al., 2004, Scaffidi et al., 1999). Another hypothesis suggests that neighbouring non-lymphoid tissues upregulate CD95 instead and commit suicide due to the absence of growth factors, relying critically on BIM (Bonfoco et al., 1998, Pellegrini et al., 2003).

1.4.3.2 B-cell maturation

B-lymphocytes are part of the adaptive immune response. B-cell development and subsequent maturation is required for maintaining self-tolerance and producing antibodies to target threats in the body (Pieper et al., 2013). Two processes that are important to producing effective B-cells are the recombination of the heavy and light chains on B-cell receptors (BCR), and

affinity maturation of antibodies in germinal centres (Merlo and Mandik-Nayak, 2013). Apoptosis becomes important in eliminating self-reactive B-cell clones throughout the development and maturation process (Hartley et al., 1993). As B-cells mature, activated B-cells proliferate upon BCR engagement and antigen presentation. However, excessive cross-linking with BCRs also triggers apoptosis (Russell et al., 1991). Apoptosis, as a result of high affinity interactions to antigens presented by DCs, can be rescued by co-stimulation provided by T-helper cells (Liu et al., 1989, Liu et al., 1997). The apoptotic machinery is definitely engaged as caspase activation has been detected during negative selection of B-cells (Chen et al., 1999). Defective B-cell development and maturation results in the development of autoimmune disorders, such as systemic lupus erythematous (SLE) (Jacobi and Diamond, 2005).

1.4.3.3 T-cell development

Apoptosis is central to the development of fully functional T-lymphocytes. T-cell development occurs in the thymus, wherein the selection process is vital for the normal homeostasis of T-cells. (Kurd and Robey, 2016). Failure to satisfy either the positive or negative selection process triggers apoptosis in immature T-cells. Bone marrow derived progenitors travel to the thymus and rely on the microenvironment for successful selection and maturation (Germain, 2002). Lymphoid progenitor cells undergo a multitude of differentiation steps defined by cell surface markers, migrating through the thymus (Zúñiga-Pflücker, 2004). The T-cell maturation process goes through positive and negative selection stages. Positive selection is a process by which T-cells are selected based on their ability to interact with the major histocompatibility (MHC) antigens with low affinity, resulting in commitment of the thymocyte to either the CD4 or CD8 specific lineage (Kisielow et al., 1988, Bevan, 1997, Barton et al., 2002). If a thymocyte fails to interact with MHC antigens presented by neighbouring cortical epithelial cells and do not receive survival signals, they undergo cell death (von Boehmer et al., 1989, Robey and Fowlkes, 1994). Conversely, if an immature T-cell interacts too strongly with self MHC peptides, acute apoptosis is triggered; this is a process known as negative selection (McPhee et al., 1979, Klein et al., 2014).

Through these two selection processes, mature T-cells that are not autoreactive and regulatory T-cells are generated (Konkel et al., 2014). Thymocytes that fail either positive or negative selection are committed to die. It was discovered that negative selection of T-cells relies on TRAIL in the extrinsic apoptotic pathway, as TRAIL deficient mice have defective thymocyte apoptosis and susceptibility to autoimmune diseases (Lamhamedi-Cherradi et al., 2003). However, on the contrary thymocytes expressing a dominant version of adaptor protein FADD actually had augmented apoptotic clearance (Newton et al., 1998). This raised questions regarding the importance of the intrinsic pathway. Despite these contradicting results, the intrinsic apoptotic pathway was also found to be crucial for thymocyte selection, implicating BIM in particular (Marsden et al., 2002). Thus, the thymus is an organ heavily reliant on functional apoptotic machinery to create the T-cell repertoire required for efficient immune responses (Spits, 2002).

1.4.3.4 Cells mediating cytotoxicity

Cytotoxic T-cells (CTLs) and natural killer (NK) cells have the ability to target cells for death. CTLs and NK cells target viruses, virally-infected cells and cancer cells (Nutt and Huntington, 2019). Two mechanisms mediate this activity – a calcium dependent and calcium independent pathway (Feig and Peter, 2007). In the calcium dependent pathway, cytolytic protein perforin and serine protease Granzyme B are released by the immune cell. In the calcium independent pathway, CD95 and CD95L upregulation and release is found on the target cell. CTLs only possess the lytic ability once activated and differentiated. On the contrary, NK cells can kill target cells spontaneously, but depend on cytokines to enhance its lytic ability (Nutt and Huntington, 2019). Target cells engage with apoptosis as exposure to CTLs was shown to cause DNA fragmentation (Duke et al., 1983). This shows that apoptosis is important for regulating immune responses.

1.4.4 Functions in disease

As the apoptotic machinery is central for tissue homeostasis, it is expected that aberrations in apoptosis and efferocytosis are important in the pathology of diseases. Alterations in apoptosis are seen in a multitude of disorders including

neurological disorders, cardiovascular diseases, immune disorders and cancer (Favaloro et al., 2012).

1.4.4.1 Defective apoptotic machinery

The apoptotic machinery fails when cells that are meant to die, evade death or when cells that are meant to stay alive, die. The neurodegenerative disorder Alzheimer's disease (AD) is underpinned by the accumulation of amyloid- ß (Aß) peptides and hyper-phosphorylation of microtubule-associated protein tau (Duyckaerts et al., 2009). This causes the loss of neurons and subsequent memory loss. Apoptosis and caspase activation have been implicated in early events of the disease, promoting progression and underlying pathology of AD (Rohn, 2010). Caspase-3 was found to be activated by the incorrectly cleaved Aß peptides, which subsequently cleaves tau (Gamblin et al., 2003). Inappropriate activation of the apoptotic pathway contributes to neuronal death in AD.

On the flip side, the suppression of apoptosis also leads to autoimmune disease and cancer (see below). Overexpression of anti-apoptotic BCL-2 proteins have been linked to the development of autoimmune diseases. An underlying pathology of SLE in patients, is the increased expression of BCL-2 in T- and B-lymphocytes (Ohsako et al., 1997). It is thought that this contributes to extended survival of self-reactive lymphocytes. Similarly, T-cell apoptosis is abrogated due to an increase in BCL-2 proteins in the gastrointestinal autoimmune disorder, Crohn's disease (Ina et al., 1999). Pathogens, such as *mycobacterium tuberculosis*, are also capable of disabling the apoptotic machinery. Once inside the cell, *M. tuberculosis* enhances anti-apoptotic protein MCL1 to support the replication of the bacteria before being released and infecting additional cells (Sly et al., 2003). These are examples of where dysregulation of the apoptotic machinery can result in the development of different diseases, depending on the context of enhancement or suppression of apoptosis.

1.4.4.2 Defective cell clearance

Dysregulations in cell clearance are also important in the development of disease, including respiratory disorder, autoimmunity, atherosclerosis and cancer (Poon et al., 2014). Impaired phagocytosis is seen in chronic pulmonary

disease (COPD) and cystic fibrosis (Hodge et al., 2003, Vandivier et al., 2002). The reduced ability to engulf apoptotic cells in these conditions stem from an increase in reactive oxygen species (ROS), which subsequently activate RhoA, negatively regulating efferocytosis (Tosello-Trampont et al., 2003, McPhillips et al., 2007). Severe asthma is an additional respiratory disorder exhibiting defective alveolar macrophage phagocytic ability, which is improved when steroid therapy is administered (Huynh et al., 2005, Woolley et al., 1996).

In the autoimmune disease SLE, an accumulation of apoptotic cells in the blood and lymph nodes are suggested to be a result of impaired efferocytosis (Herrmann et al., 1998). Mice that are deficient in the bridging molecule MFG-E8 present with SLE-like symptoms of autoantibody production and accrual of apoptotic lymphocytes (Hanayama et al., 2004). Deficiencies in the complement C1q are also linked to the pathology of SLE (Botto et al., 1998). In atherosclerosis, mature lesions are exacerbated by apoptotic cells progressing into secondary necrosis from reduced clearance (Schrijvers et al., 2005). These examples exemplify the importance of apoptotic cell clearance maintaining tissue homeostasis and preventing disease development.

1.4.5 Apoptosis and cancer

Apoptosis is central for cancer development, treatment and resistance. Escaping programmed cell death is a pillar in tumourigenesis (Hanahan and Weinberg, 2011). Broadly, there are three ways in which cancer cells can evade apoptosis: tipping the balance towards anti-apoptotic proteins, reducing caspase function and disrupting signalling of death receptors (Wong, 2011). The overexpression and amplification of BCL-2 proteins have been reported in a number of cancer types including, but by no means an exhaustive list, BCL-2 in prostate cancer and diffuse B-cell lymphoma; and MCL-1 in myeloid cell lymphoma, breast cancer and hepatocellular carcinoma (Raffo et al., 1995, Sieghart et al., 2006, Campbell et al., 2018, Consortium, 2017). An important regulator of the apoptotic machinery, p53, is either inactivated or mutated in human cancers (discussed in a later section) (Ling and Wei-Guo, 2006). Additionally, the expression of pro-apoptotic proteins IAP, is also found to be dysregulated in cancer, including pancreatic cancer (Lopes et al., 2007). These examples exemplify how cancer cells tip the scale in favour of anti-apoptotic proteins.

Cancer cells also reduce the expression of caspases in order to disarm the apoptotic machinery. Samples from breast, ovarian and cervical cancers all gave rise to a reduction in the mRNA levels of executioner caspase-3 (Devarajan et al., 2002). Furthermore, a reduction in caspase-9 expression was observed in patients with stage II colorectal cancer (Shen et al., 2010). This was further correlated with poorer prognosis for these patients. Cancer cells can also reduce the expression of death receptor CD95, which contributes to treatment resistance in leukaemia and neuroblastoma (Friesen et al., 1997, Fulda et al., 1998). Taken together, cancer cells suppress mechanisms vital in the apoptotic process in order to survive. Venetoclax, a drug that mimics BH3 proteins to engage and activate the apoptotic pathway, has been approved for the treatment of chronic lymphocytic leukaemia (CLL) (Roberts et al., 2016). Interestingly, although apoptosis is required to prevent and treat cancer, it can paradoxically be viewed as oncogenic (Ichim and Tait, 2016). Cells, such as cancer cells, that fail to die despite having the apoptotic process triggered can sustain damages contributing to genomic instability (Ichim et al., 2015). This shows that apoptosis is central to keeping homeostasis, but can also be exploited in order to facilitate tumour progression and formation.

1.4.5.1 Membrane blebbing and cell clearance in cancer

Other aspects of the apoptotic process are also altered to aid tumour progression. Interestingly, apoptotic membrane blebbing and apoptotic body formation play a part in cancer progression. In cells derived from a bladder cancer cell line, apoptotic blebs fused with each other to form spherical structures (Jinesh et al., 2013). This fusion resulted in spherical structures driven by caspase action with a reduction in stem-cell markers. It is suggested that these spherical structures are tumourigenic. Furthermore, plasma membrane blebbing is linked with increased metastatic capabilities in prostate cancer (Khan et al., 2019). Apoptotic cells also package intracellular DNA in apoptotic bodies. For example, fibroblasts can uptake and integrate DNA from lymphoma derived apoptotic bodies (Holmgren et al., 1999). It has been further shown that in fibroblasts lacking p53, integrating oncogenes from apoptotic bodies facilitated tumour formation (Bergsmedh et al., 2001). These examples show how apoptotic morphology can play a part in facilitating tumour development.

In addition to apoptosis, cancer cell clearance is also altered during tumour development. A shift in the 'eat-me' and 'don't eat-me' signals were seen in *in vivo* and human genetic studies (Julian and Olson, 2015). Several human cancers including prostate cancer and oesophageal cancer show cells that have reduced annexin expressions, an 'eat-me' signal (Paweletz et al., 2000). Additionally, 'don't-eat me' signals such as CD47 are upregulated in lung, breast and prostate cancer in order to evade cancer cell clearance (Jaiswal et al., 2009, Chao et al., 2010, Moreaux et al., 2008). However, certain experimental evidences have raised questions regarding whether tumour cells evade tumour cell clearance. Two apoptotic 'eat-me' signals, PS and calreticulin, were found to be upregulated on tumour cells (Chao et al., 2010, Utsugi et al., 1991, Woehlecke et al., 2003). Apoptotic cell clearance ensures that apoptotic cells are cleared without signalling the immune system. Tumourigenesis however, is driven by chronic inflammation (Philip et al., 2004, Lu et al., 2006). Thus two possibilities arise from this. The first suggests that defects in apoptotic cell clearance would promote an anti-tumour response as there are high levels of cell death in the tumour microenvironment (Bondanza et al., 2004). Bondanza *et al*. showed that the inhibition of PS on lymphoma cells actually increase tumour immunogenicity. However, tumour development can thrive in an inflammatory milieu and inefficient clearance may facilitate the genomic instability and angiogenic properties of cancer cells (Lu et al., 2006). This shows that apoptotic cell clearance, like apoptosis, is likely to be involved in tumourigenesis.

1.4.5.2 Immunogenic cell death

As discussed previously, apoptosis is generally considered an immunologically silent process. Furthermore, cancer cells evade tumour surveillance as they themselves can mould their immunogenicity by losing the expression of tumour specific antigens (Marincola et al., 2000). Loss of immunogenicity as well as developing immuno-tolerance and actively suppressing the immune are tactics cancer cells use to evade immune attack (Garg et al., 2015). Cells which undergo death in stressed conditions can send out signals described previously as DAMPs. When there is a chronic exposure of DAMPs, this is known as immunogenic cell death (Zhou et al., 2019). Immunogenic cell death (ICD) relies on the release of DAMPS which bind to respective pattern recognition receptors (PRRs) on antigen presenting cells (APCs) (Ronchetti et al., 1999). APCs include

macrophages and dendritic cells. Upon activation by DAMPs, APCs upregulate their co-stimulator molecules, such as CD80 and CD86 which can facilitate activation of T-cells (Khan et al., 2012). The release of DAMPs and the induction of ICD is dependent on endoplasmic reticulum (ER) stress (Vandenabeele et al., 2016). These series of events activating cytotoxic T-cell activity can be utilised for cancer therapy. Anti-cancer drugs, including type I inducers of ICD, indirectly targeting the ER to release DAMPs. Type II inducers, including hydrostatic pressure and oncolytic viruses on the other hand, target the ER directly (Rapoport and Anderson, 2019). Inducing ICD along with chemotherapy can enhance the immunogenicity of tumour cells which is an attractive therapeutic strategy for cancer (Kroemer et al., 2013).

1.5 The p53 signalling axis

A protein central to the apoptotic process and tumourigenesis itself is p53. The tumour suppressor p53 is an extensively studied transcription factor implicated in a variety of cellular functions including cell cycle arrest, DNA repair, apoptosis and senescence (Vousden and Lane, 2007, Kastenhuber and Lowe, 2017). The structure, regulation and function of p53 and its negative regulator, murine double minute (MDM) protein are explored here.

1.5.1 p53

When the p53 protein was first discovered, it was initially classified as an oncogene (Lane and Crawford, 1979). However, it was later revealed that this was actually a mutant form of p53 that was detected and the wild-type p53 functioned as a tumour suppressor (Finlay et al., 1989). Under normal circumstances, p53 activation is vital to preventing uncontrolled proliferation, genomic instability, and survival of damaged cells (Vogelstein et al., 2000). A variety of cellular stresses, including DNA damage, nutrient deficiencies and hypoxia, as well as the expression of oncogenes, can activate and stabilise p53. Widely regarded as the ‘guardian of the genome’, p53 is most well known for its function as a tumour suppressor in cancer, as a loss of p53 provides cancer cells with proliferative advantages (Lane, 1992, Hussain and Harris, 1998). Additionally, due to its role in apoptosis, hyper-activation of p53 was discovered to be important in other disorders including arthritis, neurodegenerative

diseases and ischemia (Fridman and Lowe, 2003, Vousden and Lane, 2007, Vousden and Ryan, 2009). The development of disorders suggest that p53 activity must be heavily regulated to ensure physiological levels and appropriate activity.

1.5.1.1 Structure of p53

The human p53 protein, encoded by the *TP53* gene, is a 393 amino acid protein that oligomerises and functions as a tetramer (Clore et al., 1995). At the N-terminus, there is a transactivation domain (TAD) and proline rich region (PRR), followed by a central DNA-binding domain, a flexible linker connecting the tetramerisation domain and the extreme C-terminus domain (Figure 1-4) (Joerger and Fersht, 2008). Furthermore, p53 contains a nuclear localisation sequence (NLS) and nuclear export signal (NES) motifs that allow the shuttling of p53 between the cytoplasm and nucleus (Stommel et al., 1999). The TAD is an important binding site for proteins related to its transcriptional activity and its negative regulation by MDM2 (Lu and Levine, 1995, Gu et al., 1997, Kussie et al., 1996, Schon et al., 2002). The central DNA binding domain confers the specificity for p53 to bind to DNA with the 5' –'RRRCWWGYYY'-3' (R – Arginine; C – Cysteine- W – Tryptophan; G – Glycine; Y – Tyrosine) sequence (El-Deiry et al., 1992). The reversible oligomerisation of four p53 proteins occurs via the tetramerisation domain to facilitate the function of p53 (Sakaguchi et al., 1997, Veprintsev et al., 2006). The extreme C-terminal region is subject to post-translational modifications including stabilisation through phosphorylation and degradation through ubiquitination (Rodriguez et al., 2000).

The structure of p53 contributes to its transcriptional regulatory function. The tetramerisation of p53 is loose in nature, allowing for other proteins to interact with the p53 complex (Tidow et al., 2007). For example, anti-apoptotic and pro-apoptotic BCL-2 family proteins can interact with p53 in a context-dependent manner, implicating p53 in the apoptotic process (Chipuk et al., 2005). Disruptions of p53 function can arise due to mutations. As p53 is vital for homeostatic functions, it is no surprise that more than 17,000 mutations in the *TP53* gene, inactivating p53, have been documented in more than 50% of cancer cases (Petitjean et al., 2007, Bouaoun et al., 2016). The majority of the

mutations found are located in the central DNA binding domain, whilst others are found in the tetramerisation domain (Joerger and Fersht, 2008).

Figure 1-4 The primary structure of p53. The p53 protein is a 393 amino acid protein consisting of a transactivation domain (TAD), a proline rich region (PRR), a central DNA binding domain (DBD), a tetramerisation domain (TET) and an extreme c-terminus (C-term) domain. The TAD domain at the N-terminus can bind and interact with proteins. The DBD facilitates the transcriptional regulatory function of p53. The TET domain allows p53 to oligomerise and form a tetramer in order to be fully functional. The extreme c-terminus is subject to post-translational modifications that can regulate p53 activity. Figure adapted from (Joerger and Fersht, 2008).

1.5.1.2 Regulation of p53

In normal unstressed cells, p53 levels are kept low to negate the anti-proliferative effects of p53 during development and homeostasis (Vousden and Lane, 2007). The negative regulation of p53 in a cell are carried out in three stages – regulation of stability, activity and localisation. Stability of the p53 protein is determined by the nature of the post-translational modifications on the protein (Kruse and Gu, 2008). The stabilisation of p53 is dependent on the E3 ubiquitin ligase MDM2. The levels of p53 in an unstressed cell is tightly controlled primarily by MDM2, facilitating ubiquitination and subsequent proteasomal degradation of p53 (Haupt et al., 1997). In the absence of MDM2, other E3 ligases including constitutive photomorphogenesis protein 1 (COP1) and p53-induced RING-H2 protein (Pirh2) can regulated p53 (Dornan et al., 2004, Leng et al., 2003). MDM2 can navigate p53 to both nuclear and cytoplasmic 26S proteasomes for degradation (Haupt et al., 1997). The ubiquitination-dependent degradation of p53 generally takes place in the cytoplasm (Kubbutat et al., 1997). MDM2 can further inhibit p53 transcriptional activity in the nucleus by forming a complex with p53 (Thut et al., 1997). This form of inhibition can also be achieved by MDM2 homolog, MDM4 (Francoz et al., 2006). MDM2 and p53 are linked in a negative feedback loop to regulate the levels of p53 (Figure 1-5) (discussed in a later section).

A crucial step of p53 stabilisation is the phosphorylation of residues by a variety of kinases including ataxia-telangiectasia mutated (ATM), ataxia telangiectasia and Rad3 related (ATR), checkpoint kinase (CHK) 1, and CHK2 (Kruse and Gu, 2009). It is speculated that the phosphorylation of residues on the TAD of p53 prohibits the interaction of negative regulator MDM2 with p53 (Appella and Anderson, 2001). Knock-in mutations in *in vivo* studies revealed that phosphorylation-induced stabilisation was important in DNA-damage induced apoptotic conditions (Chao et al., 2006). However, other studies have suggested that p53 can be activated regardless of phosphorylation status (Ashcroft et al., 1999, Ashcroft et al., 2000). Acetylation has also been shown to be important in stabilising and increasing p53 levels (Wang et al., 2004). The acetylation at the C-terminus of p53 blocks MDM2-mediated ubiquitination and degradation. Furthermore, phosphorylation and acetylation of p53 are highly increased upon exposure to cellular stresses which stabilises and activates p53 (Sakaguchi et al., 1998). This highlights the inverse relationship between acetylation and phosphorylation with ubiquitination in regulating p53.

The localisation of p53 is also important as it determines what functions p53 can carry out. Three models have been proposed regarding the shuttling of p53. The first model suggests that p53 binds to MDM2 in the nucleus, which promotes the export of p53-MDM2 into the cytoplasm (Tao and Levine, 1999). A second model has suggested that MDM2-ubiquitination of p53 is essential for its nuclear export (Boyd et al., 2000). A third model has stipulated that p53 can exit the nucleus independent of MDM2 (Stommel et al., 1999). There is increasing evidence to support that mono-ubiquitination of p53 by MDM2 promotes nuclear export, which is in contrast with poly-ubiquitination which commits p53 for degradation (Li et al., 2003). It is apparent that regulating p53 involves a complex network to ensure normal cellular functions can take place.

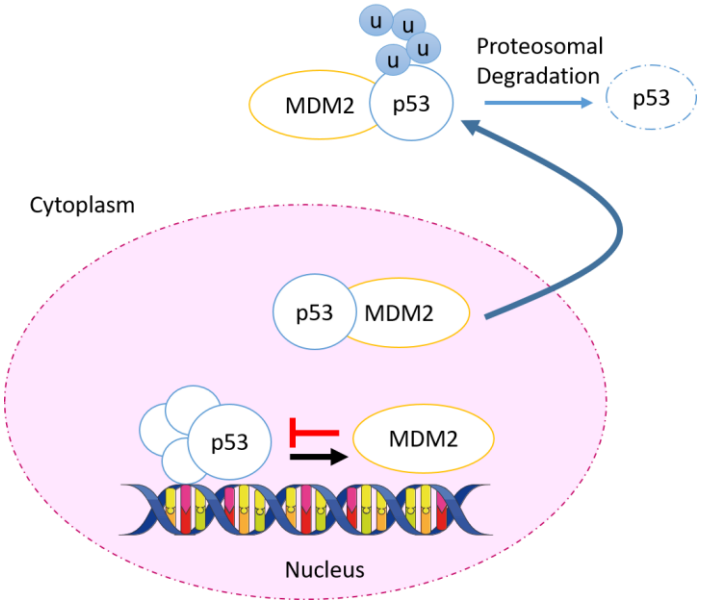

Figure 1-5 The p53-MDM2 regulatory feedback loop. The upregulation of p53 from cellular stresses induces the transcription of *MDM2*. The MDM2 protein can bind to p53 and inhibit its transcription activity. MDM2 can also facilitate shuttling p53 into the cytoplasm and the ubiquitination of p53. The ubiquitination promotes the proteosomal degradation of p53. This figure is adapted from (Nag et al., 2013). This figure was made using contents from Servier Medical Art, under the Creative Commons Attribution 3.0 Unported License. https://smart.servier.com/

1.5.2 Functions of p53

The p53 protein has both nuclear and cytoplasmic functions. Broadly, p53 is involved in a variety of cellular functions including apoptosis, autophagy, senescence, cell-cycle arrest and metabolism (Figure 1-6) (Brady and Attardi, 2010). The apoptotic and tumour suppressive functions are discussed below.

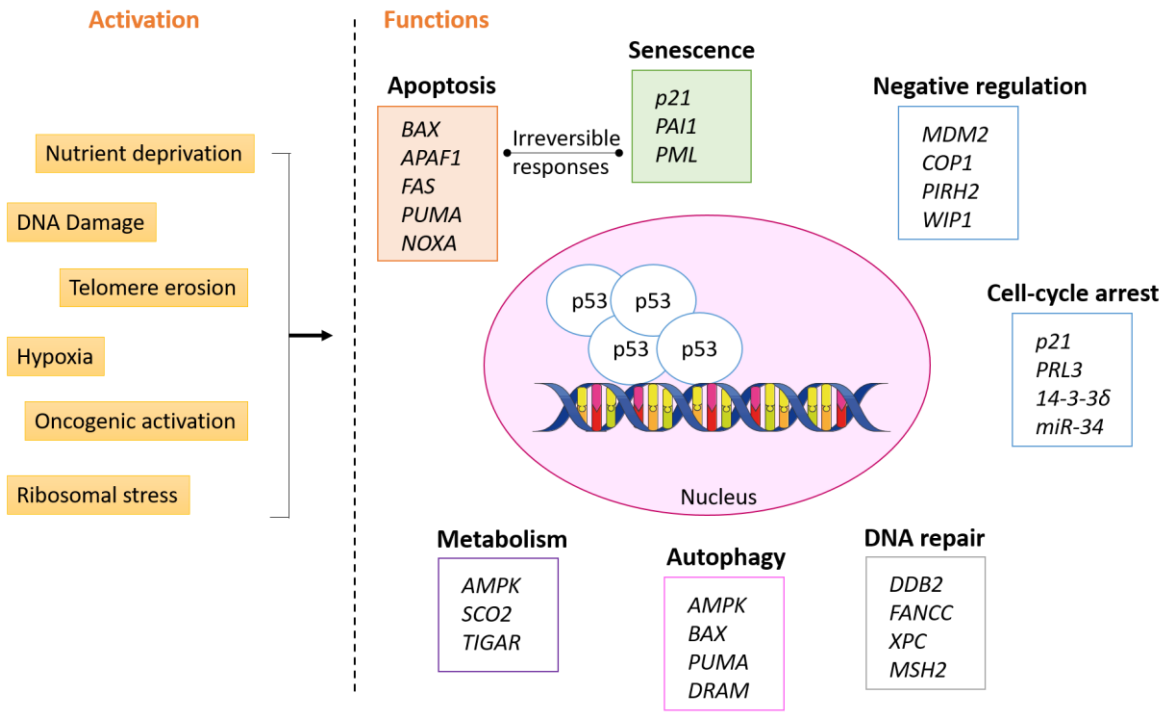

Figure 1-6 Activation and functions of p53. The p53 protein can be activated by many cellular stresses including outlined on the left. The activation of p53 then results in one or more of its cellular functions including apoptosis, senescence, autophagy, metabolism, DNA repair, cycle arrest and the negative regulation of p53 activation itself. Examples of p53-mediated target gene transcription relative to its functions are shown in the boxes. Apoptotic and senescent functions (shown in the shaded boxes) of p53 are irreversible responses whereas other p53 functions are reversible. Figure adapted from (Brady and Attardi, 2010). This figure was made using contents from Servier Medical Art, under the Creative Commons Attribution 3.0 Unported License. https://smart.servier.com/

1.5.2.1 Apoptotic functions of p53

In response to severe cellular stresses, p53 can induce irreversible apoptosis through both its transcriptional activity and its cytoplasmic activity. Both the intrinsic and extrinsic pathways of apoptosis can be triggered by p53 activation, although there is a skew towards the intrinsic pathway (Vousden and Lane, 2007). The activation of p53 leads to the upregulation of pro-apoptotic gene transcription including FAS, a death receptor in the extrinsic pathway, pro-apoptotic BCL-2 proteins BAX, PUMA and NOXA, and intrinsic apoptosome protein APAF-1 (Brady and Attardi, 2010). PUMA was revealed to be critical for p53-mediated apoptosis as cells from PUMA deficient mice are resistant to γ-irradiation *in vivo* (Jeffers et al., 2003). A loss of both PUMA and NOXA conferred resistance to radiation as well, however, studies have alluded to PUMA as a more vital mediator than NOXA in p53-mediated apoptosis (Michalak et al., 2008, Villunger et al., 2003). Additional p53 target genes include microRNAs. In respect to apoptosis, p53 can upregulate the expression of miR-34 which

subsequently targets pro-apoptotic BCL-2 proteins for degradation (Bommer et al., 2007).

Once in the cytoplasm, PUMA binds to the anti-apoptotic protein BCL-XL, allowing anti-apoptotic proteins BAX and BAK to form pores on the mitochondria (Chipuk et al., 2005). NOXA on the other hand binds to pro-apoptotic MCL-1, triggering the degradation of MCL-1 (Chen et al., 2005, Kuwana et al., 2005). Cellular stresses can also induce p53 translocation into the mitochondria, displacing MCL-1 from BAK on the mitochondria (Sykes et al., 2006). Thus, p53 can mediate apoptosis through its transcriptional and cytoplasmic functions (Fridman and Lowe, 2003).

1.5.2.2 Tumour suppressor functions of p53

The tumour suppressor p53 has been rightfully named due to its importance in sensing and responding to cellular stresses to prevent the propagation of damaged cells. Inactivation of p53 contributes the many hallmarks of cancer (Hanahan and Weinberg, 2011). There are however debates regarding which of the p53 functions are more important in perturbing tumourigenesis (Aubrey et al., 2016). Despite this, it is apparent that cooperation between multiple functions of p53 is required for its tumour suppressing functions. Apoptosis was discovered as one of the first tumour suppressing functions of p53 as apoptosis ensures that dysfunctional cells do not survive (Yonish-Rouach et al., 1991)

DNA damage repair and cell cycle arrest are two further functions of p53 that contribute tumour suppression. The p53 protein is crucial for both the acute and long-term response to DNA damage. Proteins involved in different repair mechanisms, including mismatch repair, nucleotide excision and base excision repair, interact with and are modulated by p53 (Sengupta and Harris, 2005). The p53 protein can upregulate the transcription of DNA repair proteins including MSH2 and DDB2 *(Aubrey et al., 2016)*. Cells undergo transient cell cycle arrest to allow DNA repair, after which p53 is involved in checkpoint control to maintain genomic integrity (Barboza et al., 2006). This involves the upregulation of p21, a cyclin dependent kinase inhibitor, amongst others to halt cell cycle progression (Brugarolas et al., 1995). Together, p53 helps maintain genomic stability and integrity, as cancer cells fail to repair DNA-damage resulting in accrual of

mutations in the absence of p53 (Hanahan and Weinberg, 2011). A number of experimental studies more recently have suggested that the acute DNA-damage responses mediated by p53 is not important for tumour suppression (Brady et al., 2011, Li et al., 2012). Despite this, p53 is still deemed important in DNA-damage, particularly when the acquisition of mutations can result in the inappropriate activation of oncogenes and the accumulation of DNA lesions from abnormal proliferation (Aubrey et al., 2016).

In addition to these functions, p53 mediated cellular senescence and metabolic regulation also contribute to the suppression of tumour formation. A number of p53 transcriptional target genes regulate senescence including *p21*, which was shown to be important in preventing malignant transformation of cells (Dankort et al., 2007). The p53 protein is important in maintaining homeostatic metabolic activities and responding to metabolic stresses (Berkers et al., 2013). Activating p53 promotes oxidative phosphorylation, which opposes the metabolic reprogramming towards glycolysis seen in cancer cells (Aubrey et al., 2016). This is done not only through the reduction of glucose transporters expression, but also through inhibition of glycolysis by the TP53-induced glycolysis and apoptosis regulator gene (TIGAR) (Schwartzenberg-Bar-Yoseph et al., 2004, Bensaad et al., 2006). Taken together, p53 functions are vital in order to maintain the integrity of a cell and hamper tumour formation.

1.5.3 MDM2

The murine MDMD2 protein was first discovered amplified in a transformed mouse cell line (Fakharzadeh et al., 1991, Cahilly-Snyder et al., 1987). There are three *MDM* genes, *MDM1*, *MDM2*, *MDM3*, identified on extrachromosomal nuclear bodies known as double minute. Similarly, three human MDM (also referred to as HDM) proteins have been identified, MDM1, MDM2 and MDM3 (Oliner et al., 1992). MDM1 and MDM3 are poorly understood. It was only more recently that MDM1 was identified as a binding protein of microtubules, regulating centriole duplication (Van de Mark et al., 2015). On the other hand MDM2 and its homologue MDM4 (MDMX) have been extensively studied as negative regulators of p53 (Mendoza et al., 2014).

1.5.3.1 Structure and function of MDM2

MDM2 is a 491 amino acid sequence encoding a protein that functions as an E3 ubiquitin ligase (Honda et al., 1997). The ubiquitination process relies on the E1, E2 and E3 proteins (Yang and Yu, 2003). Ubiquitin is transferred from E1 to E2, E2 to E3, and finally ligased onto a substrate from the E3 protein (Callis, 2014). The role of MDM2 is to ubiquitinate lysine residues of p53 at its C-terminus (Nakamura et al., 2000). MDM2 can also ubiquitinate itself (Fang et al., 2000, Honda and Yasuda, 2000). The functions of MDM2 are possible due to specific motifs found on the protein. At the N-terminal, MDM2 contains a p53 binding domain, followed by the NLS and NES domains, an acidic domain, zinc finger domain and a really interesting gene (RING)-finger domain at the C-terminus (Figure 1-7) (Iwakuma and Lozano, 2003). Additionally, within the RING domain, there is a nucleolar localisation signal (NoLS). The p53 binding domain allows MDM2 to bind to p53 and the RING-finger domain is required for the E3 ligase activity. The NLS and NES domains permit MDM2 to shuttle in and out of the nucleus to carry out its function. As discussed in the previous section, MDM2 tightly regulates p53 on multiple levels, including ubiquitination for degradation, shuttling of p53 back and forth between the cytoplasm and nucleus, and binding directly to p53 to inhibit its transcriptional function. These functions are carried out by the full length isoform of MDM2 (Iwakuma and Lozano, 2003).

Two isoforms of the protein can be generated – a full length p90 protein and a shorter p76 protein (Olson et al., 1993). Both isoforms are found in the cytoplasm and the nucleus. The p76 isoform does not contain the p53 binding domain, as such overexpression of the shorter isoform can antagonise the p90 isoform (Perry et al., 2000). Additional splice variants, including MDM2-A and MDM2-B in humans, are shorter forms of MDM2 that do not contain the p53 binding motif (Evans et al., 2001). There are speculations regarding the roles of the splice variants, however, it is still relatively unclear what they do (Iwakuma and Lozano, 2003).

Similar to MDM2, the homolog MDMX (also known as MDM4) contain the same sequence domain except the NLS, NES and NoLS domains (Figure 1-7) (Toledo and Wahl, 2007). However, despite containing the RING finger domain, MDM4 is catalytically inactivate and does not function as an E3 ligase (Linares et al.,

2003). MDM4 can form a heterodimer with MDM2, interacting at the RING finger domain and enhancing MDM2 ligase activity (Parant et al., 2001, Migliorini et al., 2002, Uldrijan et al., 2007). MDM2 can form a homodimer with itself, however studies have suggested that the heterodimer forms are more stable (Tanimura et al., 1999). Dimerisation of MDM2 is required for its function. MDM4 can bind and negatively regulate p53, independently from MDM2 (Francoz et al., 2006).

The importance of MDM2 and MDM4 in regulating p53 is exemplified by genetic studies. Both MDM2 and MDM4 deficiencies *in vivo* are embryonically lethal, both of which are rescued when there is a simultaneous loss of p53 (Montes de Oca Luna et al., 1995, Migliorini et al., 2002, Jones et al., 1995). Experimental studies have further suggested that there are subtle differences between the functions of MDM2 and MDM4. The loss of MDMD4 was due to an absence in cell proliferation and not the induction of apoptosis (Parant et al., 2001). Whereas MDM2 deficiency resulted in embryonic lethality due to uncontrolled p53-induced cell death (Montes de Oca Luna et al., 1995, Jones et al., 1995).

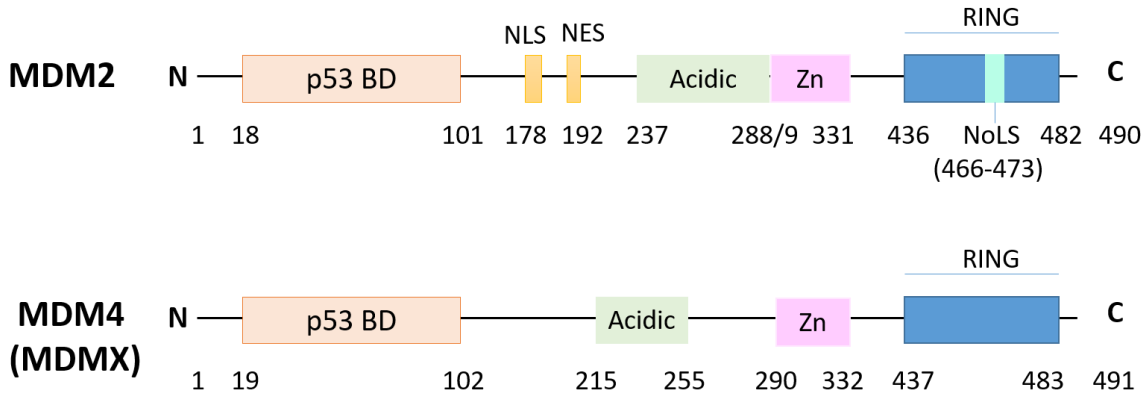

Figure 1-7 Structure of the MDM proteins. The MDM2 and MDM4 (MDMX) proteins are similar in their structure. Both contain a p53 binding domain (BD), acidic domain, zinc finger (Zn) domain, and RING finger domain. The MDM2 protein has additional nuclear localisation signal (NLS), nuclear export signal (NES) and nucleolar localisation signal (NoLS), which is absent in MDM4.

1.5.3.2 Regulation of MDM2

The regulation of MDM2 occurs at both the genetic level and the protein level. The *MDM2* gene itself contains twelve exons and two promoter regions (Figure 1-8). The two promoters, P1 and P2, are important in regulating the transcription of the gene. The P1 promoter regulates basal expression of MDM2 independently of p53, whilst the P2 promoter regulates inducible expression

generally driven by p53 (Zauberman et al., 1995, Barak et al., 1994, Jones et al., 1996). Similarly, *MDM4* also contains two promoters, whereby P1 drives constitutive expression and P2 is p53-responsive (Haupt et al., 2019). In both cases, translation of transcripts from the P2 promoter is more efficient from transcripts from the P1 promoter (Landers et al., 1997). *MDM2* P1 transcripts begin at exon 1 and skip exon 2 while P2-transcripts start from exon 2. Both however, have exon 3 to 12 in common. It is thought that the presence of two short upstream open reading frames found in exon 1 contribute to the inefficiency of P1-transcript translation (Jin et al., 2003).

A few regulators of the P1 promoter have been identified including NFκB and PTEN (Riley and Lozano, 2012). NFκB binds to the NFκB binding site on the P1 promoter to enhance the expression of MDM2 (Busuttil et al., 2010). On the contrary, PTEN negatively regulates the expression of MDM2 through a transcription factor that is currently unknown (Chang et al., 2004). The p53 protein binds to p53 response elements at the P2 promoter (Barak et al., 1994, Juven et al., 1993). This facilitates the feedback loop between MDM2 and p53 (Figure 1-5). For example, DNA damage increases p53 levels leading to enhanced *MDM2* transcription, leading to a subsequent reduction in p53 levels (Perry et al., 1993). This feedback loop keeps p53 activity in check. Additional proteins have demonstrated the ability to regulate *MDM2* transcription via the P2 promoter. *MDM2* levels can be enhanced by the binding of transcription factors Fli-1 Proto-Oncogene (Fli- 1), ETS transcription Factor and myeloid elf-1 like factor (MEF) (Truong et al., 2005); SMAD3/4 downstream of transforming growth factor ß (TGFß) signalling (Araki et al., 2010), and MYC (Slack et al., 2005).

Post-transcriptional and post-translational modifications are also important in regulating MDM2 expression and function. Post-transcriptionally, the oncogene BCR-ABL can upregulate MDM2 by enhancing the translation of *MDM2* (Trotta et al., 2003). Post-translational modifications of MDM2 have a greater impact on MDM2 function. The phosphorylation status of MDM2 alters its stability and function (Lozano, 2012). Phosphorylation of MDM2 by ATM, the kinase involved in stabilising p53 through phosphorylation, disrupts the ability of MDM2 to promote p53 translocation into the cytoplasm (Maya et al., 2001). This stabilises p53. This phosphorylation can be removed by the Wild-type p53-induced phosphatase (Wip1), a p53 target gene, in order to re-stabilise MDM2 and promote p53 for

degradation (Lu et al., 2007). This is another example of how p53 negatively regulates its own activity. Ubiquitination is another important post-translational modification regulating MDM2 activity and stability. The Herpesvirus-associated ubiquitin-specific protease (HAUSP) and the death domain-associated protein (Daxx) regulate MDM2 through ubiquitination (Lozano, 2012). Both HAUSP and Daxx prevent MDM2 auto-ubiquitination, and subsequent degradation of MDM2, in order to stabilise MDM2 and promote p53 degradation (Cummins and Vogelstein, 2004, Tang et al., 2006).

Another important regulator of MDM2 is $p14^{ARF}$ (Nag et al., 2013). The $p14^{ARF}$ protein is regarded as a tumour suppressor that sequesters MDM2 in the nucleolus (Kamijo et al., 1998, Weber et al., 2000, Sherr et al., 2005). This disrupts the function of MDM2, rending p53 stable, and promotes the degradation of MDM2. Oncogenic signalling activate $p14^{ARF}$ to suppress MDM2 activity and stabilise p53 (Pomerantz et al., 1998). The regulation of MDM2 expression has a knock-on effect on p53 stability and activity and thus must be tightly regulated to ensure homeostatic functions of p53.

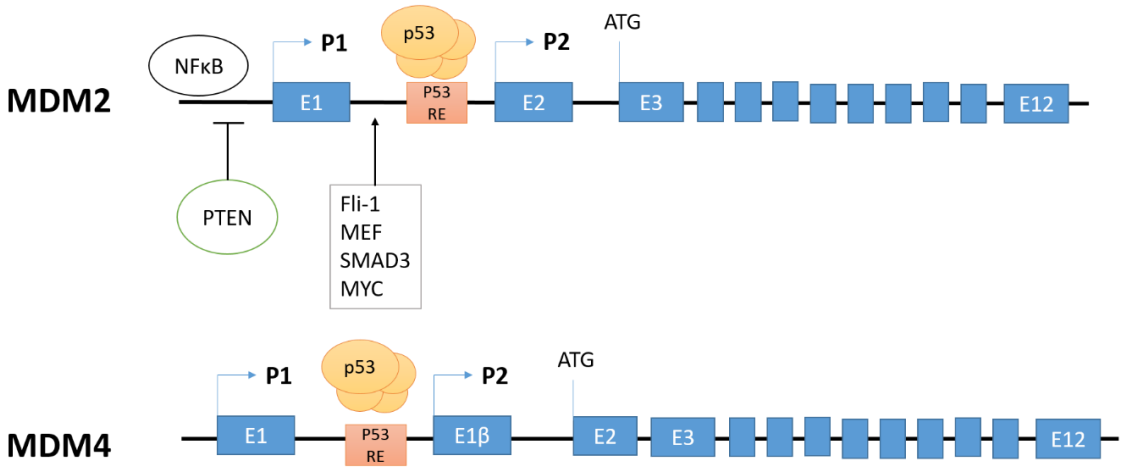

Figure 1-8 Transcriptional regulation of *MDM* genes. *MDM2* and *MDM4* genes have 2 promoters, the P1 and P2 promoter. The P1 promoter drives constitutive expression of MDM2 whilst the P2 promoter is inducible. NFκB and PTEN can induce *MDM2* transcription from the P1 promoter. Transcription factors, including Fli-1, MEF, SMAD3 and MYC, can regulate P2-*MDM2* transcription. The p53 protein can also initiate *MDM2* and *MDM4* expression via the responsive element (RE). The start codon (ATG) begins at exon 3 and 2 for *MDM2* and *MDM4* respectively.

1.5.4 The p53-MDM2 signalling axis in disease

The p53-MDM2 signalling axis is important for maintaining cellular functions and prevent the expansion of dysfunctional cells. Evidence of dysregulation in the p53-MDM2 signalling axis is evident in disease, including neurodegenerative disease and cancer (Chang et al., 2012, Karni-Schmidt et al., 2016). The role of the p53-MDM2 signalling axis in cancer is explored here.

1.5.4.1 The p53-MDM2 signalling axis in cancer

Aberrations in p53 functions have linked to multiple hallmarks of cancer including evading cell death, uncontrolled proliferation, genomic instability and alterations in metabolic activity (Vousden and Lane, 2007). The p53 protein is either mutated or inactivated in over 50% of human cancers (Hollstein et al., 1994, Ozaki and Nakagawara, 2011, Perri et al., 2016). This is further exemplified in p53 deficient mouse models developing spontaneous tumours (Donehower et al., 1992). Mutations in germline *TP53* gene cause the Li Fraumeni syndrome, a disorder characterised by a predisposition to developing cancer (Malkin et al., 1990). Cancers harbouring mutations in p53 are generally missense mutations which occur in the DNA binding domain, altering the transcriptional ability of p53 (Mantovani et al., 2019). Four hotspot mutations in the DNA binding domain, R249, R175H, R248W, R273H, are the most predominant mutations in human cancers (Hollstein et al., 1994).

Mutations can be classified as a gain of function or loss of function mutations (Ko and Prives, 1996). Gain of function mutations provide a selective advantage for cancer. For example, mutations in p53 can increase genomic instability and accumulation of mutations by promoting aberrant mitosis and check point control processes (Gualberto et al., 1998, Murphy et al., 2000). Overexpression of mutant p53 can also confer proliferative effects and resistance to apoptosis (Oren and Rotter, 2010). Certain mutations in p53 can also exert a dominant negative effect on the wild-type p53 (Willis et al., 2004). Mutant p53 proteins can form tetramers with wild-type p53, forming a complex that abrogates DNA binding ability. Furthermore, mutations in p53 can confer stability, prolonging the half-life of the protein from 20 minutes to 2 to 12 hours (Crawford et al., 1984, Cattoretti et al., 1988).

Inactivation of p53 in cancers can be achieved by upregulation of MDM2 (Oliner et al., 2016, Senturk and Manfredi, 2012). MDM2 amplification has been detected in a variety of human cancers including sarcomas (Oliner et al., 1992, Momand et al., 1998). *In vivo* models of MDM2 overexpression developed spontaneous tumours at an accelerated rate, but slower than p53 null mice (McDonnell et al., 1999). When MDM2 overexpression was combined with a loss of p53, tumour latency was similar to p53 null mice. In addition to MDM2, the loss of a locus on the *ARF* gene, epigenetic inactivation of *ARF* and mutations on ARF are frequently observed phenomena in cancer (Ko et al., 2018, Gil and Peters, 2006). Inactivation of ARF allows enhanced MDM2 activity and subsequent suppression of p53. These alterations in a cell mentioned are preferable environments for cancer.

Many therapeutic interventions have been and are developed to target the p53-MDM2 signalling axis. One of the most well developed inhibitors is the MDM2 antagonist Nutlin3a, which disrupts the binding of MDM2 and p53 (Vassilev et al., 2004). A Nutlin derivative, RG7112 has progressed into clinical trials (ClinicalTrials.gov Identifier: NCT00623870). Nutlin and nutlin derivatives are at risk of toxicities and are not as effective in cancers harbouring p53 mutations as this treatment aims to stabilise p53 (Wade et al., 2013). Other strategies for targeting p53 include stabilising the DNA binding domain of mutant p53, reinstating and reactivating the wild—type function of p53 in mutant p53 cases and gene therapy to enhance p53 levels (Roth et al., 1996, Boeckler et al., 2008, Cheok and Lane, 2017, Suzuki and Matsubara, 2011). It is clear that p53 is vital for homeostatic cellular functions, relying on apoptosis to eliminate dysfunctional cells. Thus, researching and developing therapeutic interventions that can enhance the function of p53 is important in the fight against cancer.

1.6 Rho-associated coiled-coil containing kinase (ROCK)

Another important protein family mediating changes during the apoptotic process are the effector kinases, the rho-associated coiled-coiled containing kinases (ROCKs). The structure, regulation, functions and current status of inhibitors are explored below.

1.6.1 Rho GTPases

Rho GTPases are monomeric proteins belonging to the Ras superfamily (Etienne-Manneville and Hall, 2002). Rho GTPases cycle between states of activation, bound to guanine triphosphate (GTP) facilitated by guanine exchange factors (GEFs), and inactivation, through the hydrolysis of GTP to guanine diphosphate (GDP) by GTPases-activating proteins (GAPS). Additional regulation of Rho GTPases are achieved by guanine nucleotide dissociation inhibitors (GDI) that sequester the inactivated protein in the cytosol (Haga and Ridley, 2016, Guan et al., 2013). Thus, Rho GTPases act as molecular switches responsible for controlling a variety of cellular processes involving the actin cytoskeleton, such as cell migration (Sadok and Marshall, 2014). Rho GTPases can be activated through a variety of ways. Receptor tyrosine kinases, GPCRs, cytokines and integrins are all capable of activating Rho GTPases through the activation of GEFs (Hartmann et al., 2015). There are 20 members of the Rho GTPases, including Rho, Rac and Cdc42, which interact with over 60 known effector downstream proteins (Feng et al., 2016). One of the most well characterised downstream effectors of Rho GTPases are ROCK proteins (Nakagawa et al., 1996, Ishizaki et al., 1996).

1.6.2 ROCK

ROCK proteins are serine/threonine kinases responsible for the phosphorylation of downstream targets. As such, ROCK has been extensively characterised, revealing its importance in a number of biological processes including cell migration, proliferation, adhesion, contraction and apoptosis (Kim and Ayata, 2017). Two isoforms of the serine/threonine kinase ROCK have been identified – ROCK1 (ROKß) and ROCK2 (ROKα). Apart from these two main mammalian homologues, variations of ROCK1 and ROCK2 have also been discovered. Both ROCK1 and ROCK2 belong to the AGC (protein kinase A/protein kinase G/protein kinase C) family (Ishizaki et al., 1996, Nakagawa et al., 1996).

ROCK1 and ROCK2 are ubiquitously expressed, however, there are differences in expression levels in different tissues. Higher levels of ROCK1 have been observed in lung, spleen, blood and thymus, whilst higher levels of ROCK2 are found in the brain, muscle and heart (Liu et al., 2008). Localisation of ROCK1 and ROCK2 are

largely dependent on the cell type (Hartmann et al., 2015). ROCK1 has been shown to localise predominantly in the cytoplasm (Iizuka et al., 2012). However, additional studies have also shown that ROCK1 can localise to the plasma membrane, vesicles, cell adhesion sites and centrosomes (Chevrier et al., 2002, Glyn et al., 2003, Stroeken et al., 2006). The subcellular localisation of ROCK2 has been better characterised than ROCK1. There are evidences supporting both cytosolic and nuclear localisation, as well as associations with actin, vimentin, stress fibres and centrosomes (Leung et al., 1995, Matsui et al., 1996, Tanaka et al., 2006, Ma et al., 2006, Kawabata et al., 2004, Katoh et al., 2001). Additionally, ROCK2 has been shown to localise in the cleavage furrows of cells undergoing mitosis (Inada et al., 1999, Kosako et al., 1999).

1.6.2.1 Structure of ROCK proteins

ROCK1, a 1354 amino acid protein, and ROCK2, a 1388 amino acid protein, both contain 33 exons and are located on chromosome 18 (18q11.1) and chromosome 2 (2p24) respectively (Julian and Olson, 2014). The variant of ROCK1, *Little Rock*, is the product of an inversed pseudogene on chromosome 18 (18p11.32) found mainly in vascular smooth muscle cells (Montefusco et al., 2010). The variant of ROCK2, ROCK2m, is a splice variant with an additional exon, found mainly in the skeletal muscle (Pelosi et al., 2007). The functions of these variants however still need to be determined. ROCK1 and ROCK2 are homologues that share 64% of their amino acid sequence, with a 92% homology in the kinase domain itself (Nakagawa et al., 1996). Both ROCK1 and ROCK2 contain the kinase domain on the N terminus, followed by a coiled-coiled α-helix region, and a Pleckstrin homology (PH) domain that is separated by a cysteine rich zinc finger like domain (CRD) at the C-terminus (Samuel and Olson, 2010). These 160kDa proteins contain a canonical Rho binding domain (RBD) for Rho GTPases, including RhoA, RhoB and RhoC, that is situated within the coiled-coiled domain. Other binding sites for additional regulatory proteins including RhoE, Rad and Gem, are situated near the canonical RBD. Additional RhoA binding sites have been reported in the coiled-coiled domain, stipulated to enhance binding of Rho GTPases (Blumenstein and Ahmadian, 2004). The ROCK proteins also contain cleavage sites that contribute to their function. ROCK1 contains a caspase-3 cleavage site whilst ROCK2 contains a Granzyme B cleavage site (Figure 1-9) (Coleman et al., 2001, Sebbagh et al., 2001, Sebbagh et al., 2005). This caspase-

3 cleavage site on ROCK1 is conserved across species in mammals (Chang et al., 2006).

Both ROCK proteins require the extension segments at both the N- and C-terminus ends as well as the catalytic domain to function. Crystal studies have revealed that extensions on either side of the catalytic domain on the N-terminal forms a head-to-head homodimer (Jacobs et al., 2006, Yamaguchi et al., 2006). The CRD and PH domains on the C-terminus on the other hand, remains monomeric (Wen et al., 2008). ROCK proteins themselves exist in dimers in an active form, whereby the Rho-binding regions on the coiled-coiled domain remain in parallel with each other (Dvorsky et al., 2004, Shimizu et al., 2003) (Figure 1-9). As part of the AGC kinase family, ROCK proteins show similarities in their primary and high-degree tertiary structures to other family members including dystrophia myotonica protein kinase (DMPK), myotonic dystrophy kinase related-Cdc42 related kinases (MRCK), protein kinase C (PKC), and protein kinase B (PKB/AKT) (Julian and Olson, 2014). Unlike the other AGC kinases, ROCK1 and ROCK2 do not contain the phosphorylation modifications at the activation loop or hydrophobic motif at the C-terminal when active (Yamaguchi et al., 2006). These crystal structures have been invaluable in shedding light on the structure of both ROCK proteins.

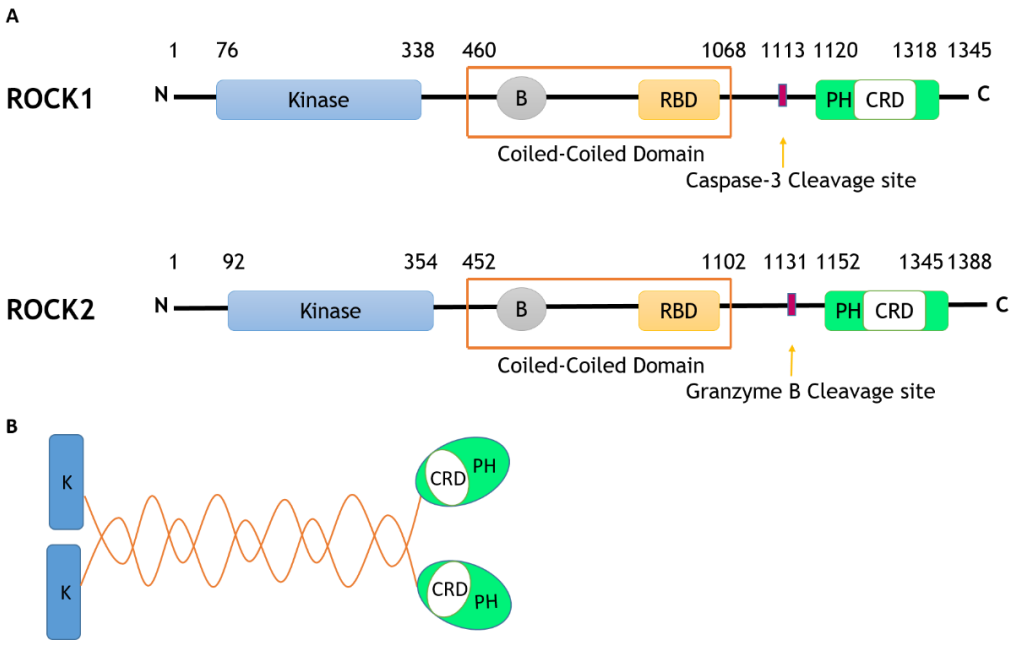

Figure 1-9 Structure of ROCK isoforms. A. Representation of the primary structure of ROCK1 and ROCK2. Both ROCK proteins contain a kinase domain (K) at the N-terminus, a coiled-coiled domain containing additional binding sites (signified with a B), a Rho binding domain (RBD), and a Pleckstrin homology (PH) domain separated by a cysteine rich domain (CRD) at the C-terminus. (figure adapted from (Julian and Olson, 2014)) **B.** Predicted ROCK structure based on crystallography experiments. The C-terminal PH and CRD domains form homodimers, while the coiled-coil regions dimerise in parallel (figure adapted from (Yamaguchi et al., 2006, Amano et al., 2010).

1.6.2.2 Conformation of ROCK proteins

Although much has been discovered regarding the structure of ROCK, there are still unclear areas regarding the conformation of the protein itself. Two models have been proposed (Figure 1-10). Initially, early studies suggest that ROCK preferentially existed in an inactive conformation. The kinase activity is inhibited through the protein folding onto itself, with the C- and N- terminals interacting with each other (Jacobs et al., 2006, Yamaguchi et al., 2006). The protein is thought to unfold upon activation, revealing the kinase domain and allowing the protein to phosphorylate downstream proteins. A more recent study looking at ROCK2, has suggested that the kinase remains in a constitutively active state. The constitutively active dimer remains anchored in the plasma membrane via its C terminal PH and CRD domains and remain in place with the help of scaffolding proteins such as Shroom (Truebestein et al., 2015). Trubestein *et al* further propose that ROCK activity is controlled by the length of the coiled-coil domain, not by Rho GTPase binding, phosphorylation, or binding to the plasma membrane itself. Instead, the length of the coiled-coil domain allows ROCK to act as a molecular ruler, positioning itself near to and engaging

its substrates. The length of the coiled-coil region is thought to be the important factor, as ROCK2 proteins with shorter coiled-coil regions despite being active showed an inability to interact with substrates and subsequent cytoskeletal defects. The mechanism as to how the kinase engages with its substrate is still unclear. How Rho GTPases interact with ROCK or how cleavage of ROCK affects the localisation and interaction with its downstream substrates is still unknown in this second model.

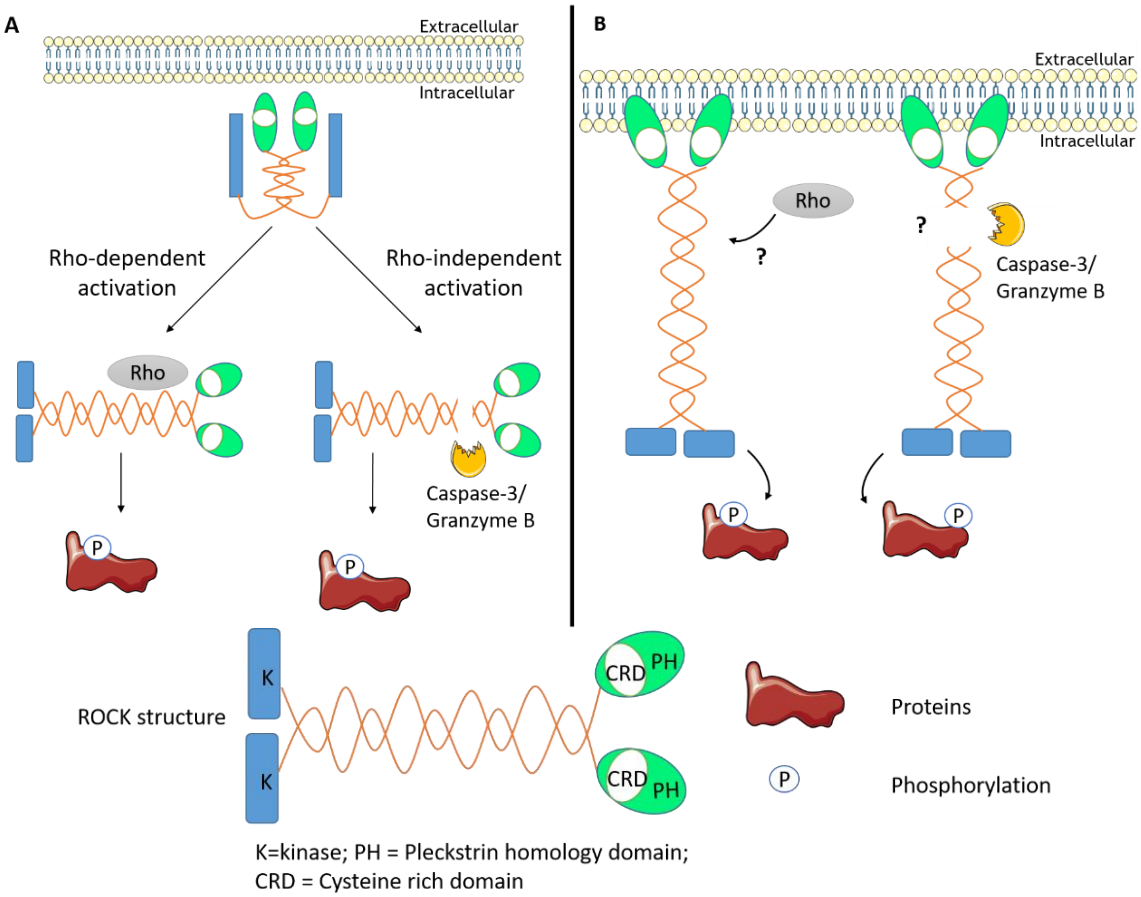

Figure 1-10 ROCK conformation models. Two models have been proposed for the conformation of ROCK. **A)**. Early studies suggest that ROCK, in its inactive state, is folded on itself. The N- and C-terminals interact with each other, hiding the kinase domain. Once activated, either in a Rho-dependent or Rho-independent fashion via cleavage by caspase-3 or granzyme B, the conformation of ROCK changes. The auto-inhibitory mechanism is disrupted, freeing up the kinase domain for downstream phosphorylation of its targets. Figure adapted from (Julian and Olson, 2014). **B).** More recent studies propose that ROCK proteins are tethered the plasma membrane itself via the PH and CRD domains. The coiled-coil domain acts as a molecular ruler, allowing interaction between the kinase and its substrate for phosphorylation. However, it is unclear how Rho binding and cleavage of ROCK fits in with this model. Figure adapted from (Truebestein et al., 2015). This figure was made using contents from Servier Medical Art, under the Creative Commons Attribution 3.0 Unported License. https://smart.servier.com/

1.6.2.3 Regulation of ROCK proteins

There are some similarities in the regulation of ROCK1 and ROCK2 owing to the overlap in their structure, whilst other modes of regulation are unique to each kinase. The most well documented mode of activation of ROCK is through the Rho GTPases. GTP-loaded RhoA and RhoC are quintessential activators, binding the RBD on the coiled-coil region on ROCK to trigger kinase activity (Ishizaki et al., 1996, Leung et al., 1996, Nakagawa et al., 1996, Matsui et al., 1996). Interacting with Rho GTPases on other binding sites on the coiled-coil domain can result in repression of ROCK activity. In particular, RhoE, Rad1 and GEM are known to inhibit ROCK activity (Ward et al., 2002, Riento et al., 2003, Komander et al., 2008). GEM and RhoE have been shown to bind to ROCK1 only, whilst Rad1 to ROCK2 only. RhoE binding towards to the N-terminus of the coiled-coil domain obstructs binding of activating Rho-GTPases. However, phosphoinositide dependent kinase 1 (PDK-1) has been reported to bind directly to ROCK1, competing with RhoE, and releasing ROCK1 from Rho-mediated inhibition (Pinner and Sahai, 2008).

In addition to Rho-dependent interactions, Rho-independent means can also regulate ROCK activity. The cleavage of ROCK proteins during apoptosis is an important regulator of its activity. ROCK1 is cleaved by caspase-3 in apoptotic cells, whilst ROCK2 is cleaved by Granzyme B, predominantly in natural killer and cytotoxic T-cells (Coleman et al., 2001, Sebbagh et al., 2001, Sebbagh et al., 2005). Severing the C-terminus constitutively activates ROCK, allowing downstream phosphorylation of its substrates. Other molecules, such as lipid mediators are able to regulate ROCK activity. Arachidonic acid (AA) can interact with ROCK via its C-terminus, while sphingosylphosphorylcholeine (SPC) can promote translocation of ROCK to the plasma membrane and sensitisation to calcium, activating the kinase (Araki et al., 2001, Fu et al., 1998, Shirao et al., 2002). Inositol-phospholipids PIP_2 and PIP_3 play further roles in spatially regulating ROCK2 in particular, to the plasma membrane via the PH domain (Yoneda et al., 2005). In addition, other proteins such as nucleophosmin has been shown to bind to ROCK2 to increase its activity (Ma et al., 2006) In contrast, Coronin1a/b was discovered to attenuate ROCK2 signalling by binding to the PH domain of the kinase (Rana and Worthylake, 2012). Collapsin response

mediator protein 2 was also shown to reduce ROCK2 activity (Yoneda et al., 2005).

Post-translational modifications have also shown to be important regulators of ROCK activity. Although phosphorylation at the activation loop is not required for ROCK activity, phosphorylation at other sites do have the ability to regulate ROCK's activity and potentially, its localisation. Both ROCK1 and ROCK2 are capable of auto-phosphorylating at S1333 on ROCK1 and S1366 on ROCK2, indicative of activation (Chuang et al., 2013, Rautou et al., 2011). It is speculated that phosphorylation at these sites regulate the localisation of ROCK proteins (Ishiuchi and Takeichi, 2011). ROCK2 phosphorylation by Polo-like 1 kinase (PLK) has been shown to enhance RhoA binding at conserved serine/threonine sites, whilst specific phosphorylation at Tyr-722 diminish RhoA binding (Lowery et al., 2007, Sinning et al., 2011). The regulation of both kinase activity and subcellular localisation of ROCK plays an important role in facilitating and controlling its functions in the cell.

1.6.3 Downstream signalling of ROCK proteins

As serine/threonine kinases, ROCK proteins phosphorylates downstream substrate targets through a consensus motif. The canonical amino acid sequence Arg/Lys-X-Ser/Thr or Arg/Lys-XX-Ser/Thr (Arg - Arginine; Lys - Lysine; Ser - Serine; Thr - Threonine; X - any amino acid) dictates the specificity of substrates for phosphorylation (Kang et al., 2007). As ROCK1 and ROCK2 have a high degree of similarity in their kinase domain, it has been speculated that they would share some common substrates. It is important to note that the amino acid sequence is also recognised by other AGC kinases including myosin II light chain (MLC) kinase (Pearce et al., 2010). A number of substrates have been identified including myosin, LIM kinase, myosin phosphatase target subunit1 (MYPT1), phosphatase and tensin homolog (PTEN), ezrin, radixin, moesin (ERM) proteins, formin homology 2 domain containing 1 (FHOD1), vimentin, RhoE, and Adducin 1 (Pearce et al., 2010). Phosphorylation of substrates can either activate or inhibit protein function. For example, phosphorylation of MLC facilitates the interaction between actin and myosin, resulting in cell contraction. Phosphorylation of MYPT1 on the other hand, inhibits its phosphatase functions on MCL, further enhancing cell contraction (Amano et al., 1996). The phosphorylation of its

substrates results in reorganisation of the actin cytoskeleton, contributing to its cellular effects including cell migration, adhesion, stress fibre formation, proliferation, and apoptotic morphology (Figure 1-11) (Julian and Olson, 2014).

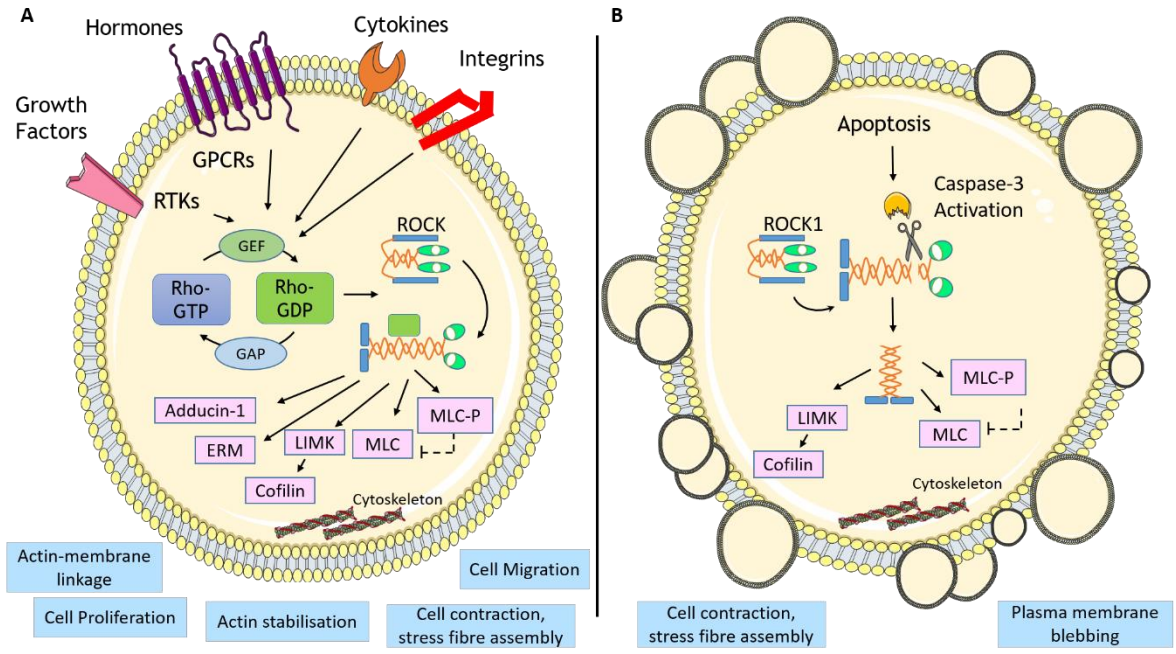

Figure 1-11 ROCK signalling cascade. A). In physiological settings, ROCK can be activated in both Rho-dependent and Rho-independent manners. Depicted is a Rho-dependent activation of ROCK. GEFs can be activated through a number of ways including, receptor tyrosine kinases (RTKs), GPCRs, cytokines and integrins. GEFs exchange GTP to GDP on Rho-GTPases that can bind and activate ROCK. ROCK can then phosphorylate a variety of substrates including MLC, regulatory subunit on myosin light chain phosphatase (MLCP), LIMK, ERMs and Adducin-1. These interact with actin and mysosin filaments, changing the cytoskeleton of a cell. This can allow for cell migration, cell contraction, stress fibre assembly, cell proliferation, actin stabilisation and actin membrane linkage. B) Representative signalling cascade for ROCK1 during apoptotic conditions. Upon apoptosis induction, caspase-3 is activated which can cleave ROCK1 (D1113). This truncated form is hyperactive, phosphorylating downstream targets including MCL, MYPT1 and LIMK. This can cause cell contraction, stress fibre assembly and the characteristic plasma membrane blebbing. Figure adapted from (Leverrier and Ridley, 2001a) (Hartmann et al., 2015). This figure was made using contents from Servier Medical Art, under the Creative Commons Attribution 3.0 Unported License. https://smart.servier.com/

1.6.4 Functions of ROCK

1.6.4.1 ROCK in cytoskeletal organisation

ROCK's most prominent function in cells is the organisation of the cytoskeleton. Interactions with actin and myosin are achieved through the phosphorylation of downstream substrates. One of the first signalling pathways identified was the phosphorylation of myosin II (Amano et al., 1996). Myosin filaments assemble and subsequently bind to actin following MLC phosphorylation. The hydrolysis of ATP following the actin-myosin interaction then enables contraction to occur

(Croft et al., 2005). In tandem, ROCK also phosphorylates MYPT1, the regulatory subunit on myosin light chain phosphatase (MLC-P). This phosphorylation inhibits MCL-P activity, enhancing MLC-mediated contraction (Feng et al., 1999). Both ROCK1 and ROCK2 can phosphorylate MYPT1, however, in vascular smooth muscle cells, ROCK2 has been shown to bind directly to MYPT1 as well (Wang et al., 2009). Similarly, ROCK stabilises actin filaments through phosphorylation of LIM kinase 1 and 2 (Maekawa et al., 1999, Ohashi et al., 2000). Activated LIM kinases phosphorylate its target cofilin. This phosphorylation inhibits the depolarisation of F-actin by cofilin, stabilising actin (Moriyama et al., 1996).

The organisation of the cytoskeletal components form contractile actin bundles, also known as stress fibres, and focal adhesions (Katoh et al., 2001, Kawabata et al., 2004, Schiller and Fassler, 2013). Focal adhesion are areas in the cell that contain proteins important for adhesion of the cell to other cells or the extracellular matrix (Schiller and Fassler, 2013). Additional functions of ROCK on the cytoskeleton are achieved through phosphorylation of adducin-1, which promote actin bundle formation (Luo and Shen, 2017), and phosphorylation of the ERM proteins, which crosslink actin and membrane-bound proteins (Fukata et al., 1998, Matsui et al., 1998). These two substrates as well as cofilin are implicated in cell migration through the formation of dynamic leading edges and filopodia (Schofield and Bernard, 2013). Together, ROCK-mediated cytoskeletal dynamics are important for numerous cellular functions including cell contraction, migration, adhesion and morphogenesis (Tojkander et al., 2012).

1.6.4.1.1 Blebbing in migration and apoptosis

The cytoskeletal reorganisation initiated by ROCK1 can cause membrane blebbing (Charras and Paluch, 2008). Cell blebbing is defined by pressure-driven spherical protrusions of the membrane, when the membrane itself detaches cortex (Pollard and Borisy, 2003). Although blebbing is often considered a characteristic morphological feature of apoptotic cells, membrane blebbing is also observed during physiological conditions including during cell division and cell spreading (Fishkind et al., 1991, Bereiter-Hahn et al., 1990). Another function of blebbing that has been documented is cell migration (Charras and Paluch, 2008). Bleb-driven cell migration has been observed during development as well as by metastatic cancer cells (Blaser et al., 2006, Friedl and Wolf, 2003).

Often, blebbing is used as an alternative to lamellipodial migration. A key difference between non-apoptotic and apoptotic membrane blebbing is the polarisation of the blebs itself. Migratory blebs are generated on the leading edge of a cell whereas apoptotic blebs are formed all around the cell (Charras and Paluch, 2008). Apoptotic blebs have been more extensively studied than migratory blebs. It is still unknown how migratory blebs are polarised and how blebbing is translated into movement. Regardless of the function, blebs are seen as an evolutionary conserved form of cell protrusion.

1.6.4.2 ROCK in cell cycle and proliferation

The role of ROCK in cell cycle progression and cell proliferation independent of cytoskeletal control is less characterised. Some studies have suggested a role for ROCK1 in regulating G1/S phase progression through cell cycle proteins (Croft and Olson, 2006, Zhang et al., 2009). These *in vitro* studies suggest that ROCK regulates the cell cycle on different levels, through increasing cyclins (D1 and A), reducing negative regulators (p21 and p27) as well as reducing the INK4 family of cyclin dependent kinase inhibitors (CDKIs). The loss of ROCK was also observed to associate with cell cycle arrest and senescence (Kumper et al., 2016). ROCK is important not only in regulating levels of proteins but also in the spatio-temporal regulation associated to cell cycle progression and ultimately mitosis. ROCK is involved in the formation of the cleavage furrow, as well as centrosome segregation and positioning during mitosis (Kosako et al., 2000, Sahai et al., 1999, Chevrier et al., 2002). ROCK promotes actin formation and disassembly of filaments, including vimentin at the cleavage furrow (Matsumura, 2005) . On the contrary, ROCK can also suppress proliferation through activation of PTEN. PTEN is responsible for inhibiting AKT/PKB, which is required for cell proliferation (Yang and Kim, 2012). These effects are dependent on cell type – ROCK inhibition was shown to suppress proliferation in smooth muscle cells and cardiac myocytes (Takeda et al., 2006, Zhao and Rivkees, 2003).

1.6.4.3 ROCK in apoptosis

As discussed in the previous section, programmed cell death results in a variety of cellular and morphological changes, particularly to the actin-cytoskeleton. The cleavage of ROCK1, not ROCK2, at the caspase-3 cleavage site forms a

hyperactive kinase. The reorganisation of the cytoskeleton and further MLC phosphorylation has proved to be crucial for apoptotic process, including cell shrinking, plasma membrane blebbing, nuclear fragmentation and apoptotic body formation (Julian and Olson, 2014). ROCK further enables the disruption of the nucleus, as well as the packaging of fragmented cellular components into apoptotic bodies (Croft et al., 2005, Coleman et al., 2001). Specialised forms of cell death triggered by NK cells result in the release of Granzyme B. In this instance, pro-apoptotic protease Granzyme B cleaves ROCK2, but not ROCK1, facilitating downstream phosphorylation of its targets and membrane blebbing. ROCK2 also leads to further activation of ROCK1 which results in reorganisation of the cytoskeleton as mentioned above (Sebbagh et al., 2005). These features allow apoptosis to remain immunologically silent, as intracellular contents such as damage associated molecular patterns (DAMPs), including nuclear histones, are largely contained within apoptotic bodies (Wickman et al., 2013). Although cells try to contain DAMPs, leakage of these molecules occur during apoptotic blebbing, which can alert and attract immune cells. This stops the progression of programmed cell death into secondary necrosis (Doran et al., 2020).

1.6.4.4 ROCK in phagocytosis

As discussed above, phagocytosis is the ultimate step to clear apoptotic cells. The Rho/ROCK signalling cascade is implicated in the negative regulation of efferocytosis (Tosello-Trampont et al., 2003, Leverrier and Ridley, 2001b), while the Inhibition of the RhoA/ROCK pathway enhanced the uptake of apoptotic cells (Tosello-Trampont et al., 2003). The enhancement of phagocytosis subsequently increases apoptotic cell clearance by macrophages (Tosello-Trampont et al., 2003, Kim et al., 2017). Signalling through Rho/Rock/ERM additionally increases phagocytic uptake of apoptotic cells through phagosome maturation (Erwig et al., 2006). Interestingly, Rho/ROCK is implicated in efferocytosis and phagocytosis via the complement receptor, but not via the Fc receptor (Olazabal et al., 2002, Caron and Hall, 1998). This is attributed to ROCK's role in reorganising the actin cytoskeleton that regulates basal engulfment.

1.6.4.5 ROCK in development

Genetic studies have given great insight into the roles of ROCK1 and ROCK2, particularly during development. Both ROCK1 and ROCK2 were found to be expressed in a variety of organs, including the heart, umbilical blood vessels and dorsal root ganglion (Shimizu et al., 2005, Thumkeo et al., 2003). Homozygous genetic deletion of ROCK1 in C57Bl/6 mice resulted in over 90% of perinatal death in mice, with defects in their eyelids and an omphalocele phenotype (Shimizu et al., 2005). ROCK2 deletion in C57Bl/6 mice were embryonically lethal, resulting in the same defects in eyelids and omphalocele phenotype, but also placental dysfunction (Thumkeo et al., 2003). The genetic studies allude to the redundant functions of the ROCK proteins during development, but equally provide insight into the importance of ROCK for cell migration and organ formation (Shi et al., 2011).

1.6.4.6 ROCK in the immune system

The role of ROCK proteins in the immune system is largely attributed to its ability to remodel the actin cytoskeleton and ROCK's less known function of altering gene expression in immune cells (Pernis et al., 2016). In T-cells, both ROCK1 and ROCK2 have been shown to trigger cytokine-mediated cell polarisation as well as transendothelial migration (TEM) downstream of RhoA activation (Heasman and Ridley, 2010, Vicente-Manzanares et al., 2002). Experimental studies using ROCK inhibitors and silencing of ROCK1/2 expression has revealed a role for ROCK in T-cell activation and differentiation. The inhibition of ROCKs resulted in a reduction of T-cell proliferation and interleukin cytokine production (Tharaux et al., 2003, Aihara et al., 2003). Interestingly, through inhibition of ROCK2, there was an absence of phosphorylation and subsequent activation of interferon regulatory factor 4 (IRF4), a transcription factor required to differentiate naïve T-cells into T-helper 17 (T_H17) cells (Biswas et al., 2010). Apart from T-cells, ROCKs have also been shown to be important in the antigen internalisation ability and motility of B-cells (Natkanski et al., 2013, Pernis et al., 2016). Furthermore, ROCKs have also been implicated in myeloid cell function. The inhibition of ROCK was shown not only to affect DC motility, but also its morphology, affecting its ability for antigen presentation (Kobayashi et al., 2001). Macrophage function can also be affected. Macrophages

can be polarised towards a more inflammatory phenotype by the activation of mitogen-activated protein kinases (MAPK) and NFκB by ROCKs (Cheng et al., 2015).

1.6.5 ROCK in disease

ROCKs are important kinases required for a numerous physiological cellular functions including organisation of the cytoskeleton to allow contraction and movement, as well as the regulation on survival, death and phagocytosis. It is therefore unsurprising that when the function of these kinases deviate from the norm, pathological conditions can arise. Accordingly, experimental studies have linked ROCK to conditions including cardiovascular diseases, autoimmunity disorders, respiratory disease and cancer (Schofield and Bernard, 2013, Pacaud and Loirand, 2010). The role of ROCK proteins in cancer is explored below.

1.6.5.1 ROCK in cancer

Cancer involves the abnormal proliferation of cells in the body, characterised by hallmark biological processes including proliferation, evasion of the immune system and cell death resistance. The progression of cancer is a multistep process that ultimately results in the transformation of cells and growth of tumours (Hanahan and Weinberg, 2011). Reorganisation and alterations in the actin cytoskeleton has proven to be important for the progression of cancer cells. Cytoskeletal changes can contribute to cell motility, invasion, metastasis as well as proliferation and the remodelling of the extracellular matrix (Morgan-Fisher et al., 2013). Recent experimental studies have shed light on the importance of ROCK signalling in modulating cellular processes that contribute mainly to tumour progression and invasion (Morgan-Fisher et al., 2013, Schofield and Bernard, 2013).Mutations in ROCK proteins have been identified in a variety of human cancers including melanoma, breast, lung, and stomach cancer (Greenman et al., 2007, Lochhead et al., 2010). High levels of ROCK1 in breast cancer and osteosarcoma have been correlated with poorer survival and increased tumour grade (Lane et al., 2008, Liu et al., 2011). Elevated ROCK2 levels were associated with more aggressive hepatocellular carcinoma and bladder cancer (Wong et al., 2009, Kamai et al., 2003). Whether increased ROCK

levels is a cause or consequence of tumour progression is still yet unknown (Hanahan and Weinberg, 2011).

The regulation of ROCK activity in cancer can come from both upstream activators, such as Rho, and binding partners of ROCK. Overexpression and over-activation of RhoA have been reported in several cancers, including breast, colon and lung cancer (Morgan-Fisher et al., 2013). In malignant melanoma and squamous cell carcinoma, PDK1 and RhoE compete to bind with ROCK1. PDK1 promotes ROCK1 activity and subsequently cell migration (Pinner and Sahai, 2008). RhoE, although antagonising PDK1, has been lost in hepatocellular carcinoma, losing the suppression of cell motility. (Riento et al., 2003, Ma et al., 2013). Cell motility and cancer survival is also dependent on the remodelling of the ECM. Enhanced ROCK activity is correlated with increased stiffness which is associated with cancer progression (Jaalouk and Lammerding, 2009). Cancer associated fibroblasts (CAF) depend on ROCK2 activity to remodel the ECM, paving the way for cancer cell migration (Gaggioli et al., 2007). This is one way in which ROCK has been proposed to promote invasiveness and metastasis. ROCK has also been suggested to mediate metastasis through epithelial-to mesenchymal transition (EMT) and E-cadherin loss (Castro et al., 2013, de Toledo et al., 2012). Further to this, ROCK promotes cell proliferation, which is another hallmark of cancer biology. Inhibiting ROCK in several cancer cell lines, including renal and prostate cancers, reduced cell proliferation (Gong et al., 2019, Abe et al., 2008). The amplification of ROCK in cancers have important implications in cancer cell proliferation, invasion and migration.

Given the involvement of ROCK in numerous facets of tumour progression, targeting ROCK is a therapeutic strategy. Inhibition of ROCK in both *in vitro* and *in vivo* settings have shown great promise. Tumour progression was reduced in mouse models of lung, hepatocellular and breast cancer when treated with ROCK inhibitors (Takamura et al., 2001, Ying et al., 2006). Experimental studies have also proposed that ROCK inhibition could prevent cancer metastasis (Morgan-Fisher et al., 2013). Thus, ROCK inhibitors have great potential in targeting different types of cancer.

1.6.6 ROCK inhibitors

ROCK1 is an attractive target given its role in different diseases including cancers, ischemic stroke and asthma (Feng et al., 2016). However, the caveat with small molecule inhibitors is the specificity; not only between the ROCK proteins but other kinases as well. Kinase inhibitors fall into two categories of inhibitor – type 1 and type 2. Type 1 inhibitors compete with ATP for the ATP binding site in the active conformation of the protein. Type 2 inhibitors bind the ATP binding site in the inactive conformation of the protein (Feng et al., 2016). The majority of ROCK inhibitors target both ROCK1 and ROCK2 given the homology in their sequence. The isoquinoline and pyridine/pyrrolopyridine based inhibitors are grouped as the classic ROCK inhibitors. Of the classic ROCK inhibitors, Fasudil (HA-1077) and Y27632 have been widely used (Asano et al., 1987, Uehata et al., 1997).

1.6.6.1 Fasudil

Fasudil is one of the first ROCK inhibitors that have been developed and the only inhibitor approved in Japan for clinical use since 1995 (Olson, 2008). Fasudil is approved for its vasodilative properties in preventing cerebral vasopsasms after subarachnoid haemorrhage and to improve blood flow following ischemic strokes (Shibuya et al., 1992). Fasudil is not selective for either isoforms of ROCK or, is it selective for ROCK alone. Fasudil can inhibit other AGC kinases, such as PKC and PKA, particularly at higher concentrations (Olson, 2008). The isoquinoline-based Fasudil binds to both ROCK proteins with moderate potency, and other AGC kinases at a 10-fold lower potency (Sasaki et al., 2002, Tamura et al., 2005). Once in the body, Fasudil is metabolised into hydroxyfasudil (Rikitake et al., 2005, Pan et al., 2013). Both molecular compounds function as type 1 inhibitors (Feng et al., 2016). Fasudil has been tested in clinical trials for multiple conditions including pulmonary hypertension, atherosclerosis and vascular resistance (Nohria et al., 2006, Ishikura et al., 2006, Kishi et al., 2005). These trials prove that Fasudil is safe in humans. Given the cellular functions of ROCK and its role in disease, it is a promising avenue to pursue, particularly in cancer. It should be noted however, that any effects of Fasudil seen in experimental conditions are likely due to its broad spectrum activity inhibiting multiple kinases, not just ROCK (Fukushima et al., 2005).

1.6.6.2 Y27632

Y27632, a ROCK inhibitor belonging to the pyridine family, is widely used in experimental studies, particularly in blood pressure regulation (Uehata et al., 1997). Like Fasudil, Y27632 is a type 1 inhibitor that binds to both ROCK1 and ROCK2. Y27632 has the ability to bind to other AGC kinases apart from ROCK proteins (Feng et al., 2016). However, unlike Fasudil, Y27632 has not been utilised in the clinic due to severe hypotension (Guan et al., 2013, Feng et al., 2016).

1.6.6.3 Other inhibitors

Other ROCK inhibitors are grouped according to their chemical structures. These include the indazole-based, pyrazole-based and pyrmidine-based ROCK inhibitors (Feng et al., 2016). Of the indazole-based, KD025 is the first reported ROCK2 specific inhibitor (Lee et al., 2014). KD025 has efficacy, treating a variety of diseases in their relevant animal models including autoimmune diseases and cancer (Zanin-Zhorov et al., 2014, Morgan-Fisher et al., 2013). There is currently great promise for KD025. It is currently being further developed for idiopathic pulmonary fibrosis, severe psoriasis and chronic graft versus host disease (Averill et al., 2018, Zanin-Zhorov et al., 2017) (Clinicaltrials.gov; NCT03640481). AT13148, a pyrazole-based ROCK inhibitor, was discovered through fragment based screening with an affinity for ROCK1 and ROCK2 as well as other AGC kinases including PKA, PKB/AKT, RSK1, p70S6K (Yap et al., 2012). AT13148 has proven to be quite effective in *in vitro* and *in vivo* models of cancer, particularly melanoma, prostate, breast, and pancreatic cancer (Sadok et al., 2015, Yap et al., 2012, Rath et al., 2018). More importantly, AT13148 has progressed into phase I clinical trials for patients with advanced solid tumours (Kumar et al., 2014).

1.6.7 Experimental background

1.6.7.1 ROCK1nc mice

The activation of the kinase ROCK1 is central to changes in the cytoskeleton important for a number of cellular processes including cell proliferation, cell cycle and migration as discussed above. During apoptosis, ROCK1 is cleaved by

caspase-3 (Figure 1-11) (Coleman et al., 2001). The removal of the C-terminus renders ROCK1 in a hyper-activated state, phosphorylating its downstream targets and facilitating cell contraction, apoptotic membrane blebbing and apoptotic body formation (Wickman et al., 2012). In order to study the role of ROCK1-mediated apoptotic membrane blebbing *in vivo*, a novel genetically-modified (GM) knock-in mouse model was created by the Olson lab and Transgenic Facility at the Beatson Institute. This C57Bl/6 model contains a single knock-in mutation altering the caspase-3 cleavage site from an aspartic acid residue to an alanine (D1113A), rendering ROCK1 resistant to caspase-3 cleavage and non-cleavable (ROCK1nc) as described by Julian (Julian, 2015). This model is important as it provides an avenue to isolate the role of ROCK1 in apoptotic blebbing while keeping the non-apoptotic functions of ROCK1 intact. ROCK1nc cells undergoing apoptosis exhibit intact biochemical features, however, they display defective blebbing and reduced forceful contractions (Julian, 2015).

The Olson lab has shown that in an acute liver damage model, ROCK1nc mice exhibited increased damage, cellular debris and neutrophilic infiltration (Julian, 2015). Interestingly, in a diethylnitrosamine (DEN) induced hepatocellular carcinoma (HCC) model and Eμ-MYC lymphoma model, ROCK1nc mice had a reduced tumour burden and an increase in cytotoxic T-cell infiltration (Julian, 2015, Naylor, 2019). Furthermore, a prolonged survival was seen in ROCK1nc mice on an Eμ-MYC lymphoma background. A reduction in tumour burden in the DEN-induced HCC model was recapitulated using the pharmacological inhibition of ROCK (Naylor, 2019). These results provide compelling evidence that ROCK1-mediate apoptotic membrane blebbing is involved in tumour development and perhaps the pharmacological inhibition of ROCK can be an attractive therapeutic strategy in certain types of cancer.

1.7 Hypotheses and aims

The first project interrogates the role of ROCK1-mediated apoptotic membrane blebbing. Deciphering the role of ROCK1 cleavage is achieved using genetic mouse models. Given the previous findings from the Olson lab regarding the role of apoptotic membrane blebbing in the liver, we sought to expand those findings into the thymus, an organ highly regulated by apoptosis. The aims of the first project are three fold. First, to address the role ROCK1-mediated blebbing in

thymic development and homeostasis. Second, to investigate apoptotic membrane blebbing and its role in cell clearance and immune cell responses. And third, to explore the role of ROCK1-mediated apoptotic membrane blebbing in an immunogenic lung cancer model.

The second part of the project looks at another aspect of the apoptotic machinery, the p53-MDM2 signalling axis. Although the oncogenic contributions of MDM2 and its relationship to p53 is well documented, less is known about the significance of the two MDM2 promoters – the basal P1 and p53-inducible P2. The aim of the second project is to tease apart the roles of the promoters in tumourigenesis using a GM approach abrogating either the P1 or P2 MDM2 promoter in the Eμ-MYC lymphoma model.

2 Materials and Methods

2.1 Materials

2.1.1 Antibodies

Table 2-1 List of primary antibodies

Antigen (Clone)	Species	Supplier	Catalogue #
α-Tubulin (B7)	Mouse	Sigma Aldrich	T9026
α-Tubulin (B7)	Rabbit	Cell Signalling Technology	2125
Caspase-3	Rabbit	Cell Signalling Technology	9662s
CD3 (SP7)	Rabbit	Vector	VP-RM01
CD4 (4SM 95)	Rat	eBioscience	14-9766-82
CD45R/B220 (RA3-6B2)	Rat	Abcam	ab64100
CD8a	Rat	eBioscience	14-0808-82
Cleaved Caspase-3 (Polyclonal)	Rabbit	Cell Signalling Technology	9661
F4/80 (CI:A3-1)	Rat	Abcam	ab6640
Ly-6G (IA8)	Rat	BioXcell	BE0075-1
ROCK1 (46/ROCK-1)	Mouse	BD Biosciences	611137
S100-A9 (M19)	Goat	Santa Cruz	sc-8115

Table 2-2 List of secondary antibodies

Antigen (Clone)	Species	Supplier	Catalogue #
Alexa Fluor 680	Goat anti-mouse	Invitrogen	A32729
Alexa Fluor 800	Donkey anti-rabbit	Thermo Scientific	SA5-10044
EnVision	Rabbit	Agilent	K4003
ImmPRESS	Goat	Vector Labs	MP-7405
ImmPress	Rabbit	Vector Labs	MP-7404

Table 2-3 List of flow cytometry antibodies

Antigen (Clone)	Supplier	Fluophore	Catalogue No
CD11b (M1/70)	Biolegend	BV570, PE	101233; 101208
CD11c (N418)	Biolegend	BV711	117349
CD25 (PC61)	Biolegend	AF700	10204
CD3 (17A2)	Biolegend	APC, PE	100236; 100206
CD4 (RM4-5)	Biolegend	APC, PerCP-Cy5.5	100516; 100539
CD44 (IM7)	Ebioscience	PE-Eflour 610	61-0441-82
CD45 (30-F11)	Biolegend	BV510	103137
CD45 (30-F11)	Ebioscience	PE-Eflour 610	61-0451-82
CD8a (53-6.7)	Biolegend	PE-Cy7	100721
CD80 (16-10A1)	Biolegend	FITC	104706
CD86 (GL1)	Biolegend	AF700	105023
F4/80 (BM8)	Biolegend	AF647, FITC	123121; 123107
Fixable Viability Dye eFlour® 780	Ebioscience	PE-Eflour780	65-0865-14
FOXP3 (MF-14)	Biolegend	AF647	126407
IgD (11-26c.2a)	Biolegend	FITC	405703
IgM (RMM-1)	Biolegend	PE	406507
Ly-6C (HK1.4)	Biolegend	BV421	128031
Ly-6G (1A8)	Biolegend	PE-Cy7	127617
MHCII [I-A/I-E] (M5/114.15.2)	Biolegend	PerCP	107623
PDCA-1 (927)	Biolegend	PerCp-Cy5.5	127021
Siglec H (551)	Biolegend	APC	129611
Streptavidin	Biologend	PE	405203
TCRß (H57-597)	Biolegend	BV421	109229
TCRγδ (GL3)	Biolegend	Biotin	118103
TruStain FcX (mouse)	Biolegend	-	101320

Table 2-4 List of primary antibodies for immunohistochemistry

Antigen (Clone)	Supplier	Catalogue No
B220/CD45R (RA3-6B2)	Abcam	Ab64100
CD3 (SP7)	Abcam	Ab16669
CD4 (4SM 95)	eBioscience	14-9766-82
CD8α (4SM 15)	eBioscience	14-0808-82
Cleaved Caspase 3	Cell Signalling Technologies	9661
F4/80 (CI:A3-1)	Abcam	Ab6640
Ly-6G (IA8)	BioXcell	BE0075-1
S100-A9 (M19)	Santa Cruz Biotechnology	Sc-8115

2.1.2 Reagents and chemicals

Table 2-5 List of reagents and chemicals

Reagent/Chemical	Supplier	Catalogue #
10x NuPAGE™ SDS Sample Reducing Agent	Invitrogen™	NP0004
4x NuPAGE™ LDS Sample Buffer	Invitrogen™	NP0007
2-Mercaptoethanol	Gibco	31350010
AdenoCre Virus (SPC-Cre)	University of Iowa Viral Core	VVC-Berns-1168
Albumin Standard	ThermoFisher Scientific	23209
Ammonium Chloride	Sigma Aldrich	A9434
Antigen unmasking solution (pH6)	Vector Labs	H-3300
Antisedan (Atipamezole)	Vetoquinol	0501267490211
Bovine Serum Albumin	Sigma Aldrich	A9647-500G
Brilliant Stain Buffer	BD Biosciences	566349
Calcium Chloride	Sigma Aldrich	21114
Cell dissociation buffer	ThermoFisher Scientific	13151014
Collagenase D	Sigma Aldrich	11088866001
Dexamethasone	Sigma Aldrich	D8893
Dexamethasone 21-phosphate disodium salt	Sigma Aldrich	D1159
DEN	Sigma Aldrich	N0258
DNase I recombinant, RNase-free	Sigma Aldrich	4716728001
Domitor (Medetomidine, 1mg.ml^{-1})	Vetoquinol	05012674902080
DMEM	ThermoFisher Scientific	21969-035
DMSO	Sigma Aldrich	D2650
EDTA	Sigma Aldrich	E0399-
Enzyme pre-treatment kit	Leica	AR9551
Epitope retrieval 2 (ER2)	Leica	AR9640
Ethanol	Fisher Scientific	64-17-5
Fasudil	LC Laboratories	F-4660
Fetal Bovine Serum	ThermoFisher Scientific	10270
Ficoll-Plaque Plus	GE Healthcare	17-1440-02

Glutaraldehyde	Sigma Aldrich	G5882
Ketamine (Narketan10, 100mg.ml^{-1})	Vetoquinol	03605877551210
L-Glutamine (200mM)	ThermoFisher Scientific	25030-032
Lipopolysaccharide (LPS)	Sigma-Aldrich	L4391
Liquid DAB	Agilent	K3468
Skimmed Milk Powder	Marvel	3025308
MEM	ThermoFisher	61100087
Methanol	Fisher Scientific	67-56-1
NuPAGE™ 4-12% Bis-Tris Gel	Invitrogen™	P0321
NuPAGE™ MES SDS Running Buffer (20x)	Invitrogen™	NP0002
NuPAGE™ MOPS SDS Running Buffer (20x)	Invitrogen™	NP0001
NuPAGE™ Transfer Buffer (20x)	Invitrogen™	NP0006
Paraformaldehyde	Electron Microscopy Service	15711
PE-Spheres	ThermoFisher Scientific	F13082
Penicillin/Streptomycin	Gibco	15140-122
Pierce Bovine Serum Albumin Standard Ampules, 2mg.ml^{-1}	Thermo Scientific	23209
Potassium Bicarbonate	Sigma Aldrich	60339
Precision Plus Protein™ All Blue Standards	BioRad	1610373
Precision Plus Protein™ Dual Colour Standard	BioRad	1610394
Halt™ Protease and Phosphatase Inhibitor Single-Use Cocktail (100X)	Thermo Fisher Scientific	1861278
RIPA Lysis and Extraction Buffer	Thermo Fisher Scientific	89900
RPMI 1640	Fisher Scientific	31870-025
Sodium Azide	Sigma	S8032
Tween-20	Sigma	P1379

2.1.3 Buffers and solutions

Table 2-6 List of buffers and solutions

Buffers and Solutions	Recipe
70% Ethanol	100% ethanol diluted in distilled water
Blotting Buffer	5% of Transfer Buffer, 20% Methanol, 75% distilled water
FACS Buffer	0.02% Sodium Azide, 1% FBS, 5mM EDTA (pH 8) with PBS up to 500ml
Neutral Buffered Formalin (10%)	100ml 37-40% formalin, 4g/l NaH_2PO4 (monobasic), 6.5g/l NaH_2PO4 (dibasic/anhydrous), 900 ml distilled water (for 1 litre solution)
MES Running Buffer 1x	MES (20x) diluted in distilled water
MOPS Running Buffer 1x	MOPS (20x) diluted in distilled water
PBS	170mM NaCl, 3.3mM KCl, 1.8mM Na2HPO4, 10.6mM H2PO4
PFA (2%)	16% PFA diluted in PBS
Red blood cell lysis (10x)	8.26g Ammonium Chloride, 1g Potassium Bicarbonate, 0.037g EDTA, distilled water up until 100ml
Sodium Cacodylate (0.1M, pH 7.4)	4.28g Sodium Cacodylate,25g Calcium Chloride, 2.5mL 0.2 M Hydrochloric Acid, make up to 200 mL with dH_2O
TBS	20mM Tris – HCl pH 7.5, 136mM NaCl
TBS-T	20mM Tris – HCl pH 7.5, 136mM NaCl, 0.1% Tween 20

2.1.4 Kits

Table 2-7 List of kits

Kit	Supplier	Catalogue #
FITC Annexin V Apoptosis Detection Kit I	Beckton Dickinson	556547
IncuCyte® pHrodo® Red Cell Labeling Kit for Phagocytosis	Essen Bioscience	4649
Pierce LDH Cytotoxicity Assay	Thermo Fisher Scientific	88953
Pierce™ BCA Protein Assay	ThermoFisher Scientific	23227
True-Nuclear™ Transcription Buffer Set	Biolegend	424401

2.1.5 Tissue isolation and culture solutions

Table 2-8 List of tissue isolation and culture solutions

Media	Composition
Complete RPMI	10% FBS, 1% L-Glutamine, 1% Pen/Strep in RPMI 1640
Complete Lymphoma RPMI	10% FBS, 1% L-Glutamine, 1% Pen/Strep, 0.1% ß-Mercaptoethanol in RPMI 1640
Freeze down medium	50% FBS, 40% RPMI, 10 % DMSO
Lung tumour isolation media	1mg.ml^{-1} collagenase D, 40 units of DNAse 1 in DMEM
Thymocyte isolation media	1mg.ml^{-1}collagenase D in RPMI

2.1.6 Other materials

Table 2-9 List of other materials

Material	Supplier	Catalogue #
0.2µM syringe filter	Life Sciences	PN4602
40 µM strainer	Greiner Bio-one	542040
70 µM strainer	Greiner Bio-one	542070
100µM yellow cell strainer for 50mL tube	Scientific Laboratories Supplies	352360
Filter paper 3MM	GE LifeSciences	3030-917
Flat bottom 96 well plates	Greiner Bio-One	655101
Flow cytometry 5ml tubes	Falcon	352052
GentleMacs tubes	Miletnyi Biotech	130096334
Nitrocellulose membrane	GE Healthcare Amersham	10600002
QiaShredder	Qiagen	79654
U-Bottom 96 well plates	Greiner Bio-One	655101

2.1.7 Equipment and software

Table 2-10 List of equipment and software

Equipment	Supplier
Attune Flow Cytometer	Thermo Fisher Scientific
FlowJo V10	FlowJo
GentleMacs	Miltenyi Biotech
Prism	Graphpad
HALO™	Indica Labs
ImageJ	
Image Lab	Biorad
Image Studio V 5.0	Licor
Incucyte	Essen Bioscience
JSM 6400 Scanning	JOEL
Sunrise™ Absorbance Reader	Tecan
ZEN	ZEISS

2.2 Methods

2.2.1 Animals

2.2.1.1 Maintenance and breeding

Mice were bred and maintained in pathogen free conditions at the Beatson Institute Animal Research Facility. All animal work carried out at the Beatson Institute is in accordance with the UK Home Office regulations in line with the Animals (Scientific Procedures) Act1986 and the European Directive 2010/63/EU policies. Ear notching and general maintenance (food, water and housing) was carried out by the Biological Services Unit at the Beatson Institute. All mice were checked regularly for health concerns. As specified in the project license (60-4225; 70-8645), mice were humanely culled by Schedule 1 techniques and a secondary method was performed for the confirmation of death.

2.2.1.2 Genotyping

Mice were routinely ear notched when pups were weaned for identification purposes. At this time tissue biopsy were sent to Transnetyx (Cordova, TN, US) for genotyping analysis. Single nucleotide polymorphism (SNP) analysis from ear notches were carried out by Taconic Biosciences (NY, US) for genetic profiling.

2.2.2 Mouse models

2.2.2.1 ROCK1nc defective apoptotic membrane blebbing model

The ROCK1 non-cleavable (ROCK1nc) mutant mouse model was generated by the Transgenic Technologies group at the Beatson Institute. Briefly, a knock-in missense mutation was introduced into the caspase-3 cleavage site of ROCK1 (D1113A) (Julian, 2015). The mice were initially a mix of 129/Sv and C57Bl/6, then further crossed onto C57Bl/6 for 5 generations and then bred to homozygosity. The ROCK1nc mouse is a constitutive whole body mutation in the ROCK1 gene. Only mice homozygous (HOM) for the non-cleavable mutation were used in experimental cohorts. Wild-type (WT) counterparts were obtained from ROCK1nc heterozygous (HET) mating pairs to ensure comparability due to the genetic background (N5, C57Bl/6). In addition, mice that express the green fluorescent protein (GFP) that were also on a C57Bl/6 background (Lifeact-EGFP,

CAG-EGFP; MGI: 4831036; (Riedl et al., 2010)) were crossed onto ROCK1nc HOM mice for phagocytosis assays.

2.2.2.2 Lung adenocarcinoma model

Two genetic models of lung adenocarcinomas were utilised – the KM and KMA models; both models have been characterised and kindly donated by the Murphy lab (University of Glasgow). In the KM model, mice bear a mutation in the *KRas* gene, lox-stop-lox (LSL) *KRas*^{G12D} (*B6.129S4-Kras*$^{tm4Tyj/J}$), and overexpression of human *c-MYC*, LSL *c-MYC* (Rosa26$^{DM.lsl-MYC}$), with the addition of a LSL-infrared red fluorescent protein (hereafter iRFP; Hprt$^{tm1(CAG-iRFP)}$; MGI6382570) (Kruspig et al., 2018, Murphy et al., 2008, Hock et al., 2017, Neidler et al., 2019). The addition of the LSL-*APOBEC3B* gene (Rosa Locus Gt(ROSA)26Sor$^{tm1(CAG-LSL-APOBEC.opt)Bea}$) onto the KM model was generated by the Strathdee lab at the Beatson Institute (unpublished data). The KMA model is a variation of the KM model. Therefore KMA mice bear the LSL-*KRas*^{G12D}, LSL-c-*MYC*, LSL-*APOBEC3B*, and LSL-*iRFP*. For the activation of conditional alleles on the KM and KMA models, a surfactant protein C (Sp-C) driven adenovirus Cre recombinase was utilised, allowing the induction of the transgenes in type II alveolar cells. The Cre recombinase allows targeted induction of genes, as the STOP cassette between the LoxP sites are removed (Houdebine, 2014). The adenovirus Sp-C Cre was delivered via intranasal inhalation to selectively target the lungs for the induction of genes (DuPage et al., 2009, Jackson et al., 2001, Neidler, 2015, Kruspig et al., 2018).

For the KM and KMA models, the desired genetic outcome were HET for Kras^{G12D}, MYC, and APOBEC3b in the KMA model. The iRFP genotype was either WT, HET (in females) or hemizygous (HEMI) (in males). Both of the lung adenocarcinoma models were crossed onto the ROCK1nc model. The models with associated genotypes are outlined in Figure 2-1 and Table 2-11.

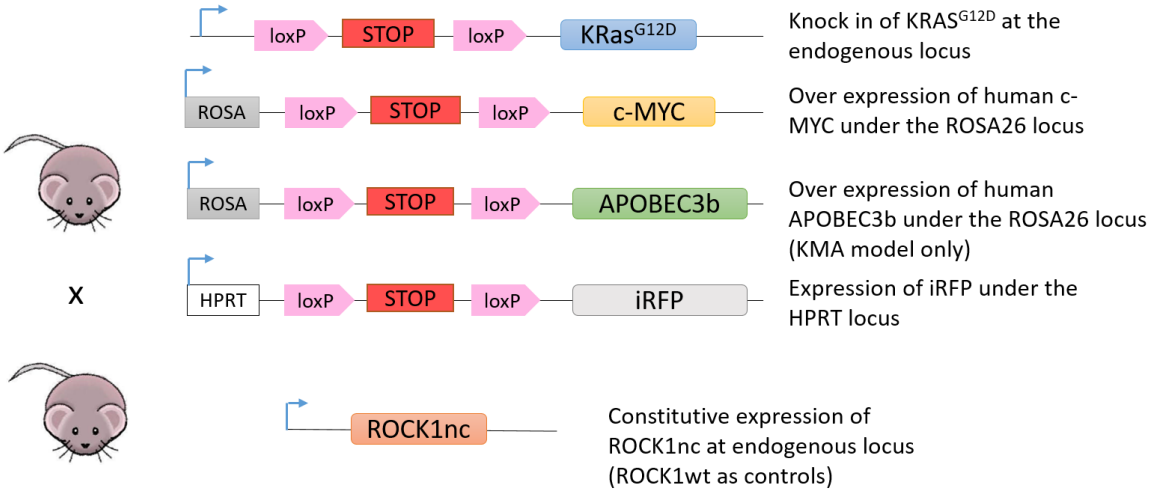

Figure 2-1 Schematic representation of the KM and KMA lung adenocarcinoma mouse model crossed onto the ROCK1nc mouse model.

Table 2-11 List of desired genetic outcomes in the KM and KMA model

Model	Transgene	Desired expression
KM-WT	LSL-*KRAS*^{G12D}	Heterozygous
	R26-LSL *MYC*	Heterozygous
	Rock1	Wild-type
	HPRT- LSL-iRFP	Wild-type Heterozygous Hemizygous
KM-NC	LSL-*KRAS*^{G12D}	Heterozygous
	R26-LSL *MYC*	Heterozygous
	Rock1nc	Homozygous
	HPRT-LSL *iRFP*	Wild-type Heterozygous Hemizygous

KMA-WT	LSL-*KRAS*^{G12D}	Heterozygous
	R26-LSL *MYC*	Heterozygous
	R26-LSL *APOBEC3*B	Heterozygous
	Rock1	Wild-type
	HPRT-LSL *iRFP*	Wild-type; Heterozygous; Hemizygous
KMA-NC	LSL-*KRAS*^{G12D}	Heterozygous
	R26-LSL *MYC*	Heterozygous
	R26-LSL-*APOBEC3*B	Heterozygous
	Rock1nc	Homozygous
	HPRT-LSL *iRFP*	Wild-type; Heterozygous; Hemizygous

2.2.2.2.1 Preparation of anaesthetic and reversal solution for viral administration

A mixture of Domitor and Ketamine diluted in 0.9% sodium chloride (NaCl) was used to anaesthetise mice in preparation for intranasal administration of adenovirus (SpC-Cre). In this instance, 100µL of Domitor and 200µL of Ketamine were diluted in 1.9mL of NaCl. A final dose of 55mg/kg Domitor and 0.27mg/kg Ketamine for females, and 49.5mg/kg of Domitor and 0.243mg/kg of ketamine for males, from the IP injection of the anaesthetic cocktail were achieved based on mouse body weight.

Antisedan was used an agent to reverse the anaesthetic effects of Domitor and Ketamine. A 100µL of Antisedan was diluted in 2.9mL of 0.9% of NaCl to achieve a 5mg/ml dose based on mouse body weight.

2.2.2.2.2 Adenovirus Sp-C Cre solution preparation and viral administration

Minimal essential Medium (MEM) was reconstituted in sterile water (0.48g in 50mL) and adjusted to a pH of 7.86. This solution was sterilised using a 0.2µM filter under sterile conditions. In sterile conditions, calcium chloride ($CaCl_2$) was diluted in sterile water to obtain a final concentration of 0.2M. Both these solutions were made the day before a scheduled induction and stored at 4°C. The MEM solution, $CaCl_2$ solution and viral aliquots of adenovirus-SPC-Cre were transported on ice to the Beatson Research Unit (BRU).

For the viral solution, a final concentration of $1x10^8$ pfu of adenovirus Sp-C Cre and 4mM of $CaCl_2$ was obtained and diluted in MEM. The virus and media were mixed first, followed by the $CaCl_2$. The resultant solution was left to precipitate for a minimum 30 minutes and maximum of 60 minutes.

For the induction of gene expression, 8-10 week old mice with the appropriate genetic backgrounds were used. Mice were anesthetised using a cocktail of Domitor and Ketamine. 45µL of the adenovirus-Sp-C Cre solution was administered via intranasal inhalation in a viral hood. Mice were then injected with antisedan directly after virus administration to reverse the effects of the anaesthetics more rapidly. Mice were kept in cages on heating plates (41°C) until fully recovered. Mice were monitored throughout the process. Health checks of all experimental cohort animals were routinely undertaken. Signs for clinical end points included laboured breathing, pinched body phenotype and weight loss. Mice were humanely culled and samples harvested at point of clinical presentation of lung tumours.

2.2.2.3 MDM2 P1-null and P2-mutant mice on an Eµ-MYC lymphoma model

Mice on an Eµ-MYC background were originally obtained from Jax (Tg(IghMyc)22Bri; 002728) (Adams et al., 1985) and stock maintained at >20 generations C57Bl/6. To study the MDM2 model, two models were generated and kindly provided by Dr. Mark Boyd (University of Liverpool) (Figure 2-2). A HET or HOM deletion of the P1 promoter was used to achieve removal of the constitutive P1 promoter. An 8 base-pair mutation was carried out on the P2 promoter to achieve a HET or HOM loss of inducible P2 function. Both the Eµ-MYC, MDM2 P1-null and Eµ-MYC, MDM2 P2-mutant cohorts were backcrossed on

the C57Bl/6 background to achieve an N>10 generation. Mice were checked regularly for health concerns. Upon presentation of clinical endpoints, mice were humanely culled and samples harvested. These end points included lymph node enlargement (15mm maximum of a single lymph node or combination of multiple); difficulties in breathing alluding to a thymic lymphoma; hunched, pinched body phenotype; weight loss; and swollen abdomen indicating a diffuse lymphoma or enlarged spleen.

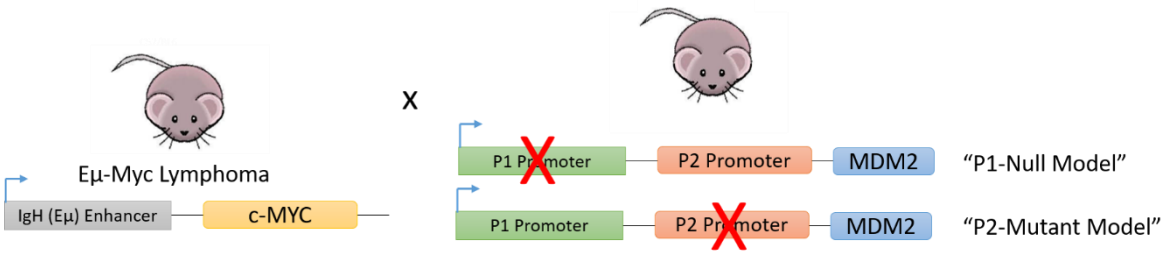

Figure 2-2 Schematic representation of the Eμ-MYC mice crossed onto the MDM2 P1 null (heterozygous/homozygous) and P2 mutated (heterozygous/homozygous) mice.

2.2.3 Tissue collection and fixation

Mice were humanely culled using increasing concentrations of carbon dioxide in a chamber followed by cervical dislocation as a secondary method. The mouse weight was recorded, and where possible blood was drawn for further analysis by cardiac puncture or through the inferior vena cava. A necropsy was performed and the appropriate organs were harvested. For formalin fixed paraffin embedded (FFPE) samples, tissues were put into 10% neutral buffered formalin. Samples were then changed over into 70% ethanol 18 to 24 hours later. If not, these were noted down and processed from formalin.

2.2.3.1 ROCK1nc mouse model

The thymus was weighed and harvested into formalin at various time points for the various *in vivo* experiments.

2.2.3.2 Lung adenocarcinoma model

For the lung mouse model, blood was drawn from the inferior vena cava. A small volume was put into EDTA tubes, mixed well and analysed on the IDEXX Procyte Dx Haematology Analyser. If enough blood was sampled, the remaining volume

was put into a heparin tube and centrifuged for 10 minutes at 10,000rpm. The plasma was then transferred to an Eppendorf and snap frozen on dry ice. The liver was harvested and weighed. The heart was then flushed with PBS and formalin was flushed through the trachea to inflate the lungs. The lungs were then put into formalin. These two procedures were only done for end point clinical tumours and not time point tumours.

Mice were also sacrificed at 8 week post intranasal inhalation. Blood was sampled as mentioned above and the liver was weighed. The right lung lobe was put into formalin and the left into PBS on ice for flow cytometry analysis. The liver and lungs of KMA mice that were HEMI or HET for iRFP were imaged *ex vivo* with the Pearl Imager to determine tumour burden and if there were any metastatic lesions in the liver.

2.2.3.3 MDM2 lymphoma model

For the lymphoma model, blood was drawn by cardiac puncture. A small volume was put into EDTA tubes, mixed well and analysed on the IDEXX Procyte Dx Haematology Analyser. If enough blood was sampled, the remaining volume was put into a heparin tube and centrifuged for 10 minutes at 10,000rpm. The plasma was then transferred to an Eppendorf and snap frozen on dry ice. The spleen, thymus and mesenteric lymph node (MLN) were weighed. If any other lymph node was enlarged, including the cervical lymph or inguinal lymph nodes, these were also weighed. Parts of any of the enlarged organs were separated into 3 parts – one part for formalin, one part snap frozen in an Eppendorf, and one part further weighed and put into cold PBS on ice. The sample put into PBS was processed into a single cell suspension and frozen down for flow cytometry analysis.

2.2.4 Histology

Formalin fixed samples were embedded into paraffin cassettes and processed for routine haematoxylin and eosin (H&E) and further immunohistochemistry (IHC) stains by the Beatson Histology Service. For both H&E and IHC stains, sections were cut from FFPE samples at 4μM of thickness.

2.2.4.1 Immunohistochemistry staining on FFPE sections

IHC stains were performed by the Beatson Histology unit. The list of antibodies, retrieval method, dilutions and secondary antibodies are shown in (Table 2-12). All primary antibodies were incubated for 35 minutes at room temperature (RT). Antigens were retrieved using 1 of 3 methods – the epitope retrieval 2(ER2), enzyme 1 (Enz1) proteinase K and antigen unmasking solution at pH6. For the secondary antibodies, the ImmPRESS or Envision kits were used. Liquid 3,3′-Diaminobenzidine-(DAB) was used as the chromogen.

Table 2-12 List of antibodies used for immunohistochemistry stains

Antibody (Clone)	Retrieval Method	Dilution	Secondary Antibody
B220/CD45R (RA3-6B2)	ER2 20 minutes	1/200	Rat ImmPRESS
Caspase 3 (ASP-175)	ER2 20 minutes	1/500	Rabbit Envision
CD3 (SP7)	ER2 20 minutes	1/100	Rabbit Envision
CD4 (4SM 95)	ER2 20 minutes	1/500	Rat ImmPRESS
CD8 (4SM 15)	ER2 20 minutes	1/500	Rat ImmPRESS
F4/80 (CI:A3-1)	Enz1 10 minutes	1/100	Rat ImmPRESS
Ly6G (IA8)	ER2 20 minutes	1/60000	Rat ImmPRESS
S100-A9 (M19)	pH6 20 minutes	1/1000	Goat ImmPRESS

2.2.4.2 Quantification of staining

All H&E and IHC tissue stains were scanned and images were analysed using HALO™. The modules utilised were area quantifications and immune profile quantifications. The area of the immune cell stains as a percentage of the tissue area was presented.

2.2.5 *In vivo* experimental procedures

2.2.5.1 Thymic development

The weights of the mouse and thymus of male and female mice (WT and HOM ROCK1nc mice) at various ages (2, 4, 6, 8 and 10 weeks) were recorded and

thymus harvested into formalin. A total of 6 sections were cut from FFPE thymi at 100μM apart. These sections were stained with H&E and analysed by HALO™.

2.2.5.2 Apoptosis under physiological conditions

The thymus from both female and male, WT and HOM ROCK1nc mice at 2, 4, 6, 8 and 10 weeks were harvested. Sections were stained for cleaved-caspase 3 as a marker for apoptotic cells.

2.2.5.3 Acute apoptosis induction by dexamethasone

Female, 8 week old (± 2 days) WT or HOM ROCK1nc mice were administered with single dose of 15mg.kg^{-1} dexamethasone-salt solution or equivalent volume of vehicle, IP. Mice were culled at 6, 12, 24 and 30 hours post IP injection. Weights of the mouse, thymus and spleen were recorded. The thymus was put into formalin.

2.2.5.4 Preparation of dexamethasone salt

Dexamethasone 21-phosphate disodium salt (dexamethasone salt) was prepared by dissolving the drug in sterile water to a concentration of 2mg/ml. In sterile conditions, the dexamethasone solution was then put through a 0.2μm syringe filter and stored at 4°C. Sterile water was used as the vehicle for control experiments. Dexamethasone salt was made fresh prior to the injection of each mouse in the experimental cohort.

2.2.5.5 Adoptive transfer of thymocytes

The thymus from either a WT or HOM ROCK1nc mouse (6-8 weeks old) were harvested and processed into a cell suspension through a 100μM filter. Red blood cells (RBC) were lysed using a RBC lysis buffer. Cells were plated out at 10x10^6 cells per 10cm dish and treated with 1μM of dexamethasone under sterile conditions. Four hours later, cells were washed twice with PBS and resuspended to 25x10^6 cells/ml in PBS. Recipient WT and HOM ROCK1nc mice (sex matched to donors) were injected IP with 200μL of cells (5x10^6 cells). Two hours after inoculation, the host mice were culled and peritoneal washout cells were collected, and analysed by flow cytometry

2.2.6 Isolation of primary cells

2.2.6.1 Isolation of thymocytes

The thymus harvested from mice were put into PBS on ice. Thymi from WT or HOM ROCK1nc were harvested and homogenised through a 100μM filter then a 40μM filter. Samples were then treated with a RBC lysis buffer for 3-5 minutes. FBS was added in order to terminate the cell lysis. Cells were resuspended in complete RPMI and counted for further use.

For immune-phenotyping studies, the thymus harvested from mice was put into PBS on ice. The thymus was cut into small pieces using scissors. Around 5mls of the thymocyte digestion mix was added to the tissue in a falcon tube. The tissue was incubated on a shaker at 37°C for 30 minutes. The tissue was then passed through a 100μM filter, followed by a RBC lysis at 1x for 3-5 minutes. The RBC lysis is terminated using FBS. Samples were then stained for flow cytometry analysis (Section 2.2.10).

2.2.6.2 Isolation of peritoneal washout cells

Carefully, the skin was dissected while the peritoneum remained intact. Up to 5mls of PBS was injected into the peritoneum slowly, and massaged for a few minutes. The mouse was then turned upside down into a petri dish, a small hole was cut in the peritoneum and the PBS was pushed out by massaging the belly with tweezers. Additional PBS was reinjected to drain out as many washout cells as possible. Cells were collected in PBS and stored on ice for further use.

2.2.7 Apoptosis assays

Thymi from WT or HOM ROCK1nc mice were harvested and isolated into suspension as previously described. Cells were then plated at $20x10^6$ cells per 9cm dish. Cells were treated either with vehicle control or 1μM of dexamethasone for 0 hours or 18 hours. For some experiments, cells treated for apoptosis induction were collected for further co-culture phagocytosis assays. Additionally, cells were also collected and washed with PBS. On one hand, cells were collected for Annexin V assays (Section 2.2.10.1). On the other, cells were centrifuged, at 1200rpm 4°C, for 10 minutes, in an eppendorf and pellets were

snap frozen and stored at -80°C for western blot analysis. Furthermore, treated cells were also utilised to image apoptotic membrane blebbing by scanning electron microscopy (Section 2.2.11.2).

2.2.7.1 Ultraviolet induction of apoptosis

Thymi from WT or HOM ROCK1nc mice were harvested and isolated into suspension as previously described. Cells were then plated at $20x10^6$ cells per 9cm dish. Cells were exposed to $0.3j.m^2$ of ultraviolet (UV) C. These cells were then used for co-culture phagocytosis assays analysed by the Incucyte (Section 2.2.11.1)

2.2.8 Phagocytosis assays

2.2.8.1 Phagocytosis of beads

Peritoneal washout cells were obtained from 6-8 week WT and HOM ROCK1nc – GFP mice. In sterile conditions, Cells were plated at a density of 160,000 cells per well in 24 well plates in complete RPMI. The phycoerythrin (PE)-spheres were added at 2:1 ratio (320,000 beads). Some wells were treated with either vehicle or 200ng/ml lipopolysaccharide (LPS). For flow cytometry analysis, cells were left in co-culture with PE-spheres for 4 hours at 37°C, 5% CO_2. At 4 hours, the supernatant and cells were collected on ice. At all wash steps, the supernatant was also collected in a tube. Cells were washed with PBS and 500µl of cell dissociation buffer was added to each well. The plate was rocked for 5 minutes at RT. The buffer was collected and wells were again washed with PBS. Tubes were then centrifuged, at 1200rpm 4°C for 5 minutes, and then resuspended in PBS for flow cytometry analysis.

In addition to flow cytometry, phagocytosis assays were also analysed using the Incucyte Zoom as follows. Plates were placed in the Incucyte Zoom for 48 hours after beads were added to the wells. Over a 44 hour period, triplicate images were taken once per hour, per well at 10x magnification. Images were then analysed using the Incucyte Zoom 2016B software.

2.2.8.2 Co-culture phagocytosis assays

Peritoneal washout cells were obtained from 6-8 week old GFP-WT or GFP-HOM ROCK1nc mice. In sterile conditions, peritoneal washout cells of each genotype were plated in triplicate in 24 well plates at a density of 40,000 cells/well. These cells were left to adhere at 37°C, 5% CO_2, prior to co-culture with donor thymocytes.

Donor thymi were obtained form 6-8 week old WT or HOM ROCK1nc mice that are sex matched to the GFP mice above. Cells were plated at $1x10^6$ cells in 10cm dishes and subjected to either vehicle, 1μM dexamethasone or $0.3j.m^2$ UVC and incubated at 37°C, 5% CO_2 for an hour. After washing the cells with PBS, cells were labelled with IncuCyte® pHrodo® red cell labelling kit for phagocytosis at 1μg/ml following the manufacturer's instructions. Cells were resuspended in complete RPMI to 400,000 cells per ml and then plated at 100μl per well in co-culture with peritoneal washout cells. Plates were then imaged using the Incucyte Zoom. Triplicate images were taken once per hour, per well at 10x magnification over a 48 hour period. Images were then analysed using the Incucyte Zoom 2016B software.

2.2.9 Isolation of tumour cells

2.2.9.1 Lung tumour cells

Lungs were harvested from mice as previously described (Section 2.2.3.2). Lungs were cut using scissors in the gentleMACS™ tubes and 5 ml of warm lung tumour isolation media was added. GentleMACS™ tubes were placed on the gentleMACS™ tissue dissociator with the heating sleeve on. Tissues were left to dissociate at 37°C for 30 minutes. Following this, tissues were passed through a 40μM strainer in 50ml falcon tubes and centrifuged at 1200rpm at 4°C for 10 minutes. Supernatant was removed and cells treated with 1x RBC lysis buffer for 3-5 minutes. FBS was then added to terminate the lysis process. Cells were then resuspended in DMEM and counted for further flow cytometry analysis.

2.2.9.2 Lymphoma tumour cells

Tumour tissues were harvested from mice as previously described (Section 2.2.3.3). Each organ was homogenised through a 40µM strainer placed on a 6cm petri dish. The cells were flushed through with 5ml of warm complete lymphoma RPMI. These cells were then layered slowly onto 5ml of ficoll in a 15ml falcon tube. Cells were centrifuged at RT for 10 minutes at 3000rpm. The lymphocyte layer was carefully pipetted out and transferred to a fresh falcon tube. Cells were counted using the cell counter and resuspended to $5x10^6$ cells per ml. If available, 3-4ml of the cells were transferred to another tube and centrifuged for 5 minutes at 1500rpm. Cells were resuspended in the same volume in freeze down medium. The cells were then put into aliquots of 1ml in appropriately labelled cryovials. Vials were put in a CoolCell and into the -80°C freezer. These cells were then used for flow cytometry analysis to assess the immune cell profile (Section 2.2.10.6).

2.2.10 Flow cytometry

2.2.10.1 Annexin V and propidium iodide for apoptotic cell detection

Thymocytes in suspension were obtained from 6-8 week old WT and ROCk1nc mice as previously described. To assess cell death using flow cytometry, dexamethasone-treated thymocytes were washed in ice cold PBS twice. Cells were then stained with Annexin V and propidium iodide (PI) according the manufacturer's instructions. Briefly, cells were resuspended in 1x Annexin V Buffer (diluted in distilled H_2O) at $1x10^6$ cells.mL^{-1}. 100µl of this cell solution was transferred to a 5ml flow cytometry tube. To this, 5µl of Annexin V and 5µl of PI were added. Samples were vortexed and left at room temperature for 15 minutes away from light. Following this, 400µl of Annexin V buffer was added and samples were run on the Attune NxT Flow Cytometer within an hour. Analysis of data was done using FloJoV10 software.

2.2.10.2 Immunophenotyping

Cells in suspension were washed and resuspended in PBS to roughly $5x10^6$ cells/ml. 200µl of cells were transferred to a 96 well U- bottom plate. All incubations were done at 4°C, and centrifugation steps at 4°C 1200rpm for 5

minutes. Cells were centrifuged and 100µl of fixable viability dye in PBS was added, and incubated for 15 minutes. Cells were centrifuged and 50 µl of FC Block in FACS buffer was added and incubated for 15 minutes. Following this, antibody cocktails were made in Brilliant Stain Buffer. The antibody cocktail was added at 50µl per well and incubated for 20-30 minutes. Cells were centrifuged, and 100µl of secondary antibody if required was added and incubated for at least 10 minutes. Cells were washed in PBS and centrifuged. For panels without intracellular staining, cells were fixed in 2% PFA for 15 minutes. For panels that required intracellular transcription factor staining (FOXP3), cells were fixed and stained for FOXP3 using True-Nuclear Transcription Buffer Set following manufacturer's instructions. All samples were then resuspended in FACS buffer post fixation and stored at 4°C. Samples were processed using the Attune NxT Flow Cytometer not more than 2 days post staining. Analysis of data was done using the FloJo V10 software.

2.2.10.3 Profiling for phagocytic cells

Peritoneal washout cells were isolated and processed for flow cytometry analysis to determine the immune cell types found in the washout cells and which cells are capable of phagocytosis. The antibody panel used in the flow cytometry analysis are shown in Table 2-13.

Table 2-13 Peritoneal washout panel for profiling and phagocytosis analysis

Antigen	Fluorophore	Concentration
CD11b	BV570	1/200
CD11c	BV711	1/200
CD19	APC	1/200
Fixable Viability Dye	Pe-Eflour 710	1/1000
F4/80	FITC	1/200
Spheres	PE	2:1 (Spheres:Cells)
TCRß	BV421	1/100

2.2.10.4 Immune profiling in the thymus

The thymi isolated from a variety of ages (4, 6, 8 and 10 weeks) of WT and ROCK1nc mice were put into a single cell suspension. Cells were counted and stained for a T-cell panel (Table 2-14) and myeloid cells (Table 2-15).

Table 2-14 T cell panel list of antibodies and concentrations for the thymus

Antigen	Fluorophore	Concentration
CD25	AF700	1/100
CD3	PE	1/200
CD4	Percp-Cy5.5	1/200
CD44	Pe-Eflour610	1/200
CD45	BV570	1/200
CD8α	PE-Cy7	1/200
Fixable Viability Dye	Pe-Eflour 710	1/1000
FOXP3	AF647	1/100
Streptavidin	BV711	1/400
TCRß	BV421	1/100
TCRγδ	Biotin	1/100

Table 2-15 Myeloid cells panel list of antibodies and concentrations for the thymus

Antigen	Fluorophore	Concentration
CD11b	BV570	1/300
CD11c	BV711	1/200
CD45	BV510	1/200
F4/80	FITC	1/200
PDCA1	Percp-Cy5.5	1/100
Siglec-H	APC	1/100

2.2.10.5 Immune profiling of KMA tumours at an 8 week time point

Cells from tumour-bearing lungs of 8 week old KMA- WT and HOM ROCK1nc mice were obtained and processed as described previously. Cells were then counted and stained for a T-cell (Table 2-16) and myeloid panel (Table 2-17).

Table 2-16 T cell panel list of antibodies and concentrations for lung tumours

Antigen	Fluorophore	Concentration
CD3	FITC	1/200
CD4	Percp-Cy5.5	1/200
CD44	Pe-Eflour 610	1/200
CD8α	Pe-Cy7	1/200
Fixable Viability Dye	Pe-Eflour 710	1/1000
FOXP3	AF647	1/100
CD19	APC-Cy7	1/200
NK1.1	BV421	1/50
Streptavidin	PE	1/400
TCRγδ	Biotin	1/100

Table 2-17 Myeloid cells panel list of antibodies and concentrations for lung tumours

Antigen (Clone)	Fluorophore	Concentration
CD11b	PE	1/300
CD11c	BV711	1/200
F4/80	AF647	1/200
Fixable Viability Dye	Pe-Eflour 710	1/1000
Ly6C	BV421	1/300
Ly6G	Pe-Cy7	1/200
MHCII	Percp-Cy5.5	1/400

2.2.10.6 Immunophenotyping of endpoint lymphoma tumours

The frozen vials of lymphoma cell suspensions were thawed and resuspended in 5ml of warm complete RPMI. Cells were then centrifuged at 1200rpm for 5

minutes at 4°C. Cells were then counted and resuspended in PBS to achieve $5x10^6$ per ml. Two different panels of antibodies were used to determine the lymphoma profile – a T-cell panel and a B-cell panel as shown below. 200µl of cells were added to each well of a 96 well plate. Cells were stained as described above and processed on the Attune Flow Cytometer within 3 days and analysed using FloJoV10 software.

Table 2-18 T cell panel list of antibodies and concentrations for lymphoma tumours

Antigen	Fluorophore	Concentration
CD3	PE	1/200
CD4	APC	1/200
CD45	BV510	1/200
CD8α	Pe-Cy7	1/200
Fixable Viability Dye	Pe-Eflour 710	1/1000

Table 2-19 B cell panel list of antibodies and concentrations for lymphoma tumours

Antigen	Fluorophore	Concentration
B220	PercpCy5.5	1/200
IgD	FITC	1/100
IgM	PE	1/100
Fixable Viability Dye	Pe-Eflour 710	1/1000

2.2.11 Microscopy

2.2.11.1 Incucyte

Phagocytosis was assessed using the Incucyte zoom microscopy system. The incucyte was utilised for imaging of both the phagocytosis of beads and apoptotic cells. Cells were visualised at 10x objective (4464) for phase, green fluorescence and red fluorescence image acquisition for 48 hours, every hour. Triplicate images were taken of each well every hour. The average of the triplicates per well for the green and red fluorescent signals were calculated.

The overlap of the red and green area normalised to background signals to determine phagocytosis.

2.2.11.2 Scanning electron microscopy

Cells were washed with ice-cold PBS. Samples were then fixed with 1.5% glutaraldehyde in 0.1M sodium cacodylate solution in suspension that was kindly supplied by Margaret Mullen (University of Glasgow) for 1 hour at room temperature. Following this, samples were washed twice in 0.1M sodium cacodylate for 10 minutes each, then stored in 0.1M sodium cacodylate solution at 4^0C until required for processing. Samples were kindly processed by Margaret Mullen (CPD method) using a JEOL 6400 Scanning microscope at the Electron Microscopy Facility at the University of Glasgow.

2.2.12 Protein extraction and analysis

2.2.12.1 Preparation of cell lysates

Frozen cell pellets were thawed. Around 30-50µl of a RIPA buffer and 1x protein inhibitor solution was added to each sample. Samples were transferred to a QiaShredder and centrifuged at room temperature at 13,000rpm for 2 minutes. Samples were transferred to a fresh Eppendorf and put on ice for 30 minutes and centrifuged at 13,000rpm for 10 minutes at 4°C. Cell lysates were transferred to a fresh Eppendorf. Protein concentrations were determined using a bicinchoninic acid (BCA) assay. Protein lysates were kept at 4°C until required for gel electrophoresis and western blotting.

2.2.12.2 Determining protein concentration

Protein concentrations were determined using a BCA assay. Briefly, a standard was created from a 2mg/ml stock of bovine serum albumin in SDS lysis buffer at 0, 0.08, 0.1, 0.2, 0.4, 1 and 2 mg/ml. In a flat 96 well plate, 10µl of either lysis buffer (blank), standard or a 1 in 2 diluted sample (in RIPA buffer) was added. 190µl of developing solution, BCA at a 50:1 ratio with Copper Sulphate was added to each well from the Pierce™ BCA Protein Assay Kit. The plate was incubated at 37°C for 30 - 60 minutes. The absorbance was measured using

Molecular Devices Microplate Reader. Concentrations of the samples were extrapolated from the standards.

2.2.12.3 SDS-Polyacrylamide gel electrophoresis

Protein samples were separated by their molecular weight based using SDS-Polyacrlamide gel electrophoresis (PAGE). The appropriate volume for 25-30µg of each sample was added to 10x NuPage SDS sample reducing agent (final 1x concentration) and 4x NuPage LDS sample buffer (final 1x concentration). Samples were boiled at 90°C for 5 minutes. Samples were centrifuged at 13,000rpm at room temperature for 5 minutes. A 1x solution of MES or MOPS were added to gel tanks. Around 25-30µL of sample was added to the appropriate wells of the precast NuPage 4-12% BIS TRIS gels, as well as 3-5µL of Precision Plus Protein Dual Colour Standard and Precision Plus Protein All Blue Standards. Gels were run using the BioRad machine at 180V until the standards were separated and tracking dye reached the bottom of the gel. Gels were then removed and used for western blotting.

2.2.13 Western Blotting

A wet transfer was utilised, to transfer gels onto nitrocellulose membranes using the Bio-Rad PowerPac HC. With each gel, the sponges, 4 filter papers and nitrocellulose membranes were pre-wet in the blotting buffer. The sponges, filter paper, membrane and gel were stacked in each cassette. The transfer was run at 100V for 1 hour. Membranes were then blocked in 5% (w/v) of milk powder in 1x TBST, for 30-60 minutes at room temperature. The primary antibodies were diluted to required concentrations in 5% Milk 1x TBST and incubated overnight, rocking at 4°C, as specified in Table 2-20.Membranes were then washed 3 times in TBST for 10 minutes each. The loading control was then added at the required concentration and membranes were incubated for 1 hour at room temperature. Blots were washed 3 times in 1x TBST for 10 minutes each. Blots were then incubated with secondary antibody in 5% Milk 1x TBS-T for 1 hour at room temperature away from light. Blots were then washed 3 times in 1x TBS-T for 10 minutes each, once in TBS for 10 minutes and stored in TBS. The protein bands were visualised using the LI-COR Odyssey System. Western blot images were then edited on the Image Studio.

Table 2-20 List of antibodies used in western blotting

Antibody	Concentration	Type
Caspase-3	1/1000	Primary
Cleaved Caspase 3	1/1000	Primary
ROCK1	1/250	Primary
AF 488	1/20000	Secondary
AF-800	1/20000	Secondary
α-Tubulin	1/2000	Loading Control

2.2.14 Release of intracellular molecules

2.2.14.1 LDH assay

Thymi were harvested from 6-8 week old WT and HOM ROCK1nc mice, then processed into a cell suspension as previously mentioned. Cells were plated in 96 well plates at 20,000 cells per well in 100µl. Cells were treated with either vehicle or 1µM of dexamethasone for 4, 8 or 24 hours. The lactate dehydrogenate (LDH) levels were analysed at 4 and 8 and 24 hours post treatment as per manufacturer's instructions. Briefly, the plate was centrifuged and 50µl of supernatant was transferred to a new 96 well flat bottom plate. To this, 50µl of the reaction mixture was added and incubated for 30 minutes at room temperature, away from light. The reaction was stopped by adding a stop solution from the manufacturer's kit. The absorbance was measured at 490nm and 680 nm using the Sunrise^{TM} Tecan machine.

2.2.15 Statistical analysis

Graphpad Prism 8 software was utilised to create graphs and carry out appropriate statistical analyses. A statistical significance of $p<0.05$ was set as a standard for all analysis. Non-parametric analysis was used in all cases. The statistical test carried out for individual experiments are stated in the figure legends. Survival curves were analysed using the Log Rank (Mantel-Cox) test.

3 ROCK1-mediated apoptotic membrane blebbing in thymic development

3.1 Introduction

3.1.1 Thymic development and homeostasis

Tissue development and tissue homeostasis both rely heavily on the apoptotic process. The thymus in particular, requires efficient apoptosis to generate functioning T-cells (Kurd and Robey, 2016). The thymus is fully developed prior to birth and involutes in humans over time from infancy to adulthood (Murray et al., 2003). Thymic involution, also known as atrophy, occurs in all vertebrates (Shanley et al., 2009). Although it is not fully understood why thymic involution occurs, this phenomenon is underpinned by a decrease in T-cell production, replacement of epithelial tissue with adipose tissue, and a decline in immune function with age (Gordon and Manley, 2011, Ge and Zhao, 2013, Palmer et al., 2018). The production of functional T-cells in the thymus begins during embryonic development but slow down as the thymus involutes. Immature T-cells (thymocytes) arriving from the bone marrow, undergo positive and negative selection to restrict the major histocompatibility complex (MHC) to either a CD4 or CD8 lineage and to eliminate self-reactive T-cells. It is estimated that over 90% of thymocytes fail either positive or negative selection, prompting apoptosis to be triggered in the majority of cells (Huesmann et al., 1991, Shortman et al., 1990). The high level of apoptotic thymocytes illustrates the elevated apoptotic activity in the thymus. However, despite the preponderance of apoptosis in the thymus, direct evidence of apoptotic cells remains elusive due to efficient cell clearance (Nakanishi et al., 2011).

3.1.2 T-cell development process

The T-cell developmental process begins with positive selection in the outer cortex and ends with negative selection in the inner medullary area (Figure 3-1) (Klein et al., 2014). During the selection stages, APCs and epithelial cells contribute to the spatio-temporal microenvironment required for T-cell development (Germain, 2002). Lymphoid progenitor cells that arrive in the thymus do not express either CD4 or CD8 MHC surface expression markers, or components of the T-cell receptor (TCR) complex (including the variable αß or

γδ chains, and CD3). Thus, these thymocytes are classed as double negatives (DN) which are further subdivided into 4 developmental stages (DN1-4) (Godfrey et al., 1993). Each double negative stage is categorised according the expression of two surface markers, CD44 and CD25, and characterised as follows: DN1, $CD25^{-}$ $CD44^{+}$; DN2, $CD25^{+}$ $CD44^{+}$; DN3, $CD25^{+}$ $CD44^{-}$; DN4, $CD25^{-}$ $CD44^{-}$. DN thymocytes can either express αß or γδ variable chain on their TCRs (Robey and Fowlkes, 1994). Following the DN stage, cells begin to express of the αß and CD3 components of the TCR complex, followed by the co-expression of both CD4 and CD8, leading to these cells being called double positives (DP). Up to 90% of the lymphoid compartment are made of DP cells in a young individual's thymus (Robey and Fowlkes, 1994). Of the DP thymocytes, around 90% of these have TCRs that engage weakly with MHC ligands on cortical epithelial cells, resulting in their failure to pass positive selection. (Merkenschlager et al., 1997). Cells failing positive selection die by neglect, which is essentially delayed apoptosis. Additionally, roughly 5% of DP cells engage too strongly with self-peptides particularly on dendritic cells, thus leading to their failure to pass negative selection as well (Matzinger and Guerder, 1989). Failing negative selection triggers acute apoptosis, yielding a small population of immature T-cells that appropriately engage with self-peptides and MHC-complexes, which will subsequently matures. Thymocytes that engage with MHC-class I peptides become CD8+ (cytotoxic) T-cells, whilst cells that interact with MHC-class II peptides become CD4+ (helper or regulatory) T-cells (Germain, 2002). These T-cells are then exported from the medulla into the blood stream.

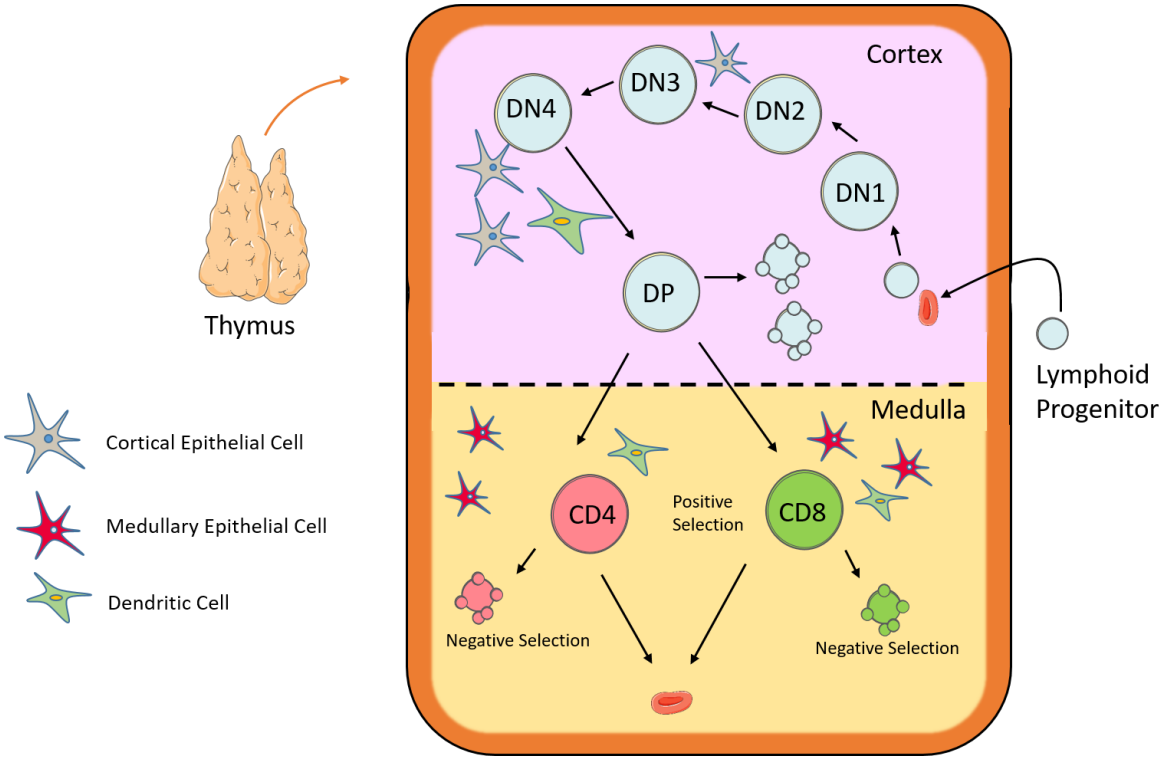

Figure 3-1 T-cell development process in the thymus. Lymphoid progenitor cells enter the cortex. The progenitor cells, or thymocytes when in the cortex, are known as double negatives (DN), as they lack lineage specific markers. There are 4 DN stages categorised based on expression of CD24 and CD44 - DN1 ($CD25^-$ $CD44^+$); DN2 ($CD25^+$ $CD44^+$); DN3 ($CD25^+$ $CD44^-$); DN4 ($CD25^-$ $CD44^-$). DN4 thymocytes turn into double positive (DP) cells as they go through rearrangement of the T-cell receptor (TCR), yielding an αβ TCR and the expression of both CD4 and CD8. DP cells interact with epithelial and dendritic cells via the major histocompatibility class (MHC) I or II. DP that interact with MHCI adequately become CD8 T-cells whilst those interacting with MHCII become CD4 T-cells. DP cells that do not engage or engage weakly with self-peptides on the MHC complex undergo cell death. DP positive cells that interact too strongly with the MHC complex also succumb to apoptosis. The single positive CD4 and CD8 cells then exit the thymus via blood vessels. This figure was adapted (Germain, 2002) and made using contents from Servier Medical Art, under the Creative Commons Attribution 3.0 Unported License. https://smart.servier.com/

3.1.3 Experimental Aims

Given the function of the thymus in the development of T-cells coupled with the important role of apoptosis, it is not surprising that ROCK1, but not ROCK2, protein levels were shown to be relatively elevated in this organ (Julian and Olson, 2014). Based on the premise of high apoptotic activity and high ROCK1 levels, the thymus was ideal to study the role of ROCK1-mediated apoptotic blebbing for effective execution of apoptosis in normal tissue homeostasis using the ROCK1nc mouse model.

Previous findings from the Olson lab have demonstrated a role for ROCK1-mediated apoptotic membrane blebbing in the context of hepatocellular

carcinoma (Julian, 2015, Naylor, 2019). This project aims to investigate the role of apoptotic membrane blebbing in a different organ, the thymus. The objective of this study is to explore the function of ROCK1-mediated apoptotic membrane blebbing in thymic homeostasis and development, looking at the anatomical properties, apoptosis, as well as cellular subtypes. Data from the tissue-specific gene expression and regulation (TiGER) showed greater levels of ROCK1 in the thymus (Julian and Olson, 2014). Additional, data from mouse RNAseq data on the bloodspot database has also shown relatively high expression of ROCK1 in lymphocytes, including T-cells (Bagger et al., 2018).

To assess the role of ROCK1-mediated apoptotic membrane blebbing, the ROCK1nc (non-cleavable) mouse model was utilised. This mouse model contains the non-cleavable form of ROCK1, as there are mutations in the caspase-3 cleavage site on all cells. Only the apoptotic membrane blebbing function of ROCK1 is disrupted whilst other biological functions of ROCK1 remain intact. Given the relatively high ROCK1 levels and apoptotic activity, as well as previous data in the lab showing that the ROCK1nc mutation does indeed affect apoptotic membrane blebbing in other cell types, I hypothesised that defective blebbing due to the ROCK1nc mutation might alter thymic development, homeostasis and the landscape of cellular populations found in the thymus.

3.2 Results

3.2.1 ROCK1nc mice exhibit normal thymic involution rates

Thymic involution occurs in both male and female vertebrates from infancy (Shanley et al., 2009). In order to assess whether this was altered in ROCK1nc mice, thymus and body weights were recorded for males and females at various ages from 2 to 10 weeks. The thymic weights were similar between the two genotypes over the various ages (Figure 3-2A, B). The weights of the thymus itself gradually increased from 2 to 6 weeks, and decreased gradually at 8 and 10 weeks for both ROCK1wt and ROCK1nc male and female mice. The body weights were also similar between the genotypes over time (data not shown). The thymic to body weight ratios of ROCK1wt and ROCK1nc were similar over the various ages within each gender as well (Figure 3-2C, D). No differences were observed in decrease in the thymic to body ratio between the genotypes for both

males and females. These data suggests that the ROCK1nc mutation does not alter the thymic weight ratios or involution rates.

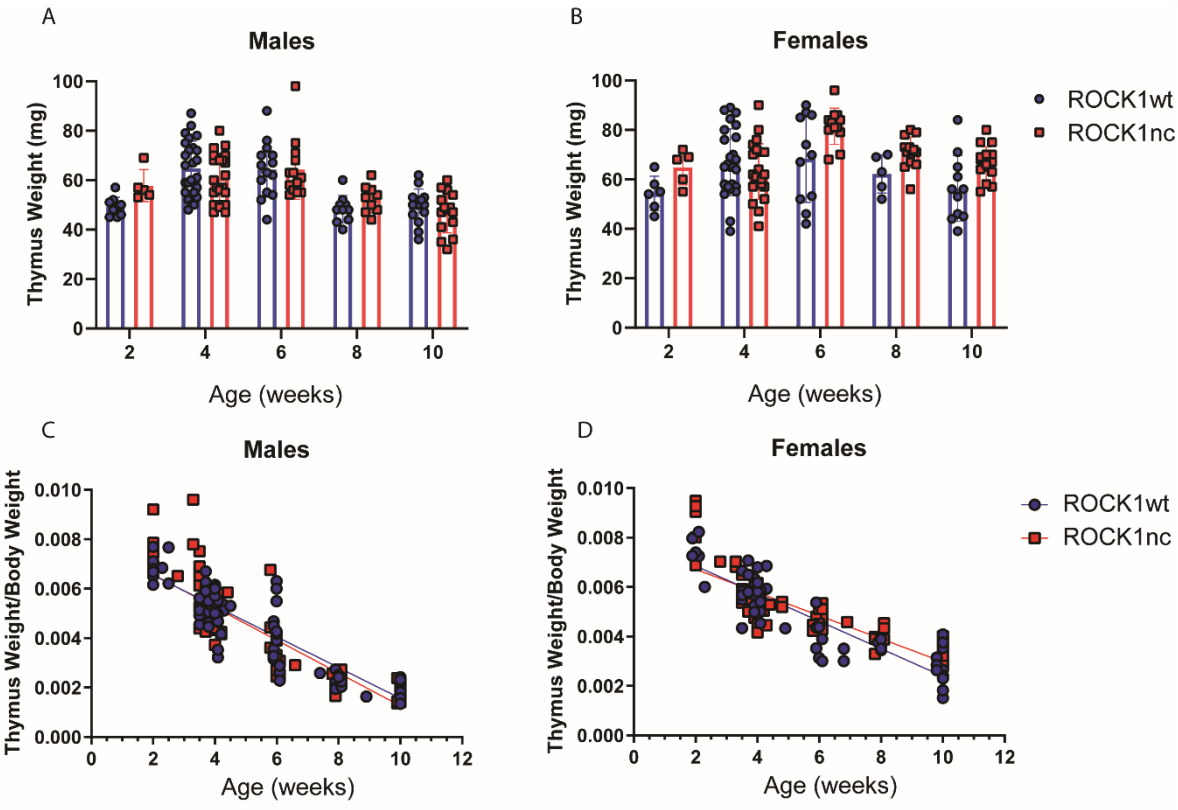

Age (wk)	ROCK1wt	ROCK1nc
2-3.4	9	5
3.5-5.4	40	31
5.5-7.4	15	14
7.5-9.4	10	9
9.5-10	14	15

Age (wk)	ROCK1wt	ROCK1nc
2-3.4	4	8
3.5-5.4	27	30
5.5-7.4	9	12
7.5-9.4	5	14
9.5-10	12	17

Figure 3-2 ROCK1nc male and female mice displayed similar thymic weights and thymic/body weight ratios and compared to ROCK1wt counterparts over time. A,B) The thymus weight (mg) of ROCK1wt and ROCK1nc male and females were recorded when harvested at the various ages (2-10 weeks). Data points represent individual mice, error bars represent mean ± SD. (Males – ROCK1wt 2wk N=9, 4wk N=26, 6wk N=14, 8wk N=10, 10wk N=14; ROCK1nc 2wk N=5, 4wk N=23, 6wk N=13, 8wk N=9, 10wk N=15; Females – ROCK1wt 2wk N=6, 4wk N=25, 6wk N=11, 8wk N=5, 10wk N=11; ROCK1nc 2wk N=5, 4wk N=23, 6wk N=12, 8wk N=14, 10wk N=17). The slope was determined from linear regression analysis. Points represent individual mice (N numbers indicated in the table).

3.2.2 ROCK1nc mutation transiently affects thymic cellularity

Thymic cellularity was also assessed and compared between ROCK1nc and ROCK1wt mice, considering also age, strain and sex of ROCK1wt mice, The thymus from male and female, ROCK1wt and ROCK1n mice were harvested at various ages (4, 6, 8 and 10 weeks) and isolated as single cell suspensions. Cells

were then counted using a CASY counter prior to immunophenotyping. Interestingly, although the cellularity at 4 and 6 weeks were comparable between genotypes, there was a significant increase in the cell count of ROCK1nc at 8 weeks (Figure 3-3). This difference however, disappeared at 10 weeks. There were no differences between the genders of each genotype at the various weeks. This could suggest that there may be a difference at 8 weeks in thymic development in ROCK1nc mice. However, the normalisation of thymic cellularity by 10 weeks would suggest that this difference is only temporary.

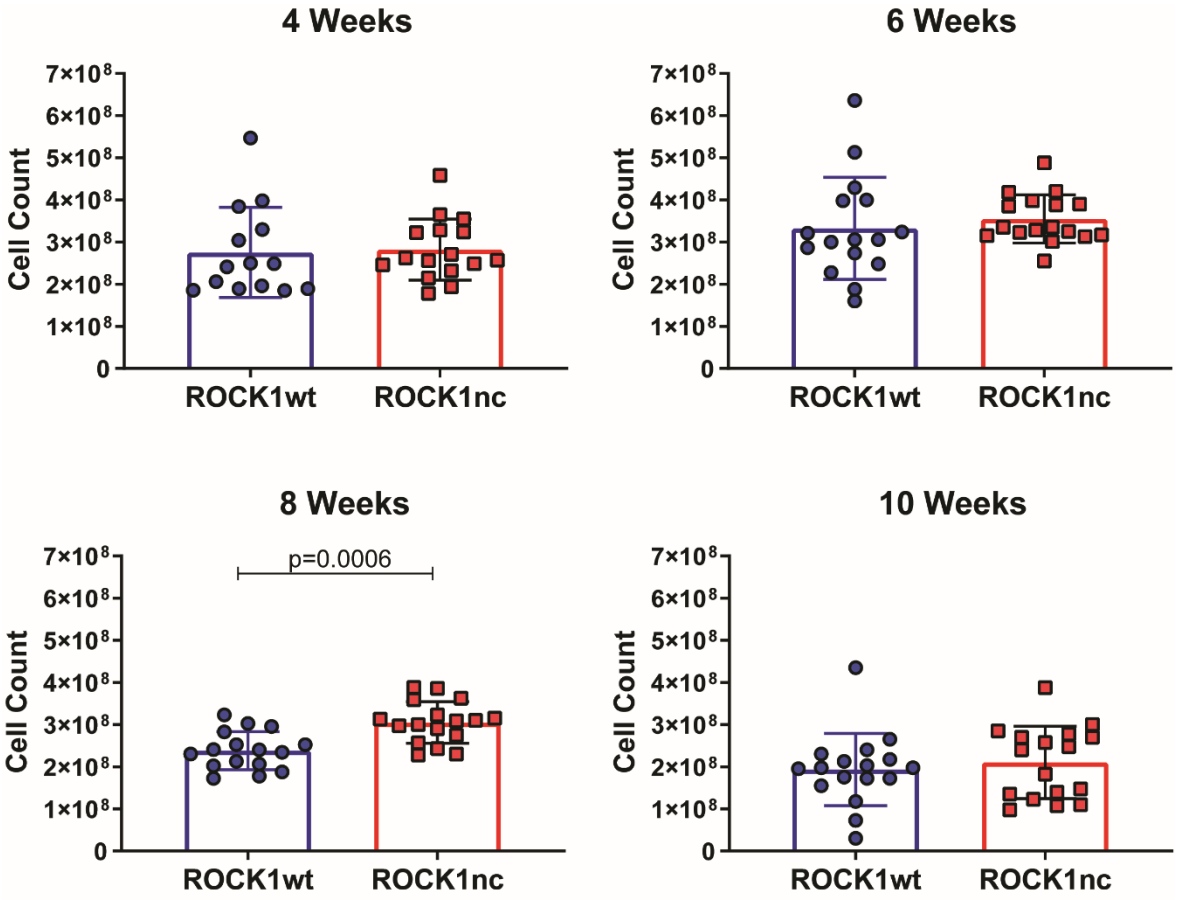

Figure 3-3 Thymic cellularity is transiently affected at 8 weeks in ROCK1nc mice. The cell counts were at comparable levels at 4, 6 and 10 weeks. Cell counts from male and female, ROCK1nc thymi were signifcantly increased at 8 weeks compared to ROCK1wt mice (p=0.0006). This difference however, disappeared at 10 weeks old. Statistical signficance was determined using the Mann-Whitney test. Points represent individual mice, error bars represent meant $\pm$ SD (4 wks – ROCK1wt N=14 (6 males, 8 females), ROCK1nc N=16 (9 males, 7 females); 6 weeks ROCK1wt N=16 (8 males, 8 females), ROCK1nc N=17 (8 males, 9 females); 8 weeks ROCk1wt N=16 (9 males, 7 females), ROCK1nc N=17 (9 males, 8 females); 10 weeks ROCK1wt N=17 (11 males, 6 females), ROCK1nc N=17 (7 males, 10 females).

3.2.3 ROCK1nc mice display normal thymic architecture

Thymic architecture is another parameter that can be used to assess thymic development. The thymus consists of two main areas, the cortex and the

medulla (Ueno et al., 2004). The cortex is the outer area where immature thymocytes sit and the medulla is the inner region where mature T-cells are found before entering the circulation. To investigate thymic architecture, formalin-fixed paraffin embedded thymi from male and female, ROCK1wt and ROCK1nc mice of various ages (2, 4, 6, 8 and 10 weeks) were sectioned 100µm apart for a total of 6 sections. Haematoxylin and eosin (H&E) stains of these sections were analysed using HALO™ software to determine the cortical and medullary areas. These two areas are histologically distinguishable on an H&E stains whereby the darker areas are the cortex and the lighter areas are the medulla (Figure 3-4).

Using a customised algorithm on HALO™, the medullary and cortical areas were determined. An average of the 6 sections was taken to assess the architecture through the thymus. No significant differences were observed in the percentage area of the cortical or medullar areas between ROCK1wt and ROCK1nc mice (Figure 3-5). There were no differences between the genders of each genotype at the various weeks. The cortex contains immature thymocytes, which far outnumber mature thymocytes found in the medulla, which is naturally reflected in the greater cortical area in both ROCK1wt and ROCK1nc thymi. The cortex was consistently around 80% of the tissue area analysed at the various ages. The medullary area, on the other hand, was consistently around 20% of the tissue area. These data suggest that the ROCK1nc mutation does not affect thymic architecture of either male or female mice at various ages.

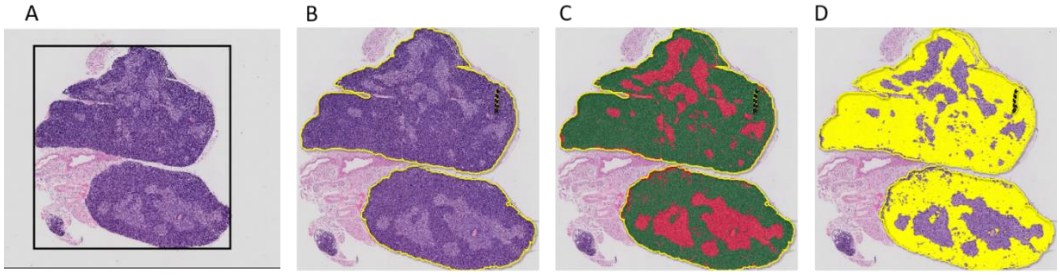

Figure 3-4 Representation of the HALO™ algorithm used to determine the cortical and medullary areas. The tissue section (A), boundary is annotated (B) as denoted by the yellow line. The software was then trained to recognise the cortical (green) and medullary (red) areas (C). The area analysed is shown in yellow (D). The areas for both the cortical and medullary area were analysed for each section.

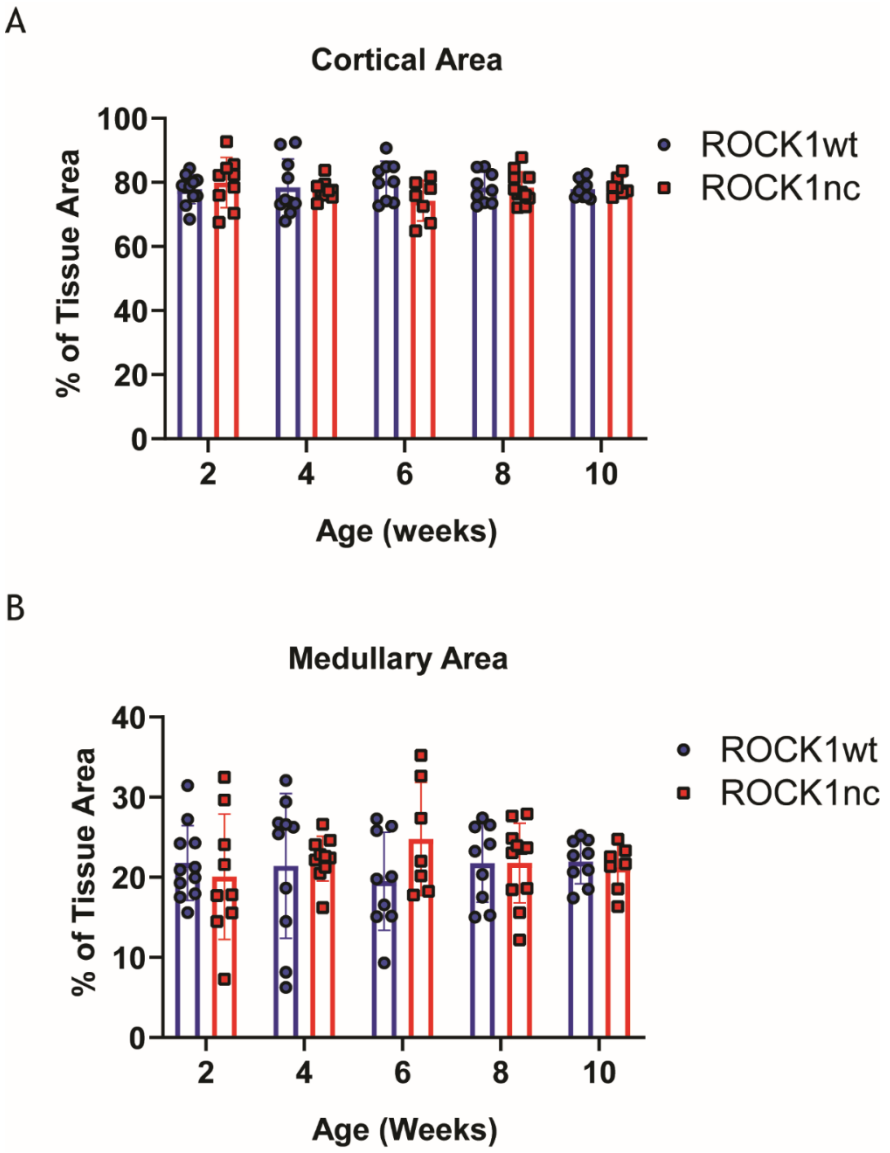

Figure 3-5 The ROCK1nc mutation does not affect thymic cortical and medullary areas. HALO™ quantification of the cortical and medullary areas from H&E stained sections of ROCK1wt and ROCK1nc thymi revealed no signifcant differences between the genotypes at the various ages (2, 4, 6, 8 and 10 weeks). Each thymi from male and female mice of each genotype was cut into 6 sections, 100µm apart. Points represent individual mice, error bars represent meant ± SD (2 weeks ROCK1wt N=11 (6 males, 5 females) ROCK1nc N=9 (5 males, 4 females); 4 weeks ROCK1wt N=10 (5 males, 5 females) ROCK1nc N=10 (5 males, 5 females); 6 weeks ROCK1wt N=9 (4 males, 5 females) ROCK1nc N=7 (4 males, 3 females); 8 weeks ROCK1wt N=9 (5 males, 4 females) ROCK1nc N=11 (6 males, 5 females).

3.2.4 Levels of apoptotic cells are unchanged in ROCK1nc thymi under physiological settings

As the ROCK1nc mutation affects apoptotic membrane blebbing, assessing residual detectable apoptotic cells would provide a good indication if clearance of the apoptotic cells was affected. Under physiological conditions, it is rare to find traces of apoptotic cells, even if there is high apoptotic activity as seen in the thymus (Elliott and Ravichandran, 2010) due to highly efficient clearance. In

order to investigate clearance, the thymus from male and female ROCK1wt and ROCK1nc mice were harvested at various ages (2, 4, 6, 8 and 10 weeks). The formalin fixed paraffin-embedded thymi were stained with antibody that detects cleaved caspase-3 (Cl. Casp3), a marker of an apoptotic cell (Figure 3-6). At the various ages, the percentage of cleaved caspase-3 positive cells were all relatively low at less than 0.5% per tissue (Figure 3-7). No significant differences were observed between the percentages of cleaved caspase-3 in ROCK1wt and ROCK1nc mouse cohorts. There were no differences between males and females in each genotype. This would indicate that the ROCK1nc mutation does not affect the levels of apoptotic cells detected and, by extension, does not affect cell clearance either.

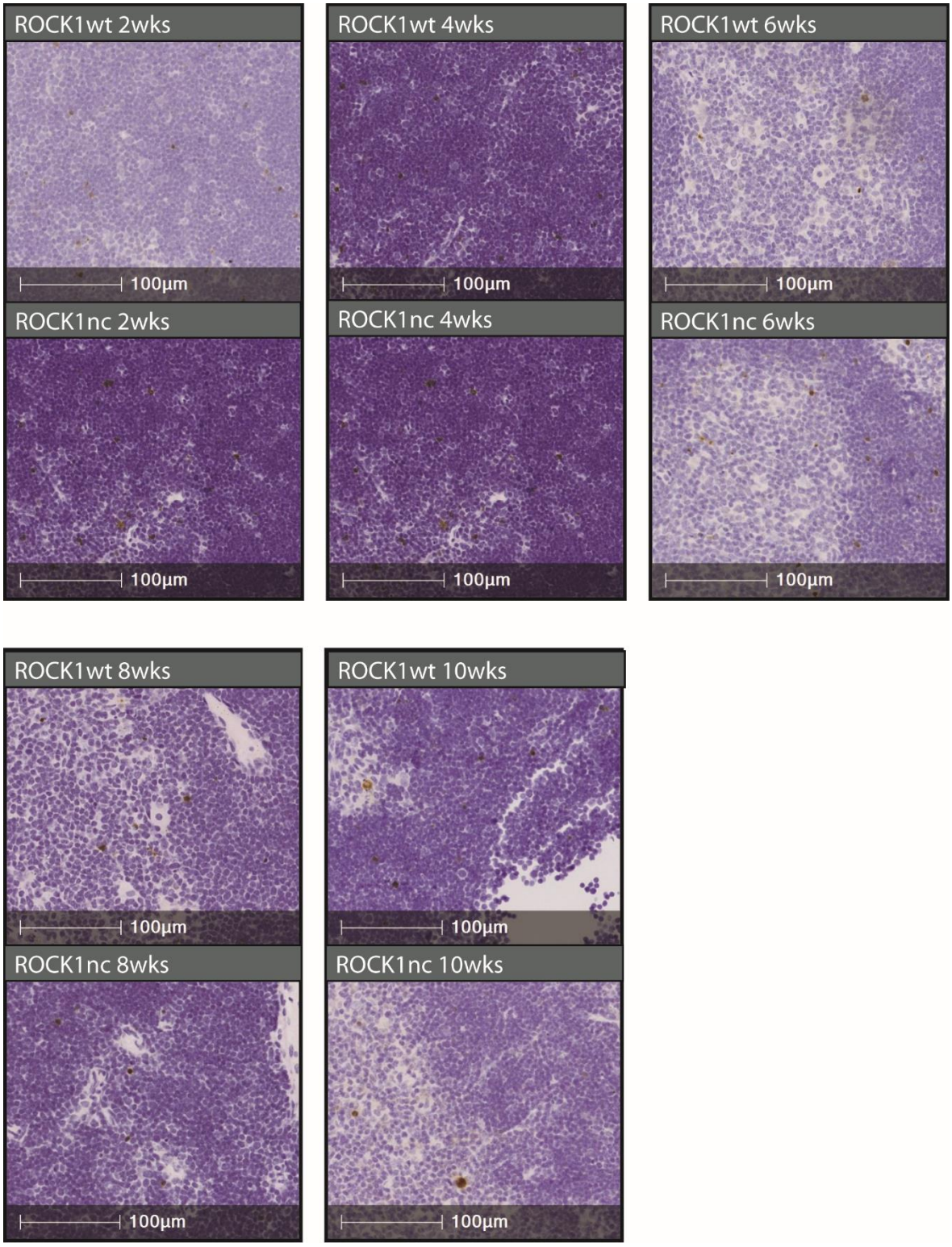

Figure 3-6 Representative cleaved caspase-3 staining of thymus sections from ROCK1wt and ROCK1nc mice. ROCK1wt and ROCK1nc male and female mice were harvested at various ages (2, 4, 6, 8 and 10 weeks). Formalin-fixed paraffin-embedded (FFPE) thymus tissues were sectioned at 4 µm and stained with antibody that detects cleaved caspase-3. Stains are at a 20x magnification and scale bars at 100 µm. Cleaved caspase-3 positive cells are brown in colour. Representative of N=7-10 per genotype, per time point.

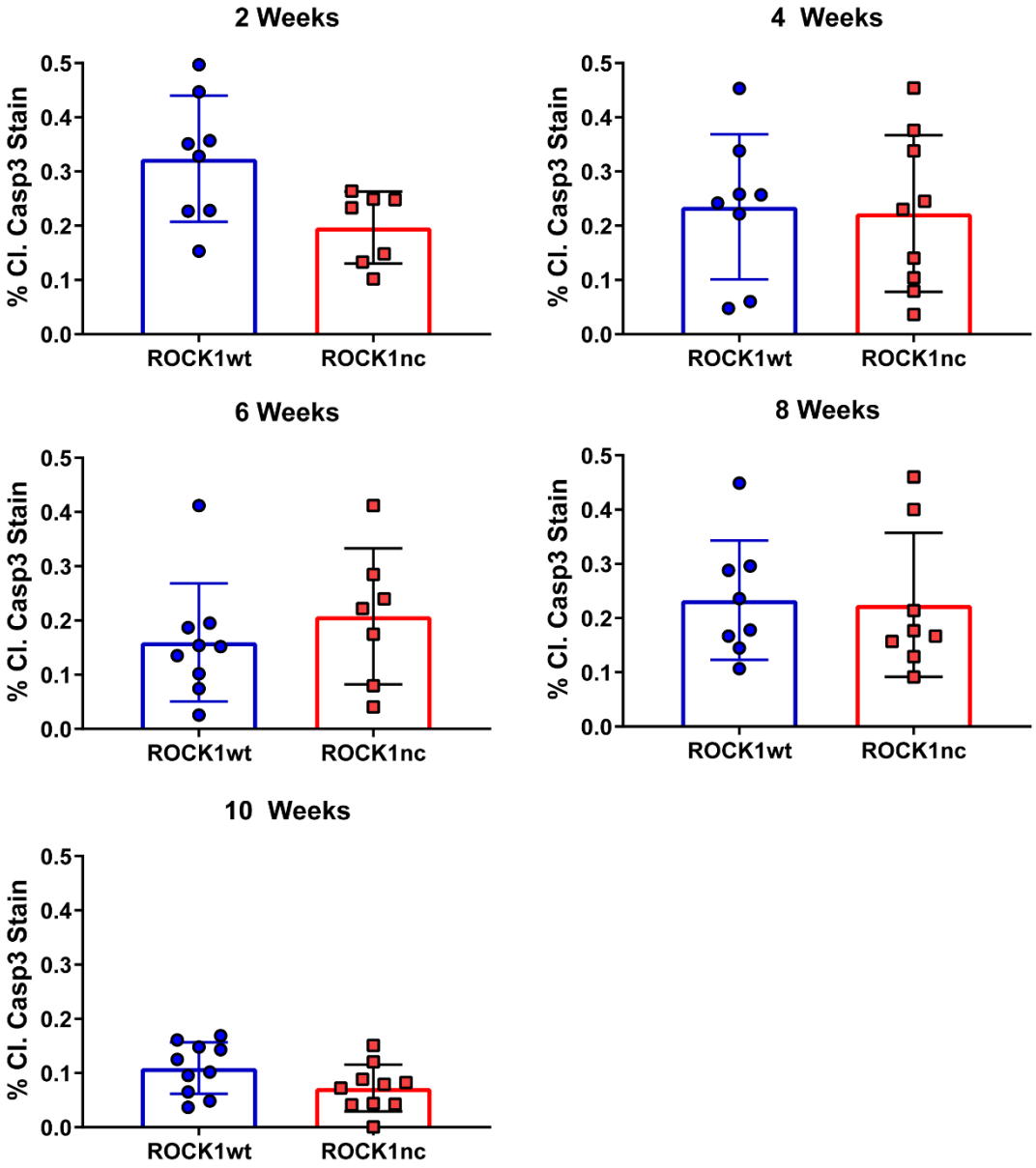

Figure 3-7 The ROCK1nc mutation does not alter the levels of detectable apoptotic cells. ROCK1wt and ROCK1nc male and female mice were harvested at various ages (2, 4, 6, 8 and 10 weeks). Formalin-fixed paraffin-embedded (FFPE) thymic tissues were sectioned at 4 µm and stained with cleaved caspase-3 (Cl.Casp3) antibody. The area of staining was quantified using HALO™. The percentage of cleaved caspase-3 staining area to tissue area of male and female ROCK1wt and ROCK1nc thymi across the various ages were determined. Data points represent individual mice, error bars represent mean ± SD. 2 weeks ROCK1wt N=8 (3 males, 5 females) ROCK1nc N=7 (4 males, 3 females); 4 weeks ROCK1wt N=8 (5 males, 3 females) ROCK1nc N=9 (4 males, 5 females); 6 weeks ROCK1wt N=9 (4 males, 5 females) ROCK1nc N= 7 (3 males, 4 females); 8 weeks ROCK1wt N=8 (4 males, 4 females) ROCK1nc N=8 (4 males, 4 females); 10 weeks ROCK1wt N=10 (5 males, 5 females) ROCK1nc N=10 (5 males, 5 females).

3.2.5 Overall physiological levels of macrophages are unchanged in ROCK1nc mice

Investigating physiological levels of macrophages is another important aspect to determine if the ROCK1nc mutation would affect this phagocytic population. Immunohistochemistry was performed by staining FFPE thymi sections from ROCK1wt and ROCK1nc mice at various ages (2, 4, 6, 8 and 10 weeks) with an antibody that detects the macrophage marker F4/80. The percentage of F4/80 cell staining in thymic tissues was below 0.7% at all ages for both genotypes (Figure 3-9). At two weeks, ROCK1nc cohorts had significantly less F4/80 staining in comparison to ROCK1wt cohorts. At all other time points, the percentage of F4/80 staining was at comparable levels between ROCK1wt and ROCK1nc cohorts. These results suggest that although there was a difference seen at a young age between the genotypes, the level of macrophages were unchanged in ROCK1nc cohorts. No differences were observed between male and female mice of each genotype. This would indicate that the ROCK1nc mutation and, by extension, defective apoptotic membrane blebbing does not affect the macrophage population, likely having no effect on cell clearance as well.

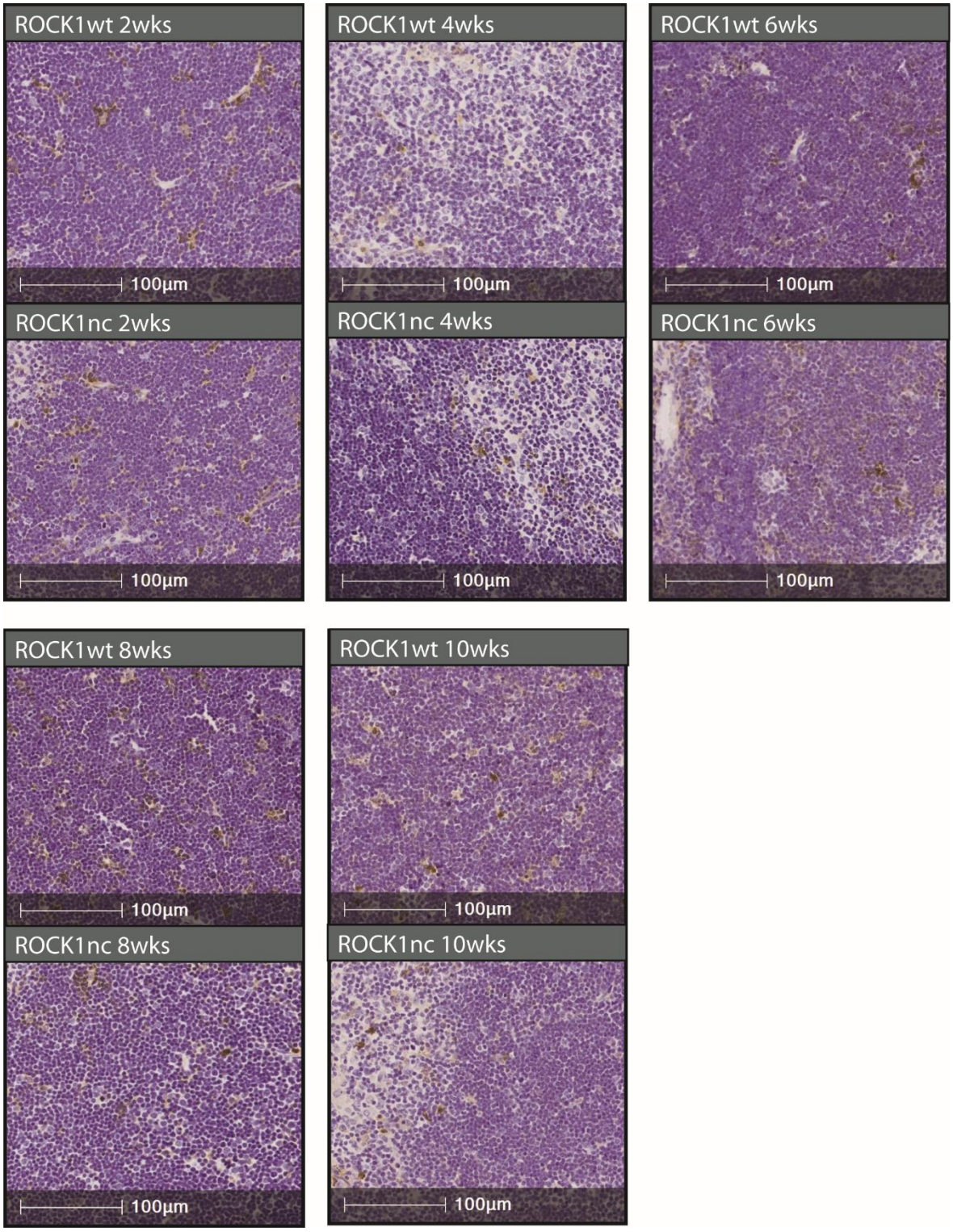

Figure 3-8 Representative F4/80 staining of thymus sections from ROCK1wt and ROCK1nc mice. ROCK1wt and ROCK1nc male and female mice were harvested at various ages (2, 4, 6, 8 and 10 weeks). FFPE thymic tissues were sectioned at 4 µm and stained with F4/80. Stains are at a 20x magnification and scale bars at 100 µm. F4/80 positive cells are brown in colour. Representative of N=7-10 per genotype, per time point.

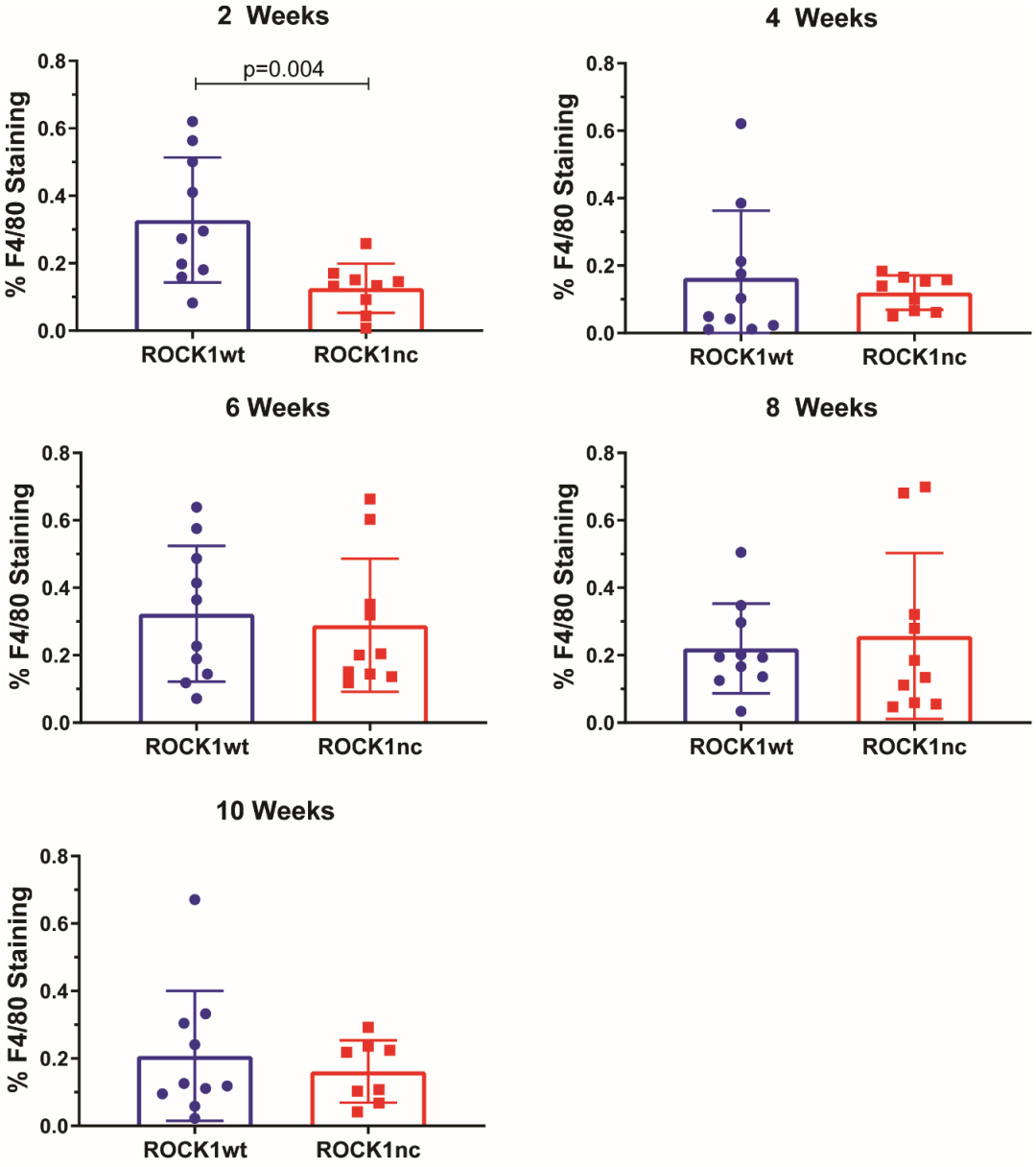

Figure 3-9 The ROCK1nc mutation did not alter the levels of macrophages. ROCK1wt and ROCK1nc male and female mice were harvested at various ages (2, 4, 6, 8 and 10 weeks). FFPE thymic tissues were sectioned at 4 µm and stained with F4/80 antibody. The area of staining was quantified using HALO™. The percentage of F4/80 stained cells relativel to total cell numbers for male and female ROCK1wt and ROCK1nc thymi across the various ages were determined. Data points represent individual mice, error bars represent mean ± SD (2 weeks N=10 (5 males, 5 females) for both genotypes; 4 weeks ROCK1wt N=10 (5 males, 5 females) ROCK1nc N=9 (5 males, 4 females); 6 weeks N=10 (5 males, 5 females) for both genotypes; 8 weeks ROCK1wt N=10 (6 males, 5 females) ROCK1nc N=10 (5 males, 5 females); 10 weeks ROCK1wt N=10 (4 males, 6 females) ROCK1nc N=8 (5 males, 3 females).

3.2.6 Characterisation of cell subsets in the thymus

Apoptosis is inherent to the T-cell developmental process. As such, investigating whether the ROCK1nc mutation would affect cellular populations would provide insight into the role of apoptotic membrane blebbing in T-cell and thymic development. Immunophenotyping of the T-cell subsets and myeloid subsets by flow cytometry was used to assess the cellular populations. Briefly, thymi

obtained from both male and female ROCK1wt and ROCK1nc mice at various ages (4, 6, 8 and 10 weeks) were isolated as single cell suspensions and subsequently stained for T-cell and myeloid antibody panels. Cells were then run on the Attune Flow cytometer and analysed using the FloJo software.

3.2.6.1 The ROCK1nc mutation display a variation of T-cell subpopulations at various ages

T-cell populations were also investigated to explore whether defective apoptotic membrane blebbing affected T-cell development. To determine this, cells isolated from thymi were stained with T-cell specific markers. In this T-cell panel, the cells of interest are double negative ($CD4^-$, $CD8^-$), double positive ($CD4^+$, $CD8^{+)}$, single positive ($CD4^+$ TCRß, $CD8^+$ TCRß), $CD4^+$ regulatory (Tregs) or γδ T-cells (Figure 3-10). The immature T-cell populations appeared to change over time (Figure 3-11). The levels of double positive cells were comparable between ROCK1wt and ROCK1nc mice at 4 weeks. At 6 and 10 weeks, the levels of double positive cells seemed to be higher in ROCK1nc mice than ROCK1wt mice, although not statistically significant. At 8 weeks, there is a statistically significant higher level of double positive cells in ROCK1nc mice compared to ROCK1wt mice.

The double negative population appeared to be variable between mice. Interestingly, mice had a significantly higher number of DN cells at 4 weeks of age. At 6 weeks, the double negative population did increase, followed by a reduction at 8 weeks and slight increase again at 10 weeks in both genotypes. There were similar levels of double negative cells between ROCK1wt and ROCK1nc mice at 6, 8 and 10 weeks. The double negative population was further divided into 4 subpopulations – DN1, DN2, DN3 and DN4. The data do show variability in both ROCK1wt and ROCK1nc cohorts at the various ages. At 4 weeks of age, the DN3 and DN4 populations were statistically significant in ROCK1nc mice. These two subpopulations were what contributed to significantly greater DN populations. At 6 weeks, there were comparable double negative cells between the two genotypes. The subpopulations of double negative cells opposed each other and ultimately cancelled each other out. There was less variability at 8 and 10 weeks in both genotypes. Although there were statistically significant greater DN1, DN2 and DN3 populations in the ROCK1nc cohort

compared to ROCK1wt cohort, there was no overall difference in the DN population.

The mature positive T-cell populations levels were also variable in ROCK1wt and ROCK1nc cohorts over time (Figure 3-12). There were comparable CD4 cellular levels at 4 weeks of age for both genotypes. The CD4 T-cell population was statistically significantly greater in ROCK1nc mice in comparison to ROCK1wt mice at 6 and 8 weeks of age. Although not statistically significant, there seemed to be greater numbers of CD4 cells in ROCK1nc mice at 10 weeks of age. Interestingly, there was a statistically significantly higher level of CD8α T-cells in ROCK1nc cohorts in comparison to ROCK1wt cohorts. Although not statistically significant at 10 weeks, there appeared to be greater numbers of CD8α T-cells in ROCK1nc mice. For both the singe positive CD4 and CD8α T-cells, there seemed to be a trend, with highest peak of cells at 6 weeks then gradually reducing at 8 and 10 weeks. The γδ T-cell population was statistically significantly higher at 6 and 8 weeks in ROCK1nc mice, whilst the regulatory T-cell populations were only statistically significantly higher at 8 weeks in ROCK1nc mice. ROCK1wt and ROCK1nc mice displayed similar levels of γδ T-cells, as well as regulatory T-cells in the thymus at 10 weeks. In all the cell populations assessed, male and female mice of each genotype had comparable levels of cells.

Taken together, the flow cytometry data suggest that there are some subtle differences between the genotypes in their T-cell distributions. Although the results were significantly different at some of the ages, there was a high degree of variability and these differences did not appear to perturb thymocyte development. Thus, within the T-cell populations explored here, most T-cell subpopulations were comparable between ROCK1wt and ROCK1nc populations. Interestingly, the CD4 and CD8α T-cell populations seem to be consistently higher in ROCK1nc mice compared to ROCK1wt mice. These results suggest that alterations of apoptotic membrane blebbing do not dramatically alter T-cell developmental processes.

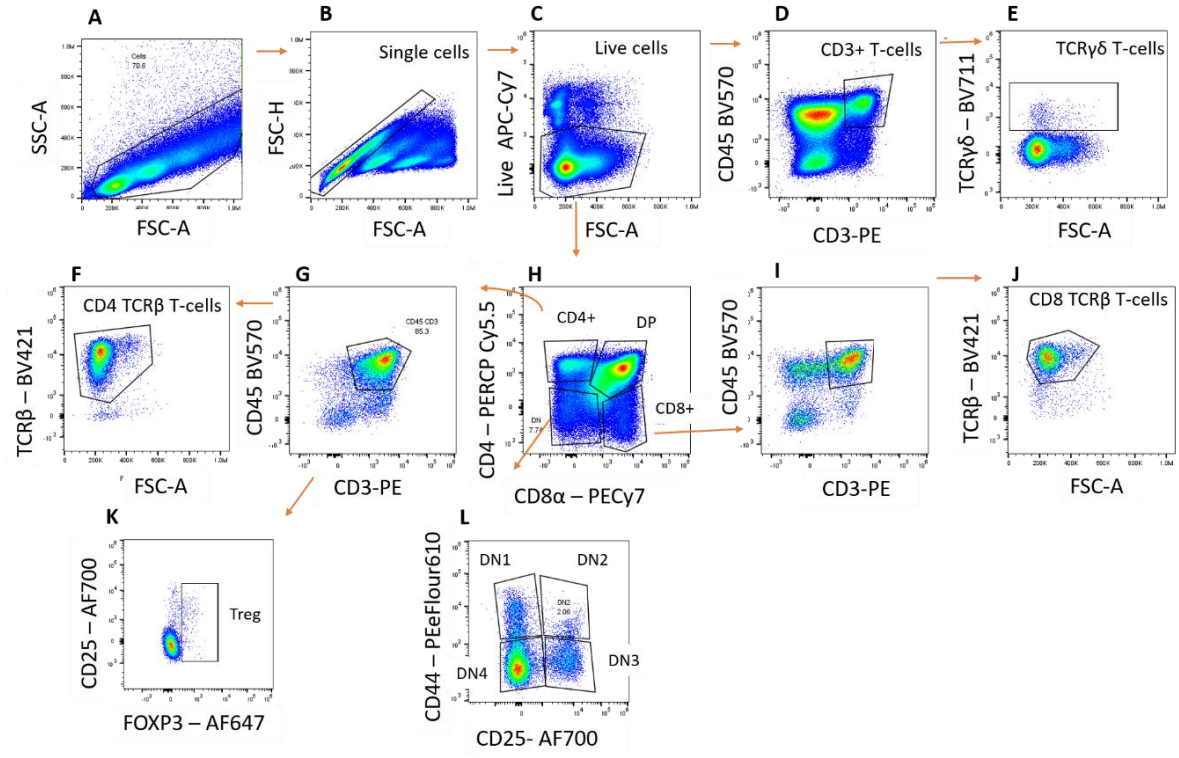

Figure 3-10 Representative flow cytometry gating strategy for T-cell phenotyping. All cells were gated in panel A, followed by a doublet exclusion in B. Gates were then applied on live cells in C. The γδ-T cells were then gated by selecting for cells that were double positive for CD45 and CD3 in panel D, followed by cells positive for the δγ T-cell receptor (TCR) in panel E. For the other cells types of interest, live cells were separated based on expression levels of CD4 and CD8 (H). Cells positive for both CD4 and CD8 are the double positive (DP) cells. Cells that were negative for CD4 and CD8 are the double negative (DN) cells. The double negatives (DN) were further subtyped based on CD25 and CD44 expression (L). These include the DN1 ($CD25^{-}$ $CD44^{+}$), DN2 ($CD25^{+}$ $CD44^{+}$), DN3 ($CD25^{+}$ $CD44^{-}$) and DN4 ($CD25^{-}$ $CD44^{-}$). The mature CD8 T-cells were gated based on CD8 positivity in panel H, followed by CD45 and CD3 positive in panel I, and finally by TCRβ positivity in panel H. Mature CD4 cells were gated on single positive CD4 cells in panel H, CD45 and CD3 positivity in panel G, and finally TCRβ positivity in panel F. Additionally, CD4 regulatory T cells (Tregs) could be identified by selecting for FOXP3 positivity in panel K, following selection in panel G. Cells were run through the Attune Flow Cytometer and analysed using FloJo.

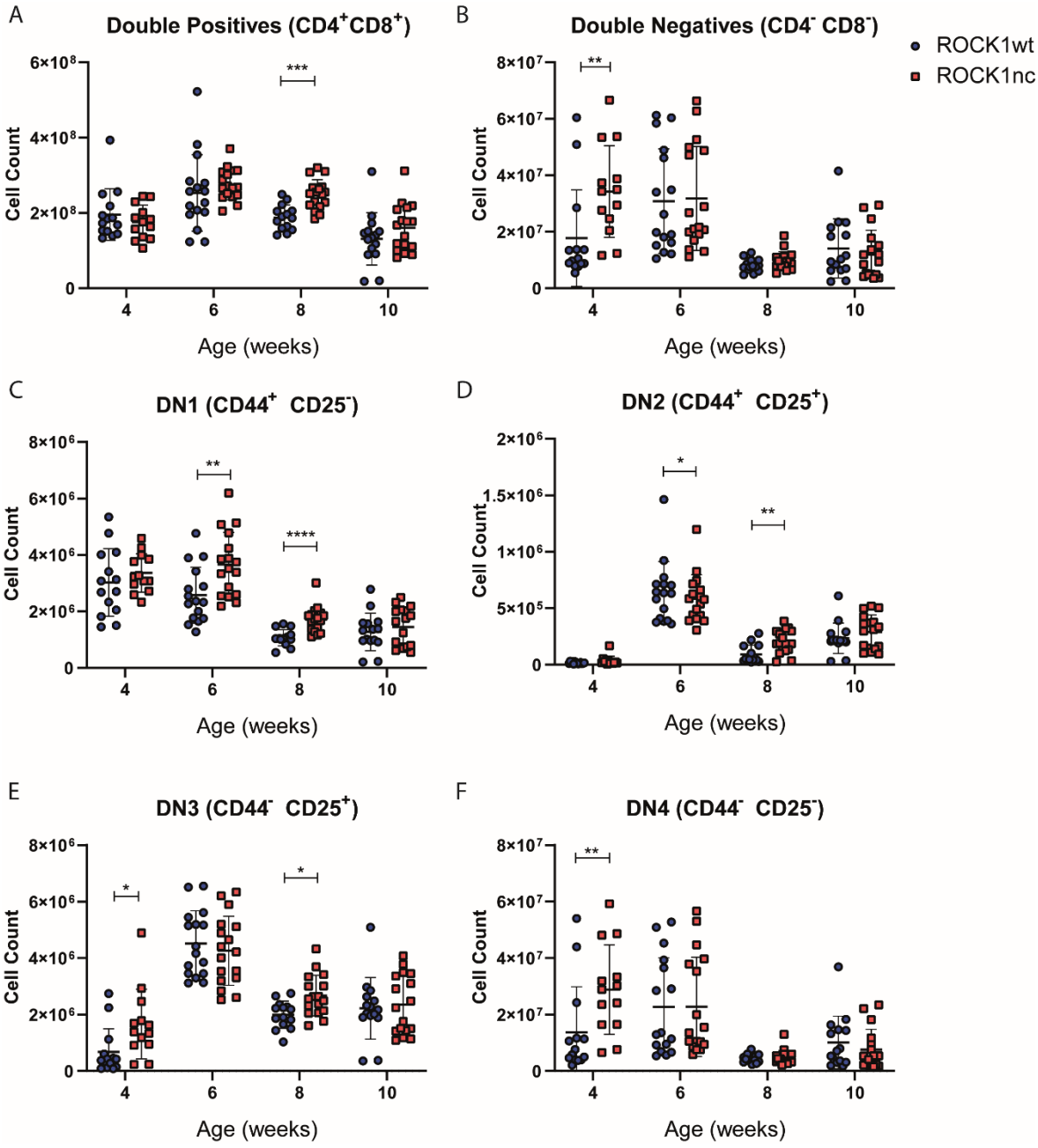

Figure 3-11 Immature T-cell populations determined by flow cytometry immune-phenotyping. Cells isolated from male and female ROCK1wt and ROCK1nc thymi at various ages (4, 6, 8 and 10 weeks) were stained for T-cell markers and analysed as per Figure 3-10. The immature T-cell subtypes include the double positives, double negatives and the double negative subtypes (DN1-DN4). Double positive cells contained the CD4+ and CD8+ surface markers. Conversely, double negatives did not contain both CD4+ and CD8+ markers. The double negatives were categorised based on CD44 and CD25 surface markers. Statistical significance was determined using the Mann-Whitney test comparing the genotypes at each time point ($p<0.05$ = *; $p<0.01$ = **; $p<-.001$ = ***), $p<0.0001$ = ****). Points represent individual mice, error bars represent mean ± SD (4 weeks ROCK1wt N=18 (10 males, 8 females) ROCK1nc N=17 (8 males, 9 females); 6 weeks ROCK1wt N=16 (8 males, 8 females) ROCK1nc N=17 (8 males, 9 females); 8 weeks ROCK1wt N=16 (9 males, 7 females) ROCK1nc N=18 (9 males, 9 females); 10 weeks ROCK1wt N=15 (9 males, 6 females) ROCK1nc N=17 (10 males, 7 females).

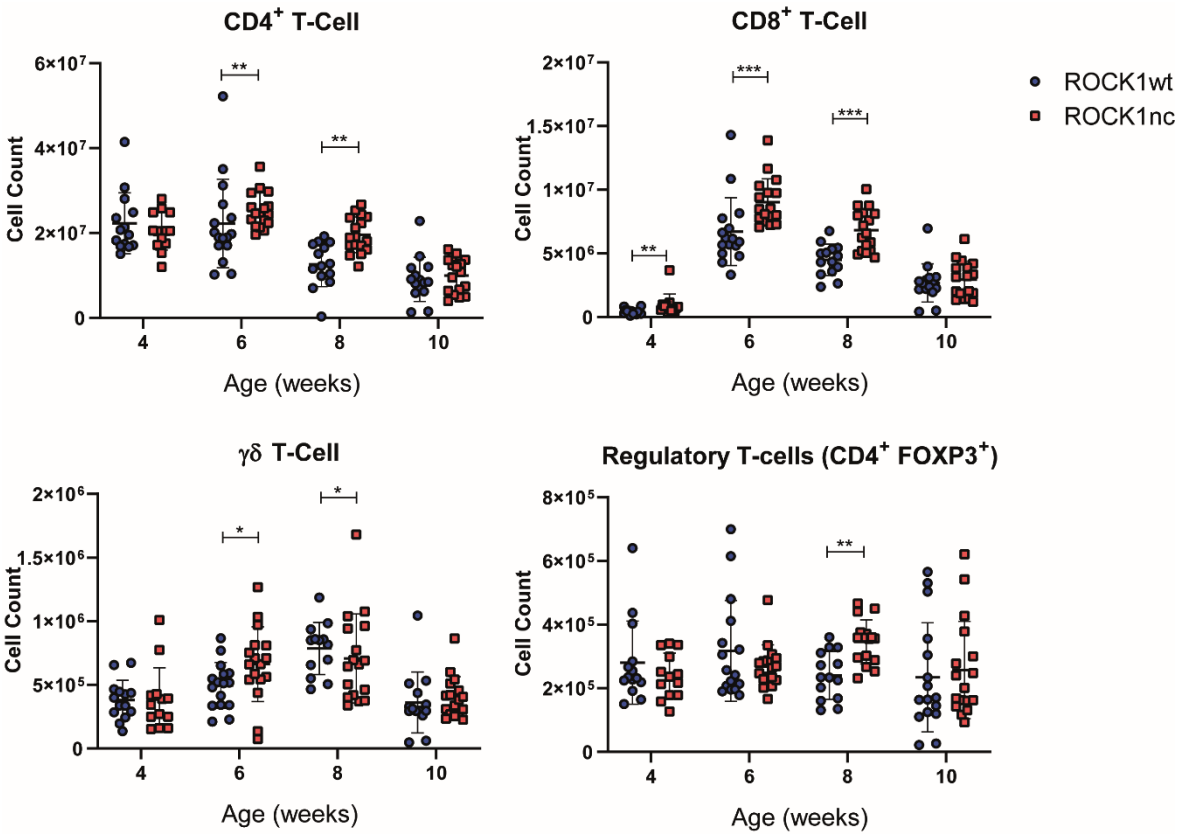

Figure 3-12 Mature T-cell populations determined by flow cytometry immune-phenotyping. Cells isolated from male and female ROCK1wt and ROCK1nc thymi at various ages (4, 6, 8 and 10 weeks) were stained for T-cell markers and analysed as per Figure 3-10. Mature cells include single positive CD4 αβ T-cells, single positive CD8 αβ T-cells, γδ T-cells and regulatory T-cells. No differences were seen in CD4+ T-cells between ROCK1wt and ROCK1nc cohorts at various ages. There were more CD8+ T-cells in the ROCK1nc cohort compared to ROCk1wt cohorts at 4, 6, and 8 weeks. Statistical significance was determined using the Mann-Whitney test comparing the genotypes at each time point ($p<0.05$ = *; $p<0.01$ = **; $p<-.001$ = ***), $p<0.0001$ = ****). Points represent individual mice, error bars represent mean ± SD (4 weeks ROCK1wt N=18 (10 males, 8 females) ROCK1nc N=17 (8 males, 9 females); 6 weeks ROCK1wt N=16 (8 males, 8 females) ROCK1nc N=17 (8 males, 9 females); 8 weeks ROCK1wt N=16 (9 males, 7 females) ROCK1nc N=18 (9 males, 9 females); 10 weeks ROCK1wt N=15 (9 males, 6 females) ROCK1nc N=17 (10 males, 7 females).

3.2.6.2 Myeloid subsets are not affected by the ROCK1n mutation

In addition to investigating the T-cell populations, the myeloid population in the thymus was also explored. As the myeloid populations are important in the T-cell development process, investigating this population could give insight into the relationship between apoptotic membrane blebbing and T-cell development. Furthermore, as macrophages are *bona fide* phagocytic cells, the ROCK1nc mutation may affect the levels of this particular cell population if there were a change to signalling from apoptotic cells. Briefly, cells were isolated as a single cell suspension from the thymus and stained with myeloid cell markers to assess macrophages and two dendritic cell (DC) populations, the classical and plasmacytoid DCs depicted in the gating strategy (Figure 3-13). Flow cytometry

data revealed a high degree of variability in the macrophage population. Despite this variability, the macrophage population was significantly greater in the ROCK1nc population at 6 and 8 weeks of age (Figure 3-14). At 10 weeks, the levels of macrophages decreased to comparable levels between cohorts of both genotypes. The DC population is split into classical DCs (CDCs) and plasmacytoid DCs (PDCs), both of which contribute to priming of T-cells (Hasegawa and Matsumoto, 2018). Analysis revealed that both ROCK1wt and ROCK1nc cohorts had similar levels of both CDCs and PDCs. No significant differences were seen at any of the cohort ages. Similar to the macrophages, both DC populations were reduced at 10 weeks compared to the previous weeks in both genotypes. There were no differences between male and female mice between the genotypes. These results indicate that apoptotic membrane blebbing does not affect the myeloid population found in the thymus.

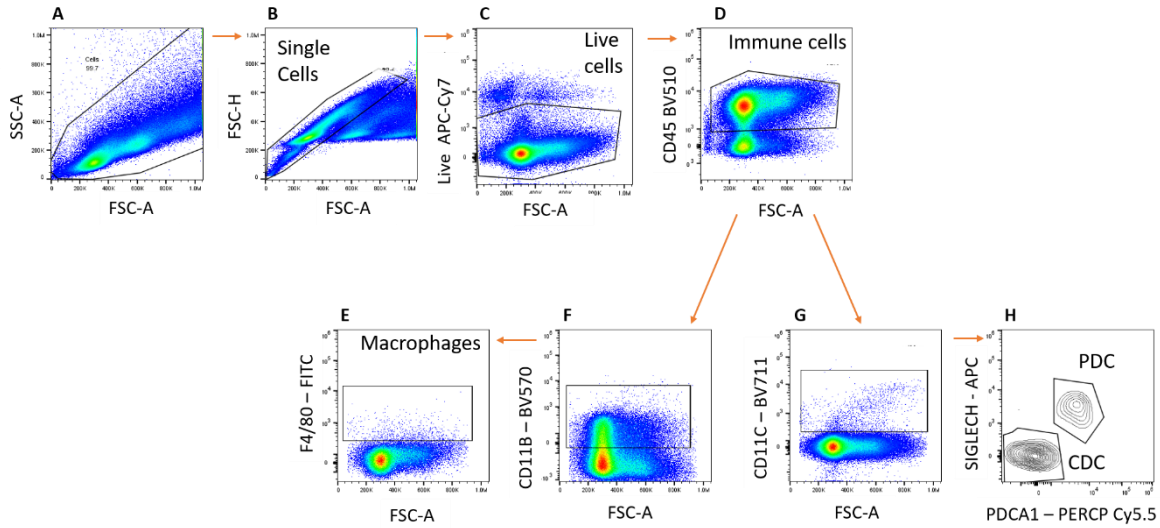

Figure 3-13 Representative flow cytometry gating strategy for myeloid cell subtypes. All cells were gated in panel A, followed by a doublet exclusion in B. Gates were then applied on live cells in panel C. Cells were then selected for the CD45 immune cell marker in panel D. Cells were then divided based on their being CD11b positive (panel F) for macrophages or CD11c positive (panel G) for dendritic cells (DCs). CD11B+ cells were then selected for F4/80 positivity (panel E). DCs were categorised into classical DCs (CDCs) or plasmacytoid DCs (PDCs) in panel H. PDCs are positive for both SIGLEC-H and PDCA-1. CDCs on the other hand are negative for both these markers. Cells were run through the Attune Flow Cytometer and analysed using FloJo

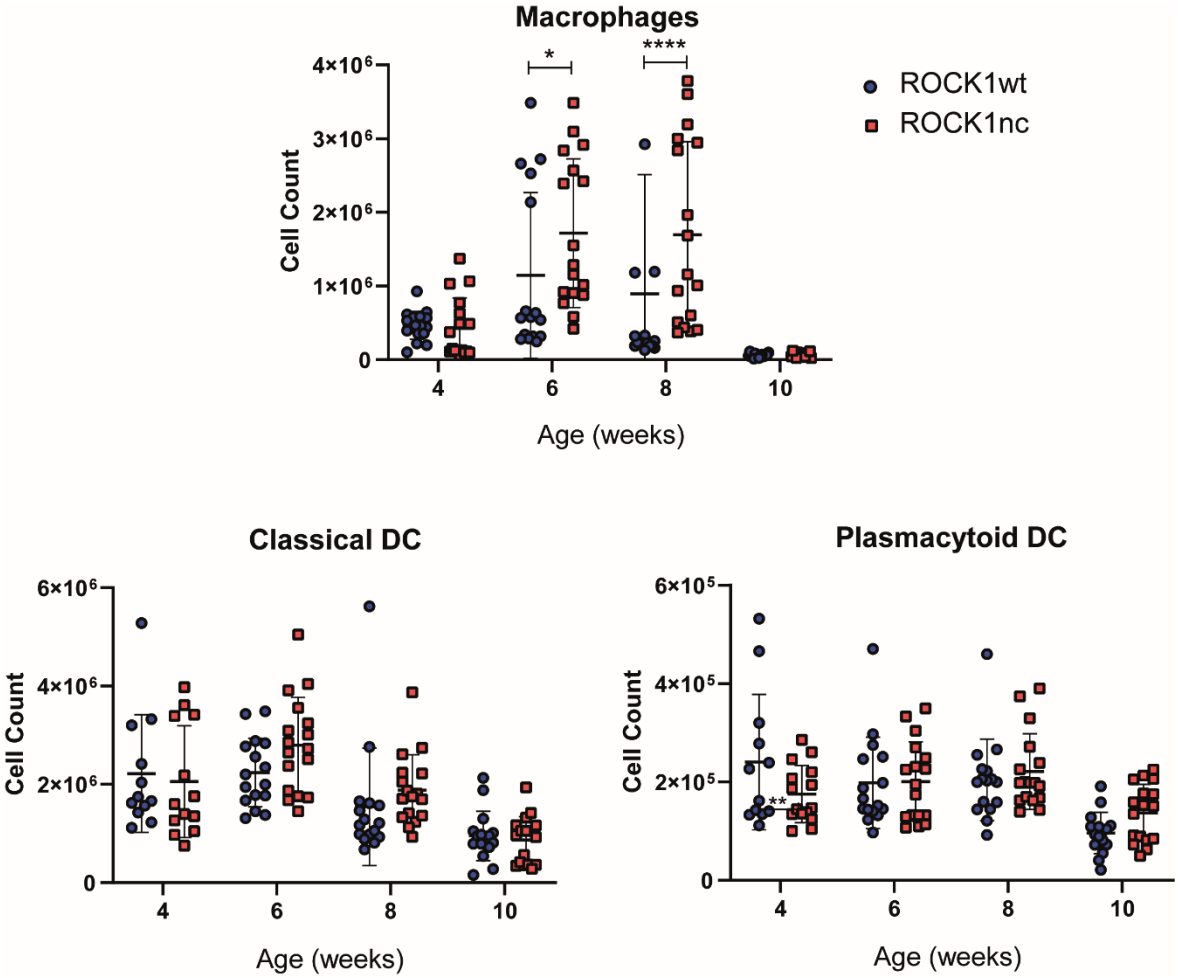

Figure 3-14 Myeloid cell populations determined by flow cytometry immuno-phenotyping. Cells isolated from male and female, ROCK1wt and ROCK1nc thymi at various ages (4, 6, 8 and 10 weeks) were stained for myeloid cell markers and analysed as per Figure 3-13. Myeloid cells analysed include macrophages and dendritic cells (DCs). Statistical significance was determined using the Mann-Whitney test comparing the genotypes at each time point ($p<0.05$ = *; $p<0.01$ = **; p<-.001 = ***), $p<0.0001$ = ****). Points represent individual mice, error bars represent meant $\pm$ SD (4 weeks ROCK1wt N=16 (8 males, 8 females) ROCK1nc N=17 (8 males, 9 females); 6 weeks N=16 (8 males, 8 females) ROCK1nc N=17 (8 males, 9 females); 8 weeks ROCK1wt N=16 (9 males, 7 females) ROCK1nc N=17 (9 males, 8 females); 10 weeks ROCK1wt N=17 (11 males, 6 females) ROCK1nc N=17 (7 males, 10 females).

3.3 Discussion

The thymus is an organ where T-cell development takes place, relying on efficient apoptosis and apoptotic cell clearance to maintain tissue development and homeostasis. Given the relatively high levels of ROCK1 in the thymus, according to the tissue gene expression and regulation database as well as the bloodspot database (Julian and Olson, 2014, Bagger et al., 2018), investigating the role apoptotic membrane blebbing in the thymus utilising the ROCK1nc mouse was the objective of my studies. This arm of the study explored the effect of the ROCK1nc mutation on thymic development, homeostasis and cell

population distribution. Post-natal thymic involution was not affected in the ROCK1nc mice cohorts. The thymus involution based on thymus size and cellularity occurred at similar rates between the genotypes in both males and females. Additionally, it is well known that the thymus in males involutes quicker than in females (Pido-Lopez et al., 2001). This was also the case in ROCK1nc mice. The fact that there were no differences in the body-weight ratios were largely supported by the similarities between ROCK1wt and ROCK1nc thymic cell counts. Any changes seen in thymic cellularity were transient in ROCK1nc mice, ultimately levelling off to similar levels in ROCK1wt mice. In addition to these parameters, the histological architecture was also investigated. The thymus consists of the outer cortex and inner medullary areas. Analysis revealed normal thymic architecture in ROCK1nc cohorts. There may be subtle differences between the genotypes, particularly at 6 weeks. Thus replotting the graph to compare the ratio of thymic cortical to medullary area may be useful to teasing apart any subtle changes. Taken together, this would suggest that the ROCK1nc mutation does not grossly affect these aspects of thymic development. Any subtle and small differences observed was negligible in the context of thymic development.

In addition to the anatomical parameters, a snapshot into the apoptotic milieu was investigated by immunohistochemistry. Formalin-fixed paraffin-embedded thymic tissues were stained with antibody that detects cleaved caspase 3, a marker of active apoptosis. These results showed that there were low levels of cleaved caspase-3 positive cells in the thymus at the various ages explored for both ROCK1wt and ROCK1nc cohorts. This is consistent with highly efficient clearance mechanisms found in the thymus. No differences were observed in ROCK1nc cohorts in comparison to ROCK1wt cohorts. This would suggest that the ROCK1nc mutation does not alter either the number of apoptotic cells found or the process of cell clearance in the thymus. To delve deeper into this, exploring cell clearance was done by assessing the levels of macrophages, a major phagocytic population. Histological stains of the macrophage marker F4/80 in thymic tissues was significantly lower in ROCK1nc mice compared to its wild-type counterparts at 2 weeks, but showed no significant differences at the later ages explored. This further strengthens the notion that the ROCK1nc mutation does not cause accumulation of apoptotic cells or an increase in macrophages.

These analysis were performed on the whole thymus, which may miss any subtleties the ROCK1nc mice may present. Performing the analysis specifically in the thymic cortical and medullary areas would allow a more accurate representation of the parameters investigated.

Following on from this, the characterisation of cellular subsets, in particular the T-cell and myeloid subsets using flow cytometry has given me further insight into how the ROCK1nc mutation might have affected the cellular populations. Within the respective T-cell populations, flow cytometry results did show variability. The majority of T-cell populations analysed, despite subtle variations, displayed comparable levels of cells between ROCK1wt and ROCK1nc mice at 10 weeks of age. This would suggest that the ROCK1nc mutation may affect the skew of immature T-cell populations as well as single positive CD4 and CD8α T-cells. These results would indicate any differences seen in the ROCK1nc mice are only transient which were ultimately resolved in adult mice. To confirm these findings, later time points of the ROCK1nc cohort would need to be investigated or more in-depth immunological analysis carried. Flow cytometry is a powerful tool to assess cell populations, however a caveat with this analysis that would have been informative in this instance is the location of the cells. Determining the location of the different cellular subtypes would help tease apart any subtleties between the genotypes.

The myeloid cell population investigated using flow cytometry was another parameter assessed. The results showed variability in the macrophage populations that evened out to similar levels at 10 weeks of age in both genotypes in a similar fashion to the T-cells. The flow cytometry data did show significantly greater macrophages in ROCK1nc cohorts at 6 and 8 weeks. However, this conflicted with the immunohistochemistry data. Immunohistochemistry analysis did not show the same results at 6 and 8 weeks. Immunohistochemistry analysis showed significantly less macrophages in ROCK1nc cohorts at 2 weeks and comparable levels of macrophages at other ages between the genotypes. Both classical and plasmacytoid populations of dendritic cells were not significantly different between both genotypes at any time points. This indicates that the phagocytic populations assessed here were not affected by the ROCK1nc mutation.

Given the high levels of apoptotic activity and ROCK1 expression in the thymus, the starting hypothesis was that the ROCK1nc mutation might have affected thymic development, homeostasis and the cellular populations therein. However, the results obtained here do not substantiate this hypothesis. The data indicated that were some differences observed in the ROCK1nc cohorts of the various parameters at the earlier time points, but the majority of what was investigated was at comparable levels to the wild-type controls. This suggests that any differences observed were likely to be transient. It is well established that cell clearance, particularly in the thymus, is extremely efficient. This explains why apoptotic cells are rarely detected, which was also observed in the low percentage of cleaved caspase-3 staining in the thymus (Figure 3-7). Perhaps there may be compensatory mechanisms in place in the thymus that overcome the effect of the ROCK1nc mutation on the morphology of apoptotic cells, or apoptotic membrane blebbing may be dispensable in the thymus and for the T-cell selection process. This would be supported by previous observations in the lab that found no significant differences in immune cell levels or any indications of an autoimmune phenotype, including glomerulonephritis, haemolytic anaemia or cytopenia, in aged ROCK1nc mouse cohorts (Julian, 2015).

In addition to what has been investigated here, additional aging of mice beyond 10 weeks until 20 weeks would confirm whether the changes seen in the ROCK1nc mice are transient. Additionally, the activation status of myeloid cells, assessed through flow cytometry, and egress of T-cells from the thymus into the periphery, including the blood stream and lymph nodes, could be explored to definitively determine if ROCK1nc absolutely does not affect thymic development and homeostasis, as well as T-cell development, with more confidence. A caveat of the system used here is the ubiquitous expression of the mutation in all cell types. It is highly possible that the mutation will yield off target effects, especially given the growing evidence of non-apoptotic functions of caspase-3 (Nakajima and Kuranaga, 2017). The cytoskeleton is important in phagocytic populations, such as macrophages, and in T-cells. Thus, performing a comparative RNAseq between apoptotic and non-apoptotic cells would be both interesting and informative. If there are changes in the ROCK1nc non-apoptotic cell population, it is plausible that this could mask any changes in apoptotic cells themselves.

The results obtained here however, suggest that the ROCK1nc mutation and, by extension, apoptotic membrane blebbing do not alter thymic development and homeostasis. It could be that under physiological conditions, the role of ROCK1-mediated apoptotic membrane blebbing is dispensable. Whether this holds true in challenged conditions and in tumour bearing settings, is explored in the upcoming chapters.

4 ROCK1nc mutation in thymic apoptosis, cell clearance and immune cell activation

4.1 Introduction

4.1.1 Apoptosis and apoptotic cell clearance

Apoptosis is a well characterised form of programmed cell death (Kerr et al., 1972). Triggering apoptosis via the intrinsic or extrinsic pathway culminates in the activation of executioner caspases, in particular, caspase-3. Once caspase-3 is cleaved and active, downstream events ensure cells undergo cell death (Kroemer et al., 2007). Cell death is underpinned by characteristic hallmark morphological changes, including cell contraction, DNA fragmentation, apoptotic membrane blebbing, and apoptotic body formation (Kerr et al., 1972, Elmore, 2007). In addition to morphological changes, cells exhibit biochemical changes as well, including the well-documented externalisation of phosphatidylserine (PS) onto the outer membrane. PS acts as an 'eat-me' signal, allowing phagocytic cells to engage and find the apoptotic cells and bodies (Ravichandran, 2003). This facilitates the uptake and clearance of the apoptotic cells by phagocytes. Phagocytes can be classed as professional and non-professional phagocytes, and include macrophages and dendritic cells (Medina and Ravichandran, 2016). Ultimately, the uptake of the dead cells and its apoptotic bodies by phagocytes facilitate homeostasis.

This apoptotic process that promotes homeostasis has been deemed to be immunologically silent. The immune system remains generally inactive as the characteristic changes seen during apoptosis allow the containment of intracellular components, which would otherwise activate immune cells and initiate an immune response (Wyllie et al., 1980). Deviation in the apoptotic machinery and clearance results in an immune response, triggered by secondary necrosis (Doran et al., 2020). The clearance of apoptotic cells, particularly in the thymus, is what helps maintain homeostasis and keeps the tissue from being overloaded with cell corpses due to the high number of apoptotic events that come with the T-cell development process.

4.1.2 Dexamethasone induces apoptosis in the thymus

Dexamethasone, a synthetic glucocorticoid, is an apoptosis-inducing agent that acts via the glucocorticoid receptor (GR) (Cifone et al., 1999). Activation of the GR intracellularly causes translocation of the complex into the nucleus, altering the transcription of genes to promote apoptosis. In parallel, intrinsic apoptosis can also be triggered resulting in the activation of caspase-3 (Bamberger et al., 1996). The activation of GRs is known to cause lymphocyte apoptosis (Smith and Cidlowski, 2010). Thymocytes in particular, are known to be highly sensitive to glucocorticoid-induced death, resulting in the release of cytochrome C and caspase activation that are characteristic of apoptotic cell death (Marchetti et al., 2003). One crucial aspect of dexamethasone-induced thymocyte apoptosis is the activation of caspase-3 (Cifone et al., 1999). In addition to the thymus, the spleen is another organ that is sensitive to the effects of dexamethasone (Ahmed and Sriranganathan, 1994). Dexamethasone is currently utilised in the clinic for a variety of conditions including leukaemia and lymphomas, due to its effect on lymphocytes (Kofler, 2000). Thus, dexamethasone was utilised for *in vitro* and *in vivo* experiments to induce apoptosis in this arm of the study.

4.1.3 Experimental Aims

Under physiological conditions, apoptosis and apoptotic cell clearance is highly regulated and efficient. Previous results showed that the ROCK1nc mutation did not impact thymic development and homeostasis. The objective of this study was to challenge the thymus and thymocytes with an apoptotic stimulus to determine if ROCK1-mediated apoptotic membrane blebbing played a role in apoptosis, cell clearance and immune cell activation. This was done using a variety of *in vitro* and *in vivo* experiments with the ROCK1nc mouse, looking at thymic clearance, efferocytosis, immune cell activation and apoptotic blebbing. I hypothesised that the ROCK1nc mutation would affect thymic clearance, efferocytosis and apoptotic membrane blebbing in challenged conditions.

4.2 Results

4.2.1 Dexamethasone induces apoptosis in ROCK1wt and ROCK1nc thymocytes

Previous findings in the Olson lab have shown that mouse embryonic fibroblasts and hepatocytes from ROCK1nc mice do not have alterations in the cell death process apart from apoptotic membrane blebbing (Julian, 2015, Naylor, 2019). To determine whether cell death biochemical processes were intact in ROCK1nc thymocytes, phosphatidylserine externalisation and protein levels were assessed. Cells that begin to undergo apoptosis are annexin V positive, denoting externalisation of PS. As cells progress further through the cell death programme, they lose their membrane integrity and thus showing positivity for both PI as well as annexin V. This culminates in only PI positivity, indicating that cells are truly dead. Cells isolated from the thymus were treated with 1 μm dexamethasone or vehicle control, *in vitro* and collected at 4 and 8 hours after treatment. Cells were evaluated for PS externalisation by flow cytometry using fluorescently-labelled annexin V, which binds to externalised PS (Figure 4-1). Healthy cells were negative for annexin V and propdium iodide (PI). Thymocytes are known to spontaneously die (Tiso et al., 1995). There was evidence of spontaneous apoptosis from freshly isolated thymocytes from ROCK1wt and ROCK1nc mice (Figure 4-2). Both ROCK1wt and ROCK1nc thymocytes that were treated with dexamethasone at 4 hours displayed roughly 10% higher levels of apoptotic cells, in comparison to vehicle control treated cells. At 8 hours post treatment, both ROCK1wt and ROCK1nc thymocytes contain almost double the amount of apoptotic cells compared to vehicle treated counterparts. At both time points, no PI positive/annexin V negative cells were detected. This would suggest that the cells were dismantled and no longer intact, likely having gone through apoptosis. However there was no difference between the ROCK1wt and ROCK1nc cells treated with dexamethasone, showing that ROCK1nc thymocytes externalise PS in the same manner as ROCK1wt thymocytes.

Using the same experimental setup, lysates were collected at 4 and 8 hours post treatment from isolated thymocytes that had been treated either with 1 μm dexamethasone or vehicle control, and processed to determine protein levels by western blotting (Figure 4-3). The ROCK1 protein presents itself as a single band

in untreated ROCK1wt and ROCK1nc thymocytes. In ROCK1wt thymocytes, at 4 hours, there was an emergence of 2 bands consistent with ROCK1 being cleaved by caspase-3. By 8 hours, only the second lower band was present, indicating that wild-type ROCK1wt was fully cleaved. On the other hand, ROCK1nc thymocytes displayed only a single ROCK1 band, confirming that the mutation is present and rendered ROCK1 resistant to caspase-mediated cleavage. Dexamethasone-treated ROCK1wt and ROCK1nc thymocytes at 4 hours saw the emergence of cleaved caspase-3, indicating that cells were beginning to undergo apoptosis. By 8 hours, both ROCK1wt and ROCK1nc thymocytes displayed a disappearance of full-length caspase-3 and comparably stronger cleaved caspase-3 bands. This indicates that the majority of the cells were apoptotic 8 hours post dexamethasone treatment in stark contrast to the vehicle control treated counterparts. This demonstrates that the biochemical pathway of apoptosis is intact in ROCK1nc thymocytes.

Taken together, both the externalisation of PS and caspase-3 cleavage by dexamethasone treatment showed that ROCK1nc thymocytes undergo cell death with no changes in the magnitude or timing of activation of apoptotic biochemical pathways.

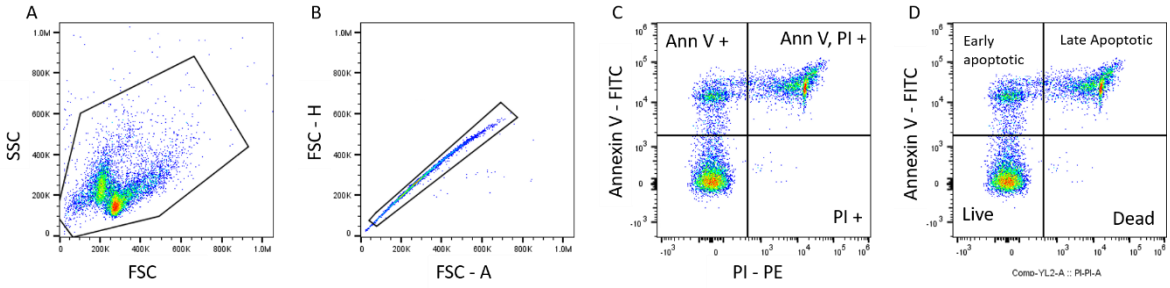

Figure 4-1 Representative flow cytometry gating strategy for annexin V and propidium iodide. Cells were gated in panel A, followed by a doublet exclusion in panel B. Cells were then segregated based on the annexin V (Ann V) and propidium iodide (PI) positivity. Early apoptotic cells are Ann V+, followed by Ann V and PI+ as cells become membrane permeable.

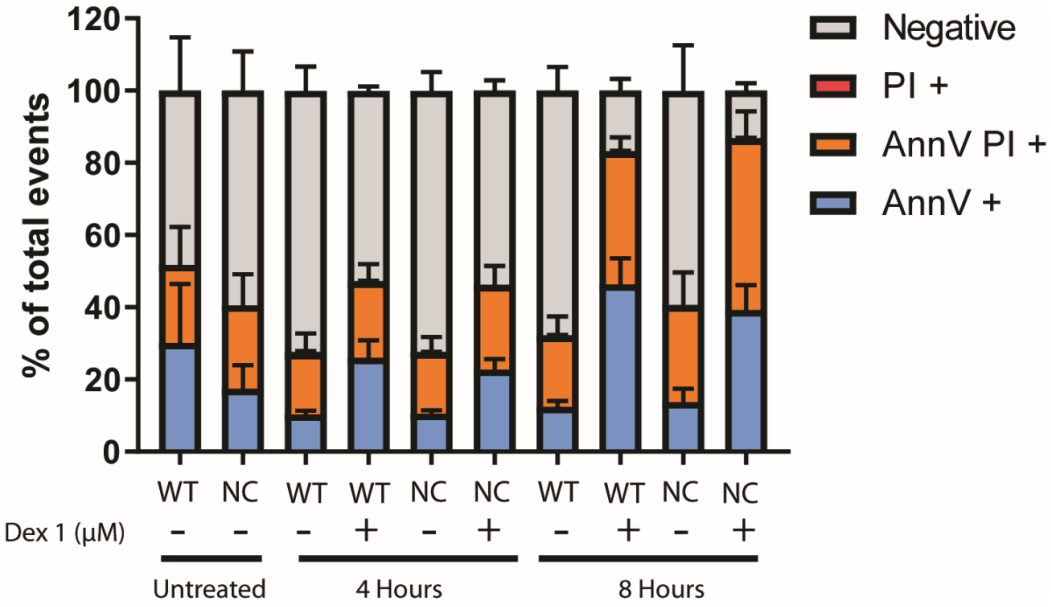

Figure 4-2 Phosphatidylserine externalisation is not altered in ROCK1nc apoptotic thymocytes. Cells isolated from 8 week old ROCK1wt and ROCK1nc mice were treated with either 1µM dexamethasone (dex) or vehicle control. Cells were collected either 4 or 8 hours post treatment and stained with annexin V (Ann V) and propidium iodide (PI). Data points show mean ± SD (N=4 per group).

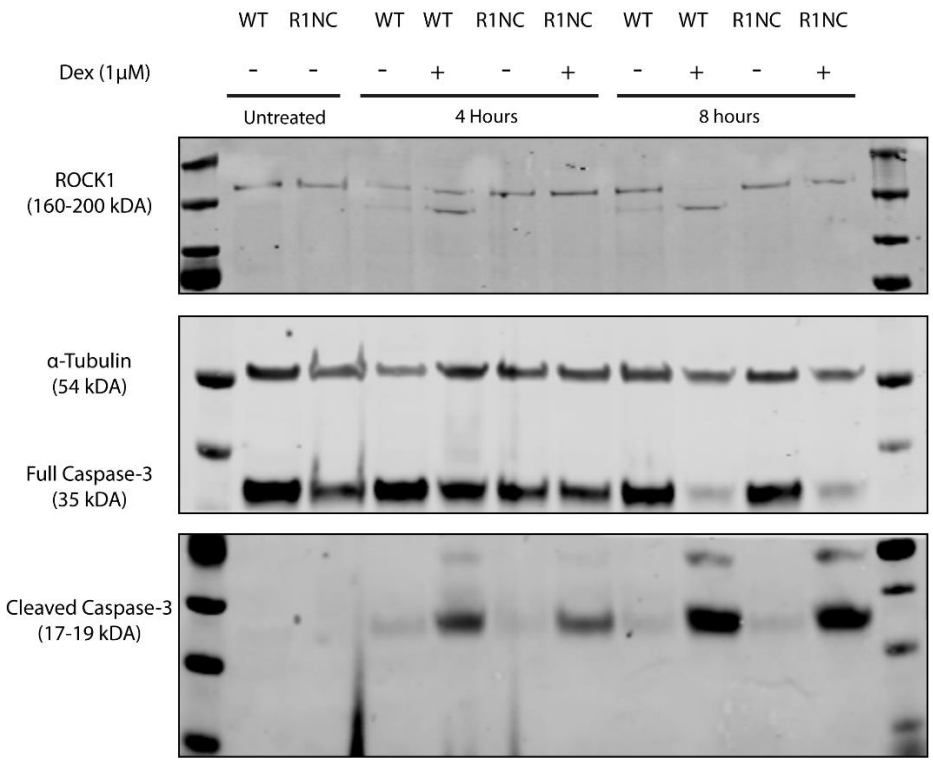

Figure 4-3 ROCK1nc thymocytes are resistant to ROCK1 cleavage and retain the biochemical pathways of apoptosis. Representative western blots showing ROCK1, full length caspase-3 and cleaved caspase-3 from untreated, dexamethasone (dex) treated (1µm), and vehicle treated ROCK1wt and ROCK1nc thymocytes (6-8 week old male and female mice) for 4 and 8 hours. Representative of 3 independent western blots.

4.2.2 Dexamethasone induces thymic and splenic weight loss in ROCK1wt and ROCK1nc mice

Dexamethasone is known to cause lymphocyte apoptosis (Smith and Cidlowski, 2010). To assess the response of the ROCK1nc mouse to apoptosis, dexamethasone-21 phosphate disodium salt (dexamethasone), was used to induce acute apoptosis *in vivo*. Dexamethasone, or vehicle control, was administered by intraperitoneal injection at 15 mg/kg to 8 week old female ROCK1wt and ROCK1nc mice. At various time points post drug administration (6, 12, 24 and 30 hours), the thymus and spleen were harvested. The percentage ratio of the thymus (Figure 4-4), and spleen (Figure 4-5) to body weight was determined. Dexamethasone caused a gradual reduction in the percentage of thymic weight to body weight. Small reductions were seen as early as 6 hours in dexamethasone-treated cohorts. By 24 hours, the thymus from both ROCK1wt and ROCK1nc mice treated with dexamethasone were significantly reduced in comparison to vehicle treated controls. This reduction was sustained to a similar level by 30 hours. The reductions in thymic weight were comparable between ROCK1wt and ROCK1nc post dexamethasone treatment. It should be noted that a statistically significant reduction was not seen at 6, 12 and 24 hours likely due to the low cohort numbers.

The spleen followed a similar trend as the thymus. Reductions were seen in the percentages of spleen to body ratio in dexamethasone-treated ROCK1wt and ROCK1nc cohorts at 6 hours. At 24 hours post dexamethasone treatment, the percentage splenic weight ratio was significantly lower in ROCK1wt and ROCK1nc cohorts compared to vehicle controls. The reduction in the percentage of splenic weight ratio was sustained at 30 hours. A loss in organ weight indicates a loss of cells. As was seen with the thymus, there was no difference between the ROCK1nc and ROCK1wt genotypes in splenic weight. Furthermore, similar to the thymic weight, a statistically significant reduction was not seen at 6, 12 and 24 hours likely due to the low cohort numbers. This would suggest that the ROCK1nc mutation has not affected acute lymphocyte apoptosis induced by dexamethasone.

The loss in thymic weight due to dexamethasone was recapitulated in the histological presentation of the tissue (Figure 4-6). The thymus obtained from

dexamethasone and vehicle treated cohorts at the various time points were fixed in formalin and embedded in paraffin. The formalin-fixed, paraffin-embedded (FFPE) thymic tissues were sectioned and stained with haematoxylin and eosin (H&E) to visualise the thymic architecture. Vehicle treated thymi displayed distinct thymic cortical (darker) and medullary (lighter) areas. At 6 and 12 hours, these thymic areas remain fairly distinct. At 24 and 30 hours however, this distinction was less obvious in dexamethasone treated ROCK1wt and ROCK1nc cohorts. The thymus seemed less densely packed particularly in the cortical area, suggesting a loss in cells that would reflect the reduction in thymic weight with dexamethasone treatment. Interestingly, although the thymic weight was reduced at 6 and 12 hours, the thymus still appeared relatively densely packed. Perhaps the clearance of apoptotic cells required more than 12 hours to see an obvious difference. It should be noted that there was variability in the thymic sections (Figure 4-6) Regardless, both ROCK1wt and ROCK1nc thymi responded to dexamethasone in a similar manner, further suggesting that acute apoptosis within the thymus was not overtly altered in the ROCK1nc mice.

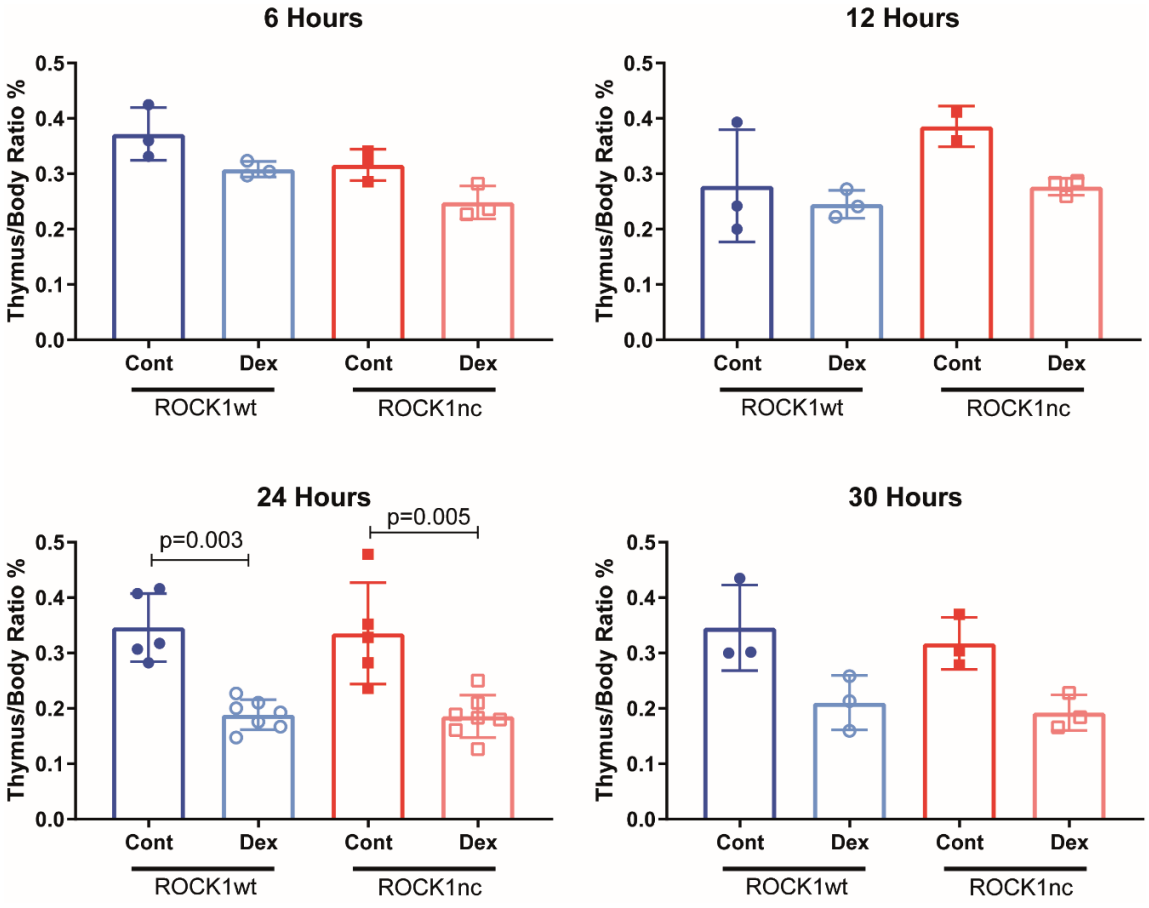

Figure 4-4 Dexamethose-induced acute apoptosis causes thymic weight loss in ROCK1wt and ROCK1nc mice. ROCK1wt and ROCK1nc 8 week old female mice were administered with dexamethasone-21 phosphate disodium salt (Dex) or vehicle control (cont) at 15 mg/kg I.P. The spleen was harvested at 6, 12, 24 and 30 hours post dex treatment. The body and spleen weights were recorded. Data points represent individual mice, error bars represent mean ± SD. Statistical signifcance was determined using a Mann-Whitney test comparing dex-treated to cont-treated cohorts per genotype (6 hours N=2-3; 12 hours N=2-3; 24 hours N=5-7; 30 hours N=2-3).

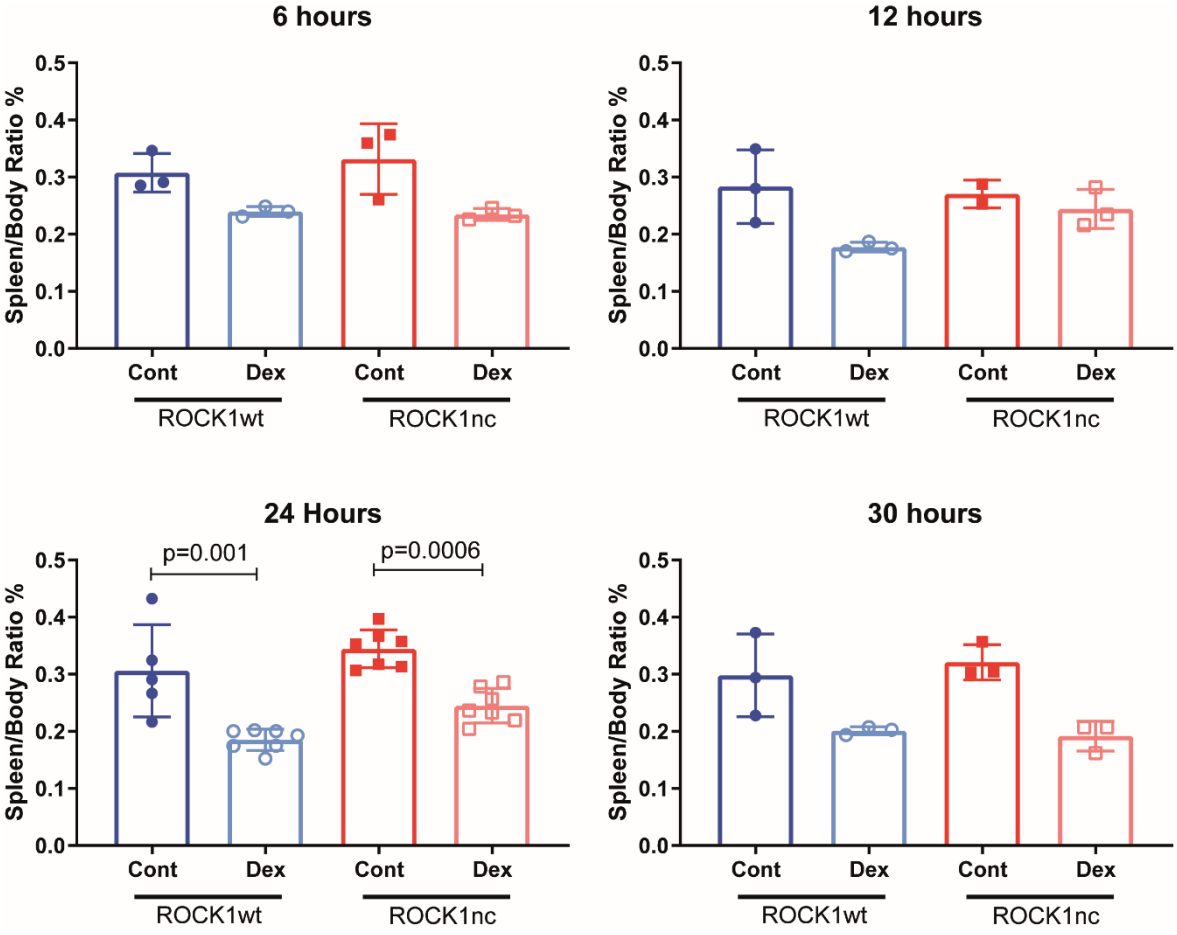

Figure 4-5 Dexamethose-induced acute apoptosis causes splenic weight loss in ROCK1wt and ROCK1nc mice. ROCK1wt and ROCK1nc, 8 week old female mice were administered with dexamethasone-21 phosphate disodium salt (Dex) or vehicle control (cont) at 15mg/kg I.P. The spleen was harvested at 6, 12, 24 and 30 hours post dex treatment. The body weight and spleen weight were recorded. Data points represent individual mice, error bars represent mean ± SD. Statistical signifcance was determined using a Mann-Whitney test comparing dex-treated to cont-treated cohorts per genotype (6 hours N=2-3; 12 hours N=2-3; 24 hours N=5-7; 30 hours N=2-3).

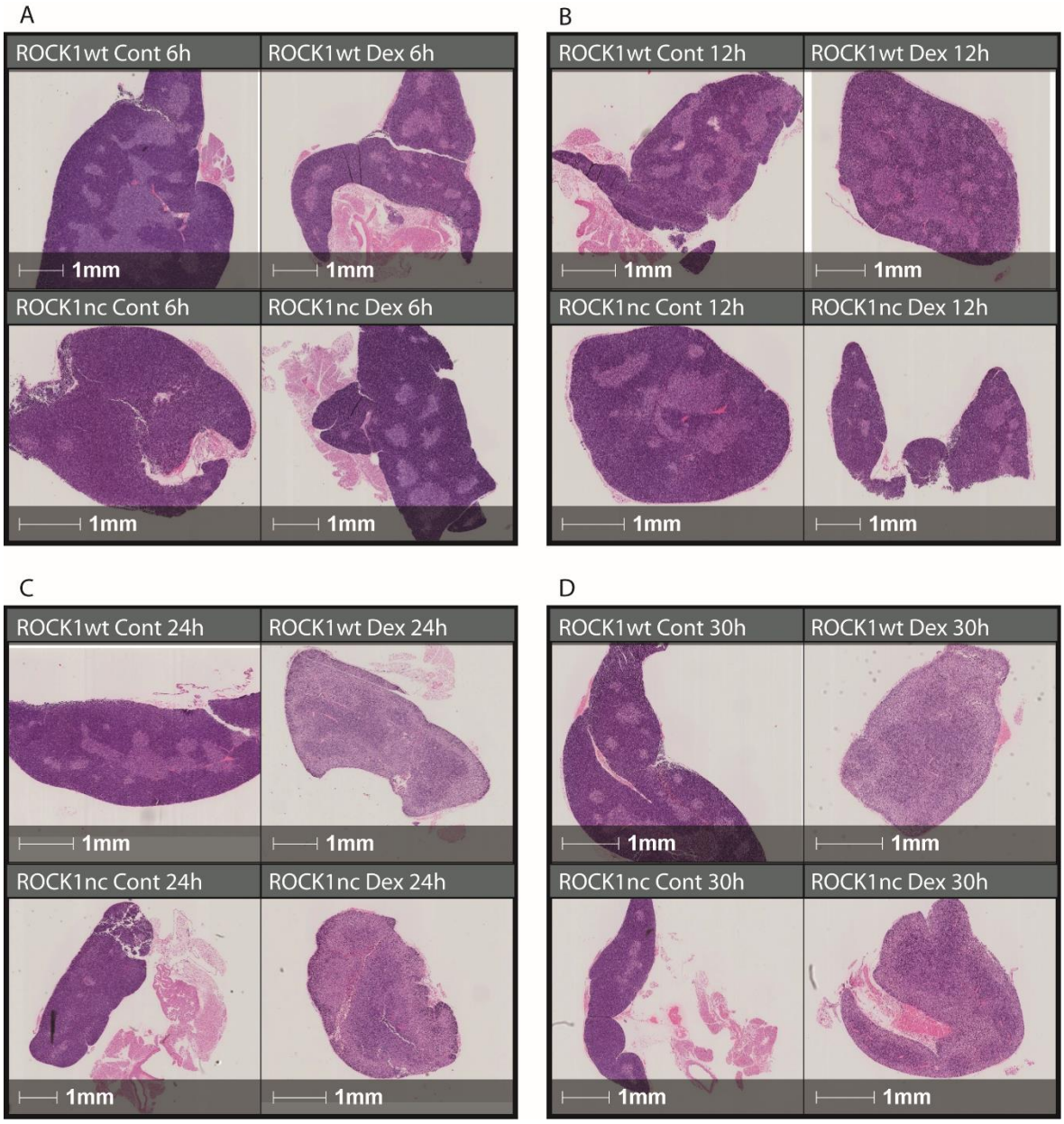

Figure 4-6 Representative H&E stains of ROCK1wt and ROCK1nc thymi. ROCK1wt and ROCK1nc, 8 week old female mice were administered with dexamethasone-21 phosphate disodium salt (Dex) or vehicle control (cont) at 15mg/kg I.P. The thymus was harvested at 6, 12, 24 and 30 hours post Dex treatment. Formalin-fixed, paraffin embedded were sectioned at 4µM and stained for haematoxylin and eosin (H&E). These are representaive of the thymus as seen in Figure 4-4. Scale bars denote 1mm in length.

4.2.3 Dexamethasone induces apoptosis *in vivo*

Following from assessing the weights of the thymus and spleen, as well as the thymic architecture, the next parameter I investigated was apoptosis. In order to examine apoptosis, FFPE embedded thymic tissues were sectioned and stained for cleaved caspase-3. Cleaved caspase-3 indicates active apoptosis, as this is generally regarded as the point of no return. Representative images showed that apoptosis was seen as early as 6 hours in both ROCK1wt and ROCK1nc

dexamethasone-treated cohorts (Figure 4-7). Cleaved caspase-3 positivity peaked at 12 hours, localising mainly in the cortex. By 24 hours, there was a dramatic reduction in cleaved caspase-3 positive cells that localised towards the tissue edges following dexamethasone treatment. At 30 hours post dexamethasone treatment, there was no evidence of apoptotic cells. The vehicle-treated conditions did not display any caspase-3 positive cells. Quantification of the percentage of cleaved caspase-3 stained cells showed an increase in ROCK1wt and ROCK1nc cohorts compared to vehicle treated mice (Figure 4-8). Roughly, a 3 fold increase in the percentage of cleaved caspase-3 staining was seen in Dex-treated ROCK1wt and ROCK1nc sections at 12 hours compared to 6 hours post treatment. It should be noted that at 6 and 12 hours post treatment, the enhanced percentage of caspase-3 staining would likely be significant if there were an increase mice numbers in ROCK1wt and ROCK1nc cohorts. Interestingly, the percentage of cleaved caspase-3 stain peaked at 12 hours, and dramatically reduced by 24 hours. The percentage of cleaved caspase-3 staining was statistically higher than vehicle controls for both genotypes. At 30 hours post treatment, the percentage of cleaved caspase-3 staining was low, comparable to vehicle-treated mice for both genotypes.

Vehicle treated mice, as expected, contained almost negligible levels of apoptotic cells. The rapid effect of dexamethasone that induced a trend of apoptotic cell detection arising at 6 hours, peaking at 12, and reducing at 24 and further at 30 hours, as well as the localisation of apoptotic cells were comparable between ROCK1wt and ROCK1nc mice. Taken together, the ROCK1nc mutation did not alter the effects of dexamethasone or the responses of the thymic tissue to dexamethasone. ROCK1nc mice exhibited no differences compared to ROCK1wt mice when treated with dexamethasone.

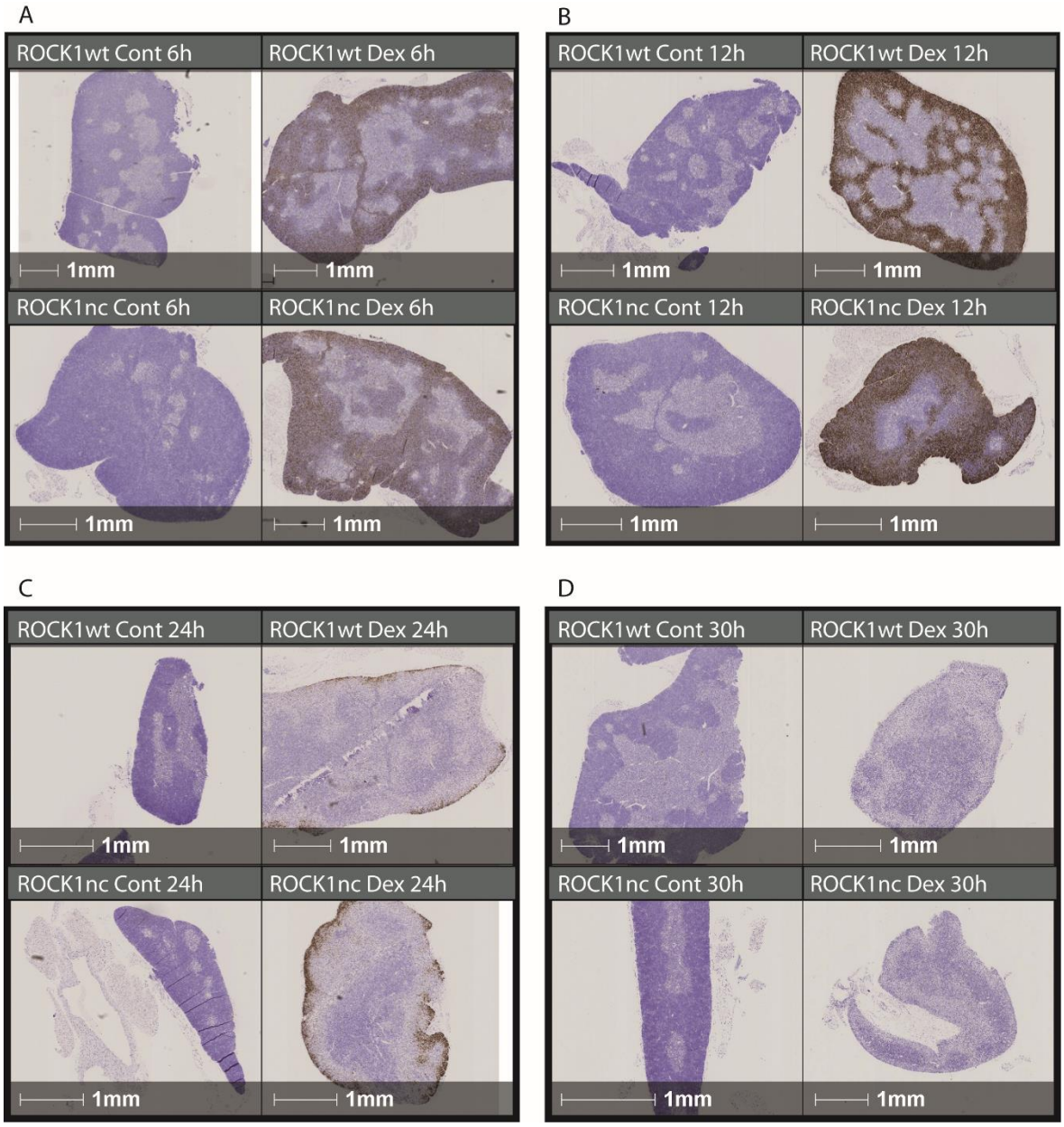

Figure 4-7 Representative cleaved caspase-3, staining of ROCK1wt and ROCK1nc thymi. ROCK1wt and ROCK1nc, 8 week old female mice were administered with dexamethasone-21 phosphate disodium salt (Dex) or vehicle control (cont) at 15 mg/kg I.P. The thymus was harvested at 6, 12, 24 and 30 hours post Dex treatment. Formalin-fixed, paraffin embedded tissues were sectioned at 4 µm and stained for cleaved caspase-3, a marker of apoptosis. Sections are representative of those quantified in Figure 4-8. (6, 12, 30 hours – N=2-3 for each genotype; 24 hours N = 5-7). Scale bars denote 1 mm in length.

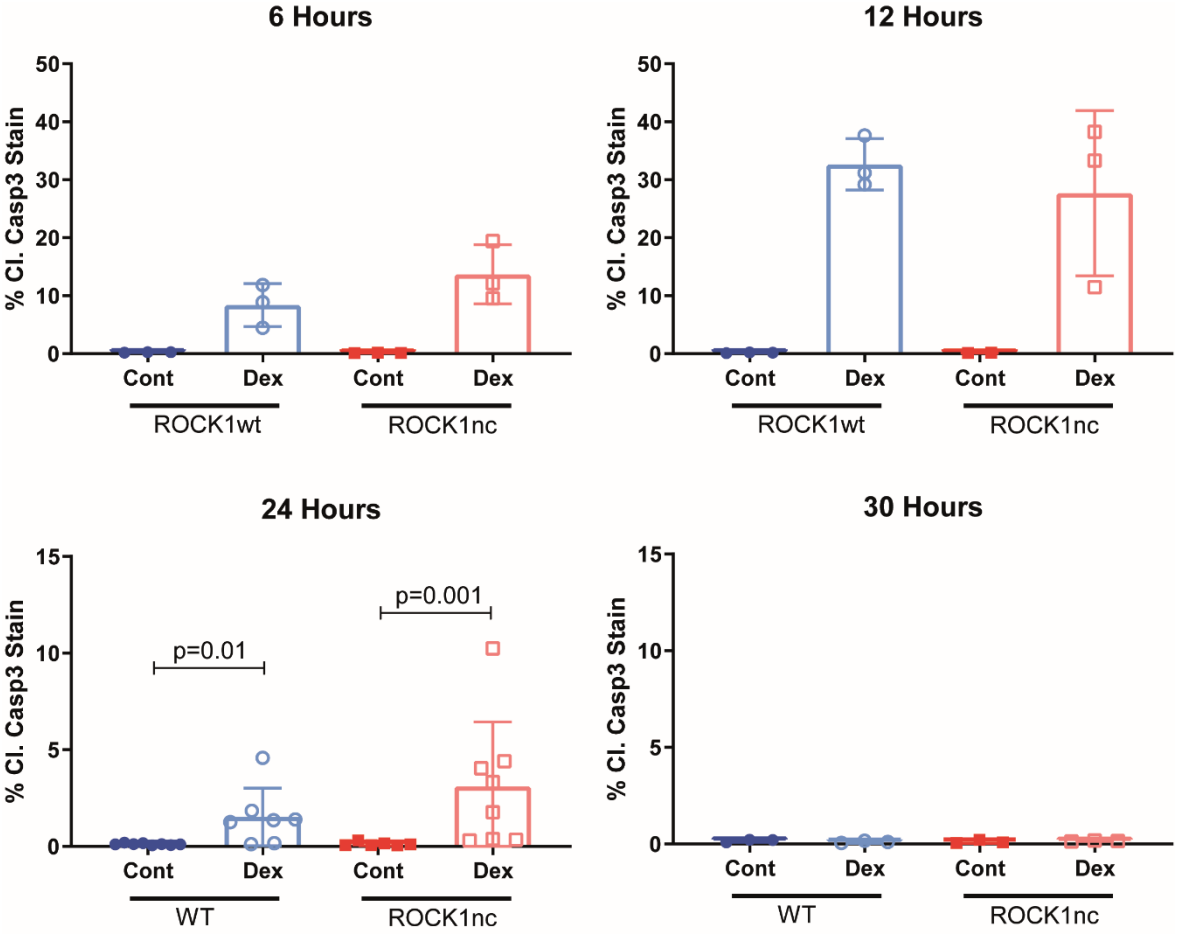

Figure 4-8 Dexamethasone-induced apoptosis occurs similarly in ROCK1wt and ROCK1nc thymic tissue. ROCK1wt and ROCK1nc 8 week old female mice were administered with dexamethasone-21 phosphate disodium salt (Dex) or vehicle control (cont) at 15 mg/kg I.P. Representative tissues were shown in Figure 4-7. The thymus was harvested at 6, 12, 24 and 30 hours post Dex treatment. Formalin-fixed, paraffin embedded tissues were sectioned at 4 µm and stained for cleaved caspase-3 (cl. casp3), a marker of apoptosis. The percentage of the area of cl. casp3 stain to tissue area was quantified using HALO™. Data points represent individual mice, error bars represent mean ± SD. Statistical signifcance was determined using a Mann-Whitney test comparing dex-treated to cont-treated cohorts per genotype. (6 hours N=2-3; 12 hours N=2-3; 24 hours N=5-7; 30 hours N=2-3). Note the scale difference for 24 and 30 hours post dex treatment.

4.2.4 Immune cell infiltration in dexamethasone treated ROCK1wt and ROCK1nc mice

In addition to causing apoptosis, 15 mg/kg dexamethasone administration to ROCK1wt and ROCK1nc female mice also caused an infiltration of macrophages and neutrophils. These two cell populations assessed as neutrophils and monocytes (the latter which differentiate into macrophages), are typically known to be first responders to sites of damage (Prame Kumar et al., 2018). FFPE thymic samples were sectioned and stained for the macrophage marker, F4/80, and subsequently quantified using HALO™ (Figure 4-9, Figure 4-10). At 6 and 12 hours post dexamethasone treatment, a small increase in the percentage of F4/80 staining, indicative of macrophage levels, was observed in both

ROCK1wt and ROCK1 treated cohorts (Figure 4-10). At later time points, 24 and 30 hours, representative images show a stark increase in the brown staining (Figure 4-9). This is reflected in the quantification, which show a significantly higher percentage of F4/80 stainingin dexamethasone treated ROCK1wt and ROCK1nc cohorts compared to vehicle treated controls. By 30 hours, the percentage of staining although not significant is still higher in dexamethasone treated cohorts for both genotypes compared to vehicle treated cohorts. The immunohistochemistry revealed that there were low number of macrophages in vehicle treated controls, consistent with what was seen previously in physiological levels (see Chapter 3). The dynamics of macrophage levels correlated with apoptotic kinetics seen previously (Figure 4-8).

In addition to macrophages, neutrophil infiltration was also investigated. The marker, anti-S100-A9 antibody was used to stain FFPE thymic tissues and quantified using HALO™ (Figure 4-11, Figure 4-12). Representative images show that levels of S100-A9 staining were barely detectable in vehicle-treated controls of both genotypes, low in dexamethasone treated ROCK1wt and ROCK1nc thymi at 6 and 12 hours post treatment, and increased at 24 and 30 hours post dexamethasone treatment in both genotypes (Figure 4-11). It should be noted, particularly at 30 hours, there was more non-specific S100-A9 staining visible in the representative images. Interestingly, despite the non-specific staining, the cells positive for S100-A9 appeared to localise towards the edges. Once quantified, the percentage of S100-A9 staining, indicative of neutrophil levels, were only slightly increased in dexamethasone treated ROCK1wt and ROCK1nc cohorts at 6 and 12 hours (Figure 4-12). By 24 hours, there was a statistically significant increase in the percentage of S100-A9 staining in dexamethasone-treated cohorts compared to vehicle treated cohorts of both genotypes. Levels of S100-A9 staining decreased slightly by 30 hours for both genotypes. Similar to the trend with macrophages, the levels of neutrophils seemed to peak at 24 hours, which coincided with the apoptotic cell dynamics.

Taken together, these data sets show that the *in vivo* challenge with dexamethasone resulted in an increase in neutrophils and macrophages in the thymus. This response was seen in the ROCK1nc mice as well as wild-type counterparts. This suggests that the ROCK1nc mutation does not impair or

exacerbate the infiltration of phagocytic cells in response to apoptosis-inducing damage *in vivo*.

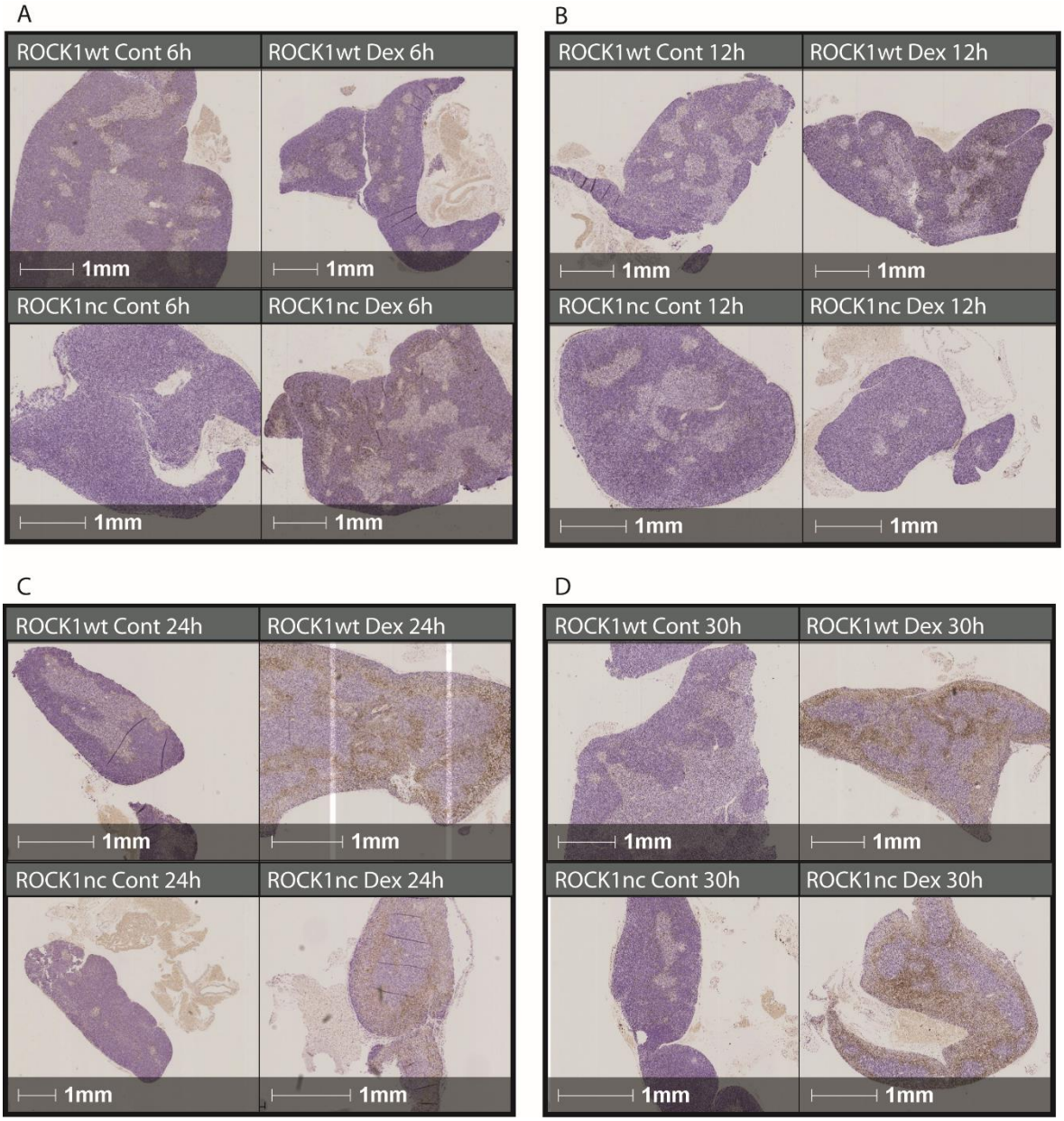

Figure 4-9 Representative F4/80 staining of ROCK1wt and ROCK1nc thymi. ROCK1wt and ROCK1nc 8 week old female mice were administered with dexamethasone-21 phosphate disodium salt (Dex) or vehicle control (cont) at 15 mg/kg I.P. The thymus was harvested at 6, 12, 24 and 30 hours post Dex treatment. Formalin-fixed, paraffin embedded tissues were sectioned at 4 µm and stained for F4/80, a marker of macrophages. Sections are representative of those quantified Figure 4-10. (6, 12, 30 hours – N=2-3 for each genotype; 24 hours N = 5-7). Scale bars denote 1 mm in length.

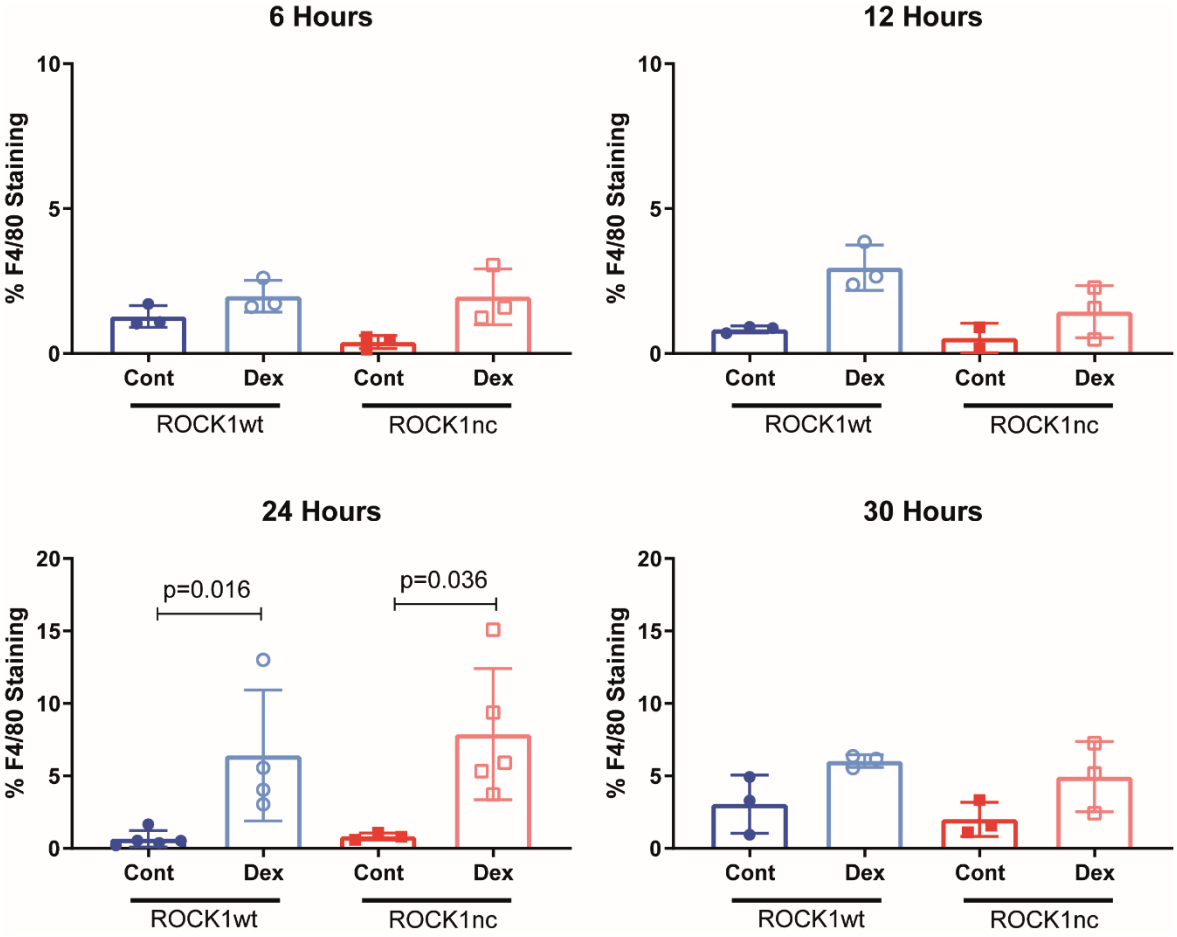

Figure 4-10 Dexamethasone-induced acute apoptosis resulted in macrophage infiltration in both ROCK1wt and ROCK1nc thymi. ROCK1wt and ROCK1nc 8 week old female mice were administered with dexamethasone-21 phosphate disodium salt (Dex) or vehicle control (cont) at 15 mg/kg I.P. Representative tissues were shown in Figure 4-9. The thymus was harvested at 6, 12, 24 and 30 hours post Dex treatment. Formalin-fixed, paraffin embedded tissues were sectioned at 4 µm and stained for F4/80, a macrophage marker. The percentage of the area of F4/80 staining to tissue area was quantified using HALO™. Data points represent individual mice, error bars represent mean ± SD. Statistical signifcance was determined using a Mann-Whitney test comparing Dex-treated to cont-treated cohorts per genotype. (6 hours N=2-3; 12 hours N=2-3; 24 hours N=5-7; 30 hours N=2-3). Note the scale difference for 6 and 12 hours post dex treatment.

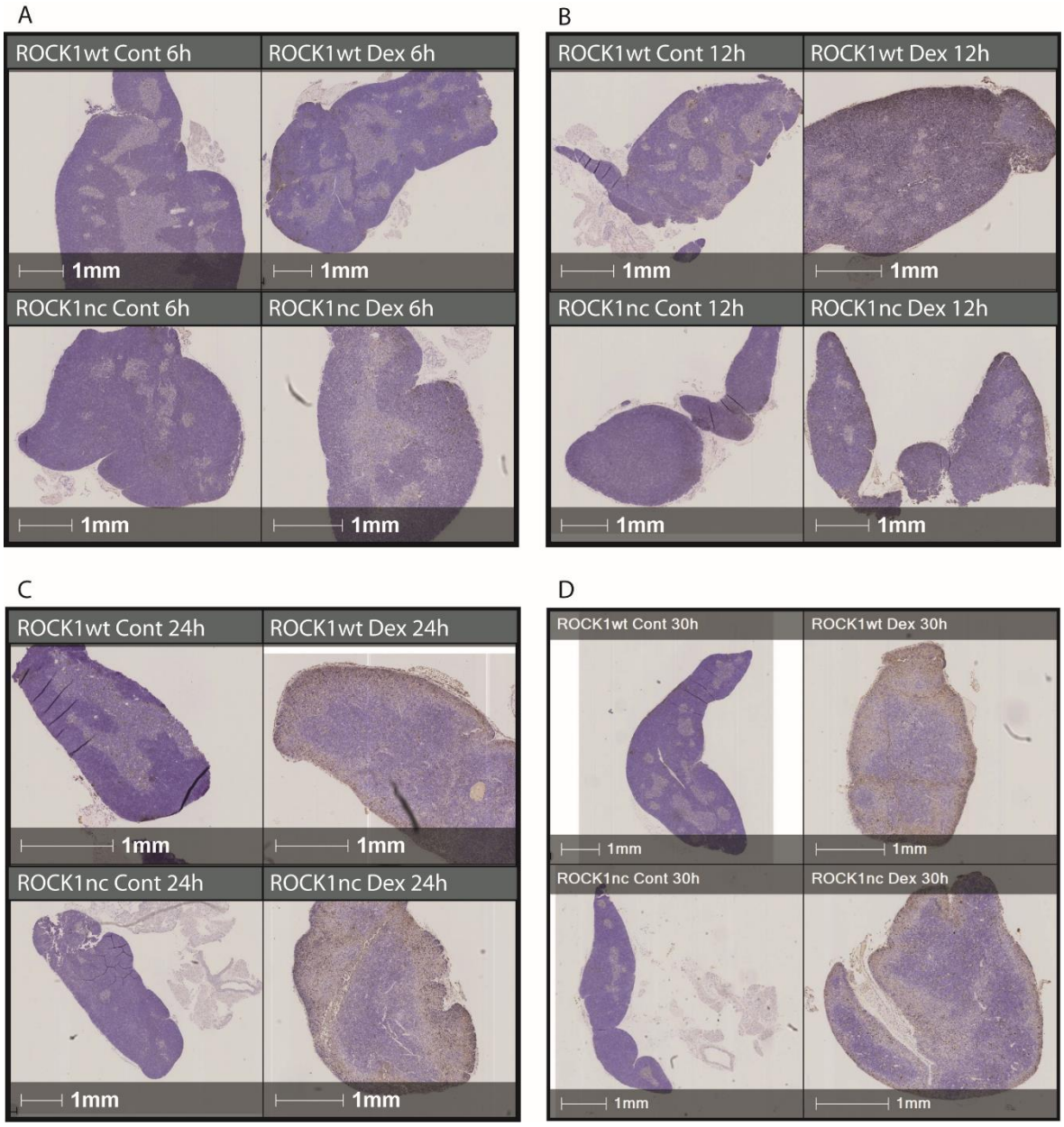

Figure 4-11 Representative S100-A9 staining of ROCK1wt and ROCK1nc thymi. ROCK1wt and ROCK1nc 8 week old female mice were administered with dexamethasone-21 phosphate disodium salt (Dex) or vehicle control (cont) at 15 mg/kg I.P. The thymus was harvested at 6, 12, 24 and 30 hours post dex treatment. Formalin-fixed, paraffin embedded tissues were sectioned at 4 µm and stained for S100-A9, a marker of neutrophils. Sections are representative of those quantified Figure 4-10. (6, 12, 30 hours – N=2-3 for each genotype; 24 hours N = 5-7). Scale bars denote 1 mm in length

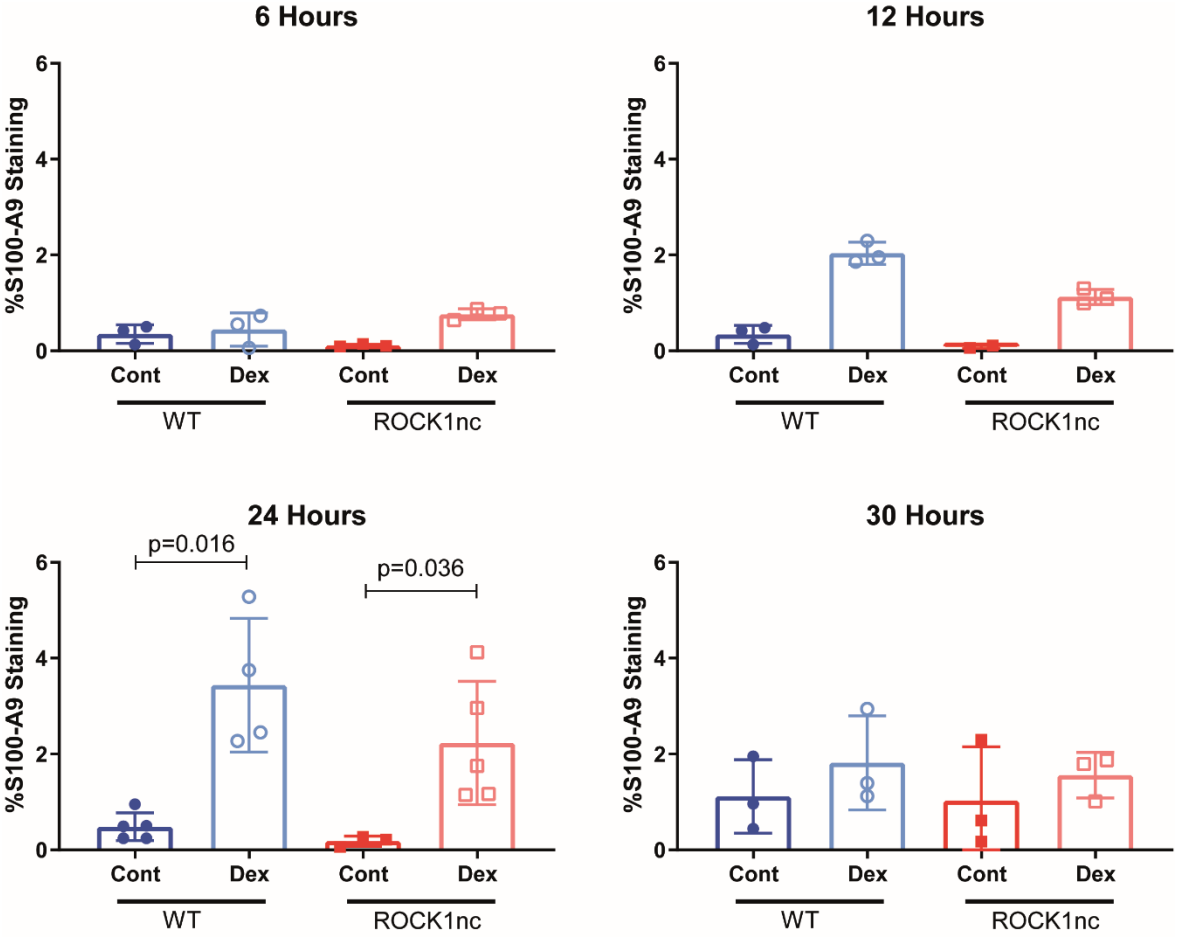

Figure 4-12 Dexamethasone-induced acute apoptosis resulted in neutrophil infiltration equally in ROCK1wt and ROCK1nc mice. ROCK1wt and ROCK1nc 8 week old female mice were administered with dexamethasone-21 phosphate disodium salt (Dex) or vehicle control (cont) at 15 mg/kg I.P. Representative tissues were shown in Figure 4-11. The thymus was harvested at 6, 12, 24 and 30 hours post Dex treatment. Formalin-fixed, paraffin embedded tissues were sectioned at 4 µm and stained for S100-A9, a neutrophil marker. The percentage of the area of S100-A9 staining to tissue area was quantified using HALO™. Data points represent individual mice, error bars represent mean ± SD. Statistical signifcance was determined using a Mann-Whitney test comparing Dex-treated to cont-treated cohorts per genotype. (6 hours N=2-3; 12 hours N=2-3; 24 hours N=5-7; 30 hours N=2-3). Note the scale difference for 6 and 12 hours post dex treatment.

4.2.5 Apoptotic thymocytes result in higher levels of immune cells in the ROCK1nc peritoneum

Thus far, there did not appear to be any perturbation in ROCK1nc mice compared to ROCK1wt mice. As the ROCK1nc mutation is found in all cell types, isolating the immune response to apoptotic cells using an adoptive transfer experimental model allowed me to assess the ROCK1nc mutation in two ways – the apoptotic cells and the ability of the immune system to respond to the apoptotic cells. The adoptive transfer experiment consisted of 4 combinations, administering apoptotic ROCK1nc thymocytes into ROCK1wt and ROCK1nc host mice, as well as ROCK1wt thymocytes into ROCK1wt and ROCK1nc host mice

(Figure 4-13). Briefly, donor thymocytes from either ROCK1nc or ROCK1wt mice were isolated into suspension and treated *ex vivo* with 1 μm dexamethasone for 4 hours. Following treatment, ROCK1wt or ROCK1nc recipient mice were subject to intraperitoneal (IP) injection of $5x10^6$ cells of the treated cells. It should be noted that apoptotic cells from the same preparations were injected into ROCK1wt and ROCK1nc mice. Mice were culled 2 hours post injection. The peritoneal washout cells were collected and subsequently stained for immune cell markers for flow cytometry analysis. The gating strategy depicts the cellular populations assessed, including T-cells, monocytes, macrophages, dendritic cells, neutrophils, as well as surface activation markers including CD80, CD86, and the major histocompatibility class II (MHC-II) (Figure 4-14).

The adoptive transfer experiments carried out was done with all possible combinations (Figure 4-13). Donor ROCK1wt thymocytes were injected in ROCK1wt and ROCK1nc mice, and vice versa with ROCK1nc thymocytes into ROCK1wt and ROCK1nc mice. Interestingly, the immune cell populations assessed were higher in ROCK1nc recipients, regardless of donor origin, compared to ROCK1wt recipients (Figure 4-15, Figure 4-16). There were significantly higher level of monocytes that were recruited to the peritoneum regardless of donor genotype, in ROCK1nc recipients (Figure 4-15). In a similar fashion, ROCK1nc recipients had a higher dendritic cell count from ROCK1wt and ROCK1nc donor thymocytes. ROCK1nc thymocytes in ROCK1nc recipients were statistically significantly to ROCK1wt recipients injected with ROCK1nc thymocytes. No differences were observed in the combinations of conditions for the levels of neutrophils recruited to the peritoneum. Furthermore, ROCK1nc recipients yielded higher T-cell counts compared to ROCK1wt recipients. ROCK1wt recipients injected with apoptotic ROCK1nc thymocytes did yield significantly lower T-cells in comparison to ROCK1nc recipients injected with ROCK1nc thymocytes.

Consistent with a general increase of immune cells, the macrophage population was significantly increased in ROCK1nc recipients, regardless of donor genotype (Figure 4-16). The macrophage activation status can be assessed with the surface markers, MHCII, CD80 CD86. These three markers are co-stimulatory molecules that are upregulated on antigen presenting cells, implying a more inflammatory-like macrophage. Interestingly, the mean fluorescence intensity

(MFI), which signifies the level of the surface staining, was significantly lower in macrophages from ROCK1nc recipients, regardless of donor genotype, compared to ROCK1wt recipients. The intensity of CD80 and CD86 were at comparable levels in the different conditions. Despite higher levels of macrophages in the ROCK1nc host, lower levels of co-stimulatory molecules could allude to an anti-inflammatory phenotype of the cells, regardless of donors.

Taken together, these data would suggest that the ROCK1nc mutation in the whole body recipient does yield a different response to injected apoptotic cells. Interestingly however the genotype of the donor apoptotic thymocytes themselves did not matter as much as the genotype of the recipient itself. This experiment suggests that the ROCK1nc mutation could affect cell clearance and the immune response towards apoptotic cells.

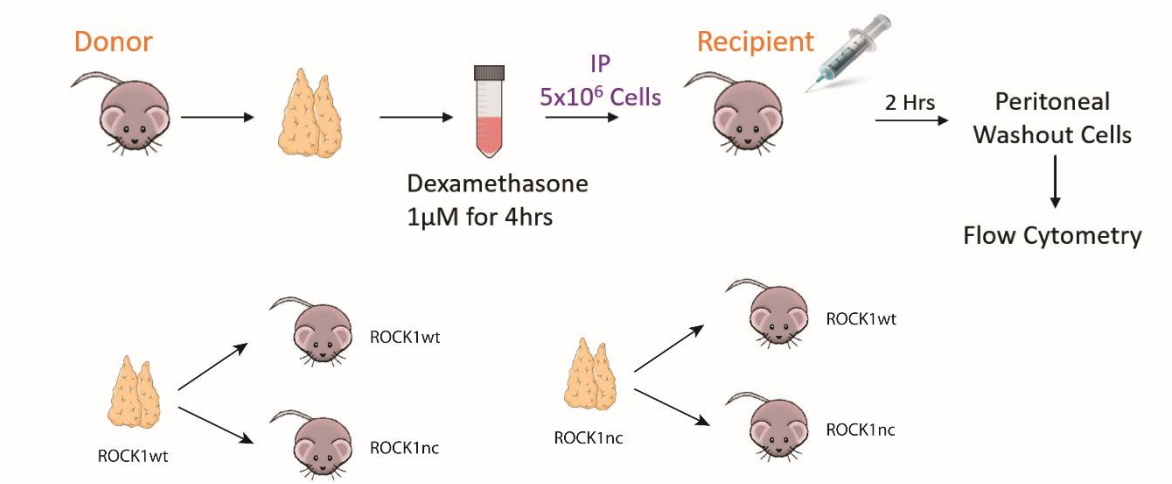

Figure 4-13 Schematic representation of the adoptive transfer experimental setup. A schematic representation of the adoptive transfer experiment. Donor and recipient mice were from the same colony, thus were matched in their genetic background as C57Bl/6 mice. Donor and recipient mice were further age (6-8 weeks) and gender matched. The thymus from ROCK1wt or ROCK1nc donor mice were isolated into suspension and treated *ex vivo* with 1 µm dexamethasone for 4 hours. Treated cells were then injected intraperitoneal (IP) at $5x10^6$ cells to the appropriate recipients. The peritoneal washout cells were obtained 2 hours after cellular injections and stained with cell surface markers for assessment by flow cytometry.

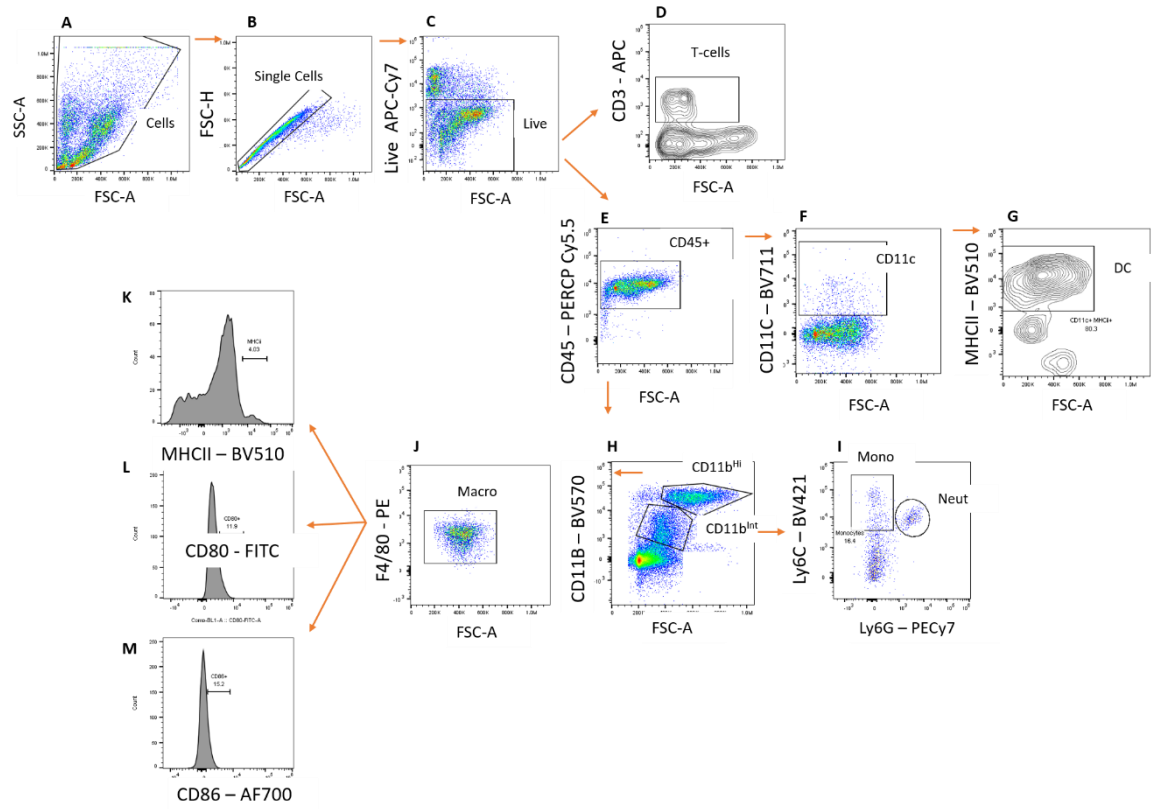

Figure 4-14 Representative gating strategy for the detection of immune cells. All cells were gated in panel A, selected for single cells in panel B, and gated for live cells in panel C. T-cells were gated based on CD-3 positivity (panel D). Immune cells were selected based on CD45 positivity (panel E). Cells were then categorised based on CD11c positive (panel F) and subsequent MHCII positivity (panel G) to select for dendritic cells. Additionally, cells were gated for their CD11b positive (panel H). CD11b positive cells were further gated based on the Ly6C and Ly6G (panel I) positivity. Ly6C positive cells were the monocyte population whilst double positive Ly6C and Ly6G cells are the neutrophils. On the other hand, CD11b positive cells were also gated on the F4/80 marker, a macrophage surface marker (panel J). Macrophages were assessed for their activation status looking at MHCII (panel K) CD80 (panel L), and CD86 (panel M). Cells were run through the Attune flow cytometer and analysed using FloJo.

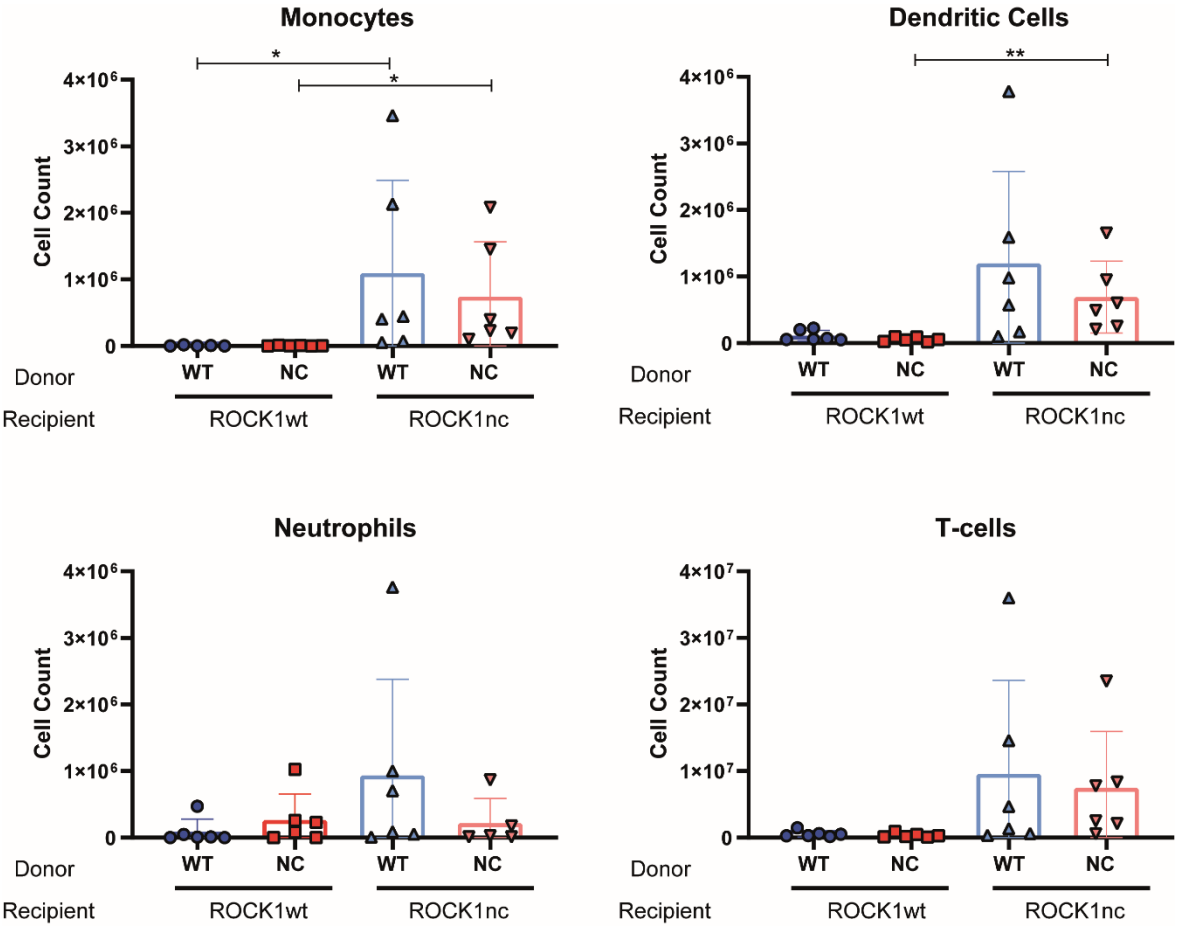

Figure 4-15 Immune cell populations are increased in ROCK1nc recipients. The thymus from ROCK1wt (WT) or ROCK1nc (NC) donor mice, were isolated into suspension and treated *ex vivo* with 1µM of dexamethasone for 4 hours. Treated cells were then injected intraperitoneal (IP) at $5x10^6$ cells into the appropriate recipients. It should be noted that the same cell prep at each injection was administered to the recipients. The peritoneal washout cells were obtained 2 hours after cellular injections and stained with cell surface markers for assessment by flow cytometry. Cell types assessed were monocytes, dendritic cells, neutrophils and T-cells. Data points represent individual mice, error bars represent mean ± SD. Statistical signifcance was determined using the Kruskal-Wallis test (*p<0.05; **p<0.01). (N=10 total donor mice; N=6 for each recipient group).

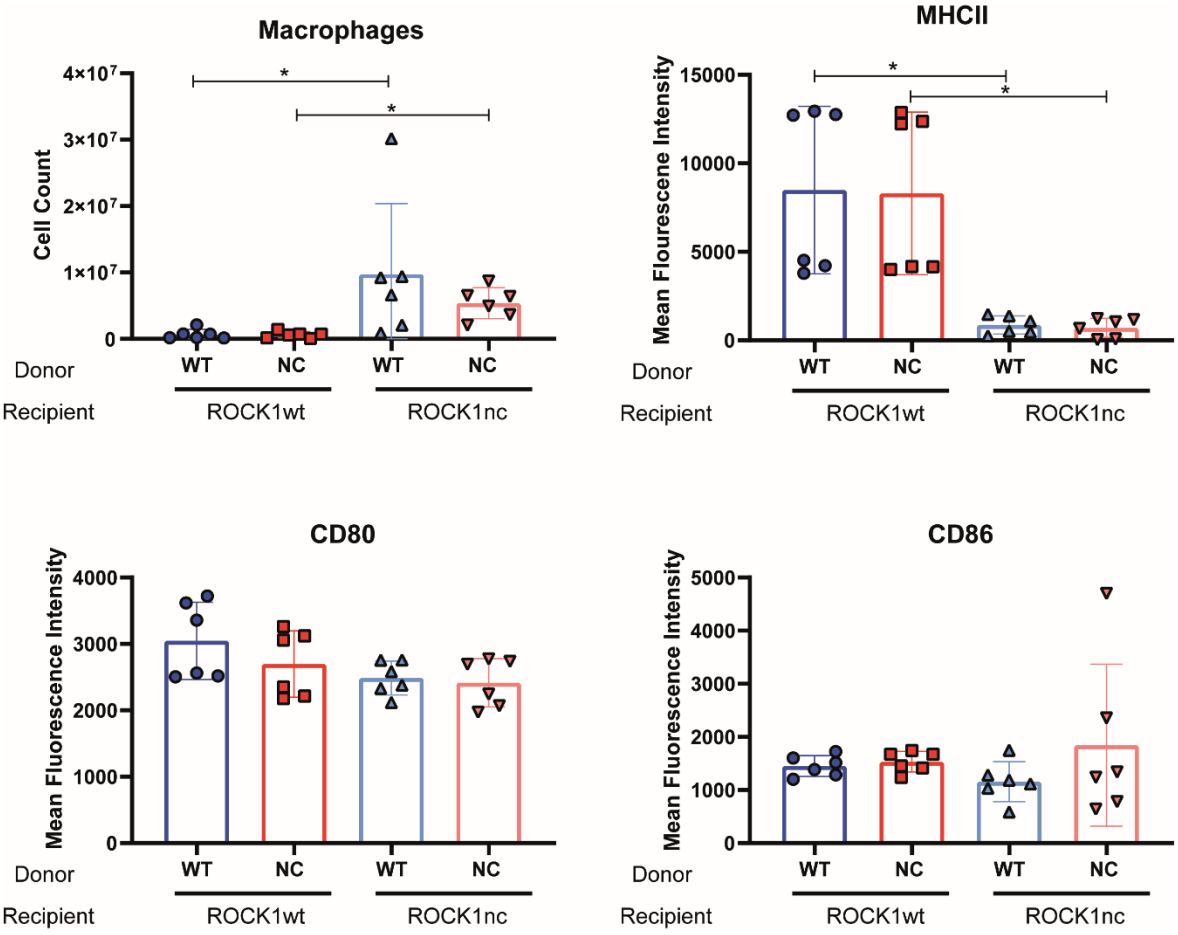

Figure 4-16 Higher levels of macrophages with lower levels of activation are found in ROCK1nc recipients. The thymus from ROCK1wt (WT) or ROCK1nc (NC) donor mice were isolated into suspension and treated *ex vivo* with 1 µm dexamethasone for 4 hours. Treated cells were then injected intraperitoneal (IP) at $5x10^6$ cells to the appropriate recipients. It should be noted that the same cell prep at each injection was administered to the recipients. The peritoneal washout cells were obtained 2 hours after cellular injections and stained with cell surface markers for assessment by flow cytometry. Macrophage populations and co-stimulatory molecules MHCII, CD80 and CD86 were also assessed. The mean fluorescence intensity signifies level of staining, taking into account the cell number. Data points represent individual mice, error bars represent mean ± SD. Statistical signifcance was determined using the Kruskal-Wallis test (*p<0.05; **p<0.01). (N=10 total donor mice; N=6 for each recipient group).

4.2.6 Phagocytosis is temporarily altered with the ROCK1nc mutation

Phagocytosis, or efferocytosis, is required for efficient cell clearance of apoptotic cells. As the ROCK1nc mutation is found all cells, including phagocytic cells, phagocytosis assays were utilised to explore how the mutation would affect not only apoptotic cells but also immune cells. Cells were obtained from the peritoneum of ROCK1wt and ROCK1nc mice and analysed for their immune cell makeup and phagocytic ability by flow cytometry (Figure 4-17). The peritoneal cell populations were composed of a variety of cells, including macrophages, dendritic cells, B-cells and T-cells (Figure 4-17A). Flow cytometry

results show that B-cells were the most abundant cell type found in the peritoneal washouts in both ROCK1wt and ROCK1nc mice. However, whilst T-cells next predominate the cell population of the ROCK1wt mice, it appeared that macrophages out-numbered T-cells in the ROCK1nc mice. Dendritic cells were the least abundant cell types in both genotypes.

The next step was to assess the phagocytic ability of the immune cells analysed. To this end, peritoneal washout cells from ROCK1wt and ROCK1nc mice were plated and incubated with fluorescent beads at a 2:1 ratio (beads:cells). Cells were harvested for flow cytometry analysis at 45 minutes and 4 hours post incubation to determine phagocytic capability. In addition to the beads, the inflammatory agent lipopolysaccharide (LPS) was added to some conditions to assess whether inducing immune cell activation would influence the ability of cells to undergo phagocytosis. In all cases, macrophages were the cell population that was positive for the fluorescent beads, suggesting that macrophages phagocytosed the beads (Figure 4-17). At 45 minutes post incubation, the macrophage populations from both ROCK1wt and ROCK1nc mice showed a similar intensity of bead fluorescence. The addition of LPS did not alter the intensity of fluorescence with the macrophages for either genotype. At 4 hours post incubation however, there was a significantly greater fluorescence intensity in ROCK1nc macrophages in comparison to ROCK1wt macrophages. The addition of LPS appeared to have further increased the fluorescence intensity in ROCK1wt macrophages, but not ROCK1nc macrophages. These data suggest that ROCK1nc macrophages have uptake more fluorescent beads, and are therefore more phagocytic prior to stimulation.

To extend these findings, phagocytosis was assessed using the Incucyte live cell imaging system, allowing for dynamic measurements over time. Using the same methods as previously discussed, the whole population of cells from peritoneal ROCK1wt and ROCK1wt washouts were incubated with fluorescent beads with and without LPS. Plates were then imaged using the Incucyte over 48 hours and analysed for overlapping fluorescence signals as a means to measure phagocytosis. Results show that ROCK1nc and ROCK1wt washout cells had increasing fluorescent signals over time (Figure 4-18A). ROCK1wt and ROCK1nc cells in this assay behaved in the same manner. Interestingly, the addition of LPS resulted in lower fluorescence intensity than without LPS.

Following on from bead internalisation, the Incucyte was also used to measure phagocytosis of apoptotic cells. In order to do this, ROCK1wt and ROCK1nc mice were crossed onto a Lifeact-green fluorescent protein (GFP) mouse to obtain fluorescently labelled peritoneal washout cells. The peritoneal washout cells from GFP-ROCK1wt and GFP-ROCK1nc mice were isolated and plated to adhere prior to co-incubation with apoptotic cells. Thymocytes isolated from ROCK1wt and ROCK1nc mice were subject to either control, dexamethasone (1 μM) or UVC (0.3 J/m^2) treatment for an hour then labelled with a specific dye, pHrodo, that fluoresces only when there is a marked pH change as occurs inside a lysosome. Donor thymocytes were plated with peritoneal washout cells at a 1:1 ratio. Plates were then imaged using the Incucyte and analysed for overlapping fluorescent signals. All conditions were accounted for, *i.e.* donor thymocytes from both ROCK1wt and ROCK1nc mice were plated with washout cells from the two genotypes. Apoptotic cells treated with vehicle control from both ROCK1wt and ROCK1nc did not yield different signals when co-incubated with peritoneal cells from either genotype (Figure 4-18B). Interestingly, in the dexamethasone-treated thymocytes, ROCK1nc thymocytes with ROCK1nc peritoneal washout cells seemed to have a trend for greater overlap compared to the other conditions (Figure 4-18C). ROCK1nc thymocytes when co-incubated with ROCK1wt washout cells also seemed to yield a higher overlap in fluorescence. However, the UVC-treated thymocytes of both genotypes resulted in similar percentage overlaps for all conditions (Figure 4-18D). The results here suggest that whilst under control and UVC inductions there were no differences in the phagocytic ability of peritoneal wash out cells, washout cells did have an increased affinity to phagocytose ROCK1nc thymocytes pre-treated with dexamethasone.

The flow cytometry data showed that although there was a mixed population of cells, macrophages were likely to be the predominant phagocytic population. The ROCK1nc mutation may have affected the phagocytic population. At early time points post incubation, flow cytometry data indicated that ROCK1nc cells may be capable of more phagocytosis. However, this may be resolved as the Incucyte data, which looks at phagocytosis at more long term durations, would suggest that the uptake of beads was similar between the two genotypes. However, co-incubation with apoptotic ROCK1nc thymocytes treated with

dexamethasone resulted in a higher level of phagocytosis regardless of the genotype of the phagocytic cells.

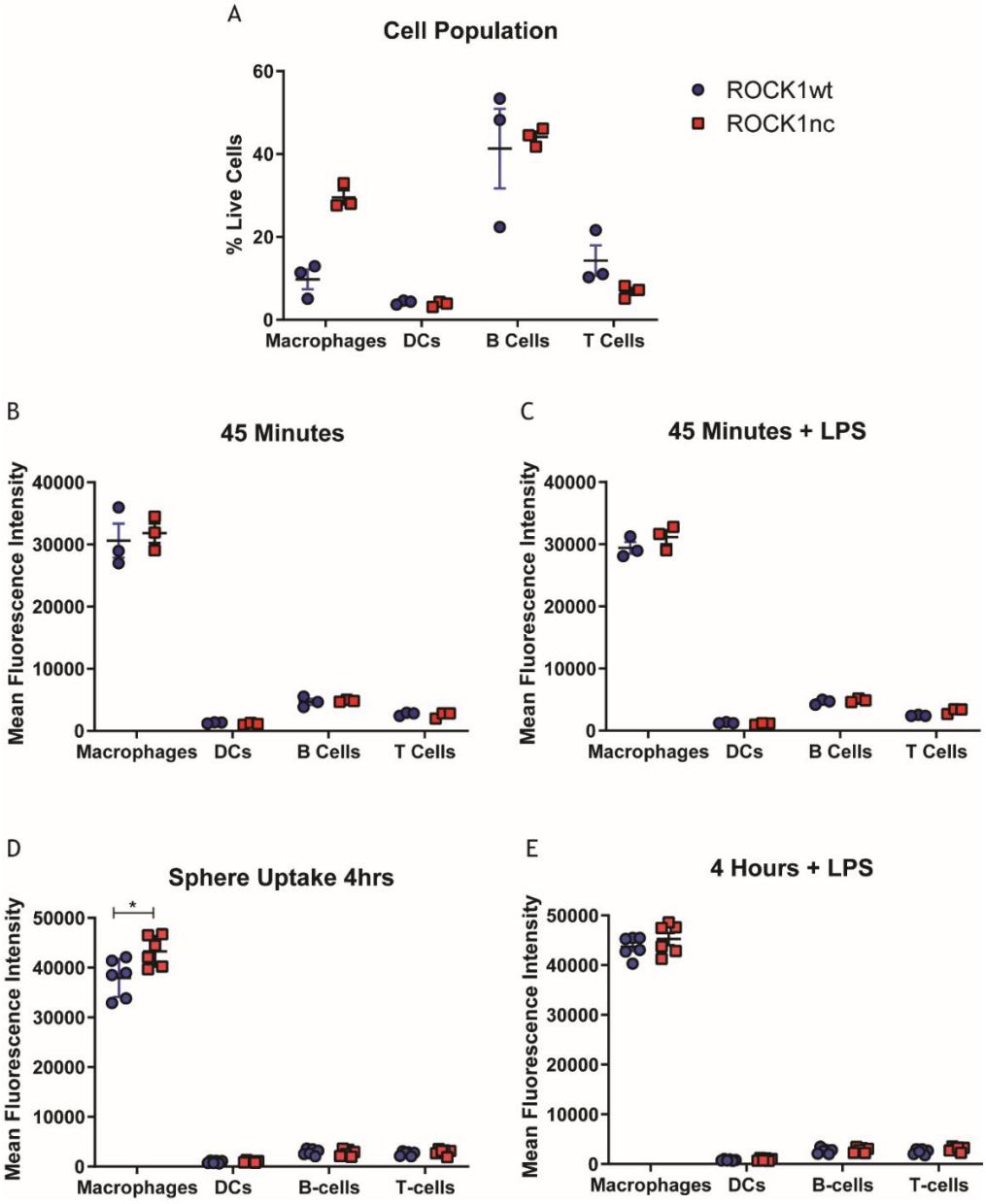

Figure 4-17 ROCK1nc macrophages may have greater phagocytic abilities in the short term. **P**eritoneal washout cells were isolated from ROCK1wt and ROCK1nc mice and assessed for the immune cell subtypes and their ability to uptake fluorescent beads. A) Flow cytometry results showing cell populations in peritoneal washouts. B,C/D, E) The washout cells were incubated at a 2:1 ratio (fluorescent beads:cells) with and without lipopolysaccharide (LPS 200 ng/ml). Cells were harvested 45 minutes (B/C) and 4 hours (D/E) post co-incubation and stained for immune cells (as in A). Flow cytometry data was analysed using FloJo V10 to determine the phagocytic ability of the immune cells by looking at positivity of the fluorescent beads. Data points represent individual mice, error bars represent mean ± SD. Statistical signifcance was determined using the Kruskal-Wallis test (*p<0.05;). (N=3 for immune cell characterisation and 45 minute time points; N=6 for 4 hour time points).

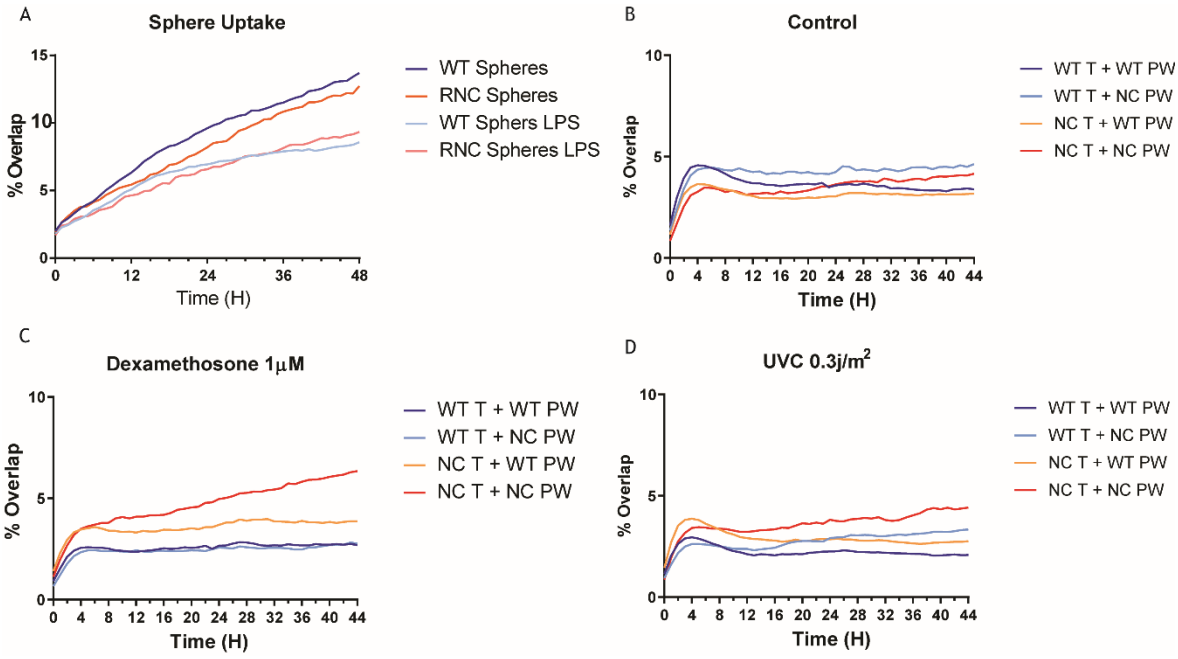

Figure 4-18 The ROCK1nc mutation does not alter phagocytosis in the long term. A) Peritoneal washout cells were isolated from ROCK1wt (WT) and ROCK1nc (RNC) mice. Cells were co-incubated with fluorescent beads at a 1:1 ratio, with or without the addition of lipopolysaccharide (LPS 200 ng/ml). Plates were then put into the Incucyte and imaged once every hour with 3 phase contrast and red fluorescent signal images per well for a period of 48 hours. Images were analysed for the overlap between cells and fluorescent signals as a readout for phagocytosis. C/D) Peritoneal washout cells (PW) were isolated from GFP-ROCK1wt and GFP-ROCK1nc mice. Thymocytes (T) obtained from ROCK1wt and ROCK1nc mice were pre-treated with either vehicle control, dexamethasone (1 μM), or UVC (0.3 J/m^2), labelled with pHrodo dye, then co-incubated with washout cells at 1:1 ratio. Plates were put into the Incucyte and imaged once every hour with 3 images per well for a phase contrast, green and red fluorescent signals for 44 hours. Control wells were used for spectral unmixing to normalise the signal intensities and bleed-through between the signals. Images were analysed for the overlap between cells and fluorescent signals as a readout of phagocytosis. The line represents the mean (N=5 biological replicates, with triplicates per experiment). Due to the great variability, the error bars are not shown.

4.2.7 The ROCK1nc mutation does not alter the release of intracellular contents from apoptotic thymocytes

Apoptotic cells are often self-contained, limiting the release of intracellular contents that could otherwise provoke an immune response. Cells that die via necrosis, or secondary necrosis, release intracellular contents known as damage associated molecular patterns (DAMPs) such as adenosine triphosphate (ATP) (Rock and Kono, 2008). If the ROCK1nc mutation alters the apoptotic morphology, this could alter the release of intracellular contents from apoptotic thymocytes. In order to investigate this, a lactate dehydrogenase (LDH) assay was used to assess the release of intracellular contents using LDH as a proxy. Briefly, thymocytes isolated from ROCK1wt and ROCK1nc mice were treated with dexamethasone (1 μM) for 4, 8 and 24 hours. Post incubation, LDH release was assessed using a chemiluminescence assay. The results show that there were no

increases in the levels of LDH detection with the treatment of dexamethasone at 4, 8 or 24 hours for either ROCK1wt or ROCK1nc thymocytes (Figure 4-19). In fact, the detection of LDH has not altered over time regardless of treatment and regardless of genotype. The results of this assay would suggest that neither dexamethasone treatment nor the ROCK1nc mutation altered the release of LDH.

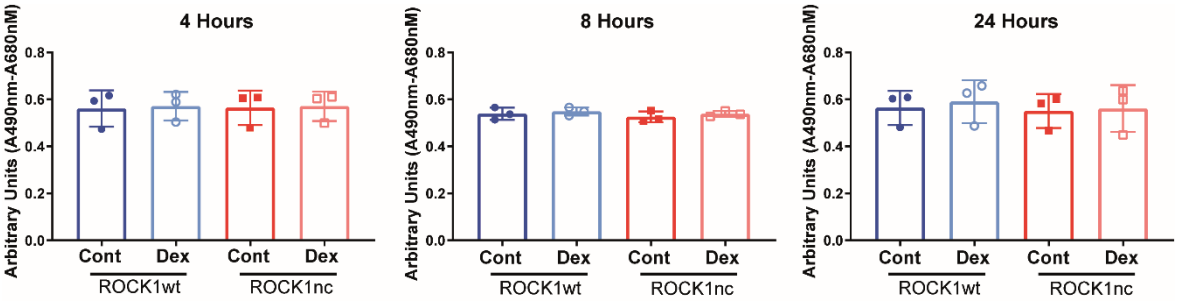

Figure 4-19 The release of intracellular content was unchanged in ROCK1nc apoptotic thymocytes. Thymocytes isolated from the thymus of ROCK1wt and ROCK1nc mice were treated with a vehicle control (cont) or dexamethasone (Dex) at 1 µM. At 4, 8 and 24 hours post treatment, an LDH assay was performed to detect the levels of LDH in the supernatant, a marker of the release of intracellular contents. Data points represent individual mice, error bars represent mean ± SEM (N=3 per group).

4.2.8 Apoptotic thymocytes do not conclusively bleb

So far, any differences between ROCK1wt and ROCK1nc were subtle or not sustained for long periods of time. The obvious question following these experiments is whether thymocytes bleb. In order to investigate this, thymocytes isolated from the thymus of ROCK1wt and ROCK1nc mice were treated with a vehicle control or dexamethasone. Cells were then fixed and imaged using scanning electron microscopy (SEM) 4 and 8 hours after dexamethasone treatment. Thymocytes are small in diameter, ranging roughly from 4-7 µm according to the literature (Abe and Ito, 1970). The microscopy images showed that the thymocytes from ROCK1wt and ROCK1nc mice were indeed approximately 4-7 µm in diameter (Figure 4-20, Figure 4-21). At 4 hours, ROCK1wt and ROCK1nc thymocytes looked relatively healthy. As thymocytes often undergo spontaneous apoptosis when outside of the thymus, a small number of cells had some small circular membrane areas, likely to be blebs. In the vehicle control group, the majority of ROCK1wt and ROCK1nc thymocytes appeared to be round and healthy (Figure 4-20). Representative images do show a thymocyte with what could be described as a bleb in the ROCK1wt control

condition (red circle). In the dexamethasone-treated ROCK1wt thymocytes, more cells had a distinct morphology. It could be interpreted that these cells were apoptotic. Only a minority of cells showed this morphology. The ROCK1nc thymocytes did not seem to deviate far from the round shape, but rather seemed somewhat smoother on their surface.

At 8 hours, control treated ROCK1wt and ROCK1nc thymocytes appeared similar in their morphologies (Figure 4-21). Dexamethasone-treated thymocytes had more cells with an altered morphology. The representative images suggest that the dexamethasone-treated ROCK1wt may have apoptotic blebs, however this is the minority of the population. ROCK1nc thymocytes treated with dexamethasone did display some degree of altered cellular morphology, including cells that are oval-like and distorted. However, this altered morphology did not precisely resemble the round blebs seen in the ROCK1wt thymocytes. There was a low number of cells in both genotypes that exhibited altered morphology at 4 and 8 hours. Although it does seem that some thymocytes displayed apoptotic blebs in the ROCK1wt condition, it was not obvious as with other cell types, including mouse embryonic fibroblasts and hepatocytes (Julian, 2015, Naylor, 2019). Due to the variability, small numbers and inconsistencies in morphology, quantifications were not feasible. Therefore, it was difficult to conclusively determine if thymocytes do indeed display apoptotic membrane blebs or in the case of the ROCK1nc cells, display deficient apoptotic blebbing.

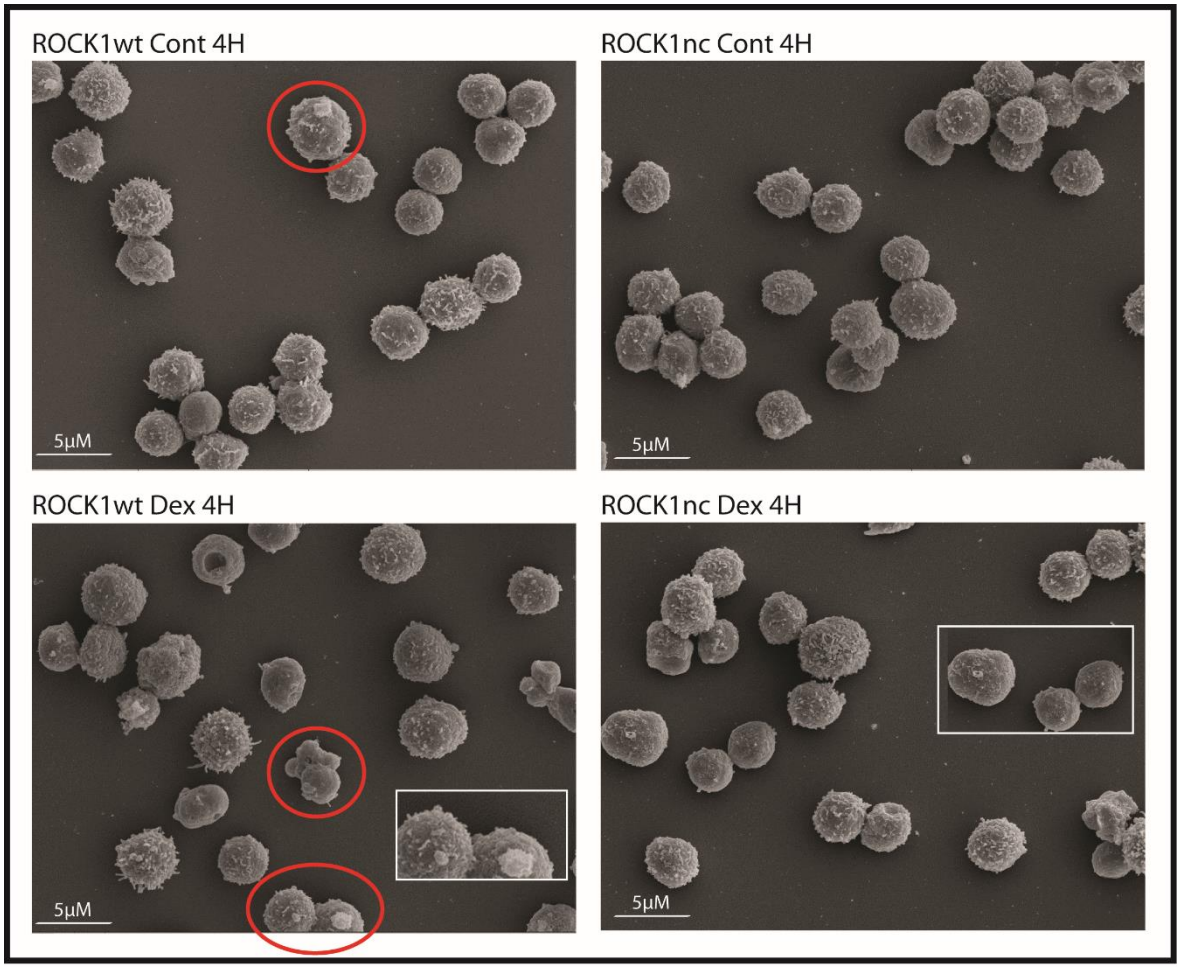

Figure 4-20 Representative scanning electron microscopy images of ROCK1wt and ROCK1nc thymocytes at 4 hours post dexamethasone treatment. Thymocytes were isolated from the thymus of ROCK1wt and ROCK1nc mice. Cells were treated with either a vehicle control (cont) or 1 µm dexamethasone (Dex) for 4 hours. Cells were then fixed and processed for scanning electron microscopy (SEM). These images were taken by Margaret Mullen at the University of Glasgow, with the JOEL 6400 scanning electron microscope. Red circles denote cells that seemed to have the blebbing phenotype in the ROCK1wt cells. The white squares are close up images of some of the cells found. This is representative of 2 biological replicates. Scale bars denote 5 µm in length.

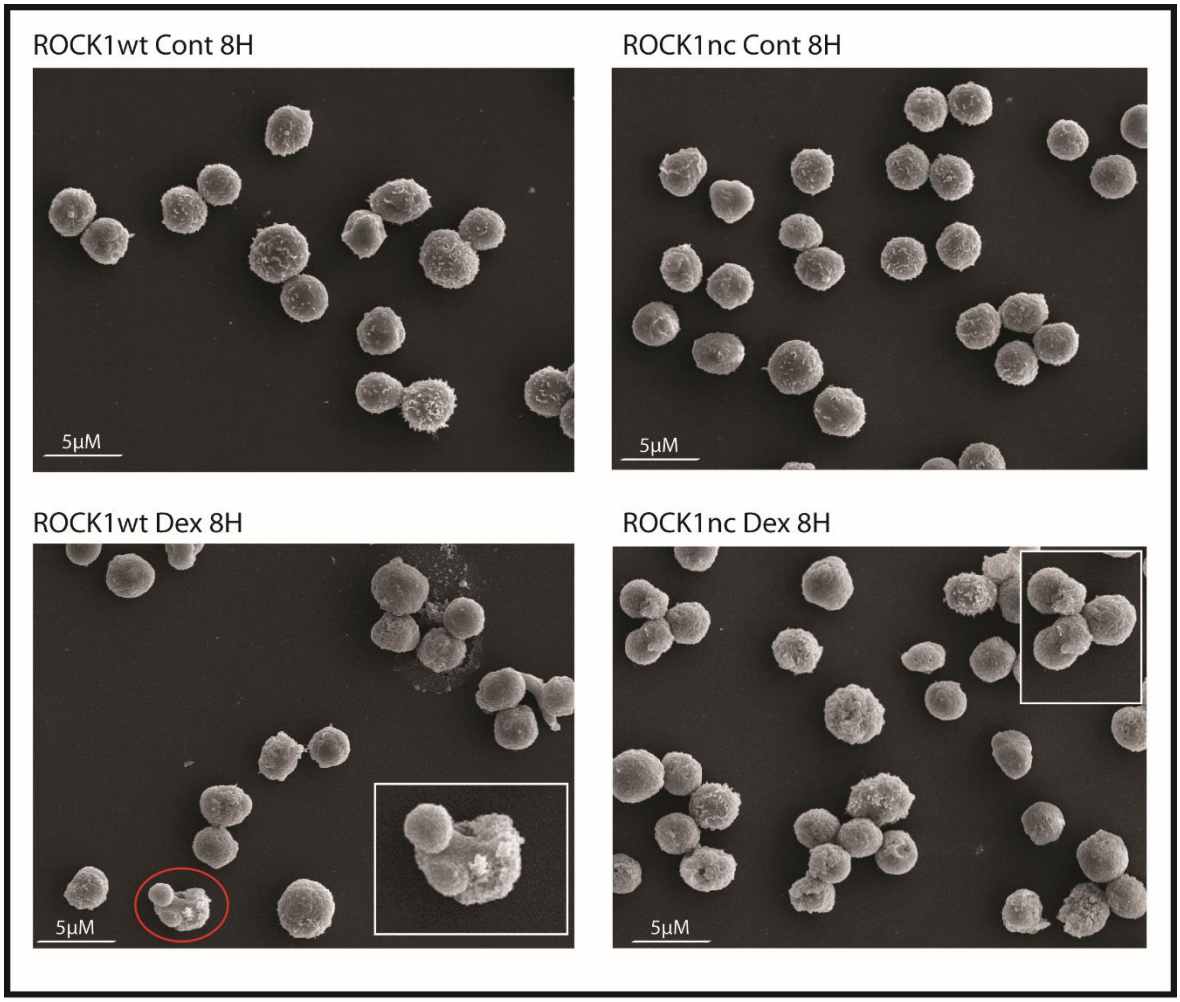

Figure 4-21 Representative scanning electron microscopy images of ROCK1wt and ROCK1nc thymocytes at 8 hours. Thymocytes were isolated from the thymus of ROCK1wt and ROCK1nc mice. Cells were treated with either a vehicle control (cont) or 1 µm dexamethasone (Dex) for 8 hours. Cells were then fixed and processed for scanning electron microscopy (SEM). These images were taken by Margaret Mullen at the University of Glasgow, with the JOEL 6400 scanning electron microscope. Red circles denote cells that seemed to have the blebbing phenotype in the ROCK1wt cells. The white squares are close up images of some of the cells found. This is representative of 2 biological replicates. Scale bars denote 5 µm in length

4.3 Discussion

This arm of the study was concerned with investigating the effects of the ROCK1nc mutation on apoptosis, cell clearance and immune responses. To this end, isolated thymocytes and mice were challenged in acute conditions. Dexamethasone, a glucocorticoid agonist that is known to cause lymphocyte apoptosis, was used to induce apoptosis in thymocytes (Cifone et al., 1999). Results from flow cytometry and western blotting revealed that dexamethasone did induce thymocyte death in both ROCK1wt and ROCK1nc cells to a similar degree. Thymocyte death was detected as early as 4 hours and at a more pronounced level by 8 hours for both genotypes. Additionally, western blots

showed that like ROCK1wt thymocytes, apoptotic ROCK1nc thymocytes display caspase-3 cleavage, confirming that apoptosis was occurring. The ROCK1nc mutation did not affect the biochemical mechanism of apoptosis and the kinetics of apoptosis at the points investigated. This set of results indicates that the ROCK1nc mutation did alter the ability of cells to undergo apoptosis or alter the apoptotic machinery.

The next step was to investigate the role of apoptotic membrane blebbing *in vivo* by introducing the apoptosis inducing agent, dexamethasone. Administering dexamethasone IP to ROCK1wt and ROCK1nc mice resulted in reductions in thymic and splenic weights. This is consistent with the selectivity of dexamethasone, as this drug targets lymphocytes. Reductions in the percentages of thymic and splenic to body ratios were seen at 6 hours. At 24 hours, a significant reduction was observed in thymic and splenic weight loss for both genotypes in dexamethasone-treated mice compared to vehicle-treated mice. This loss was sustained at 30 hours post dexamethasone treatment in both genotypes as well. In both instances, no differences were seen between the genotypes in dexamethasone treated mice. It should be noted that although statistical significance was not seen at other time points, this would be due to low numbers of mice sampled. For example, it is possible that the 30 hour time point would have been significant with a greater cohort number. From the thymi harvested in these experiments, vehicle-treated ROCK1wt and ROCK1nc mice had the same architecture, including the cortex and medulla, as untreated thymic tissues. The thymus of both ROCK1wt and ROCK1nc mice were similar to vehicle treated thymi at 6 and 12 hours post treatment. Interestingly, at 24 and 30 hours, the cortical areas were lighter suggesting a loss of cells in both ROCK1wt and ROCK1nc cohorts.

This was confirmed when the apoptotic levels were investigated using cleaved-caspase 3 staining. The cleaved caspase-3 staining revealed that cell death was evident at 6 hours and peaked at 12 hours. The majority of cleaved caspase-3 positive cells were found in the cortex. By 24 hours, the localisation of cleaved caspase-3 positive cells was at the edges, which disappeared by 30 hours. This reflects what was seen with the H&E stains, as the cortical cells were likely to be dead and cleared by 24 hours, hence why the cortical areas were lighter. The mode of action of dexamethasone targeting lymphocytes, particularly in the

cortex has been described (Ahmed and Sriranganathan, 1994). The kinetics observed in these experiments were similar to previously described results. Previous data have shown that dexamethasone-induced apoptosis was highly evident at 18 hours and barely detected at 24 hours (Ahmed and Sriranganathan, 1994). In addition to cleaved caspase-3 staining, another assay to assess apoptosis, the terminal deoxynucleotidyl transferase dUTP nick end labeling (TUNEL) assay, should be carried out to confirm the immunohistochemistry results observed here.

The cell death observed in the thymus from dexamethasone triggered recruitment of macrophages and neutrophils. Macrophages and neutrophils are generally the first responders at sites of damage. As such, results showed that there was a significant increase in the levels of neutrophils and macrophages at 24 hours post dexamethasone treatment compared to vehicle-treated cohorts. This was observed in both ROCK1wt and ROCK1nc genotypes. By 30 hours, the levels of these immune cells did decrease, which coincided with the kinetics of apoptosis that dexamethasone induced. Overall, this study investigating the acute effects of dexamethasone showed that the kinetics of apoptosis and responses to acute apoptosis induction in ROCK1nc mice was similar to ROCK1wt mice.

This set of results is in contrast to what might have been expected. Given the high apoptotic activity and ROCK1 levels in thymocytes, I expected that there would be a difference in the clearance of the dead cells, however this was not the case. This could suggest that the apoptotic morphology may not be important in thymic clearance or perhaps there were compensating mechanisms to ensure efficient clearance despite aberrations in apoptotic morphology. It is known that there are professional and nonprofessional phagocytes which are crucial to maintaining thymic homeostasis (Arandjelovic and Ravichandran, 2015). Nonprofessional phagocytes in the thymus, such as thymic epithelial cells, can aid in eliminating apoptotic cells. Additionally, as there are far greater thymocytes in comparison to macrophages, it has been proposed that macrophages phagocytose multiple apoptotic cells and corpses. Furthermore, although SEM images could not confirm apoptotic membrane blebbing in ROCK1wt and deficient apoptotic membrane blebbing in ROCK1nc thymocytes, ROCK1nc thymocytes did not look necrotic. Previous findings in the Olson lab

using mouse embryonic fibroblasts and hepatocytes have shown a necrotic-like phenotypes in ROCK1nc cells, which did not seem to occur in ROCK1nc thymocytes at the time points investigated (Julian, 2015, Naylor, 2019). Given the combination of both professional and non-professional phagocyte clearance and a potentially non-necrotic phenotype in ROCK1nc thymocytes, these factors could perhaps explain why results observed in ROCK1wt and ROCK1nc mice were similar upon dexamethasone challenge.

Following on from this, another method was utilised in order to explore the effect of the ROCK1nc mutation on apoptotic thymocytes would have in regards to immune responses and immune infiltrations. To this end, an adoptive transfer assay was carried out in which the effects of the apoptotic cells and resident phagocytic cells could be functionally separated, to compare to the ROCK1nc mouse that is a whole animal model. Across the board, the immune cell populations were higher in ROCK1nc recipients. Interestingly, the recipient genotype seemed to contribute to the changes more than the genotype of the donor apoptotic cells themselves. This indicates that the genotype of the apoptotic thymocytes and potentially, how the cells die is not as important. There are a few ways to interpret this set of results. One hypothesis is that the immune system is not as efficient as clearing out the apoptotic cells in the ROCK1nc mice. As more T-cells were observed, this was likely due to a combination of the thymocytes and infiltrating T-cells. In addition, the macrophage population, although higher in ROCK1nc recipients, had lower levels of MHCII.

In contrast, a more plausible hypothesis is that the ROCK1nc cells are trained and conditioned to respond differently than ROCK1wt cells due to higher inflammatory environment from defective apoptotic blebbing. The cells in the ROCK1nc mice are in a constant state of inflammation and thus have to adapt to deal, which is reflected in in the results shown here. The higher influx of immune cells coupled with the low activation status is consistent with previous results seen in the Olson lab. The ROCK1nc mice had lower levels of cytokines to begin with under physiological conditions, which could be an adaption to deal with the higher inflammatory state from defective apoptotic membrane blebbing (Julian, 2015). Taken together, these experiments suggest that ROCK1nc

mutation could affect a recipient mouse and its response to apoptotic cells regardless of the donor apoptotic cell genotype.

To interrogate this further, phagocytosis was investigated *in vitro*. ROCK1nc mice had higher levels of macrophages in comparison to ROCK1wt mice. It was also these macrophages which had the greater propensity to take up fluorescent beads as a surrogate of phagocytosis. This was shown at 4 hours post beads incubation, where ROCK1nc macrophages did have a significantly higher level of fluorescence, likely indicating higher phagocytic activity. This would suggest that at this time point, the ROCK1nc mutation has had an effect on the phagocytic cells. Despite this difference in the short term, in the long term using microscopy to analyse phagocytosis, elevated phagocytic capabilities of ROCK1nc macrophages was not sustained. However, flow cytometry is more accurate in discerning the different cell types and phagocytic levels and therefore, should be performed at a later time point. Levels of fluorescence in the peritoneal washout cells were comparable between ROCK1wt and ROCK1nc cells when co-incubated with beads. As seen with the flow cytometry data, the addition of LPS also reduced phagocytic activity as lower percentages of overlap between fluorescence and cells were observed. This phenomenon has been described in the literature, as LPS does inhibit the ability of macrophages to phagocytose (Feng et al., 2011).

The temporary increase in phagocytosis could be attributed to two main reasons – an off target effect of the ROCK1nc mutation or the activation of macrophages and immune cells prior to isolation. Given the non-apoptotic role of caspase-3 in macrophage polarity cytoskeletal reorganisation (Liu et al., 2016b), this could explain the enhanced phagocytosis at the shorter time point. Equally, as ROCK1nc mice seem to have a different, more anti-inflammatory milieu (Julian, 2015), this could explain the higher phagocytic capabilities as phagocytes can engulf more when not activated (Feng et al., 2011). Using bone marrow derived macrophages, and not peritoneal macrophages, for example could mitigate any changes the phagocytes may undergo in a whole body system. To this end, it would be important to assess the phenotypes and antigen presentation capabilities of the phagocytes, macrophages and dendritic cells. Utilising the ovalbumin-specific t-cell receptor transgenic mouse model (OT1 and OT2 system), antigen presentation capabilities of the phagocytes can be examined.

Isolated thymocytes from ROCK1wt and ROCK1nc were also pre-treated with either a vehicle control or death inducing agent, and labelled with pHrodo dye that fluoresces inside the acidic environment of lysosomes. Given the flow cytometry data, it was assumed that the washout cells responsible for phagocytosing the apoptotic cells were macrophages. As expected, vehicle treated thymocytes did not yield a difference when co-incubated with peritoneal washout cells irrespective of genotype. Dexamethasone treated ROCK1nc thymocytes in combination with ROCK1nc washout cells trended to having a greater percentage of fluorescence overlap. Out of the 5 biological repeats, 3 showed the same trend. This could possibly indicate that the ROCK1nc mutation could affect phagocytosis, especially when co-incubated with ROCK1nc washout cells. Results seen in the phagocytosis experiments indicate that there are no overall differences in how ROCK1nc phagocytes and ROCK1nc apoptotic thymocytes behave.

The flow cytometry data did point to a significant increase in phagocytic capability of ROCK1nc macrophages, however, this appeared to transient as it was not sustained in the longer term assays. It would be insightful to repeat these using flow cytometry analysis at longer time points, such as 8, 18, 24 and 48 hours to determine if the enhanced phagocytosis seen in ROCK1nc macrophages is indeed transient using the same methodology where a difference was observed. A caveat of the flow cytometry experiments should be noted: Cells positive for fluorescence could have beads stuck to their surface rather than phagocytosed, giving a false positive. Preliminary results using confocal microscopy and z-stacks did suggest that beads were taken up by cells and not stuck on their surface (data not shown).

A key parameter to determining if the ROCK1nc mutation affects apoptotic cell morphology is the release of intracellular contents. The LDH assay was used as a surrogate marker for the release of intracellular contents. Surprisingly, the results obtained from this assay showed that dexamethasone did not increase the detected levels of LDH at 4, 8 or 24 hours post treatment compared to vehicle treated ROCK1wt and ROCK1nc thymocytes. Thymocytes are much smaller than other cells, so it could be that the levels of LDH release are low or even undetectable. Increasing the cell numbers or inducing apoptosis using other means such as UVC are two ways that could be used to optimise the assay and to

compare the results further. Other assays to detect the release of immunogenic contents, such as ATP or high mobility group box 1 (HMGB1), might perhaps be more informative to determine if ROCK1nc thymocytes had altered apoptotic morphology.

Given all the results obtained, mice with the ROCK1nc mutation either had comparable results to ROCK1wt cohorts, or subtle or short term differences. SEM was used to visualise the morphology of thymocytes as they are small in nature and cannot be well resolved with normal microscopes. SEM images at 4 and 8 hours showed that dexamethasone treatment seemed to be causing morphological changes in some thymocytes that were more obvious in ROCK1wt cells than ROCK1nc cells. At 8 hours post dexamethasone, more cells did have an altered morphology, particularly in ROCK1wt cells, but this was not conclusively quantified. ROCK1nc cells appeared to have a smoother texture, although it is difficult to conclude with certainty that these are deficient in blebbing.

Previous published data provided evidence that thymocytes do bleb when treated with acrylonitrile (Mikhutkina et al., 2004). This was shown with phase contrast microscopy in the study by Mikhutkina *et al.*, although these observations were confounded by blurry images showing putative apoptotic blebs on the surface of the thymocytes. Moreover, Jurkat human T-cells have been shown to bleb when the death ligand agonist, Fas, was administered (Tixeira et al., 2020). The apoptotic membrane blebbing observed with Jurkat cells was abrogated when a ROCK inhibitor was used, giving confidence that thymocytes did indeed bleb in a ROCK-dependent manner. However, the extent to which they bleb may not be as profound as other cells. Previous results in the lab with other cell types, particularly mouse embryonic fibroblasts have displayed canonical blebbing and obvious deficiencies in apoptotic blebbing in MEFs bearing the ROCK1nc mutation (Julian, 2015). One possibility as to why thymocytes may not bleb to the same extent is their small size and low cytoplasm to nucleus ratio. Thymocytes are small, largely made up of their nucleus. Apoptotic membrane blebbing relies on forceful contraction that causes blebs to protrude that are filled with cytoplasmic fluid. Perhaps, as thymocytes have less cytoplasm and area for contractile forces to occur, smaller and infrequent blebs may arise when cells undergo apoptosis. Although dexamethasone did cause apoptosis, using other apoptotic inducers such as BH3

mimetic drugs to see if the thymocytes behaved in a similar manner might shed more light on apoptotic membrane blebbing in thymocytes.

The results shown here indicate that the ROCK1nc mutation has either no observable effect, or subtle, small or transient effectson thymocyte apoptosis, immune cell responses and cell clearance. There is an indication that phagocytes may respond differently with the ROCK1nc mutation. However, why this may be is still unclear. For the most part, ROCK1nc thymocytes behaved in a similar manner to ROCK1wt cells both *in vivo* and *in vitro*. The results in this chapter have not supported my initial hypothesis, which could indicate that the thymus, an organ brimming with apoptotic activity, does not rely heavily on apoptotic membrane blebbing for efficient cell clearance. This would imply that ROCK1-mediated apoptotic membrane blebbing could be dispensable in this tissue, even when challenged with an apoptotic stimuli.

5 Impact of the ROCK1nc mutation in a genetic model of lung tumourigenesis

5.1 Introduction

5.1.1 KRAS and MYC driven lung adenocarcinoma

Lung cancer is considered one of the leading causes of cancer-related death worldwide (CRUK, 2017). Lung cancers can be characterised based on their histological profile into non-small cell lung cancer (NSCLC) and small cell lung cancer (SLC), with the majority of cases being NSCLC (van Zandwijk et al., 1995). NSLCs are further subdivided into adenocarcinoma, bronchioalveolar carcinoma, large cell carcinoma and squamous cell carcinomas (Kwon and Berns, 2013). Of the subtypes of NSCLC, lung adenocarcinomas (LuADs) account for 50% of the cases observed (Ischenko et al., 2017). A multitude of genetic mutations found in NSCLCs contribute to the heterogeneity of the disease (Vogelstein et al., 2013). In LuADs, oncogenic mutations in the Kirsten rat sarcoma viral oncogene homologue (KRAS) protein are highly prevalent, occurring in roughly 30% of cases (2014). *KRAS* mutations are prognostic markers for poorer outcomes (Graziano et al., 1999). Of the activating mutations in *KRAS*, the G12D point mutation is one of the more common oncogenic mutations (Ferrer et al., 2018). Activating *KRAS* mutations promote tumourigenesis through enhanced cell proliferation, migration and survival via the mitogen activated protein kinase (MAPK), phosphoinositide 3- kinase (PI3K) and the small GTPase, including Rho, effector pathways (Downward, 2003, O'Hagan and Heyer, 2011).

In addition to *KRAS*, amplification of *MYC* is also observed in NSCLC patients (Iwakawa et al., 2011, Massó-Vallés et al., 2020). *MYC* amplification occurs in over 20% of LuADS, associated with poor prognosis of patients harbouring this oncogenic amplification (Iwakawa et al., 2011). The MYC protein regulates a variety of cellular processes including cell proliferation, but also, cell death. A delicate balance in the levels of MYC determine which pathway a cell takes. A modest overexpression of MYC promotes cell proliferation, while a large increase in MYC pushes a cell towards death (Neidler et al., 2019). In addition to the proliferative effects, oncogenic amplification of MYC promotes invasion and metastasis, as well as angiogenesis (Rapp et al., 2009, Wolfer et al., 2010,

Shchors et al., 2006). A modest augmentation in MYC expression is seen more frequently in LuADs in comparison to the high amplification of MYC (Seo et al., 2014).

Recapitulating LuAD by utilising genetically modified mouse models (GEMs) has significantly increased our understanding of the disease. $KRAS^{G12D}$ combined with deregulation of MYC cooperate to drive the formation of LuADs (Kortlever et al., 2017, Kruspig et al., 2018). Kortlever *et. al.* have elegantly demonstrated that the cooperation of $KRAS^{G12D}$ and amplification of MYC in an inducible model of LuAD that results in an immunosuppressive and inflammatory environment in lung tumours (Kortlever et al., 2017). Mice with oncogenic $KRAS^{G12D}$ and overexpression of MYC will be referred to here as the KM model. The KM model is associated with an increase in macrophage infiltration and a reduction in cells that target the tumour itself, including T-cells and neutrophils. This immuno-suppressive effect is largely driven by MYC itself (Kortlever et al., 2017, Topper et al., 2017). Additional studies have shown that KRAS can also contribute to the immunosuppressive environment found in tumours by stabilising the programmed death ligand 1 (PDL1) protein (Coelho et al., 2017). These studies collectively establish the roles of KRAS and MYC in suppressing the immune system in this GEM model of LuAD.

5.1.2 APOBEC3b drives mutagenesis

The apolipoprotein B mRNA editing enzyme catalytic subunit 3B (APOBEC3B), one of seven APOBEC proteins, is a cytosine deaminase. APOBEC3B can deaminate deoxycytidine (C) on single-stranded DNA into deoxyuridine (U) (Henderson and Fenton, 2015). DNA base alterations by members of the APOBEC family were initially recognised as an immune response against viral agents (Harris et al., 2003, Mangeat et al., 2003). Evidence linking APOBEC proteins and carcinogenesis emerged over 20 years ago (Yamanaka et al., 1995). More recent evidence implicates APOBEC3B in causing mutations in human cancers, as this protein is amplified in tumour tissues and cancer cell lines, particularly in breast, ovarian and lung cancers (Roberts et al., 2012, Harris et al., 2003, Burns et al., 2013, Leonard et al., 2013). As APOBEC3B was shown to be significantly increased in human LuAD samples, it was hypothesised that the heterogeneity observed in human LuAD tumours may be attributed to the mutational load

brought on by APOBEC3B (Swanton et al., 2015). Furthermore, a retrospective study demonstrated a correlation between elevated levels of APOBEC3B with poorer prognosis of NSCLC patients (Yan et al., 2016). These studies established an association between APOBEC3B and tumourigenesis. As these findings are still relatively novel, GEM models studying the role of APOBEC3B, particularly in conjunction with other mutations, in lung cancer have not yet been reported.

5.1.3 Experimental Aims

In this chapter, the aim was to assess whether the ROCK1nc mutation, and by extension apoptotic membrane blebbing, would affect tumourigenesis. This will help discern the role of ROCK1 cleavage in tumourigenesis. Two lung adenocarcinoma models were utilised in this study – the KM ($KRAS^{G12D}$, cMYC overexpression) and the KMA model ($KRAS^{G12D}$, cMYC overexpression, APOBEC3B overexpression). The unpublished data on the KMA model showed an extension of survival and enhanced immunogenicity in comparison to the KM model (Murphy lab, unpublished observations). Given the relationship between immunogenicity and apoptosis, the KMA model was chosen to address if apoptotic membrane blebbing played a role in an immunological model of tumourigenesis. The KM model was utilised as a control to determine if the mutation might also impact an immunologically silent lung cancer model (Kortlever et al., 2017). Furthermore, ROCK1 was shown to be overexpressed in NSCLC lung tissues, correlating with poorer prognosis of patients (Hu et al., 2019). With the addition of the ROCK1nc mutation to the KMA model, the hypothesis was that the abrogated apoptotic membrane blebbing would negate the survival extension. However, based on the fact that ROCK1nc delayed liver cancer in a carcinogenic model (Olson lab, unpublished) ROCK1nc mutation could in fact further the survival benefit seen with APOBEC3B conditional overexpression, by potentially contributing to the immuno-surveillance of tumours (Julian, 2015).

5.1.3.1 Autochthonous Lung Adenocarcinoma Models

The models used in this arm of the study are based on an autochthonous lung adenocarcinoma model developed in the Murphy lab (Beatson Institute). The expression of the transgenes (MYC, $KRAS^{G12D,}$ APOBEC3B) in the mouse models, were induced by expression of Cre recombinase from an adenoviral vector. Cre recombinase expression was under the control of the surfactant protein c (Sp-C)-promoter, targeting recombination of alleles in type II alveolar cells (Glasser et al., 1991, Linnoila et al., 1992, Neidler, 2015). Mice expressing $KRAS^{G12D}$ and *MYC* were denoted as KM, whilst mice additionally expressing APOBEC3B were called KMA. A mixture of mice with and without the expression of near-infrared fluorescent protein (iRFP) were also utilised in the KM and KMA cohorts (Hock et al., 2017). KM mice develop tumours that resemble human lung adenocarcinoma (Neidler et al., 2019). Interestingly, when this model was combined with a conditionally expressed APOBEC3B transgene (Beatson Institute, D. Strathdee lab), an extension in survival was observed (Murphy lab, unpublished observations).

It is speculated that tumours in the KMA model are more immunogenic due to higher mutational loads. Thus, increased immune-surveillance may play a part in extending survival beyond what is seen with the KM model. Mice bearing the ROCK1nc mutation were crossed to the two lung cancer models utilised in this study (KM and KMA). The mouse cohorts used to investigate the role of ROCK1-mediated apoptotic membrane blebbing in lung adenocarcinoma are outlined in the table below (Table 5-1).

Mouse Cohort	Genotypes
KM-WT	*LSL-KRAS*^{G12D} (Het); *LSL-MYC* (HET); ROCK1 (WT); LSL-iRFP (WT/HET/HEMI)
KM-NC	*LSL-KRAS*^{G12D} (Het); *LSL-MYC* (HET); ROCK1 (NC mutation HOM); LSL-iRFP (WT/HET/HEMI)
KMA-WT	*LSL-KRAS*^{G12D} (Het); *LSL-MYC* (HET); *LSL*-APOBEC3B (HET); ROCK1 (WT); LSL-iRFP (WT/HET/HEMI)
KMA-NC	*LSL-KRAS*^{G12D} (Het); *LSL-MYC* (HET); *LSL*-APOBEC3B (HET); ROCK1 (NC mutation HOM); LSL-iRFP (WT/HET/HEMI)

Table 5-1 Experimental cohorts denoting genetic alleles in ROCK1 mice on KM or KMA models. There were 4 main cohorts used in this study – KM-WT, KM-NC, KMA-WT, KMA-NC. KM mice contain the *LSL-KRAS*^{G12D}*, LSL-MYC,* and variable *LSL-iRFP* expression. KMA mice contain the same alleles as the KM with the addition of *LSL-APOBEC3B*. WT cohorts contain endogenous expression of wild-type ROCK1 while NC cohorts contain a homozygous ROCK1nc mutation.

5.2 Results

5.2.1 The ROCK1nc mutation accelerates tumourigenesis in the KMA lung adenocarcinoma model

KMA mice at the age of 8-10 weeks were administered with adenoviral Sp-C-Cre via intranasal inhalation to induce the genetic alleles specifically in the lungs. The ROCK1nc mutation is ubiquitously-expressed mutation. KMA mice wild-type for the ROCK1nc mutation (KMA-WT) or homozygous for the ROCK1nc mutation (KMA-NC) were aged and harvested at clinical endpoint. The end-point clinical signs that indicate lung tumours include breathing difficulties, weight loss and a pinched body phenotype. Interestingly, the addition of the ROCK1nc mutation significantly accelerated tumourigenesis (p=0.0021), with a median survival of 112 days compared to 153.5 days for KMA-WT mice (Figure 5-1). This acceleration was observed in both male and female mice. The expression of the iRFP reporter did not alter the survival of these mice. This survival analysis has shown that the full body ROCK1nc mutation, and by extension, defective apoptotic blebbing, plays a role in accelerating tumourigenesis.

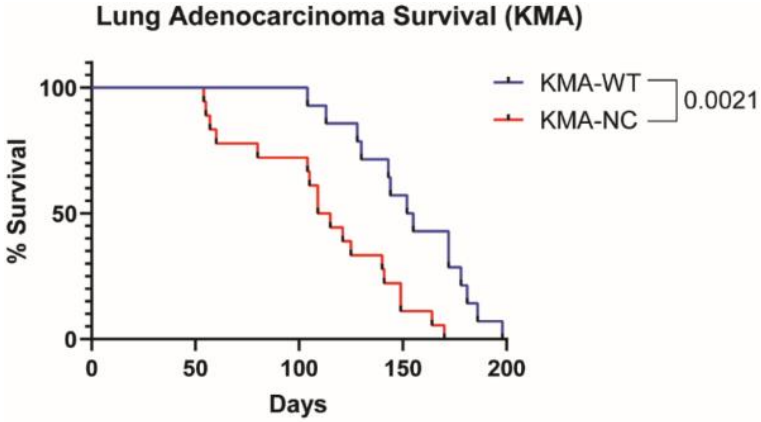

Cohort	Median Survival (Days)
KMA-WT	153.5
KMA-NC	112

Figure 5-1 The ROCK1nc mutation accelerates tumourigenesis in the KMA lung adenocarcinoma model. Kaplan-Meier survival curve for KMA-WT and KMA-NC mice showing accelerated tumourigenesis in KMA mice bearing the ROCK1nc mutation. Mice were administered with a Sp-C Cre adenovirus via intranasal inhalation at 8-10 weeks of age to induce the expression $KRAS^{G12D}$, MYC and APOBEC3B in type II alveolar cells. The ROCK1nc mutation is expressed in all cell types from birth. Median survival was 153.5 days for ROCK1wt cohorts, and 112 days for ROCK1nc cohorts from the date of viral induction. Lines represent the percentage of live mice. Statistical significance was determined using the Log-rank (Mantel-Cox) test. (KMA-WT – N=14, 10 males, 4 females (9 iRFP mice); KMA-NC – N=14, 10 males, 4 females (8 iRFP mice)).

5.2.1.1 The lung tumour burden at clinical endpoint is comparable between KMA-WT and KMA-NC mice

The lungs of mice harvested at clinical endpoint were fixed in formalin and embedded in paraffin. FFPE lung samples were then sectioned into 3 different levels, at 100 µm apart. These sections were stained with hematoxylin and eosin (H&E) and tumour burden was quantified using HALO™ image analysis software (Figure 5-2). Representative images show the algorithm-determined tumour (red) and lung tissue (green) areas (Figure 5-2A). The percentage average of the tumour areas was comparable between KMA-WT and KMA-NC mice (Figure 5-2B). This model does not often have liver metastasis. However, the liver weights were also noted in the event that the ROCK1nc mutation promoted metastasis. No macro-metastases in the liver were observed, which was reflected in the comparable ratios of liver to body weights in both genotypes (Figure 5-2C). As some mice in both cohorts expressed the iRFP reporter gene in their lungs, this was used as an independent means to assess tumour burden. Although there was variability in the fluorescence intensity in the KMA-NC cohort, both genotypes displayed similar levels of iRFP expression (Figure 5-2F). To confirm that

metastasis had not occurred, liver images were also taken and no IRFP positivity was detected (data not shown). The fluorescence tumour data sets reiterate the results seen with the histology data; indicating that the ROCK1nc mutation did not alter tumour burden at clinical endpoint, despite the accelerated tumourigenesis observed.

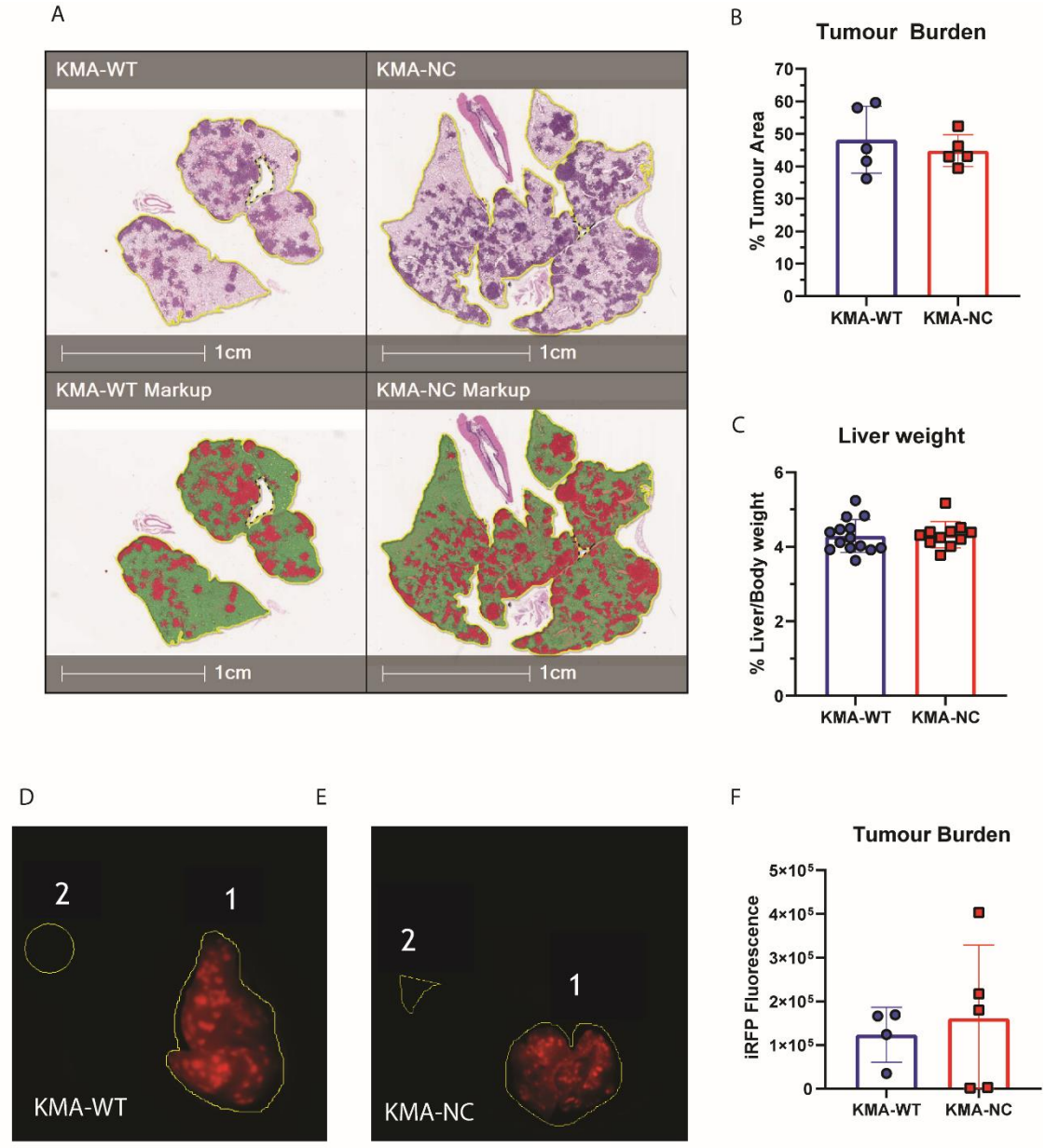

Figure 5-2 The ROCK1nc mutation did not alter endpoint tumour burden in the KMA lung cancer model. KMA-WT and KMA-NC mice were harvested at clinical endpoint post induction via intranasal inhalation (Sp-C Cre $1x10^8$ pfu). The tumour burden was determined using histology by H&E stains. Sections of FFPE tissues were cut 100 µm apart, for a total of 3 sections. Sections were then quantified using Halo™ A) Representative images of one section showing the H&E stains of lung tissues and a marked-up image depicting lung tissue (green) and tumour tissue (red). B) Halo™ quantifications of the average percentage of tumour area, by calculating the tumour area as a percentage of the tissue area of each level and averaging the 3 levels. Data points represent individual mice showing an average of the 3 sections per mouse, error bars represent mean ± SD (N=5 per genotype). C) The percentage liver to body weight ratios of KMA-WT and KMA-NC mice. Data points represent individual mice, error bars represent mean ± SD (KMA-WT N=11, KMA-NC N=7) D, E) Representative images of iRFP-positive lung tissues. 1 depicts the lung tissue and 2 the background signal. F) Quantification of fluorescent signals by HALO™ from lung tissues were measured by reducing the fluorescent signal by the background signal. Data points represent individual mice, error bars represent mean ± SD (KMA-WT N=4, KMA-NC N=5). Scale bars denote 1 cm in length.

5.2.2 KMA-NC mice have more apoptotic cells in endpoint tumours

To probe the differences seen in survival when the ROCK1nc mutation was present, levels of cell apoptosis in the lung tumours were assessed. This was done using immunohistochemistry on FFPE lung samples from clinical endpoints in KMA-WT and KMA-NC mice. Representative images reflect the low number of cleaved caspase-3 positive cells in both KMA-WT and KMA-NC lung samples (Figure 5-3). When quantified using HALO™, KMA-NC mice have a statistically significantly higher percentage of cleaved caspase-3 staining when compared to KMA-WT mice (Figure 5-3). Although there was a higher percentage of staining in the KMA-NC cohort, both cohorts still have a very low percentage of apoptotic cells, at less than 0.1%. Despite the low levels of apoptotic cells, this set of results suggest that the addition of the ROCK1nc mutation to the KMA model may result in a higher level of apoptotic cells detected in these tumours.

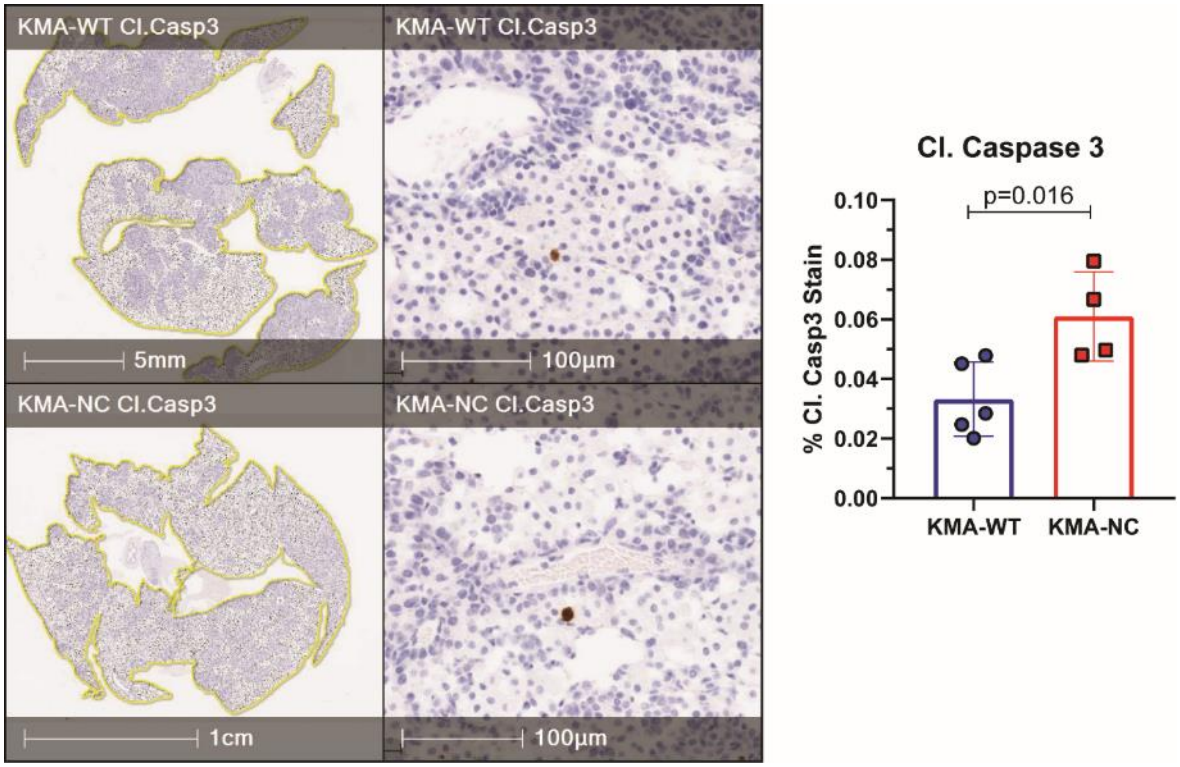

Figure 5-3 KMA-NC lung tumours have greater levels of cleaved caspase-3 staining. FFPE lung tissue samples from KMA-WT and KMA-NC mice at clinical endpoint were sectioned (4µm), and stained for cleaved caspase-3 (Cl. Casp3). Left - Representative images showing KMA-WT and KMA-NC lung tissue stained with Cl.Casp3 and quantified using Halo™. Scale bars are shown in the images. Left panel shows the whole tissue at 2x magnification and the right panel shows a 20x magnification. Right - Data points show the average percentage of Cl.Casp3 stain area to tissue area. Each point represents individual mice, error bars represent mean ± SD. (N=5 KMA-WT; N=4 KMA-NC).

5.2.3 Immune cell profile assessments of KMA mice

5.2.3.1 Histological assessment of immune cells of KMA mice at clinical endpoint

One hypothesis on how APOBEC3B expression might delay MYC/KRas induced tumourigenesis is that there is increased immune cell infiltration. Therefore, it was interesting to compare the immune cell status of the lung samples obtained from KMA-WT and KMA-NC tumours. Immunohistochemistry was used to stain for T-cell populations, CD4 and CD8 T-cells, as well as myeloid cells, macrophages and neutrophils. These sections were then quantified using HALO™. Representative images of the CD4 stain showed low numbers of positive cells (Figure 5-4A). This was reflected in the quantifications, with less than 0.8% CD4 stain area to tissue area (Figure 5-4B). There seemed to be a slightly lower level of CD4 positive T-cells in the KMA-NC lung samples in comparison to KMA-WT samples. Similarly, there were low levels of CD8α positive T-cells in both KMA-WT and KMA-NC lung tissues (Figure 5-4C, D). In a similar fashion to the CD4 positive T-cells, there was a slightly lower percentage of CD8α stained area in KMA-NC mice in comparison to KMA-WT mice (Figure 5-4D). In both instances, there was quite high variability between the mice in KMA-WT samples (Figure 5-4B, D). There also seemed to be a fairly similar percentage of CD4 and CD8α staining area in the tissues. Largely, the CD4 and CD8α T-cell populations in the lungs at clinical endpoint were slightly lower in the KMA-NC mice compared to KMA-WT mice.

The macrophage population was investigated using antibody staining for the macrophage-selective F4/80 epitope by immunohistochemistry. The representative images show the presence of macrophages in both the KMA-WT and KMA-NC lung tissues (Figure 5-5A). The quantifications of the sections using HALO™ showed that there was a comparable percentage of F4/80 stained area between the two genotypes at clinical endpoint (Figure 5-5B). Similarly, the neutrophil population was assessed using antibody staining for the Ly6G epitope by immunohistochemistry. Representative images show that there were some neutrophils in the lungs of both KMA-WT and KMA-NC mice (Figure 5-5C). When quantified, although there seemed to be a lower percentage of Ly6G stained area in the KMA-NC cohort, this was not statistically significant (Figure 5-5D). The myeloid population investigated, similar to the T-cell population, seemed to

be fairly comparable between the genotypes at this time point. There were however, more macrophages found in the lung samples than the other cell types. It should be noted that for these four cell types, there was no specific localisation of the immune cells to the tumour area. The immune cells were generally distributed throughout the tissues. With the caveat that only a small number of tumours have been assessed, these results suggest that the ROCK1nc mutation did not overtly affect the immune landscape in the KMA model.

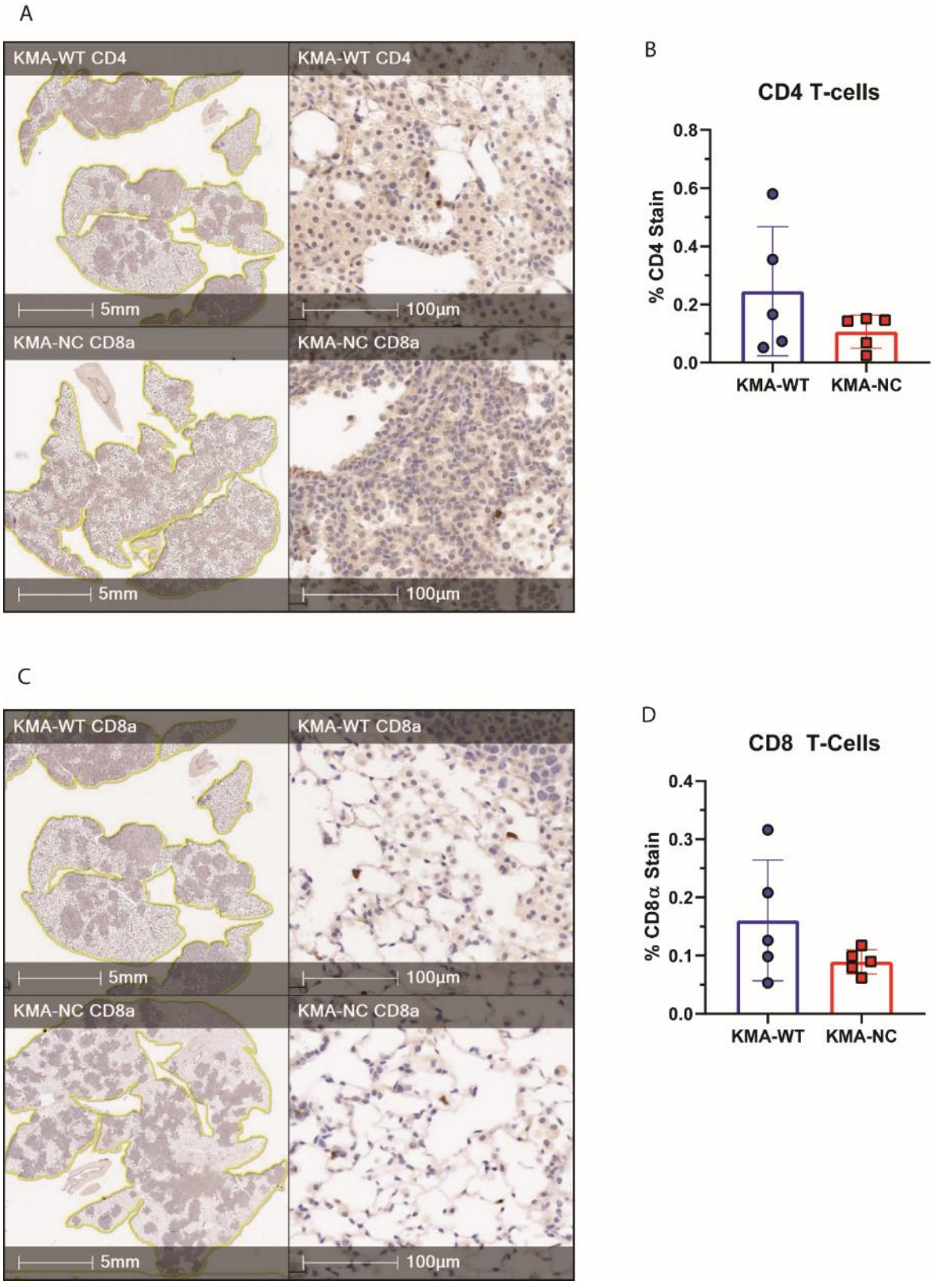

Figure 5-4 Representative staining and quantification of CD4 and CD8α T-cells. FFPE lung tissue samples from KMA-WT and KMA-NC mice at clinical endpoint were sectioned (4 µm) and stained for CD4 and CD8α T-cells. A, C) Representative images showing KMA-WT and KMA-NC lung tissues stained with CD4 (A) and CD8α antibodies (C). These were quantified using Halo™. Scale bars are shown in the images at 5 mm (left) and 100 µm (right). Left panesl show the whole tissue and right panels show a 20x magnification. B) Data points show the average percentage of CD4 (B) and CD8α (D) stained area to tissue area. Each point represents individual mice, error bars represent mean ± SD. (N=5 for both genotypes).

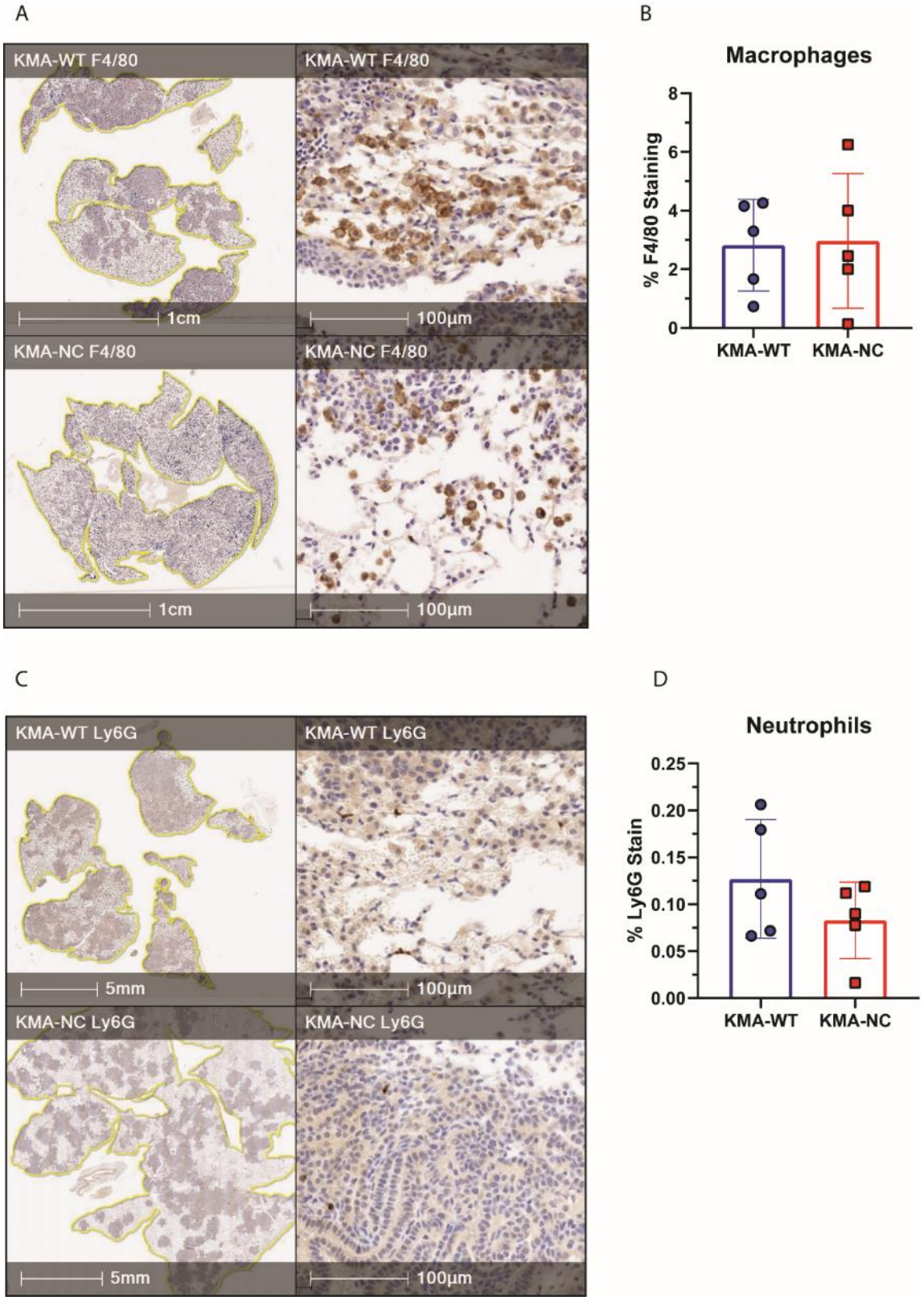

Figure 5-5 KMA-WT and KMA-NC mice have fairly similar levels of myeloid cells at clinical endpoint. FFPE lung tissue samples from KMA-WT and KMA-NC mice at clinical endpoint were sectioned (4µm) and stained for F4/80, a macrophage marker, or Ly6G, a neutrophil marker. A, C) Representative images showing KMA-WT and KMA-NC lung tissues stained with F4/80 (A) and Ly6G (C). These were quantified using Halo™. Scale bars are shown in the images at 5 mm (left) and 100 µm (right). Left panels show the whole tissue and the right panels show a 20x magnification. B) Data points show the average percentage of F4/80 (B) and Ly6G (D) stained area to tissue area. Each point represents individual mice, error bars represent mean ± SD. (N=5 for both genotypes).

5.2.3.2 Circulating immune cells at clinical endpoint are unchanged

The circulating immune cells at clinical endpoint were also determined using the IDEXX ProCyte Dx* (IDEXX). The results from blood samples revealed that there were no differences between KMA-WT and KMA-NC mice in their white blood cell, lymphocyte, monocyte or neutrophil counts (Figure 5-6). This collectively shows that at clinical endpoint, the ROCK1nc mutation had not altered the immune cell populations in circulation or in the tumour.

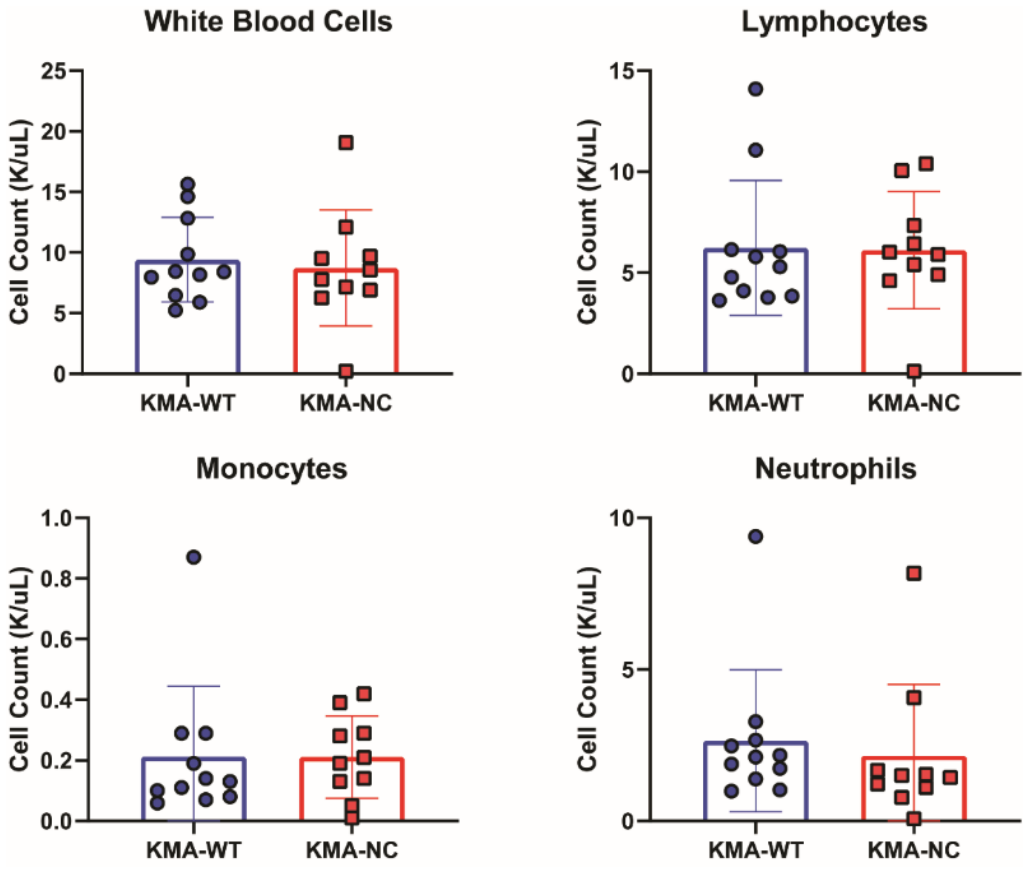

Figure 5-6 Circulating immune cells were equivalent in KMA-WT and KMA-NC mice. Circulating white blood cells, lymphocytes, monocytes and neutrophils were counted from blood samples from KMA-WT and KMA-NC mice at clinical endpoint. Samples were run on the IDEXX ProCyte Dx*; Data points represent individual mice, error bars showing mean ± SD (KMA-WT N=11; KMA-NC N=10).

5.2.4 KMA mice bearing the ROCK1nc mutation have a greater tumour burden at an 8 week time point

As a survival difference was observed between KMA-WT and KMA-NC cohorts, but no differences in tumour burden were detected, understanding how the ROCK1nc mutation accelerates tumourigenesis was important. An earlier time point was therefore investigated. KMA-WT and KMA-NC mice at 8 weeks post

intranasal inhalation were harvested and assessed for tumour burden and immune cell populations. The tumour burden was investigated through immunohistochemistry. FFPE lung tissues from 8 week post genetic recombination were sectioned at 3 different levels, at 100 µm apart in order to obtain a holistic picture of the lung. These sections were stained with H&E and then quantified using HALO™ (Figure 5-7A). Representative images show that the tumours found in the lung were dense and darker than neighbouring cells. The algorithm on HALO™ discriminates the normal tissue (green) from tumour tissue (red). The average percentage of tumour area within lung tissues showed a marked statistically-significant increase in tumour burden in KMA-NC mice compared to KMA-WT mice at 8 weeks (Figure 5-7B; p=0.028). The liver weights of mice were also taken as a rough indication of metastatic burden. The percentage of liver to body weight ratios were comparable between KMA-WT and KMA-NC mice (Figure 5-7C). Furthermore, no metastases were visually observed in the livers histologically, nor in the iRFP images of the KMA-WT or KMA-NC mice (data not shown).

As some of the mice in both cohorts contained the reporter allele iRFP, the Pearl Imaging system was also used to quantify tumour burden in lung and liver tissues. Representative images show the tumour cells in red in KMA-WT and KMA-NC mice (Figure 5-7D). Pearl quantifications were analysed based on signal intensity subtracted from background intensity. The iRFP fluorescence was also statistically significantly greater in KMA-NC mice compared to KMA-WT (Figure 5-7F; p=0.036). This complements the histological data, as both methods showed that KMA-NC mice have a greater tumour burden than KMA-WT mice. Pearl imaging also confirmed the absence of detectable metastatic cells in the liver (data not shown). This data set at 8 weeks showed that the ROCK1nc mutation increased tumour burden in the KMA model. The KMA-NC mice consistently showed worse prognosis compared to KMA-WT mice, which is sustained not only at clinical endpoint but also at this 8 week time point. A higher tumour burden at this pre-clinical stage in the KMA-NC cohort would contribute to the accelerated tumourigenesis in these mice (Figure 5-1).

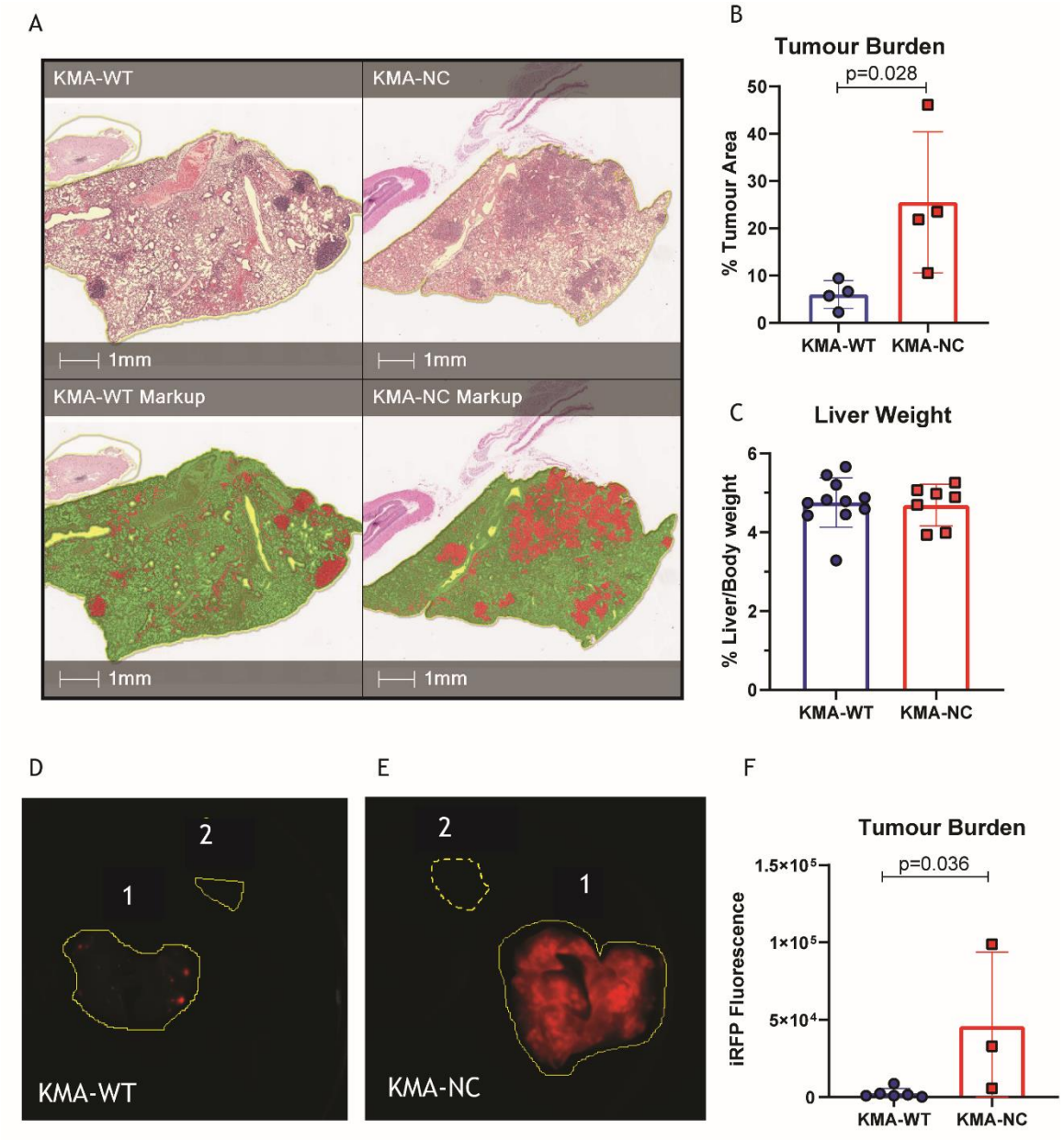

Figure 5-7 KMA mice bearing the ROCK1nc mutation have a higher tumour burden at an 8 week time point. KMA-WT and KMA-NC mice were harvested at 8 weeks post induction via intranasal inhalation (Sp-C Cre 1x10^8 pfu). The tumour burden was determined using histology by H&E stains. Sections from FFPE were cut at 100 µm apart, for a total of 3 sections. Sections were then quantified using Halo™ A) Representative images of one section showing the H&E stains of lung tissues and a marked-up image depicting the lung tissue (green) and tumour tissue (red). B) Halo™ quantifications of the average percentage of tumour area, by calculating the tumour area as a percentage of the total tissue area of each level and averaging the 3 levels. Data points represent individual mice showing an average of the 3 sections per mouse, error bars represent mean ± SD (N=4 per genotype). C) The percentage of liver to body weight ratios of KMA-WT and KMA-NC mice. Data points represent individual mice, error bars represent mean ± SD (KMA-WT N=11, KMA-NC N=7) D,E) Representative images of iRFP positive lung tissues. 1 depicts the lung tissue and 2 the background signal. F) Quantification of fluorescent signals from lung tissues measured by reducing the fluorescent signal by the background signal. Data points represent individual mice, error bars represent mean ± SD (KMA-WT N=6, KMA-NC N=3).

5.2.5 Increased apoptotic cells in the lungs of KMA-NC mice at an 8 week time point

As the ROCK1nc mutation affects apoptotic membrane blebbing, the next parameter investigated was apoptosis. This was done using an antibody that detects cleaved caspase-3 stain by immunohistochemistry. FFPE lung samples were sectioned at 3 levels, at 100 µm apart and stained for cleaved caspase-3. KMA-WT and KMA-NC mice displayed visually low numbers of cleaved caspase-3 positive cells, denoted with the brown colour (Figure 5-8A). Stains were then quantified using HALO™ and averages over the three levels were determined. The average percentage of cleaved caspase-3 to tissue area was greater in three of the four KMA-NC mice compared to KMA-WT mice. It should be noted however, that both cohorts had relatively low levels of cleaved caspse-3 staining at less than 0.05%. Therefore, although there seems to be greater levels of apoptotic cells in the KMA-NC model, the significance of overall low levels is still unknown.

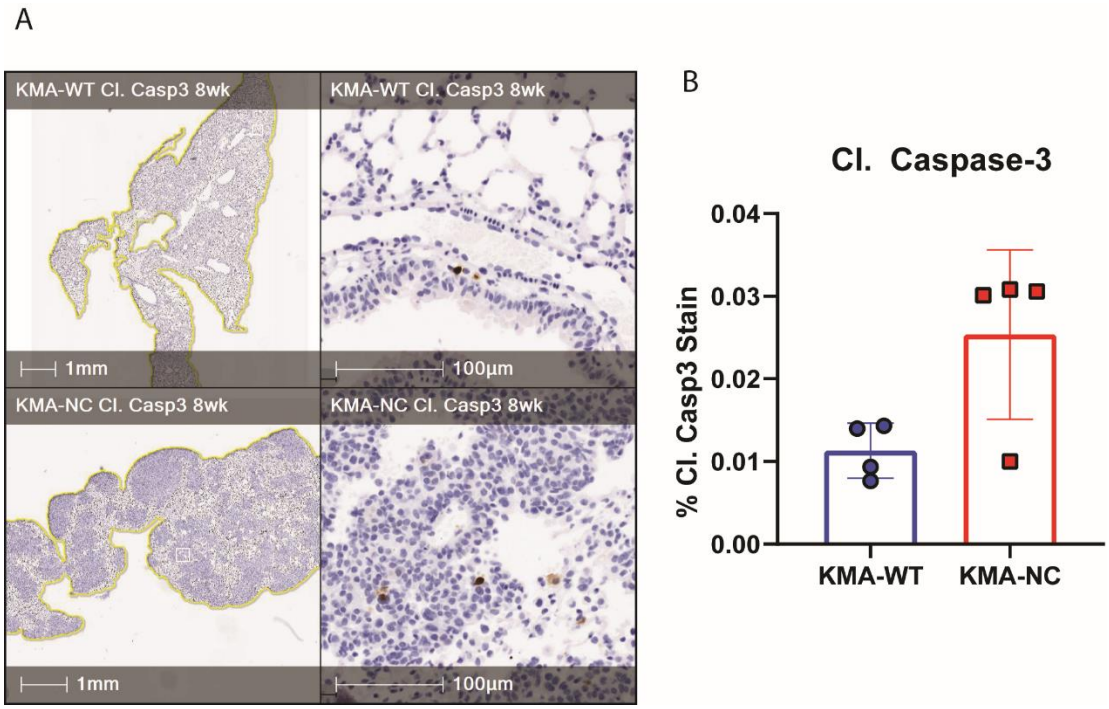

Figure 5-8 Lung samples from KMA-NC mice display greater levels of apoptotic cells at 8 weeks. FFPE lung tissue samples from KMA-WT and KMA-NC mice at 8 weeks were sectioned (4 µm), at 100 µm apart for a total of 3 levels, and stained for cleaved caspase-3 (Cl.C3). A) Representative images showing KMA-WT and KMA-NC lung tissue stained with Cl.C3, quantified using Halo™. Scale bars are shown in the images at 1 mm (left) and 100 µm (right). Left panels show the whole tissue and the right panels show a 20x magnification. B) Data points show the average percentage of Cl.C3 stained area to tissue area. Each point represents individual mice, error bars represent mean ± SD. A Mann-Whitney statistical test was performed and no significant differences were found (N=4 for both genotypes).

5.2.6 8 Immune cell profiling of KMA mice at 8 weeks post induction

Characterising the immune landscape in the tumours of KMA mice is an important aspect to understand what is driving the change in tumour susceptibility, given that the KMA model is believed to be immunogenic. Additionally, is it widely established that there is a relationship between the presence and activation of immune cells, and tumour development (Gajewski et al., 2013). In order to characterise the immune cell profiles in the 8 week cohort, three approaches were taken – flow cytometry and immunohistochemistry to assess immune cell populations in the lungs, and the IDEXX ProCyte Dx* to analyse immune cell populations in the circulation.

5.2.6.1 Flow cytometry analysis of immune cells at 8 weeks post induction

Flow cytometry analysis on lung samples of 8 week KMA-WT and KMA-NC mice was carried out to assess the T-cell populations and myeloid populations in the lungs. The T-cell populations studied include CD4 T-cells, CD8α T-cells, natural killer (NK) cells, NK T-cells, γδ T-cells and regulatory T-cells. Additionally, the activation status of CD4 and CD8 cells were also assessed through the expression of the surface marker CD44. The representative gating strategy for T-cells is shown in Figure 5-9. Flow cytometry results show that there were comparable levels of the T-cell and natural killer populations between KMA-WT and KMA-NC mice (Figure 1-10). The regulatory T-cell population however, seemed to be higher in some of the KMA-NC mice. There were also no differences observed in the activation status of the T-cell populations as seen by equivalent levels of cells positive for the expression of CD44 between the two genotypes.

In addition to the T-cell panel, a myeloid panel was applied to interrogate macrophages, dendritic cells, neutrophil and monocyte populations (Figure 5-11). The monocyte population was split based on the level of Ly6C staining into low/intermediate and high Ly6C expression. Monocytes that were low/intermediate for Ly6C expression are generally regarded as anti-inflammatory, whilst higher Ly6C expression correlates with an inflammatory signature (Peng et al., 2009). Similar to the T-cell panel, cells in the myeloid panel were at comparable levels between KMA-WT and KMA-NC mice at this 8 week time point. The only population that seemed to have fewer cells in the

KMA-NC cohorts in comparison to the KMA-WT cohorts were the dendritic cells. Across the analysis, it should be noted that there was one data point in the KMA-NC cohorts that was higher than the rest which belonged to the same mouse for both panels. The flow cytometry data suggested that at 8 weeks post-induction the levels of immune cells were largely comparable between KMA-WT and KMA-NC cohorts.

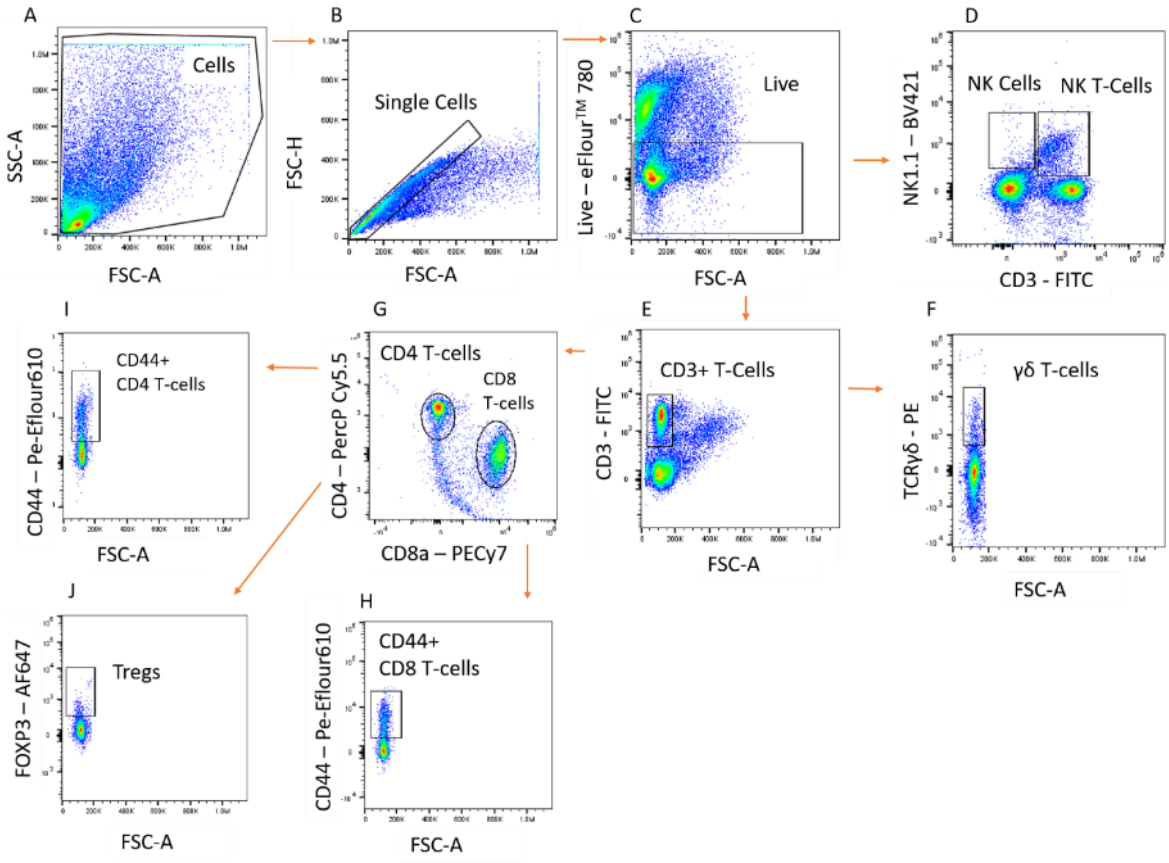

Figure 5-9 Representative gating strategy for T-cells from lung samples of 8 week old KMA-WT and KMA-NC mice. Cells were stained using a T-cell antibody panel, run through the Attune NxT Flow cytometer and analysed using FloJo software. All cells were gated in panel A, followed by doublet cell exclusion (B). Gates were then applied on live cells (C). Natural Killer (NK) and NK T-cells were distinguished based on NK1.1 single positivity or dual positivity for NK1.1 and CD3 expression (D). T-cells were gated for their CD3 positivity (E). The γδ T-cells were then classified based on the γδ T-cell receptor (TCR) positivity (F). T-cells were also distinguished based on their CD4 or CD8α positivity, showing the CD4 T-cell and CD8α T-cell populations (G). The activation status of T-cells were determined using the marker CD44 on CD8α T-cells (H), and CD4 T-cells (I). Regulatory T-cells (Tregs) were also determined from CD4 T-cells (J).

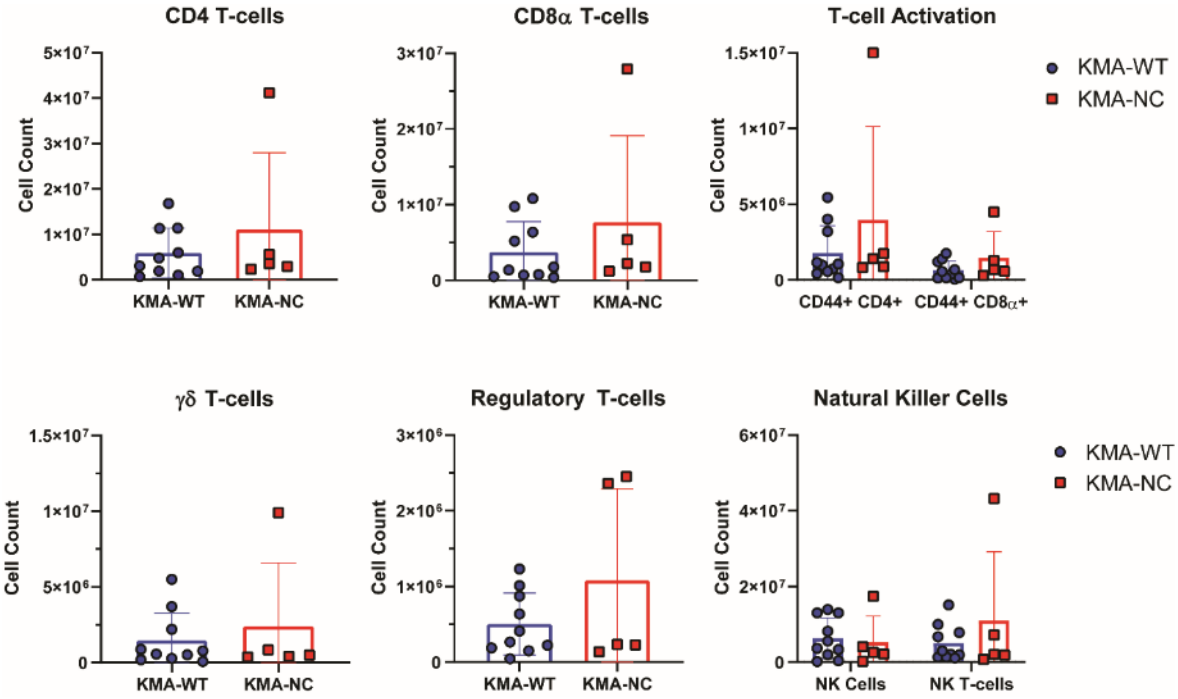

Figure 5-10 T-cell populations in KMA lungs were not different in ROCK1nc mutant mice compared to wild-type. KMA-WT and KMA-NC mice were induced by viral induction via intranasal inhalation and tissue harvested at an 8-week time point. The right side of the lungs were isolated and stained to assess T-cell populations by flow cytometry. The T-cell populations assessed were CD4 T-cells, CD8α T-cells, γδ T-cells, regulatory T-cells, natural killer (NK) cells, and NK T-cells. The activation status of CD4 and CD8α T-cells was investigated using the CD44 marker. The cell count of each population was extrapolated to represent the count in the whole lung. Data points represent individual mice, error bars represent mean ± SD. (N=KMA-WT N=10; KMA-NC N=5).

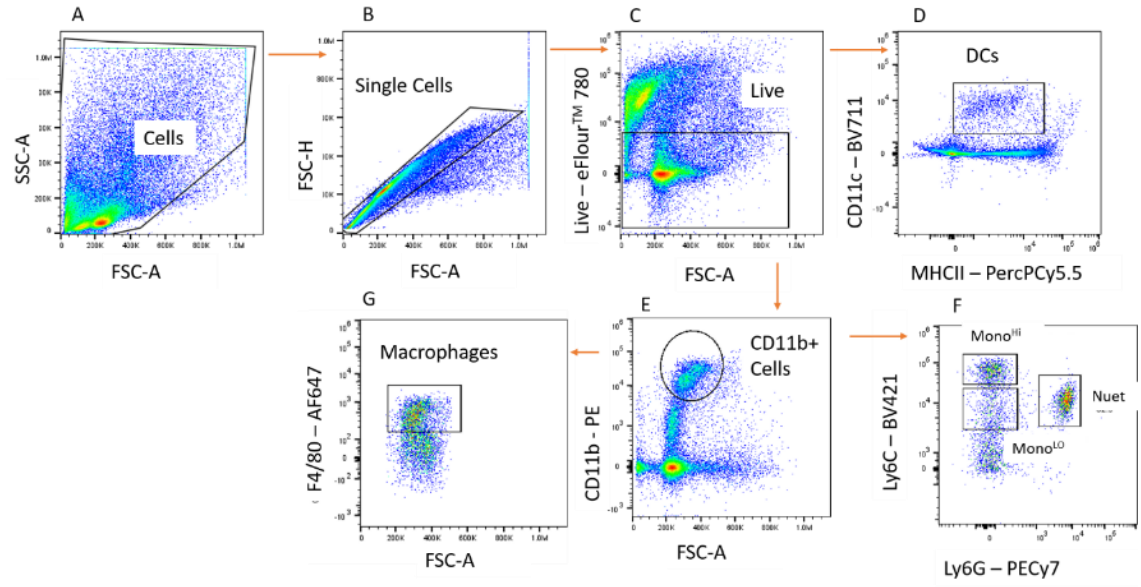

Figure 5-11 Representative gating strategy for myeloid cell populations from lung samples at an 8 week time point from KMA-WT and KMA-NC mice. Cells were stained using a myeloid antibody panel, run through the Attune NxT Flow cytometer and analysed using FloJo All cells were gated in panel A, followed by a doublet cell exclusion (B). Gates were then applied on live cells (C). Dendritic cells were then classified based on the CD11c and MHCII positivity (D). Live cells were also gated on CD11b positivity (E). Macrophages were positive for F4/80 (G). Monocytes and neutrophils were distinguished by their Ly6C and Ly6G expression (F). Monocytes were classed as $Ly6C^{High}$ or $Ly6C^{Intermediate/low}$ expression. Neutrophils were positive for both Ly6C and Ly6G.

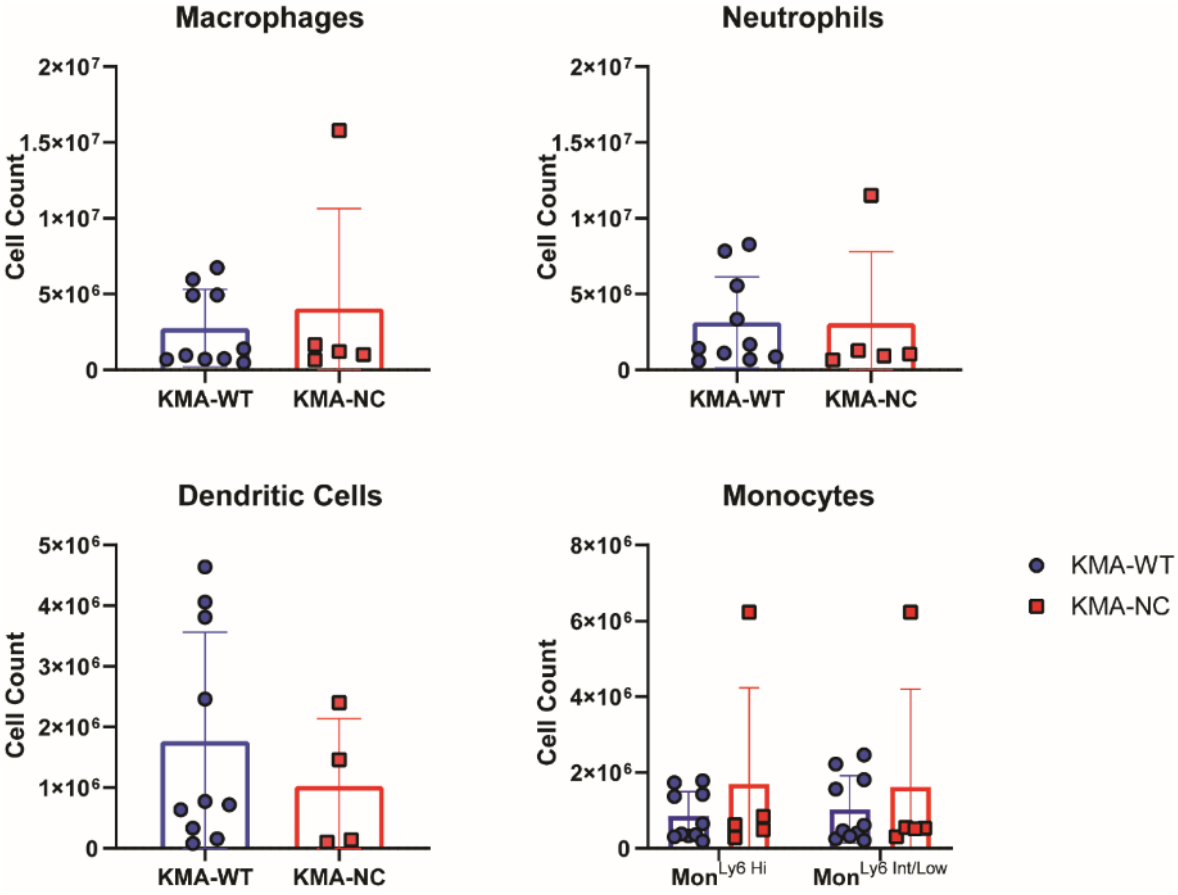

Figure 5-12 Myeloid cell populations in the lungs were comparable between KMA-WT and KMA-NC mice at an 8-week timepoint. KMA-WT and KMA-NC mice were induced by viral induction via intranasal inhalation and tissue harvested at an 8-week timepoint. The right side of the lungs were isolated and stained to assess myeloid cell populations. Levels of macrophages, neutrophils, dendritic cells and monocytes, distinguished on the level of Ly6C expression (Intermedia/Low, and High) are shown for KMA-WT (blue) and KMA-NC (red). The cell count of each population was extrapolated to represent the count in the whole lung. Data points represent individual mice, error bars represent mean ± SD. (N=KMA-WT N=10; KMA-NC N=5).

5.2.6.2 Histological assessment of immune cells at an 8 week time point

In addition to flow cytometry, immunohistochemistry analysis of CD4 and CD8α positive T cells, macrophages and neutrophils was also carried out. FFPE lung tissues from KMA-WT and KMA-NC mice 8 week post intranasal inhalation of Adeno-Cre were cut and processed in the same manner as the H&E samples. Three sections 100 µm apart were obtained, stained and then quantified using HALO™. For the T-cells, an anti-CD4 and anti-CD8 antibody staining was used to distinguish between the two populations of T-cells (Figure 5-13). Representative images show the presence of both CD4 and CD8α T-cells (Figure 5-13A, C). When quantified and averaged, the percentage of CD4 positive staining area to tissue area appeared to be slightly higher in the KMA-NC cohorts (Figure 5-13B)

although there were only small numbers analysed. For the CD8α T- cell population, no differences were observed in the average percentage of CD8α positive staining area to tissue area (Figure 5-13D). It is also worth noting that there were relatively low levels of T-cells present at less than 1.5% per tissue area.

To assess the levels of macrophages, the percentage of F4/80 staining to tissue area was quantified (Figure 5-14A, B). Due to the variability in the KMA-NC population, although it may seem that there was a greater average percentage of macrophages, it is likely to be comparable to KMA-WT tumours. The neutrophil population was investigated using anti-Ly6G antibody staining and quantified (Figure 5-14C, D). Although the neutrophil population might seem to be higher in the KMA-WT cohort, there was considerable variability between the mice in this instance. Similar to endpoint tumours, there were more macrophages than any other cell type investigated here, although still quite a low percentage (<1%) relative to the total tissue area.

It should also be noted that none of the immune stains that were carried out had particular localisations and were found throughout the lung tissue. None of the comparisons were significantly different. However, it might be argued that there seemed to be some trends observed with the CD4 T-cells. To consolidate these findings, additional samples would need to be analysed to robustly demonstrate if the trends held up, and to counteract the variability seen in the macrophage and neutrophil analyses. Thus far, however there did not appear to be any major differences in the immune populations between the KMA-WT and KMA-NC populations at the 8 week timepoint in the lungs of this genetic model.

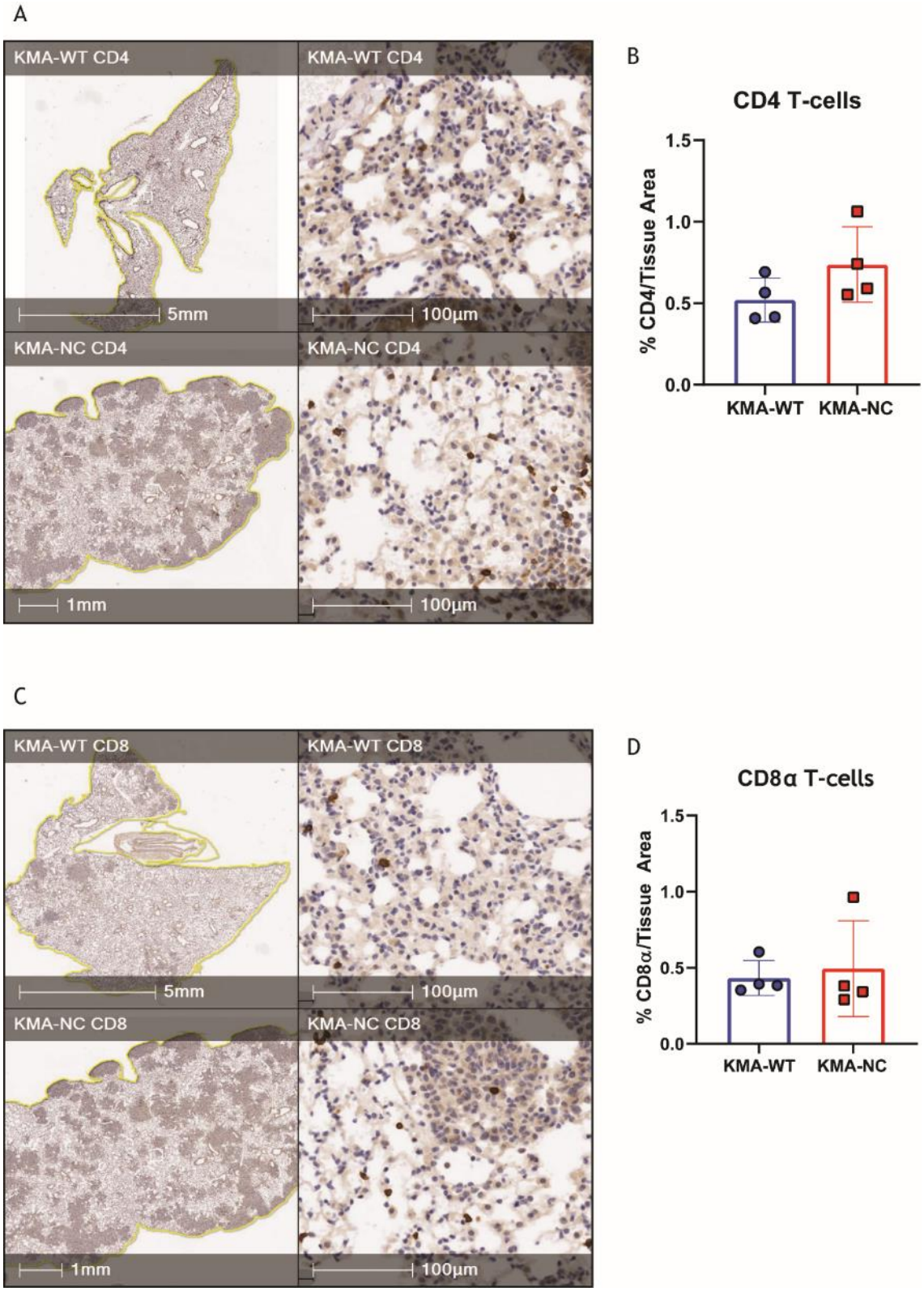

Figure 5-13 KMA-NC and KMA-WT mice have comparable levels of CD4 and CD8α T-cells in lungs harvested at an 8 week time point. FFPE lung tissue samples from KMA-WT and KMA-NC harvested at an 8 week timepoint post transgene induction were sectioned (4 µm), at 100 µm apart for a total of 3 levels, and stained for CD4 and CD8α positive T cells. A, C) Representative images showing KMA-WT and KMA-NC lung tissues stained with CD4 (A) and CD8α (C) at 1 level, quantified using Halo™. Scale bars are shown in the images. Left panels show the whole tissue and the rights panel show a 20x magnification. B) Data points show the average percentage of CD4 (B) and CD8α (D) stained area to tissue area (in yellow outline). Statistical test: Mann-Whitney Test; no significant difference. Each point represents individual mice, error bars represent mean ± SD. (N=4 for both genotypes).

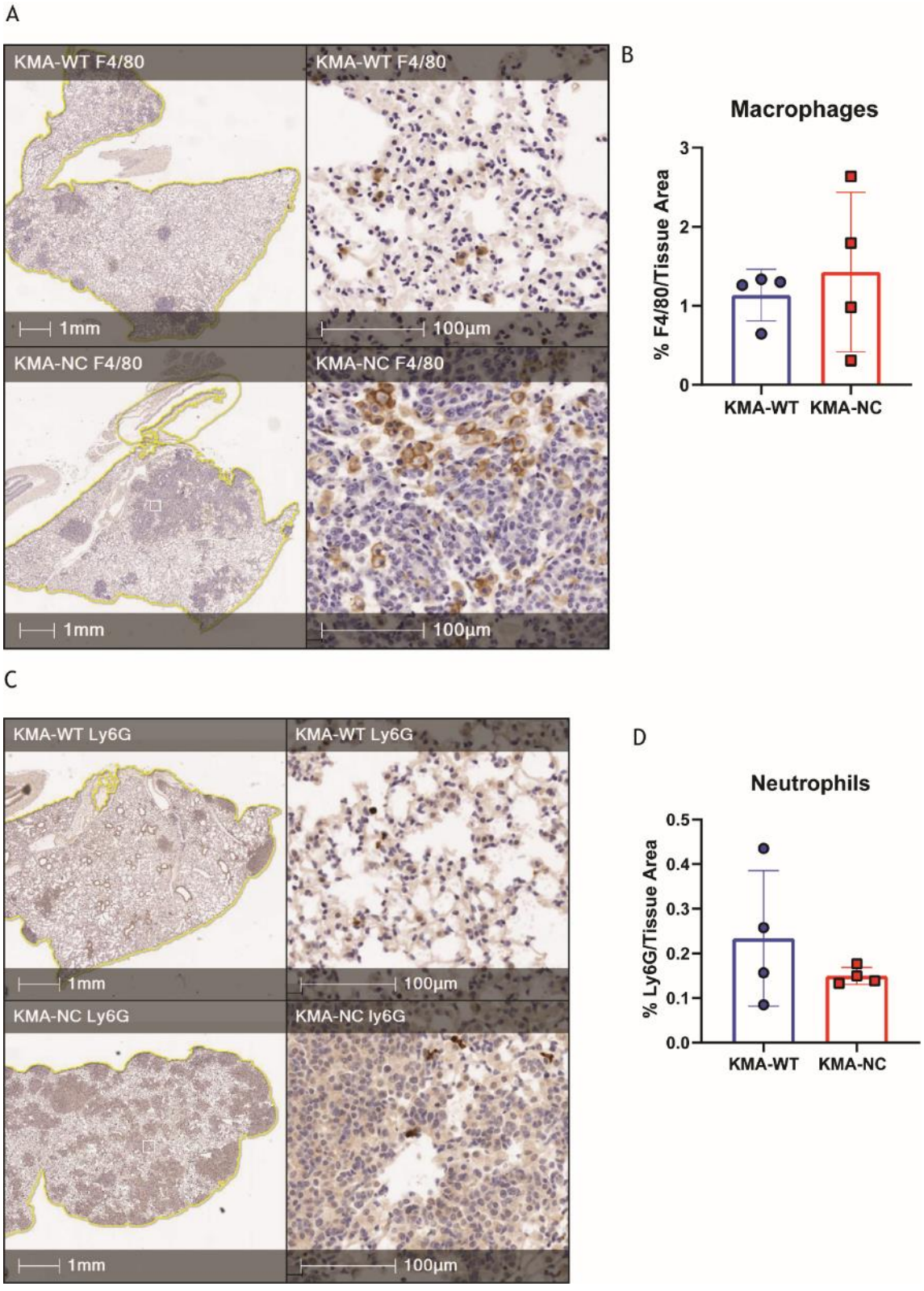

Figure 5-14 Levels of macrophages and neutrophils were comparable in KMA-NC lung samples relative to KMA-WT at 8 weeks. FFPE lung tissue samples from KMA-WT and KMA-NC at 8 weeks were sectioned (4 µm), at 100 µm apart for a total of 3 levels, and stained for F4/80, a macrophage marker, and Ly6G, a neutrophil marker. A, C) Representative images showing KMA-WT and KMA-NC lung tissue stained with F4/80 (A) and Ly6G (C) at 1 level, quantified using Halo™. Scale bars are shown in the images. Left panels show the whole tissue and the right panels show a 20x magnification. B) Data points show the average percentage of F4/80 (B) and Ly6G (D) stained area to tissue area. Each point represents individual mice, error bars represent mean ± SD. Statistical test: Mann-Whitney test; no significant difference (N=4 for both genotypes).

5.2.6.3 Circulating immune cells are unchanged at 8 weeks post viral induction in KMA-NC mice

Finally, the circulating immune cell populations were also assessed in KMA-WT compared to KMA-NC mice at the 8-week time point. Results showed that there are no significant differences in the levels of white blood cells in the KMA-NC mice compared to KMA-WT mice (Figure 5-15). There may be a slight trend to an increase in the white blood cells in the KMA-NC mice, which might be due to the higher lymphocyte levels. The monocyte and neutrophil populations were at comparable levels between the two genotypes. This suggests that there are no differences between the two genotypes in regards to circulating white blood cells.

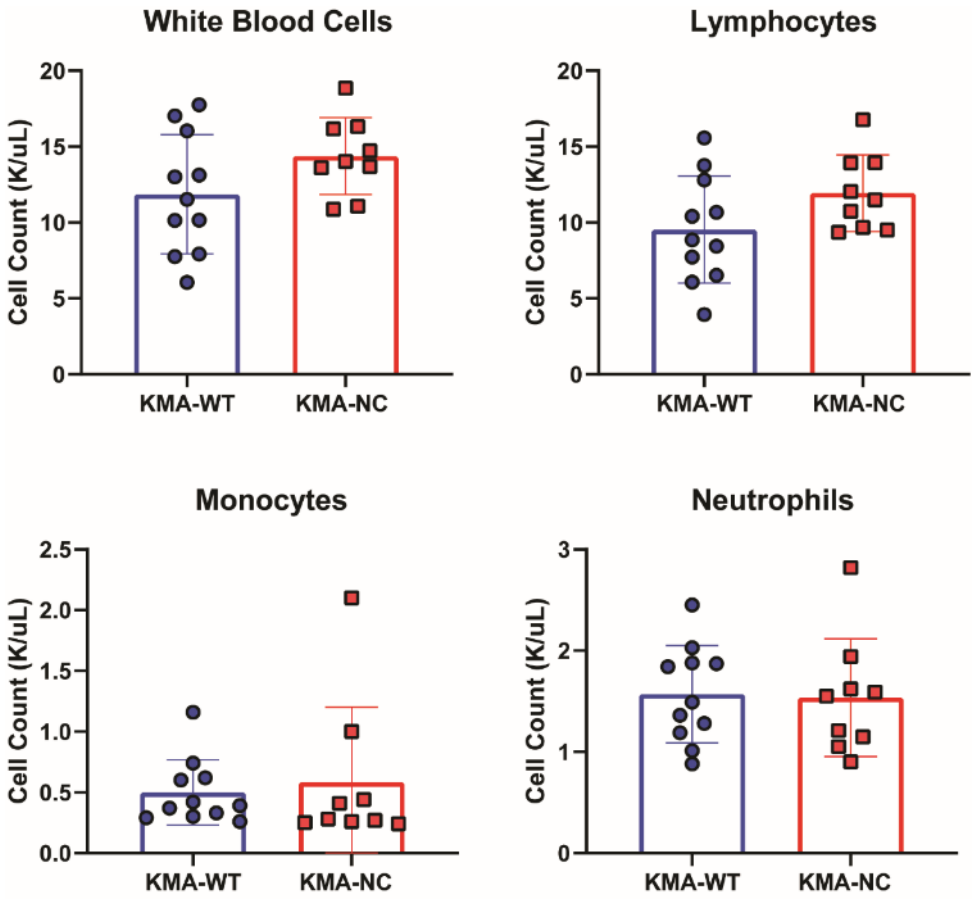

Figure 5-15 No differences were observed in white blood cell populations circulating in the blood of KMA-NC and KMA-WT mice at 8 weeks. Circulating white blood cells, lymphocytes, monocytes and neutrophils were determined from blood samples from KMA-WT and KMA-NC mice at 8 weeks. Samples were run on the IDEXX ProCyte Dx*; Data points represent individual mice, error bars showing mean ± SD (KMA-WT N=11; KMA-NC N=9).

5.2.7 KM-NC mice succumb to lung tumours faster than KM-WT mice

The addition of the ROCK1nc mutation to the KMA model led to a significant differences in survival, with the mice expressing ROCK1nc succumbing to tumourigenesis faster. Whilst one hypothesis was that this may be due to the modulation of immunogenicity in the APOBEC3B lung cancer model, the ROCK1nc allele was also crossed into the KM lung mouse model to assess effects in a non-immunogenic model. KM-WT and KM-NC mice were administered with the Sp-C-Cre adenovirus via intranasal inhalation at 8-10 weeks old and left to age. When clinical presentations of lung tumours were observed, mice were harvested. The clinical signs of lung tumours were the same as in the KMA mice, including difficulties in breathing, a pinched phenotype and weight loss. The addition of the ROCK1nc mutation to the KM lung adenocarcinoma model also accelerated tumourigenesis (Figure 5-16). This acceleration was observed in both male and female mice. The presence of the iRFP reporter did not affect the survival of the mice. The median survival days of the KM-NC cohort was 102 days, which was significantly lower than the KM-WT cohort at 119 days ($p=0.025$). Defective apoptotic membrane blebbing resulted in a poorer outcome in the KM model as well as in the KMA model.

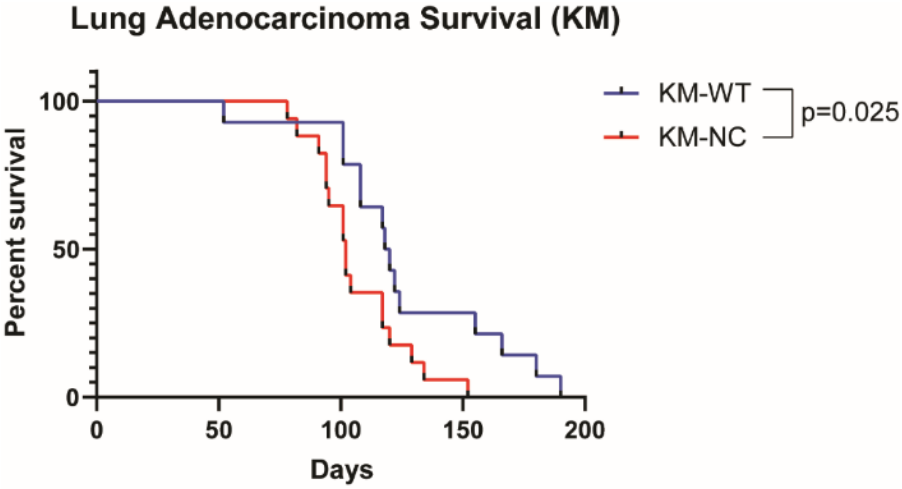

Cohort	Median Survival (Days)
KM-WT	119
KM-NC	102

Figure 5-16 The ROCK1nc mutation accelerated tumourigenesis in genetic mouse model (KM) of lung adenocarcinoma mice. Kaplan-Meier survival curve for KM-WT and KM-NC mice. Mice were administered with $1x10^8$ pfu of Sp-C Cre adenovirus via intranasal inhalation at 8-10 weeks of age to induce the expression $KRAS^{G12D}$ and MYC in type II alveolar cells. The ROCK1nc mutation is expressed in all cell types from birth. Median survival was 119 days for ROCK1wt cohorts, and 102 days for ROCK1nc cohorts from the date of viral induction. Lines represent the percentage of live mice. Statistical significance was determined using the Log-rank (Mantel-Cox) test. (KMA-WT – N=16, 7 males, 9 females (5 iRFP mice); KMA-NC – N=17, 10 males, 7 females (8 iRFP mice)).

5.2.7.1 Endpoint tumour burden in KM-NC and KM-WT are similar

Lung tissues harvested from mice at clinical endpoint were fixed in formalin. FFPE samples were sectioned at 3 levels, at a 100 µm apart, and subsequently stained with H&E. These tissue sections were quantified using HALO™ and averaged (Figure 5-17). Representative images show lung tissue (green) and tumour tissue (red) areas that were determined using the HALO™ algorithm (Figure 5-17A). The average percentage tumour area of KM-WT and KM-NC mice wert similar at clinical endpoint (Figure 5-17B). As liver metastasis was possible, liver weights were noted. No visible metastases were observed when harvesting the mice and there were no differences observed in the percentage of liver to body weight ratios between the genotypes (Figure 5-17C). The fluorescence of the iRFP marker was not imaged in this particular case and therefore liver metastasis can't be ruled out, however, given previous KMA experiments and others in the KM model, this is unlikely (Kruspig et al., 2018) These results shows that despite the accelerated tumourigeneses, the endpoint tumour burden was comparable between the two genotypes.

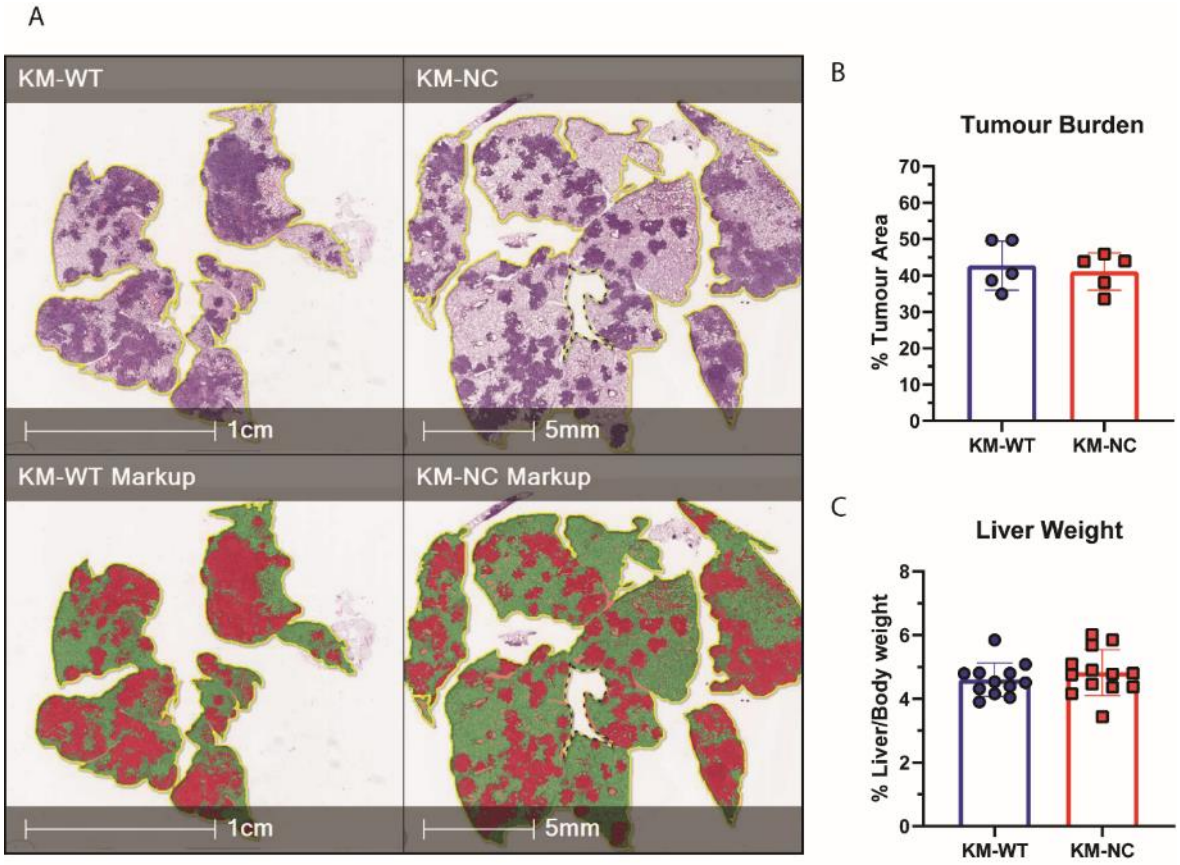

Figure 5-17 Endpoint tumour burdens are similar between KM-WT and KM-NC mice. KM-WT and KM-NC mice were harvested at clinical endpoint, post induction (Sp-C Cre $1x10^8$ pfu). The tumour burden was determined using histology by H&E stains. Sections from FFPE were cut at 100 µm apart, for a total of 3 sections. Sections were then quantified using Halo™ A) Representative images of one section showing the H&E stains of lung tissues and a marked-up image depicting the lung tissue (green) and tumour tissue (red). B) Halo™ quantifications of the average percentage of tumour area, by calculating the tumour area as a percentage of the tissue area of each level and averaging the 3 levels. Data points represent individual mice showing an average of the 3 sections per mouse, error bars represent mean ± SD (N= per genotype). C) The percentage of liver to body weight ratios of KM-WT and KM-NC mice. Data points represent individual mice, error bars represent mean ± SD (KMA-WT N=12, KMA-NC N=13).

5.2.8 KM-NC mice have greater levels of apoptotic cells

Cell death was explored in the endpoint lung tissues of KM-WT and KM-NC mice using immunohistochemistry. The sections were stained with antibody against cleaved caspase-3 and quantified using HALO™. Representative images show that there was a low number of caspase-3 positive cells in both KMA-WT and KMA-NC lungs (Figure 5-18A). When quantified, there was a statistically significantly (p=0.03) greater percentage of cleaved caspase 3 stained area in KM-NC mice in comparison to KM-WT mice, although there were relatively low percentages of cleaved caspase-3 staining in both genotypes. The immunohistochemistry data showed that the addition of the ROCK1nc mutation altered the levels of apoptotic cells found in the lung tumours.

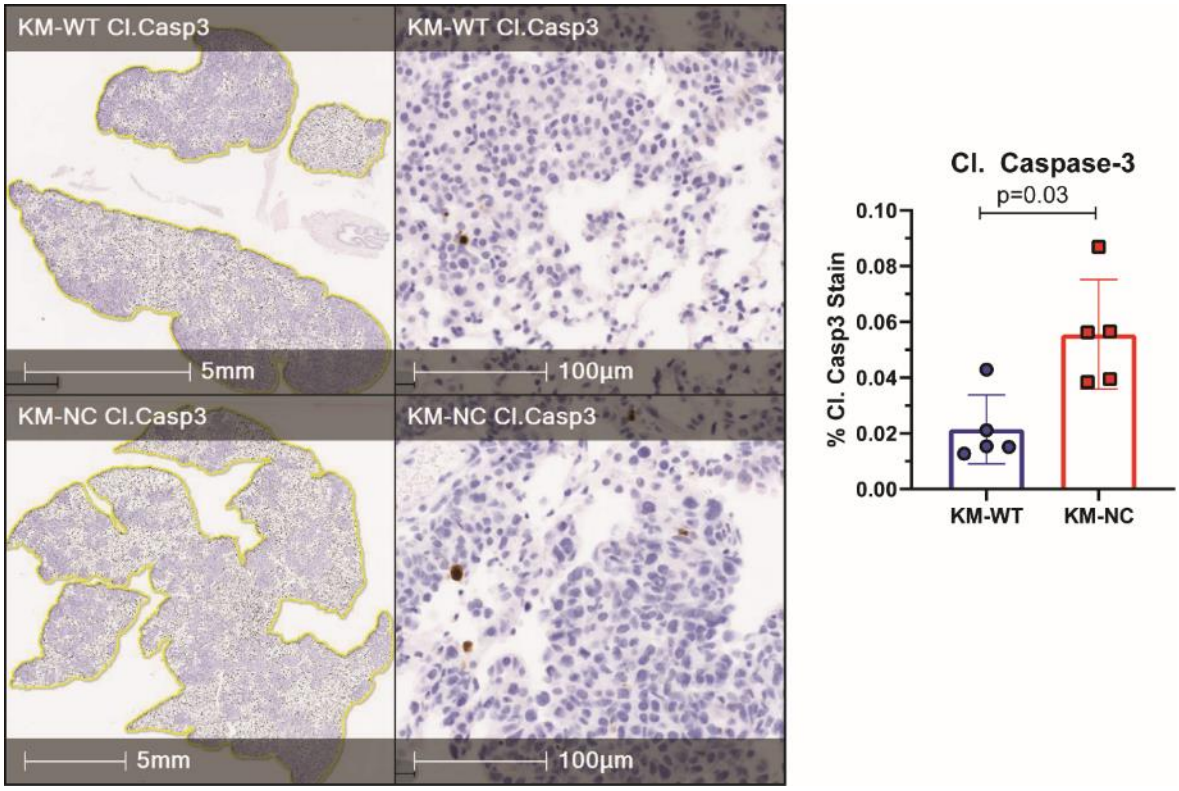

Figure 5-18 KM-NC mice have a greater percentage of cleaved caspase-3 staining in endpoint tumours. FFPE lung tissue samples from KM-WT and KM-NC at endpoint were sectioned (4 µm) and stained for cleaved caspase-3 (Cl.C3). A) Representative images showing KMA-WT and KMA-NC lung tissue stained with Cl.C3 of 1 levels, quantified using Halo™. Scale bars are shown in the images at 1 mm (left) and 100 µm (right). Left panels show the whole tissue and the right panels show a 20x magnification. B) Data points show the average percentage of Cl.C3 stain area to tissue area. Each point represents individual mice, error bars represent mean ± SD. Statistical test: Mann-Whitney; no significant differences (N=5 for both genotypes).

5.2.9 Immune cell profiles of KM mice

5.2.9.1 Assessment of immune cells in KM mice by immunohistochemistry

The CD4 and CD8α T-cell populations and myeloid populations, macrophages and neutrophils, were also investigated in the KM model by immunohistochemistry. Sections of lung tissue from KM-WT and KM-NC mice were stained with anti-CD4 and CD8α antibodies to assess the levels of T-cells at clinical endpoint. Representative images show that there are both CD4 and CD8α positive T-cells present in the lungs of both cohorts (Figure 5-19A, C). The CD4 and CD8α T-cell populations were comparable between KM-NC mice and KM-WT mice (Figure 5-19B, D).

The representative images show the presence of both macrophages and neutrophils in the endpoint tumours of both genotypes (Figure 5-20A, C). The

KM-NC cohort seems to have a greater percentage of F4/80 staining in comparison to KM-WT (Figure 5-20B). Although the KM-NC cohort might appear to have a greater percentage of F4/80 staining in comparison to KM-WT, this is likely due to an outlier of one mouse with low levels of F4/80 staining. Similarly, for the neutrophils, the KM-NC and KM-WT cohorts had similar levels of Ly6G staining (Figure 5-20D). It is important to note that the level of macrophages and neutrophil staining is relatively low. The addition of the ROCK1nc mutation to this KM model did not seem to particularly alter the levels of immune cells in endpoint tumours.

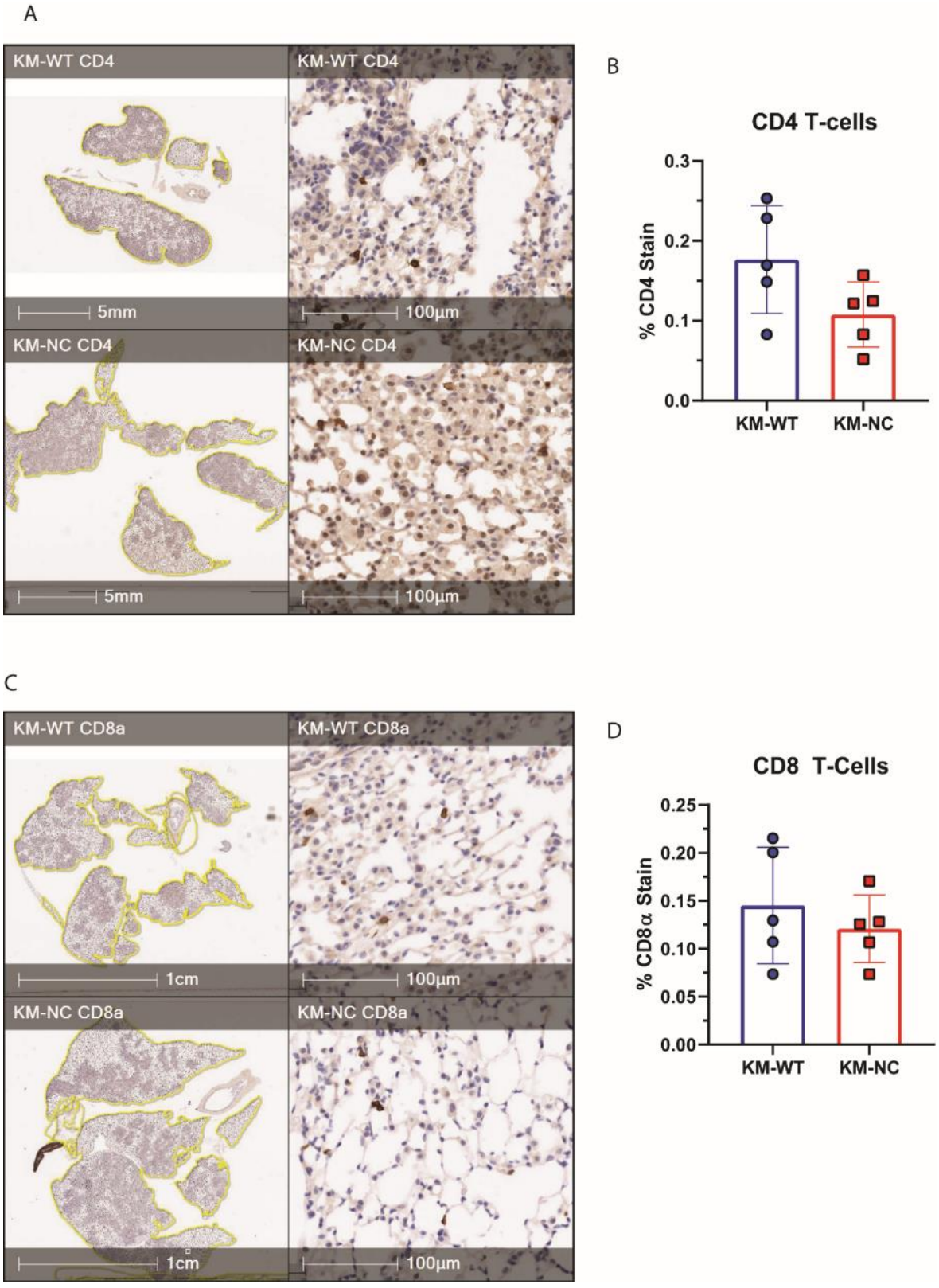

Figure 5-19 T-cells populations were comparable between KM-WT and KM-NC mice in endpoint lung tumours. FFPE lung tissue from KM-WT and KM-NC mice at endpoint were sectioned (4 µm), at 100 µm apart for a total of 3 levels, and stained for CD4 and CD8α positive T-cells. A, C) Representative images showing KM-WT and KM-NC lung tissue stained for CD4 (A) and CD8α (C) then quantified using Halo™. Scale bars are shown in the images. Left panels show the whole tissue and the right panels show a 20x magnification. B) Data points show the average percentage of CD4 (B) and CD8α (D) stained area to tissue area. Each point represents individual mice, error bars represent mean ± SD. Statistical test: Mann-Whitney Test; no significant differences (N=5 for both genotypes).

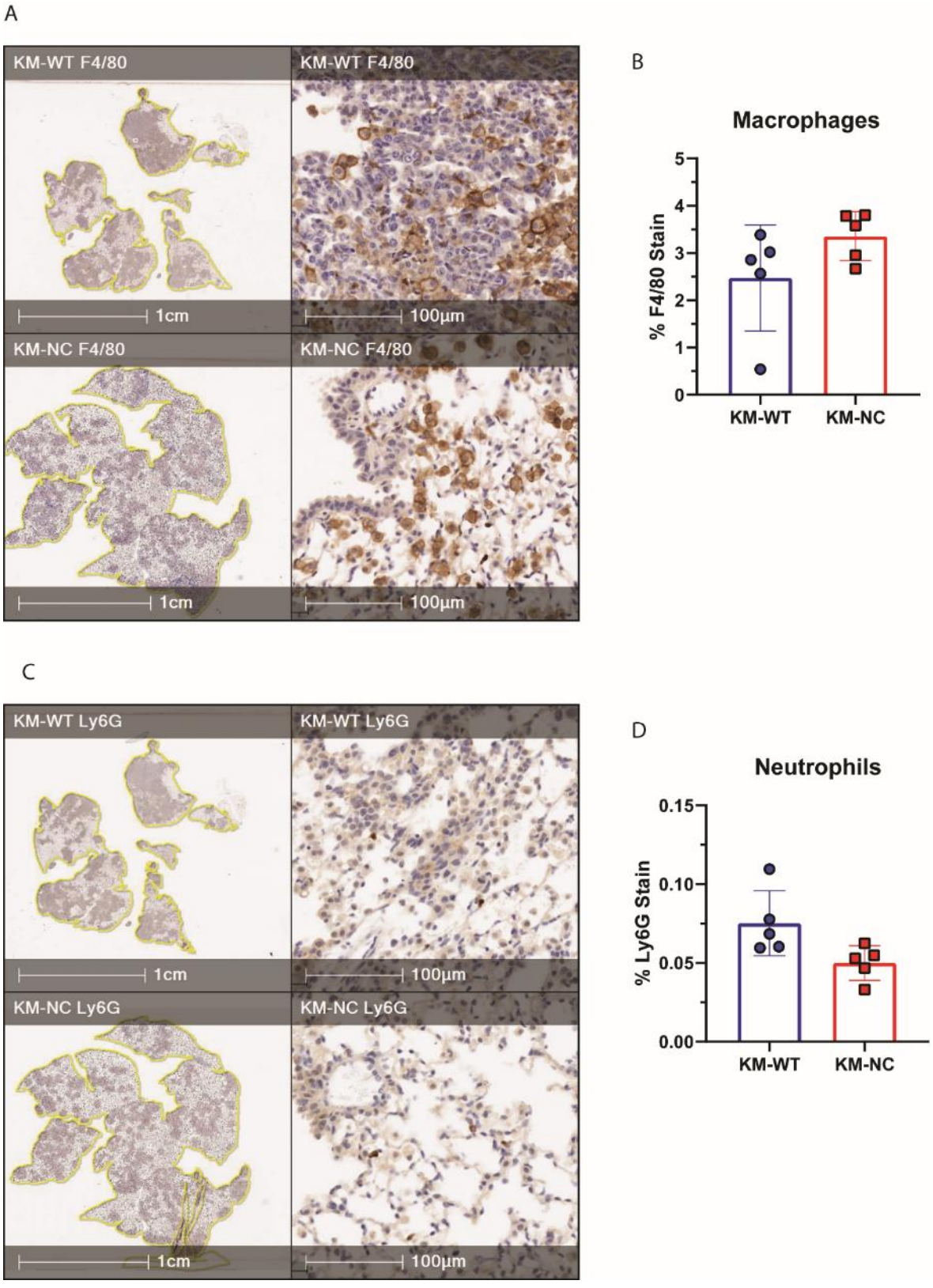

Figure 5-20 Myeloid populations were similar in KM-NC and KM-WT endpoint lung tumours. FFPE lung tissues from KM-WT and KM-NC mice at clinical endpoint were sectioned (4 µm) stained for F4/80, a macrophage marker, or Ly6G, a neutrophil marker. A, C) Representative images showing KM-WT and KM-NC lung tissue stained with F4/80 (A) and Ly6G (C), and quantified using Halo™. Scale bars are shown in the images. Left panels show the whole tissue and the right panels show a 20x magnification. B) Data points show the average percentage of F4/80 (B) and Ly6G (D) stained area to tissue area. Each point represents individual mice, error bars represent mean ± SD. Statistical test; Mann-Whitney; no statistical difference. (N=5 for both genotypes).

5.2.9.2 Circulating immune cell levels are comparable between KM-WT and KM-NC mice

Circulating immune cells were analysed in the KM cohorts. White blood cell counts, lymphocytes and neutrophils numbers were comparable between the two genotypes (Figure 5-21). The monocyte count was higher in a few KM-NC mice, however there was a high degree of variability in this cohort (Figure 5-21). The monocyte count appeared to be higher in the KM-NC cohort, however there were variabilities between the mice (Figure 5-21). Overall, these results show that there were no differences in the white blood cell populations circulating in the blood of KM-WT and KM-NC mice.

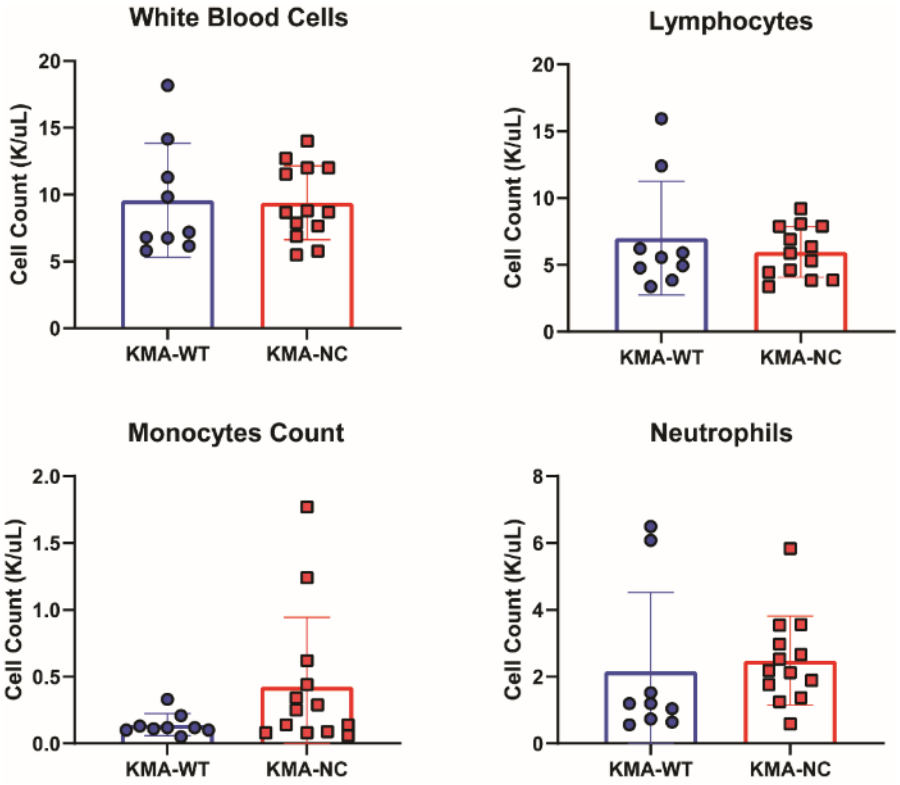

Figure 5-21 No differences were observed in immune cell populations circulating in the blood of KM-WT and KM-NC mice. Circulating white blood cells, lymphocytes, monocytes and neutrophils were determined from blood samples from KM-WT and KM-NC mice at clinical endpoint. Samples were run on the IDEXX ProCyte Dx*; Data points represent individual mice, error bars showing mean ± SD (KM-WT N=9; KM-NC N=13).

5.3 Discussion

The ROCK1nc mutation disrupts apoptotic cell morphology. Previous chapters showed that apoptotic cell membrane blebbing was largely dispensable for physiological and acute challenges in the thymus. When introduced into a cancer setting, however, apoptotic membrane blebbing has shown to be important in hepatocellular carcinoma (HCC) (Julian, 2015, Naylor, 2019), and now, lung adenocarcinoma. The KM lung model is a well-characterised mouse model to study non-small cell lung carcinoma (Kortlever et al., 2017). The addition of elevated APOBEC3B expression to the KM model was carried out by the Murphy lab, resulting in increased heterogeneity and immunogenicity in this lung cancer model (data not shown, unpublished observations). The KMA model was chosen to study the ROCK1nc model because of these attributes as there is a strong correlation between apoptosis and the immune system, particularly in the ROCK1nc HCC model (Julian, 2015).

The addition of the ROCK1nc mutation to the KMA model accelerated tumourigenesis and shortened survival. This set of results supports the initial hypothesis and contradicts what was seen with the HCC model. KMA-NC mice had a median survival of around 40 days less than KMA-WT mice. Despite this acceleration in death, the endpoint tumour burden in the KMA-NC mice was comparable to KMA-NC mice. Interestingly, at an earlier 8 week time point after oncogenic activation, the tumour burden was significantly higher in KMA-NC mice. This particular lung adenocarcinoma model is not known for being metastatic, which was not altered by the addition of the ROCK1nc mutation. The ROCK1nc mutation was not expected to affect any of the biological functions that ROCK mediates apart from the apoptotic membrane blebbing morphology. Thus, this set of results show that defective apoptotic membrane blebbing may worsen lung tumourigenesis. This is contrast to what was seen in the diethylnitrosamine (DEN) HCC model (Julian, 2015). In the DEN-HCC model, the ROCK1nc mutation reduced the tumour burden at 6 and 9 months after induction. The HCC model relies on a carcinogenic insult, which may respond differently to a genetic model in the way that apoptosis manifests and clearance is controlled. Furthermore, the lung and liver are two different organs, therefore these organs could respond differently to aberrant apoptotic membrane blebbing.

The ROCK1nc mutation was also crossed to the KM model to understand whether the difference seen in the KMA model was specific to the immunogenicity imparted by APOBEC3B over-expression. Contrary to expectations, the addition of the ROCK1nc mutation the KM model also accelerated tumourigenesis. Although defective apoptotic membrane blebbing worsened the survival outcome, the tumour burden at clinical endpoint was comparable to its wild-type counterparts. It can be speculated that at an earlier time point, the tumour burden would be greater in the KM-NC mice than the KM-WT mice. To confirm this hypothesis, an earlier 8 week time point could be investigated.

In both the KMA and KM models, the lung tumour samples obtained at clinical endpoint displayed statistically significantly higher levels of apoptotic cells with the ROCK1nc mutation. Similarly, although not statistically significant, there were also greater levels of cleaved caspase-3 staining in KMA-NC mice at the 8 week time point. The percentage of cleaved caspse-3 staining was lower at 8 weeks than at clinical endpoint in both genotypes. This could suggest that there was an increase in apoptosis over time. However, it should be noted that there were still a relatively low number of apoptotic cells in both models, at less than 0.1%. There have been studies that have shown that elevated cleaved caspase-3 levels in human cancer, including ovarian and colorectal cancer, is associated with poorer prognosis (Hu et al., 2014). Perhaps the levels of cleaved caspase-3 positive cells is important for tumourigenesis. In addition to cleaved caspase-3, a terminal deoxynucleotidyl transferase dUTP nick end labelling (TUNEL) assay could be done to confirm the levels of apoptotic cells and accumulation of apoptotic debris.

The low levels of apoptosis were unexpected. It was thought that enhanced apoptosis would extend survival, rather than contribute to tumourigenesis. One explanation could be the levels of MYC found in the tumours. The oncogene MYC has dual functions depending on the level found in the cell; at moderate levels, MYC drives proliferation, whilst MYC at high levels drives apoptosis (Murphy et al., 2008). Perhaps the proliferative signals dominate over the apoptotic signals. To confirm the proliferation status of the tumour cells, a 5-bromo-2'-deoxyuridine (BrdU) labelling experiment or Ki67 stain by immunohistochemistry could be performed. Furthermore, if tumour cells have high MYC levels, it is often accompanied by the inactivation of the apoptotic machinery (Schmitt and

Lowe, 2002, Finch et al., 2006). Another hypothesis would be that the apoptotic machinery is disabled in many of the tumour cells, thus, only a small number of cells were caspase-3 positive. To double check the apoptotic status in these tumours, western blotting for ROCK1, cleaved caspase-3 and the Bcl-2 apoptotic related proteins would be informative.

The KMA model was chosen as an example of an immunogenic tumour model, and so the immune cell profiles were investigated in the tumours. The results obtained in this study suggest that the ROCK1nc mutation did not alter the immune cell landscape in endpoint tumours or in circulation in the KMA model. Similar results were seen in the KM model, confirming that the ROCK1nc mutation did not alter the immune milieu. This was in contrast to what was observed in the HCC model, as increased neutrophils and CD8α T-cells were observed in ROCK1nc HCC tumours (Julian, 2015), which correlated with a lower tumour burden in the ROCK1nc mice. This suggests a relationship between apoptotic morphology and immune cell landscape. Furthermore, previous results in the Murphy lab showed that KMA tumours have a greater level of CD8α T-cells in comparison to the KM model (unpublished data). Due to these reasons, it was surprising that the ROCK1nc mutation did not make a difference to the immune landscape. . It would be interesting to assess if the phagocytic capabilities of macrophages and dendritic cells for tumour cells are functional in the KM/KMA models. Phagocytosis assays would be helpful in determining if phagocytosis of the tumour cells was impaired, and thereby making them difficult to be efficiently cleared. For example, apoptotic lung cells could be co-cultured with bone marrow derived macrophages to assess phagocytic ability and clearance.

Based on these exciting results it is obviously important to deciphering how apoptotic membrane blebbing contributes to tumourigenesis and the clinical relevance of this observation. The crucial analysis would be to determine the apoptotic morphology of both healthy and tumour cells in the lungs. This could be done using scanning electron microscopy and time lapse microscopy. In addition, the release of intracellular contents from tumour cells would be informative. If the lung tumour cells have a disrupted apoptotic morphology, this could skew cell death towards a more necrotic phenotype – the release of intracellular content and necrosis has been with poorer prognosis in patients (Liu and Jiao, 2019). For example, detecting damage associated molecular patterns

(DAMPs) including ATP or HMGB1 in the tumours *in vivo* or using the lactate dehydrogenase LDH assay on apoptotic tumour and lung cells *in vitro* could shed light on the apoptotic status of the cells. Furthermore, understanding the levels of ROCK1 in the lung under physiological conditions and how it compares to a tumour setting would also be important.

From a clinical standpoint, given the results in this study, a ROCK inhibitor might not be suitable treatment for lung cancer. However, ROCK inhibitors do not only inhibit the apoptotic morphology but also the biological functions of ROCK1 that could contribute to tumourigenesis by promoting cell migration and angiogenesis (Croft et al., 2004). Another study has further shown a relationship between poor prognosis and elevated ROCK1 levels in patients (Hu et al., 2019). Abolishing all biological functions of ROCK using an inhibitor *in vitro* abrogated cell migration, invasion and adhesion (Hu et al., 2019). Furthermore, the use of the ROCK inhibitor Fasudil, reduced the tumour burden in a DEN-induced HCC model, recapitulating what was seen in the ROCK1nc, DEN-HCC model (Naylor, 2019, Julian, 2015) Another interesting study highlighted the effect of ROCK inhibitors and immunogenic cell death in promoting anti-tumour immunity in both syngeneic and genetic mouse mammary tumour models (Nam et al., 2018). Nam *et. al.* demonstrated that in the presence of ROCK inhibitor, phagocytes have a greater ability to clear tumour cells; the ROCK inhibitor specifically modulates the phagocytic ability of phagocytes and enhances T-cell priming by dendritic cells (Nam et al., 2018). These studies would suggest that a ROCK inhibitor may be beneficial as it underscores the contributions of the biological ROCK in tumourigenesis. As the ROCK1nc mouse model specifically dissects the role of apoptotic membrane blebbing, preliminary experiments are currently ongoing in KMA-WT cohorts treated with ROCK inhibitor, Fasudil. This drug would inhibit all the functions of ROCK, not only apoptotic membrane blebbing. It should be noted that although Fasudil does primarily target ROCK, it does also inhibit other kinases including protein kinase A. Whether a ROCK inhibitor would be useful in the lung adenocarcinoma model remains to be seen.

The mechanism as to how this might occur is yet to be elucidated. Initial experiments into understanding how the lung and tumour cells die, as well as how the phagocytic cells clear tumour cells would be important. Performing *in vitro* experiments from isolated lung cancer cells from a ROCK1nc and ROCK1wt

background to assess morphology and release of intracellular content upon apoptotic stimuli should be done. Furthermore, performing RNA sequencing on endpoint lung tumours would provide some direction into what pathways are important in tumourigenesis as currently, a mechanism is unknown.

To interrogate the role of apoptotic membrane blebbing in tumourigenesis, understanding the role of apoptosis in tumours in necessary. Apoptosis is traditionally known to be immunologically silent. However, paradoxically, higher levels of apoptosis correlate with more aggressive tumours (Leoncini et al., 1993, Gregory et al., 2016, Gregory and Paterson, 2018). In aggressive tumours, the levels of apoptotic cells range between 5-10% depending on the cancer type in comparison to 0.5-2% in non-aggressive cancers (Ucker and Levine, 2018) It is also established that upon apoptosis, phagocytes including macrophages are recruited (Gregory and Devitt, 2004). The concept, onco-regenerative niche was developed to reflect the role of apoptosis in shaping tissue regeneration and aggressive malignant disease mediated by tissue-associated macrophages and extracellular vesicles (Gregory and Paterson, 2018). The suppression of apoptosis in B-cell non Hodgkin lymphoma xenografts resulted in a reduction in tumour associated macrophages and improved prognosis, suggesting that apoptosis can be important in modulating tumour activity (Ford et al., 2015). Additionally, extracellular vesicles from apoptotic endothelial cells have also shown immunomodulatory capabilities (Dieudé et al., 2015). It is then plausible then that extracellular vesicles from tumour cells can do the same.

To this end, although a phenotype was observed in the KMA and KM model, alternative tumour models would perhaps be more intuitive and straightforward in deciphering the role of blebs in anti-tumour immunity. Using a transplant model system in a variety of ways could be more promising at deciphering the role of blebbing. For example, ROCK1nc lung tumour cells or fragments could be transplanted into ROCK1wt mice to assess tumour growth and clearance by immuno-surveillance of the tumour. Additionally, choosing a model system in which cell death is important and could promote tumourigenesis may be a better model system to address apoptotic membrane blebbing. It is also know that apoptosis can facilitate tissue regeneration, best characterised in the HCC model (El-Serag and Rudolph, 2007). Furthermore, T-cell lymphomas can arise due to higher susceptibility of older T-cells to apoptosis (Martins et al., 2014, Moreno,

2014) and in an aggressive B-cell xenograft model, apoptosis was shown to be important in transforming macrophages (Ford et al., 2015). Thus, using a T-cell lymphoma model or an aggressive B-cell lymphoma model may be more appropriate.

In summary, the addition of the ROCK1nc mutation to two lung adenocarcinoma models, KMA and KM, resulted in accelerated tumourigenesis. This would suggest that defective apoptotic membrane blebbing propagates carcinogenesis irrespective of the ability of APOBEC3B to induce heterogenic and immunogenic tumours.

6 The role of the MDM2 P1 and P2 promoters in lymphomagenesis

6.1 Introduction

6.1.1 Overview of the MDM2 protein structure, function and regulation

Murine double minute 2 (MDM2), belonging to the MDM family of proteins, is most notable for its negative regulation of the tumour suppressor p53. (Iwakuma and Lozano, 2003). As an E3 ubiquitin ligase, MDM2 can ubiquitinate its substrate, such as p53, which targets the protein for subsequent degradation (Nakamura et al., 2000). The p53-MDM2 axis has been extensively studied. The tumour suppressor p53 is responsible for regulating the gene expression of a variety of proteins involved in apoptosis in both the intrinsic and extrinsic pathways, including *Bax* and *Fas* (Haupt et al., 2003). The loss of MDM2 contrbutes to unregulated p53, which results in p53-induced apoptosis(de Rozieres et al., 2000). As such, MDM2 is highly important in maintaining levels of p53 which ultimately can contribute to determining if a cell lives or dies.

The relationship between the two proteins has been exemplified in *in vivo* models as mice deficient in the MDM2 protein are embryonically lethal (Montes de Oca Luna et al., 1995). This phenotype is however rescued by a deletion of *TP53* in tandem with *Mdm2*. The MDM2 protein functions as either a homodimer or a heterodimer, with MDMX (also known as MDM4 in humans). The homolog MDMX resides out of the nucleus (Toledo and Wahl, 2007). Despite this, the loss of MDMX *in vivo* results in the same phenotype as MDM2 deletion and is similarly rescued by the loss of p53 (Migliorini et al., 2002). Without tight regulation of MDM2, there are repercussions on p53 and its functions. This is translated into a pathological phenotype, including cancer. Multiple human tumours exhibit an amplification of MDM2, which in turns represses the tumour suppressor p53 (Rayburn et al., 2005). Thus, MDM2 can act as an oncogene if left unchecked.

Although MDM2 is most notable for its interaction and control of p53, with a p53 binding domain in its structure; it can also interact with other proteins and have p53 independent functions (Ganguli and Wasylyk, 2003). Utilising both *in vitro* and *in vivo* studies, MDM2 has been shown to be involved in a myriad of

biological functions including cell differentiation and cell cycle control (Riley and Lozano, 2012). Given the importance of the MDM2-p53 axis as well as the p53-independent functions of MDM2, tight regulation of MDM2 is required. This is achieved at both the transcription level (discussed next) and post-translational level (Lozano, 2012). The function of MDM2 can be negatively controlled by post-translational modifications, such as phosphorylation, and its negative regulator $p14^{ARF}$ (Nag et al., 2013). The protein $p14^{ARF}$ retains MDM2 in the nucleolus, disrupting its function. These regulations are important in maintaining levels of MDM2 during homeostasis. Disruptions in these pathways often yields enhanced MDM2 functions. Thus, there are many parts in the MDM2-p53 axis that need to function correctly in order to maintain homeostasis.

6.1.2 The MDM2 promoters

The transcription of the *Mdm2* gene is controlled by two promoters – P1 and P2 (Figure 6-1). The P1 promoter is upstream of exon1 whilst the P2 is upstream of exon 2. The P1 promoter regulates the transcription of basal MDM2 expression and functions independent of p53. The P2 promoter, on the other hand, controls the expression of MDM2 induced by p53, under stressed conditions (Zauberman et al., 1995, Barak et al., 1994, Jones et al., 1996). This constitutes the feedback loop in the MDM2-p53 axis; higher levels of p53 induce the expression of MDM2, which in turn repress p53 (Lahav et al., 2004). The p53 protein binds to a response element upstream of exon 2 in *Mdm2*, driving transcription of MDM2.The transcription start site of the gene itself begins at exon 3. The transcript length depends on the promoter. The P1 promoter produces a longer transcript than the P2 promoter (Landers et al., 1997). Transcripts from the P1 promoter are translated 8 times less efficiently than P2 transcripts (Jin et al., 2003). Once translated, the MDM2 proteins are identical. The function of the MDM2 P2 promoter is currently better understood than the P1. It has been shown however that higher levels of the P1 transcript in conjunction with lower levels of p53 transcripts result in a poorer prognosis in human pancreatic adenocarcinomas (Grochola et al., 2011).

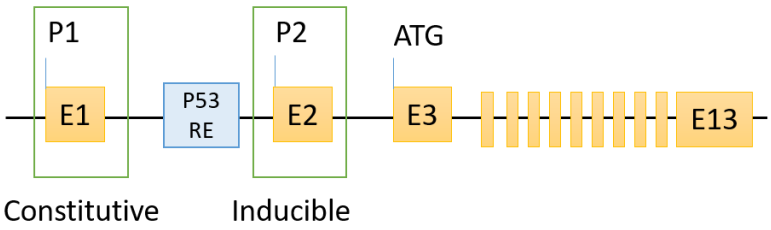

Figure 6-1 *Mdm2* transcription driven by the constitutive P1 promoter and inducible P2 promoter. The *Mdm2* gene contains 13 exons (E). Constitutive expression of MDM2 is driven by the P1 promoter. Under conditions of stress, p53 can bind to the responsive element (RE) upstream of the P2 promoter to drive upregulation of MDM2, which in turn suppresses p53. This is part of the regulatory loop for the MDM2-p53 axis. The transcription start site begins at E3. The P1 transcript is longer than the P2 transcript. Once translated, the protein is the same size (90kDa).

6.1.3 MDM2 in lymphoma

MDM2 is highly important in regulating homeostasis in cells. The oncogenic role of MDM2 in human cancers have been well documented, including leukemias and lymphoma (Wang et al., 2008). The MDM2 protein was found to be overexpressed in lymphomas, including non-Hodgkin's lymphoma, Burkitt's lymphoma and Myc-driven lymphomas (Watanabe et al., 1996, Eischen et al., 1999, Wilda et al., 2004). The Eμ-MYC transgenic mouse is a model of Burkitts lymphoma in which overexpression of c-MYC in B-cells leads to lymphomagenesis (Adams et al., 1985). Inactivation of p53 in this model was commonly observed, whilst an overexpression of MDM2 was also found to occur (Eischen et al., 1999). Of note, overexpression of MDM2 using a genetically engineered mouse (GEM) model also predisposed to mice to spontaneous tumour formation, including lymphomas (Jones et al., 1998).

6.1.4 Experimental background

The project discussed in this chapter stemmed from findings in the Sansom lab (Beatson Institute) on teasing apart the role of the P1- and P2- MDM2 promoters in intestinal cancer using the $Apc^{Min/+}$ mouse model of intestinal cancer. This was achieved through the use of mice with genetically engineered perturbations in either P1 or P2 promoter regions of MDM2. The 'MDM2 P1-knockout (P1-null)' model and 'MDM2 P2-mutant' model were generated by and in collaboration with Dr. Mark Boyd (University of Liverpool). In the P1-null mice, the P1 *Mdm2* promoter was deleted yielding a heterozygous deletion (P1-het) or homozygous deletion (P1-null), but transcription from P2 is unaffected. In the 'P2-mutant'

mouse, 8 base pairs in the P2 promoter region were mutated which essentially abolishes ability to transcribe from this promoter, but transcription from P1 is unaffected. The P1-null and P2-mutant mouse lines were then crossed onto the *Apc*$^{Min/+}$ model. Interestingly, perturbation in tumour onset was observed in the P1-null model but not in the P2-mutant model. Mice with a heterozygous deletion of the P1 promoter had delayed intestinal tumourigenesis (unpublished data). Furthermore, none of the P1-promoter null mice reached endpoint with intestinal tumours. However, this data was confounded because before mice could develop symptoms of intestinal tumours, all P1-null mice had succumbed to thymic lymphoma. This was a highly unexpected phenotype as lymphomas do not normally occur in this intestinal model.

6.1.5 Experimental aims

The functions of MDM2 are well understood, however, the individual roles and the contribution of the P1 and P2 promoters in tumourigenesis is not well characterised. Both the P1 and P2 mouse models were crossed onto the Eμ-MYC lymphoma model. The rationale for this study was i) as a follow up to the emergence of lymphomas in the *Apc*$^{Min/+}$-model to determine if disruption of one or either of the MDM2 promoters made lymphoid cells more tumour prone and, ii) in a model known to be susceptible to p53 loss (Eischen et al., 1999) could this dissect out the p53-dependent and p53-independent functions of MDM2.

6.2 Results

6.2.1 Heterozygous loss of the P1 or P2 *Mdm2* promoters have opposite effect in lymphomagenesis

To assess whether the status of the P1 and P2 MDM2 promoters had an effect on tumourigenesis and overall survival, mice on an Eμ-MYC background were crossed to the P1-knockout and P2-mutant mouse models. The effect of both the heterozygous and homozygous loss of the P1 promoter, and the heterozygous and homozygous disruption of the P2 promoter were explored in this model. All mice had been backcrossed to a C57Bl/6 background (N10) and littermate controls were used in each colony. Mice were aged and harvested upon clinical presentation of lymphoma or up until 330 days (roughly 11 months). Signs of lymphomagenesis included the enlargement of the lymph nodes, laboured

breathing which often signifies a thymic lymphoma, and distended abdomen for signs of splenic lymphomas. It should be noted that WT mice from the P1-null and P2-mutant cohorts were combined for the analysis as the survival curves were similar to each other and not statistically significantly different.

In the P1-null cohort, both the heterozygous and homozygous loss of the P1 promoter delayed lymphomagenesis in comparison to the wild-type MDM2 counterparts (Figure 6-2A). The heterozygous loss of the P1 promoter has statistically significantly delayed the tumourigenesis in this model ($p=0.03$). At the time of writing, the P1-null cohort is still ongoing and is not yet matured and as such fails to reach statistical significance. However it appears that survival is extended (Figure 6-2A). It should be noted that mice null for the P1 promoter have reduced fertility, therefore it took longer to obtain mice with the correct genotype in this cohort. Furthermore, there is a higher number of females in comparison to males in the P1 cohorts, therefore it is still unknown whether this phenotype is the same in males. The Eμ-MYC lymphoma is known to have a high penetrance rate, with over 90% of mice developing lymphomas by 6 months on a mixed C57Bl/6 background (Harris et al., 1988). MDM2-WT mice did result in a relatively high percentage of disease incidence at the 330 day mark (11 months). The percentage incidence of P1-HET mice was much lower at 42%, whilst the P1-HOM cohort thus far, has a disease penetrance of 67%. The heterozygous and homozygous loss of the P1 promoter not only delayed tumourigenesis, but also seemed to reduce penetration at the specified time point. Both the hetero- and homozygous loss of the P1 promoter behaves in a similar manner, suggesting that constitutive P1 promoter driving basal levels of MDM2 is likely to contribute to tumourigenesis.

Interestingly, the heterozygous mutation of the P2 promoter significantly accelerated tumourigenesis in comparison to its MDM2 wild-type counterparts (Figure 6-2B; $p=0.015$). This acceleration in lymphomagenesis in the heterozygous P2 cohorts is seen in both males and females. Mice with a homozygous loss of the P2 promoter does have a lower median survival than WT cohorts; however, there are 5 mice in this cohort that contribute to the tail on the survival graph (% Incidence – WT - 82% vs HOM 64%; Median Survival – WT 152 days vs HOM 123 days). This is seen in both male and female mice in the P2-HOM cohort. The P2 cohorts are completed and mature, and indicates that losing one

allele of the p53-inducible P2 promoter accelerates lymphomagenesis whilst the homozygous loss of the P2 promoter does not seem to alter tumourigenesis overall.

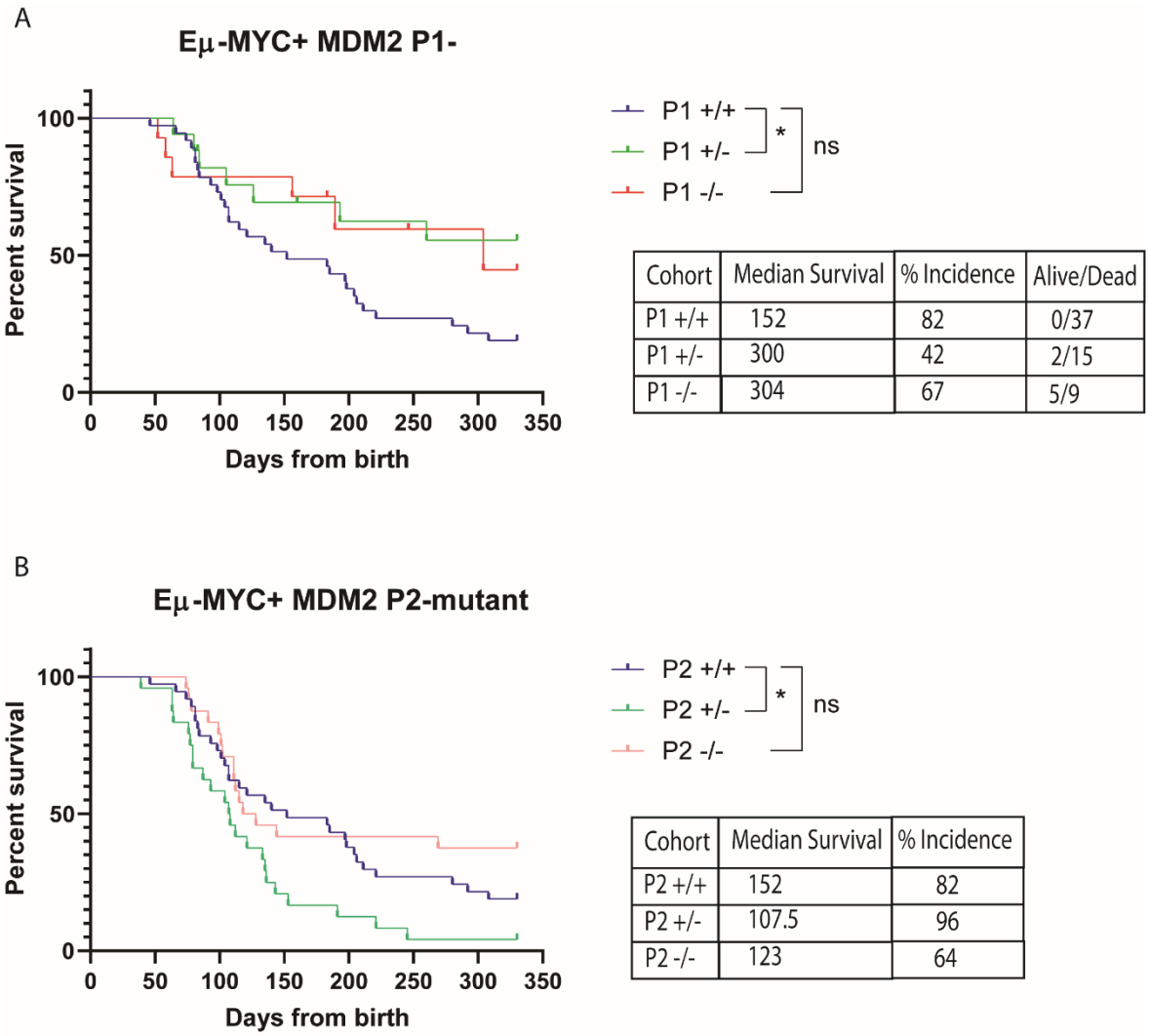

Cohort	Median Survival	% Incidence	Alive/Dead
P1 +/+	152	82	0/37
P1 +/-	300	42	2/15
P1 -/-	304	67	5/9

Cohort	Median Survival	% Incidence
P2 +/+	152	82
P2 +/-	107.5	96
P2 -/-	123	64

Figure 6-2 The heterozygous loss of the P1 and P2 MDM2 promoter have opposing effects on lymphomagenesis in the Eμ-MYC model. All the mice in both experimental cohorts are Eμ-MYC positive. In the P1-null cohort, the P1 promoter is either wild-type (P1 +/+), a heterozygous loss (P1 +/-) or a homozygous loss (P1 -/-). In the P2-mutant cohort, P2 promoter is either wild-type (P2 +/+), a heterozygous mutation (P2 +/-) or a homozygous mutation (P2 -/-). The median survival (days) are shown in the tables. Lines represent the percentage of alive mice. Statistical significance was determined using the Log-rank (Mantel-Cox) test. (P1 +/+ N= 18 (8 males & 10 females); P1 +/-N=14 (4 males, 10 females); P1 -/-N=14 (3 males, 11 females); (P2 +/+ N= 19, 8 males & 11 females; P2 +/-N=24 (8 males, 16 females); P2 -/-N=23 (10 males, 13 females).

6.2.2 Distribution of disease is unchanged in the P1 and P2 MDM2 experimental cohorts

As well as differences in survival in the P1-null and P2-mutant experimental cohorts, the disease distribution was also assessed. At endpoint, Eμ-MYC+ mice present with clinical signs of lymphoma which can be categorised into 3

different groups – lymphoma, thymic lymphoma and multicentric lymphoma. Lymphomas present as enlargements of the lymph nodes and/or spleen, while thymic lymphomas predominately manifest as an enlarged thymus Mice with multicentric lymphoma have an enlargement of the lymph nodes, spleen and the thymus. As some differences were seen in the survival analyses, understanding if the altered MDM2 status could skew the disease profile was important. The type of lymphoma that the mice in both the P1-null and P2-mutant experimental arms succumbed to and their age was recorded.

All three types of lymphoma categories are found in both the P1 and P2 cohorts (Figure 6-3). The heterozygous loss of the P1 promoter (P1-HET) cohort only contains one mouse that succumbed to thymic lymphoma (Figure 6-3A, B). Similarly, there is an even distribution of the three types of lymphomas in the P1 HOM cohort (Figure 6-3A). When compared to each of the genotypes, the P1-HET cohort had two mice that succumbed to lymphomas whilst none of the mice in the P1-HOM cohort so far have been harvested due to lymphomas at the330 day time point (Figure 6-3A, B). Furthermore, there are low numbers of mice in both the P1-HET and P1-HOM cohort that succumbed to thymic lymphomas (Figure 6-3). The results shown in the P1-null cohorts are a reflection of what is seen in the survival curves. The type of lymphomas and age that the mice were harvested due to lymphoma in the P1-HET and P1-HOM is likely a reflection of the enhanced survival seen in these two cohorts. The disease distribution in the P2 experimental arm is generally fairly distributed between the three types of lymphomas for each genotype (Figure 6-3C). The data also seems to suggest that P2-HET and P2-HOM mice succumbed to lymphomas slightly earlier than their WT counterparts (Figure 6-3C). This is again reflective of the lower median survival of the P2-HET and P2-HOM cohorts. Overall, for both the P1 and P2 experimental cohorts, there was no significant skew towards any lymphoma category.

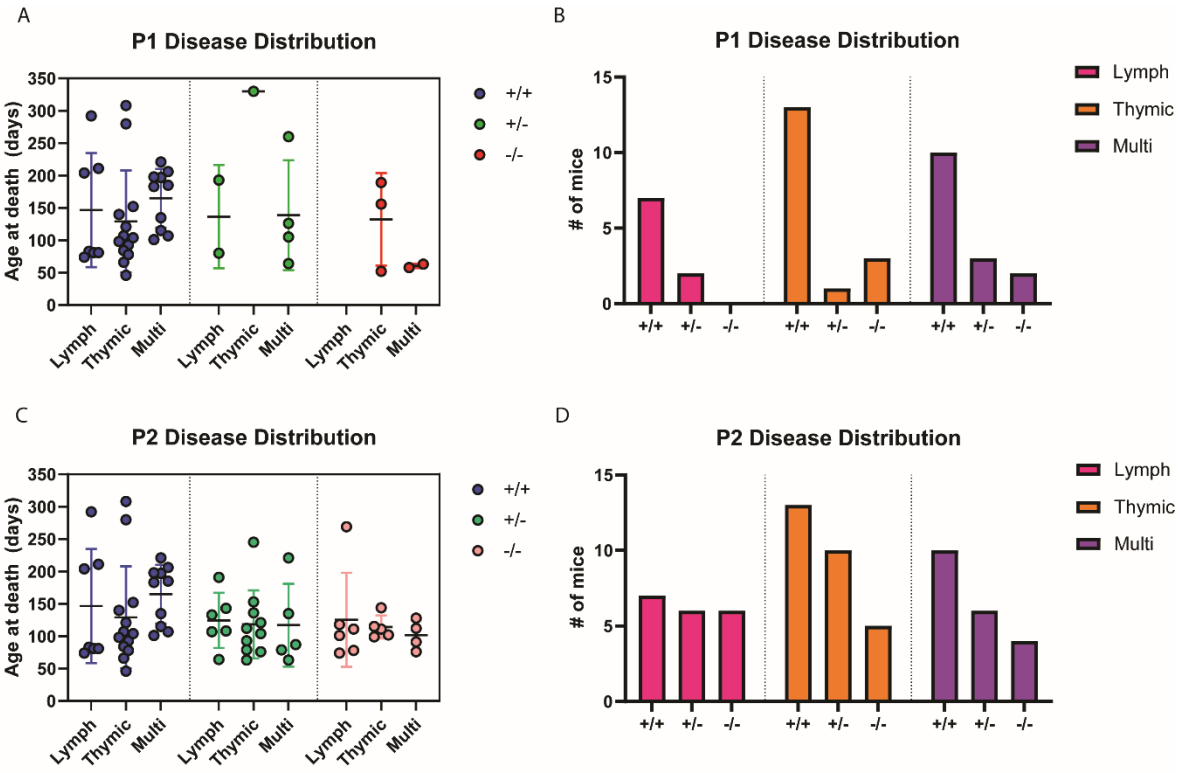

Figure 6-3 The disease distribution profiles of the MDM2 P1-null and P2 mutant, Eμ-MYC cohorts at the 330 day time point. The disease category of wildtype (+/+), heterozygous loss (+/-) and homozygous loss (-/-) of the MDM2 P1-null and P2-mutant, Eμ-MYC+ mice were recorded at clinical endpoint. The disease distribution per genotype and the age of death of the P1 (A), and P2 (C) are shown. Data points represent individual mice. Error bars represent mean ± SD. Statistical test: Kruskal-Wallis (P1 +/+ N=17; P1 +/- N=9; P1 -/- N=7) (P2 +/+ N=18; P2 +/- N=22; P2 -/- N=17). B/D) Data sets shown based on number of mice in the disease category for the P1-null and P2-mutant experimental cohorts. A/C) WT- Blue, HET- Green, HOM-Red/Pink; B/D) Pink – Lymphoma; Orange – Thymic lymphoma; Purple - Multicentric

6.2.3 Organ weights are unchanged in the MDM2 P1 and P2 experimental cohorts at endpoint

In addition to the disease distribution, another parameter to assess whether the *Mdm2* status altered the tumour profile at endpoint is the mouse and organ weights. The body and organ weights of the P1 and P2 mice were recorded at clinical endpoint. The organs that were weighed include the spleen, thymus, and mesenteric lymph node (MLN) as this can be used as a proxy for disease burden. In the P1 experimental arm, generally, the P1-HOM mice seemed to have a slightly lower body weight compared to P1-HET and P1-WT mice (Figure 6-4). Despite this, the percentage of the spleen, thymus and MLN weight to body weight ratio is relatively comparable between the WT, P1-HET and P1-HOM cohorts. In the P2 experimental arm, the body weight of the WT, P2-HET and P2-HOM mice are comparable (Figure 6-5). The spleen, thymic and MLN weights to body weight percentages are also comparable between the genotypes. As the

skew of disease distribution was not different between the genotypes in the P1 and P2 experimental arm, the results obtained here are as expected.

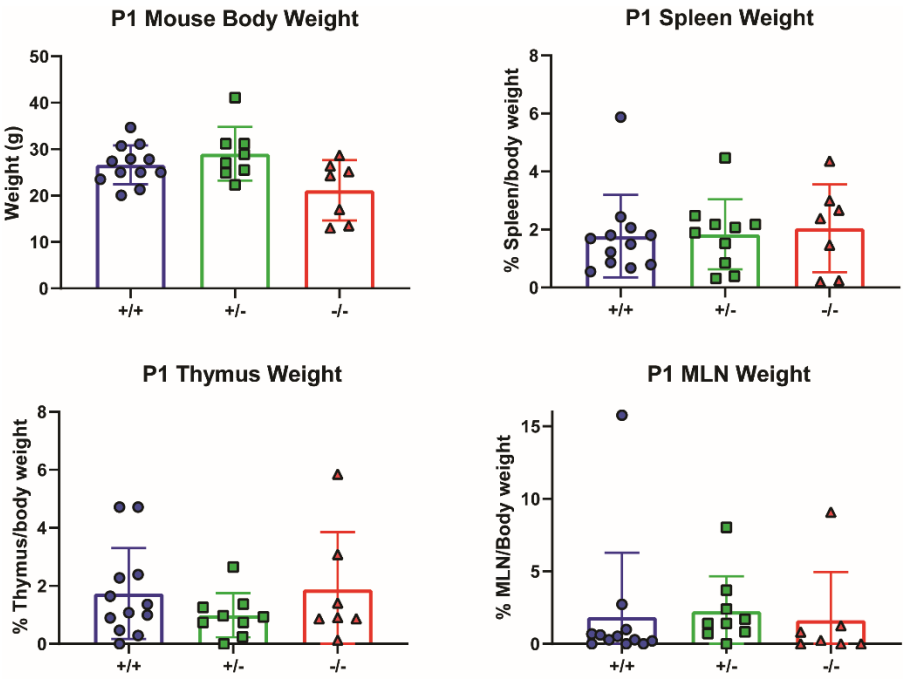

Figure 6-4 Body and organ weights of Eμ-MYC; MDM2-P1-null mice are comparable to MDM2-P1-WT controls. The body, spleen, thymus and mesenteric lymph node (MLN) weights were recorded for wild-type P1 (+/+) mice, mice with a heterzygous loss of the P1 promoter (+/-) and mice with a homozygous loss of the P1 promoter (-/-), all on an Eμ-MYC background. The percentage of organ to body weights were then calculuated. The data points represent individual mice. Error bars represent mean ± SD. Statistical test: Kruskal-Wallis (+/+ N=12, +/- N=9-10; -/- N=7).

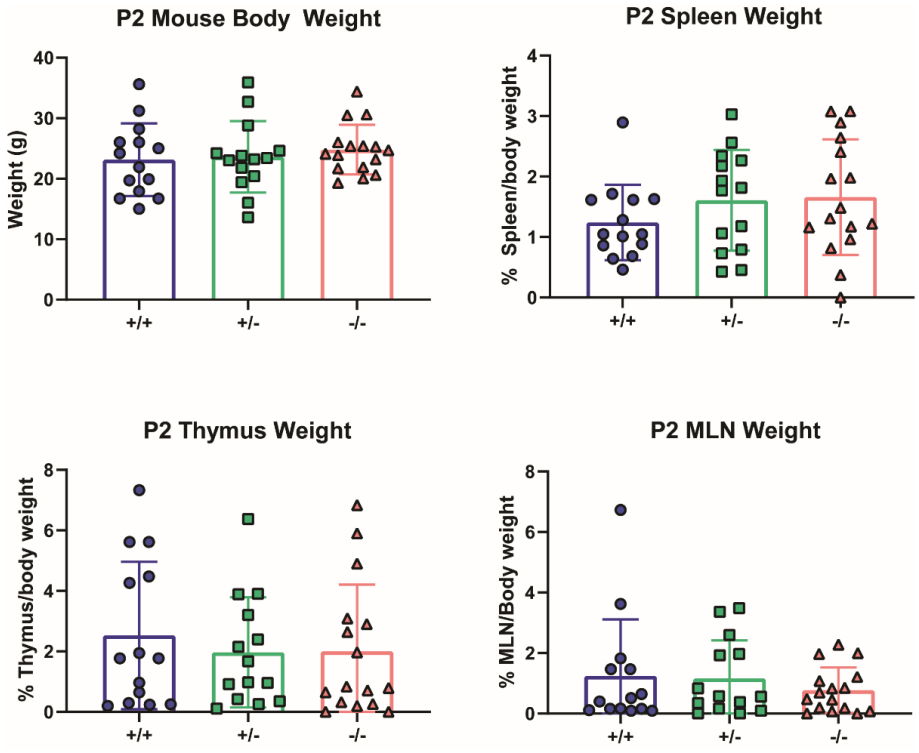

Figure 6-5 Body and organ weights of Eμ-MYC; MDM2-P2- mutant mice are comparable to MDM2-P2-WT controls. The body, spleen, thymus and mesenteric lymph node (MLN) weights were recorded for wild-type P2 (+/+) mice, mice with a heterzygous loss of the P2 promoter (+/-) and mice with a homozygous loss of the P2 promoter (-/-), all on an Eμ-MYC background. The percentage of organ to body weights were then calculuated. The data points represent individual mice. Error bars represent mean ± SD. Statistical test: Kruskal-Wallis (+/+ N=13, +/- N=14; -/- N=16).

6.2.4 Histological analysis of Eμ-MYC, MDM2 P1-null and P2-mutant lymphoma tumours

As mentioned previously, the Eμ-MYC model is characterised by an expansion of the B-cell population as the MYC oncogene expression is driven by the immunoglobulin heavy chain promoter. Immunohistochemistry was performed on formalin fixed, paraffin embedded (FFPE) tumour samples. Haematoxylin and eosin (H&E) stains showed dense cells indicative of tumour area (Figure 6-6). The representative high magnification image show clusters of large blast like cells which were found in all genotypes (Figure 6-6B). To confirm that the tumours were B-cell lymphoma, tumours were stained for the B-cell marker, CD45R (B220) by immunohistochemistry (Figure 6-7). In both the P1-null and P2-mutant cohorts, the CD45R stain confirmed that the majority of the tumour tissues were indeed B-cell lymphomas. Interestingly, two P1 HOM thymic lymphoma tumours were negative for the CD45R stain. This indicates that the thymic lymphomas in this sample are unlikely to be of B-cell origin.

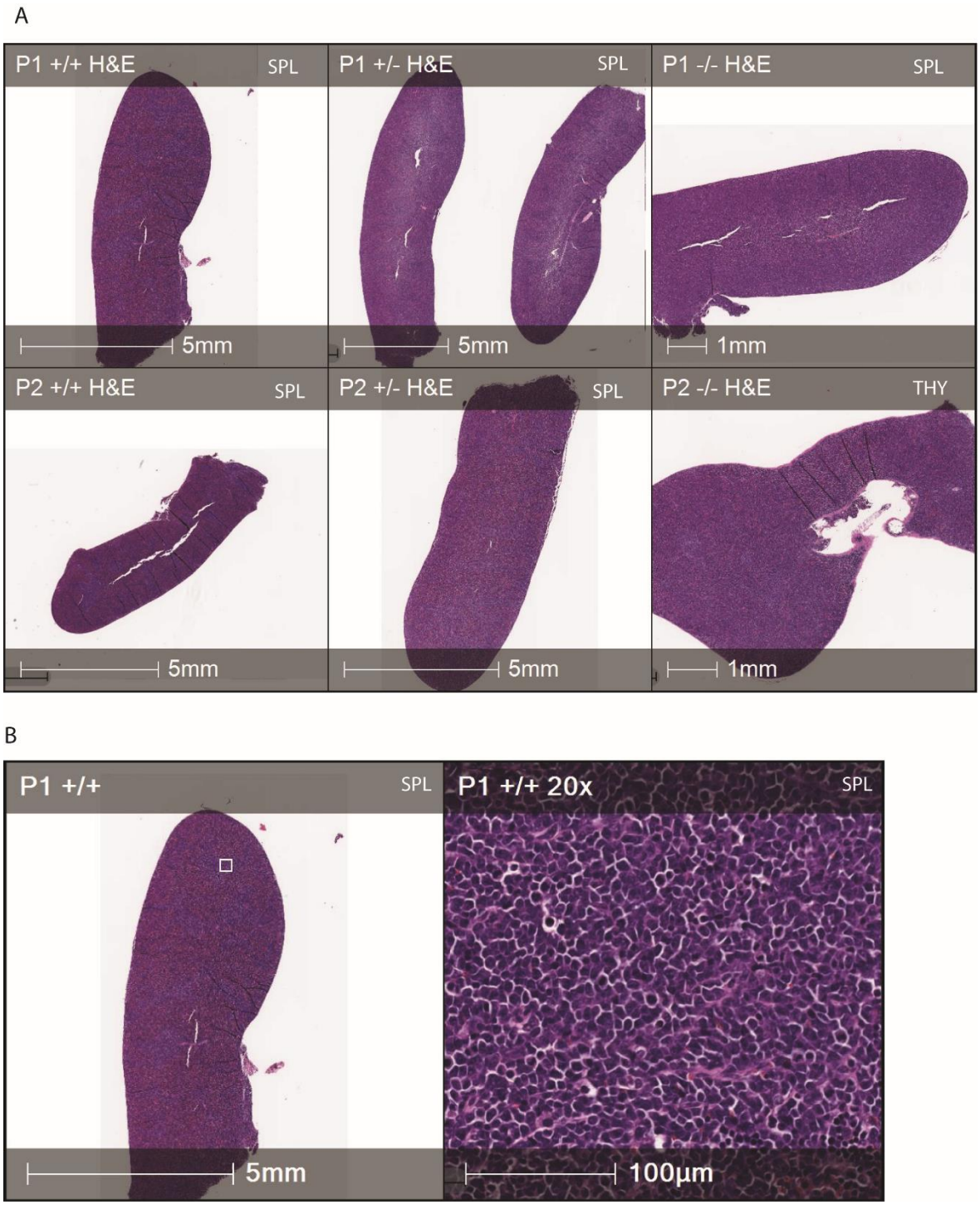

Figure 6-6 Representative H&E staining in the Eμ-MYC; P1-null, Eμ-MYC; P2-mutant lymphomas. FFPE endpoint tumours from the P1-null and P2mutant, Eμ-MYC cohorts were sectioned (4μM) and stained for hematoxylin and eosin (H&E). P1 WT (+/+) N=3, P1 HET (+/-) N=6, P1 HOM (-/-) N=6; P2 WT (+/+) N=3, P2 HET (+/-) N=6, P2 HOM (-/-) N=6. Scale bars are denoted in the images. SPL=Spleen, THY=thymus

A

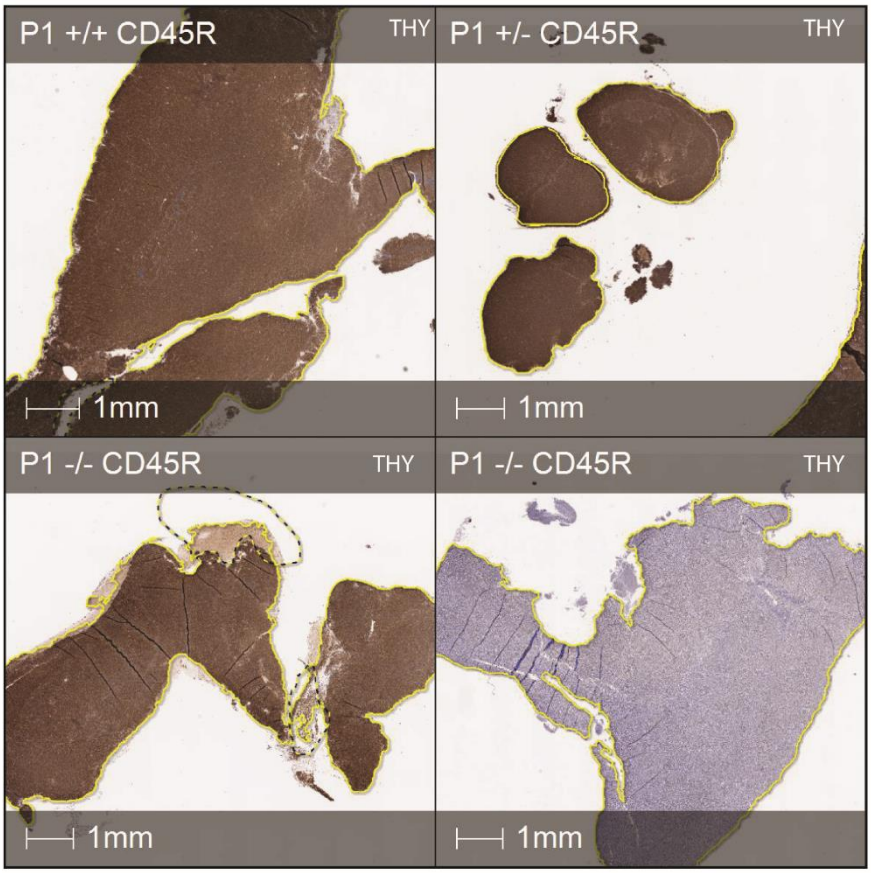

Cohort	CD45R+/# Samples
P1 +/+	3/3
P1 +/-	6/6
P1 -/-	4/6

B

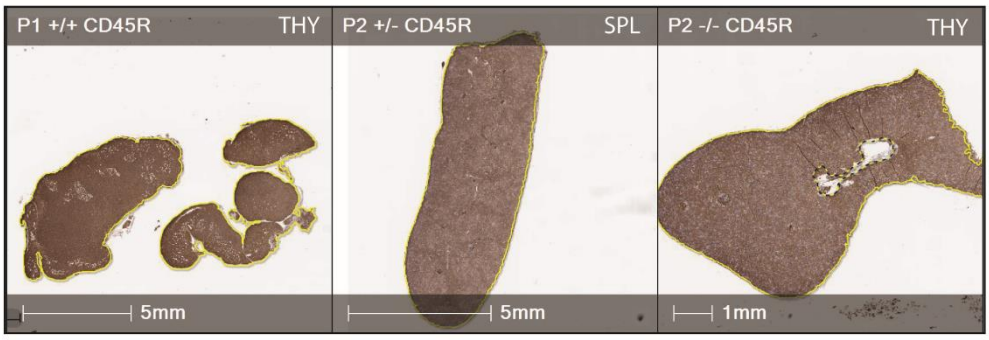

Cohort	CD45R+/# Samples
P2 +/+	3/3
P2 +/-	6/6
P2 -/-	6/6

Figure 6-7 Representative immunohistochemistry images stained for CD45R in Eμ-MYC; P1-null and Eμ-MYC; P2-mutant mice FFPE tumour tissues at endpoint in Eμ-MYC, MDM2 P1-null and P2-mutant cohorts. Tissues were sectioned (4μM) and stained for the B-cell marker, CD45R (B220). P1 WT (+/+) N=3, P1 HET (+/-) N=6, P1 HOM (-/-) N=6; P2 WT (+/+) N=3, P2 HET (+/-) N=6, P2 HOM (-/-) N=6. Scale bars are denoted in the images. SPL=Spleen, THY=thymus

6.2.5 Endpoint Eμ-MYC lymphomas have similar apoptotic levels regardless of the status of MDM2

The MDM2 protein is tightly linked to p53; one of the functions of p53 is to induce apoptosis. To understand whether the MDM2 status has altered the levels of apoptotic cells in tumours at endpoint, immunohistochemistry was performed. Endpoint tissue samples were sectioned and stained with cleaved caspase-3 and quantified using HALO™. Representative images in the both the P1-null and P2-mutant experimental arms show that there are cleaved caspase-3 positive cells found in the tumours (Figure 6-8A, B). Levels of cleaved caspase-3 were compared between the genotypes in the P1 experimental arm (Figure 6-8C) or P2 experimental cohorts (Figure 6-8D). Overall, the MDM2 status does not seem to affect the apoptotic levels found in endpoint Eμ-MYC lymphomas.

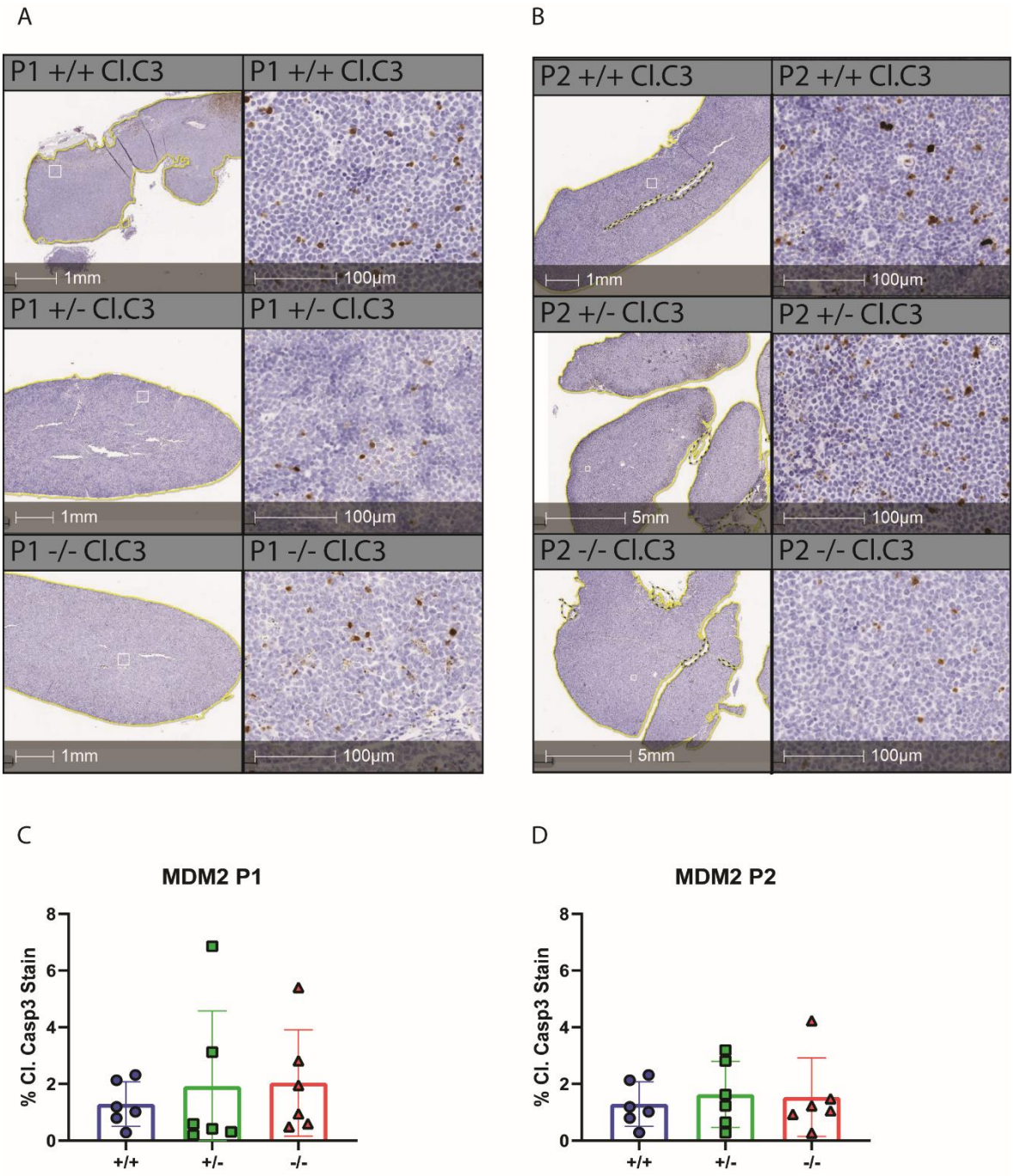

Figure 6-8 No changes to the apoptotic status of Eμ-MYC lymphomas when crossed with MDM2-isoform specific deleted mice. FFPE endpoint tumours from Eμ-MYC, MDM2 P1-null and P2-mutant cohorts were sectioned (4μM) and stained for cleaved caspase-3 (Cl .C3). Representative stains are shown for the P1 cohort (A) and P2 cohort (C). The stain area was quantified using HALO™ and presented as the percentage of cleaved caspase-3 stain area to tissue area (B, D). Data points represent individual mice, error bars represent mean ± SD. The WT samples from both cohorts were combined. Statistical test: Kruskal-Wallis P1 WT (+/+) N=3, P1 HET (+/-) N=6, P1 HOM (-/-) N=6; P2 WT (+/+) N=3, P2 HET (+/-) N=6, P2 HOM (-/-) N=6. Scale bars are denoted in the images.

6.2.6 Flow cytometric analysis of endpoint Eμ-MYC, MDM2 P1-null and P2-mutant tumours

To further investigate the effect of the MDM2 status on disease profile, flow cytometry analyses was performed to determine and confirm the tumour cell type. As the Eμ-MYC model is known to drive the proliferation of B-cells and, sometimes, T-cells, the tumour bearing organs at endpoint were harvested for flow cytometry analysis to investigate the B-cell and T-cell populations. The maturity of the B-cells are of interest in this experiment to assess whether the genetic manipulations in the P1 or P2 MDM2 promoters have altered the disease origin. Tumour bearing organs were processed into a single cell suspension and stained for B- and T-cell markers. B-cell were determined using the B220 marker and the maturity was classified using the immunoglobulin M (IgM) and immunoglobulin G (IgG) surface markers (Figure 6-9). Cells that are negative for IgM and IgD are categorised as pre-B cells and B-cells with surface Ig markers are classified as B-cells. The tumours are classified as having either a predominantly pre-B, B-cell or mixed B-cell population.

As this is an Eμ-MYC model, as shown by immunohistochemistry this was a predominantly a B-cell cancer. This was confirmed with this flow cytometry analysis as tumours were predominantly composed of B-lineage cells (T-cell data not shown). Additionally, if there were multiple enlarged organs, the individual organs were stained and analysed. Each individual mouse had a similar B-cell profile regardless of organ. The tumours of WT mice contained a combination of a pre-B and B-cell population (Figure 6-10A). The P1-HET cohorts were all pre-B tumours, whilst the two samples that had B-cells in the P1-HOM cohorts were pre-B and B-cell tumours (Figure 6-10A). Interestingly, two of the P1-HOM mice did not have any B-cells and low T-cell numbers as well (gating strategy shown in Figure 6-9C; data not shown). In the P2 experimental arm, the P2-HET and P2-HOM cohorts were contained a mixture of pre-B and B-cell tumours. There were low and comparable numbers of T-cells between the genotypes as well (data not shown). The results obtained here infers that in the P1 HOM group, there potentially could be a skew towards a more immature phenotype. The P2-HET and P2-HOM contained a mixture of the B-cell populations. Thus, it is unlikely that the genetic alterations in either of the MDM2 promoters have skewed the disease phenotype.

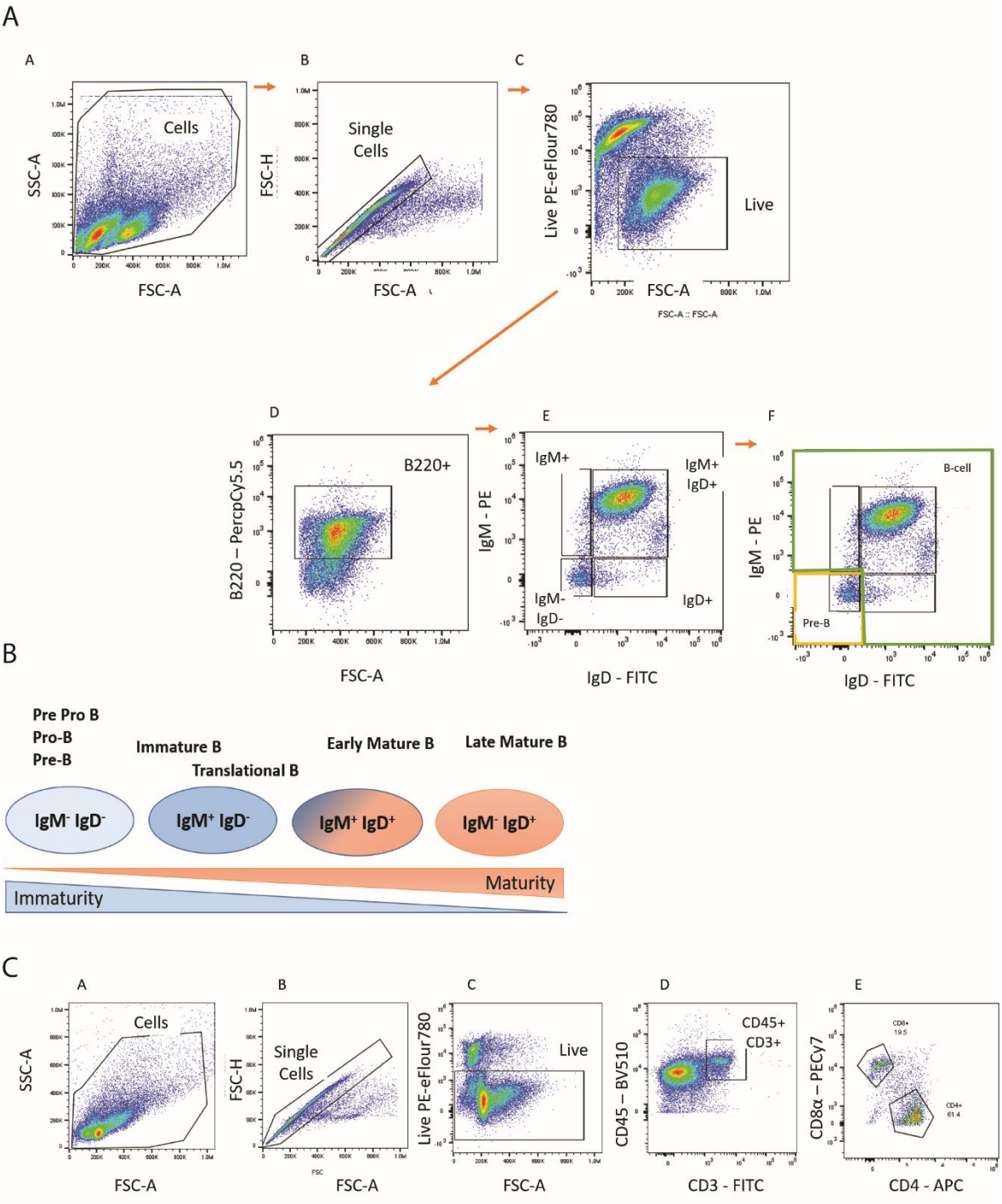

Figure 6-9 The B-cell and T-cell gating strategy for Eμ-MYC; MDM2 P1 and P2 genotypes. A) B-cell gating strategy: Cells were gated based on size and granularity followed by a doublet exclusion and positive selection for live cells. Cells were then gated for the B220 B-cell surface marker. The B-cells were then gated based on IgM and IgD surface expression marker. Cells that are negative for surface Ig markers, IgM and IgD, are pre B-cells. Cells that are positive Ig markers are deemed as B-Cells. B) A schematic showing the transition of B-cell from immaturity and maturity depending on surface Ig staining. C) T-cell gating strategy: Cells were gated based on size and granularity, followed by a doublet exclusion and positive selection for live cells. Cells were then gated for the CD45 and CD3-cell surface markers. The T-cells were then gated based on CD4 and CD8α surface expression markers.

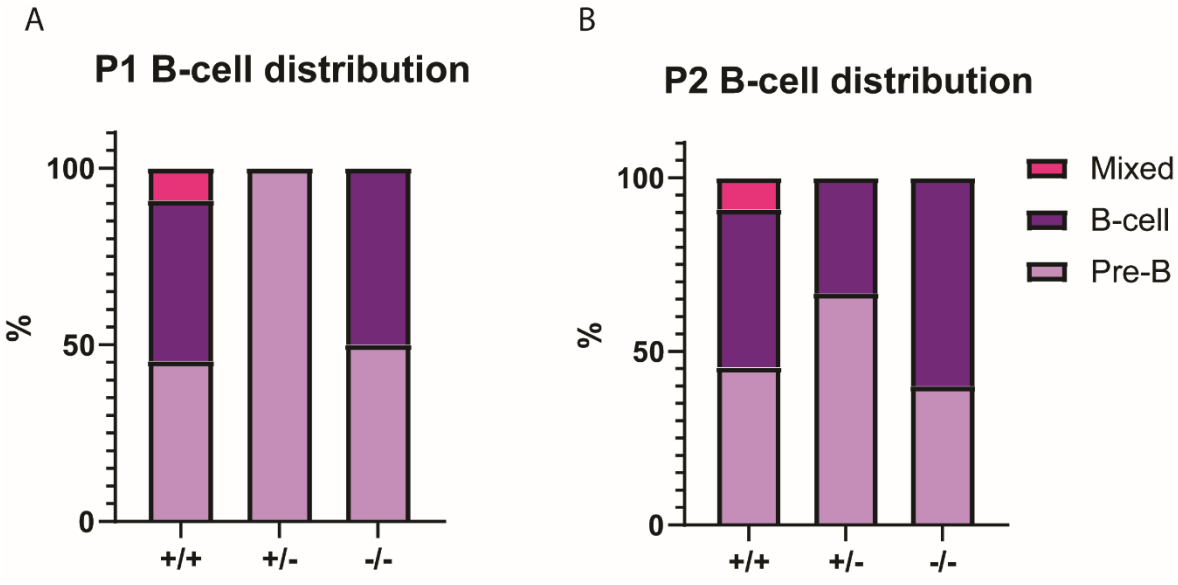

Figure 6-10 Immunophenotyping of B cell lymphomas in the Eμ-MYC; MDM2-P1-null and Eμ-MYC;MDM2-P2-mutant cohorts. Enlarged tumour organs were processed and stained as shown in Figure 6-9. If multiple organs from the same mouse were obtained, the average percentage for the B-cell populations were calculated. If mice had over 50% of a certain population, they were classed as pre-B or B-cell. If there was a mix between the populations, then it was classified as mixed B-cell population. The wild-type data points were combined from the P1 and P2 experimental arms (P1/P2 +/+ N=9; P1 +/- N=4, -/- N=2; P2 +/- N=3, -/- N=5).

6.2.7 Circulating immune cells are unchanged at clinical endpoint in Eμ-MYC lymphomas with the deletion of the MDM2 promoters

Whilst the Eμ-MYC tumours present as lymphomas, haematology analysis of the circulation was also carried out as dissemination of lymphoma cells in the blood and leukaemia can arise (Kelly et al., 2007). Results from the IDEXX haem analyser show that there were no overall differences in the total white blood cell count found between the P1-null and wild type genotypes (Figure 6-11). When looking at lymphocytes, the P1 HOM cohort trended towards a lower number of lymphocytes in comparison to both P1 WT and P1 HET cohorts. This trend is true for the neutrophils as well while monocytes are similar between all the genotypes. The P2-HET and P2-HOM mice have lower white blood cell counts in the circulation compared to WT mice at clinical endpoint. Consistently, the P2-HOM mice showed lower levels of circulating lymphocytes, monocytes and neutrophils compared to wild type controls.

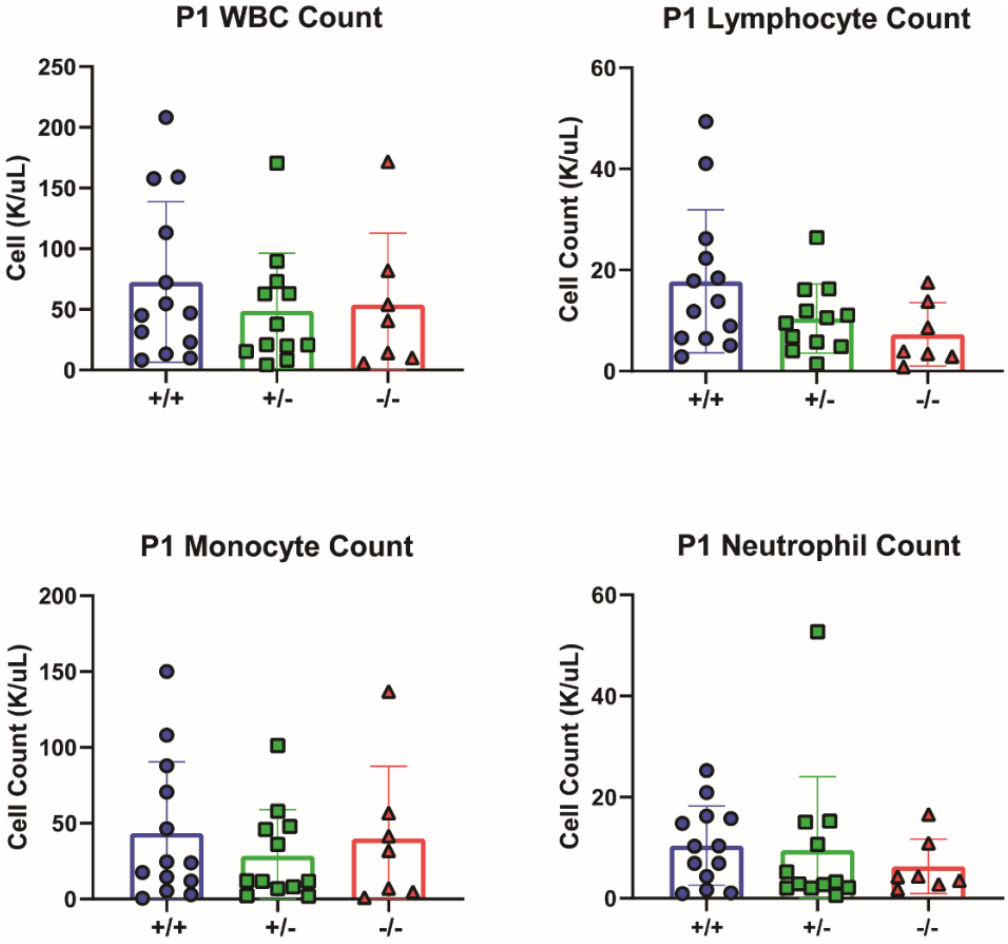

Figure 6-11 Circulating immune cell profiles in lymphoma-bearing Eμ-MYC; P1-null mice. Circulating white blood cells, lymphocytes, monocytes and neutrophils were determined from blood samples from P1 WT (+/+), P1 HET (+/-) and P1 HOM (-/-) mice. Samples were run on the IDEXX ProCyte Dx*; Data points represent individual mice, error bars showing mean ± SD. Statistical test: Kruskal-Wallis. (+/+ N=13; +/- N=12; -/- N=7).

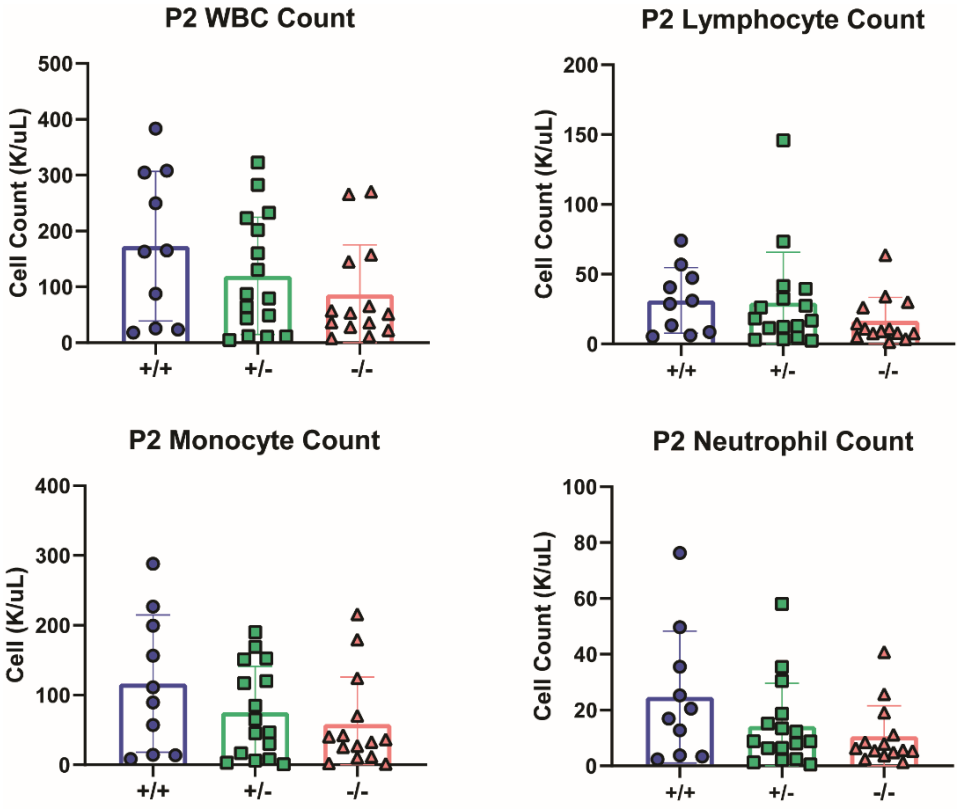

Figure 6-12 Circulating immune cell profiles in lymphoma-bearing Eμ-MYC; P2-mutant mice. Circulating white blood cells, lymphocytes, monocytes and neutrophils were determined from blood samples from P2 WT (+/+), P2 HET (+/-) and P2 HOM (-/-) mice. Samples were run on the IDEXX ProCyte Dx*; Data points represent individual mice, error bars showing mean ± SD. Statistical test: Kruskal-Wallis (+/+ N=10; +/- N=15; -/- N=14).

6.3 Discussion

The role of MDM2 in its ability to regulate p53 is well studied. More recently, the p53-independent functions of MDM2 have also been investigated (Bohlman and Manfredi, 2014). Although the discovery of the two MDM2 promoters was described over 20 years ago, the p53-responsive P2 promoter has been better studied than the constitutive P1 promoter (Barak et al., 1994). Furthermore, the role of MDM2 as an oncogene in tumourigenesis and cancer resistance has also been well established (Jones et al., 1998, Hou et al., 2019). However, the contribution of the individual promoters towards tumourigenesis has not been investigated. Data from the Sansom lab has shown interesting and surprising results particularly in regards to the P1 promoter. Mice null for the MDM2 P1 promoter were protected against intestinal adenomas in an $Apc^{Min/+}$ driven model. All of the P1-knockout mice in this model did however, did succumb to thymic lymphomas. This phenotype in the $Apc^{Min/+}$ MDM2 P1-null mice was reversed when crossed onto a p53 knockout model. The p53 knockout mice no

longer had thymic lymphomas and succumbed to intestinal tumours once again. This suggests an involvement of p53 in delaying intestinal tumourigenesis, but promoting thymic lymphomas in conjunction with a loss of the P1 promoter.

This unusual phenotype led to studying the role of the MDM2 promoters in other tumour types including lymphoma. Interestingly, as shown here, a heterozygous loss of the P1 promoter significantly delayed lymphomagenesis and early indications are that homozygous loss of the P1 promoter also increases mouse survival on the Eμ-MYC lymphoma model. In contrast to this, loss of function of the P2 promoter (in both heterozygous and homozygous animals) actually led to an accelerated tumourigenesis. This suggests that the P1 promoter is perhaps associated with the oncogenic effects of MDM2, whilst the P2 promoter with tumour suppressive effects. However, this was not the case in the intestinal model as mutations in the P2-promoter had no effect in the $Apc^{Min/+}$ model and exacerbated tumourigenesis overall in the P1-null context. Perhaps the roles of the promoters is then context dependent. It is well known that deregulation in the MDM2-p53 axis can cooperate with MYC to accelerate lymphomagenesis (Eischen et al., 1999, Schmitt et al., 1999, Grabow et al., 2016). In Eμ-MYC tumours, spontaneous inactivation of p53 or $p14^{ARF}$, or upregulation of MDM2 often occur (Eischen et al., 1999). If a loss of p53 ensues, then perhaps the P2 MDM2 promoter might be dispensable. What is unknown is in the absence of p53, what factors may regulate or interact with the P2 promoter.

One hypothesis to explain why there is an extended survival in the P1-null cohorts could be due to the levels of p53 itself. The P1 promoter drives basal levels of MDM2, which can regulate p53. In the Eμ-MYC model, there is a pre-neoplastic stage at 4-6 weeks of age where mice develop hyperplasia (Keller et al., 2010). Perhaps during the initial stages of tumourigenesis, tumour cells can accumulate p53 levels that clear out early lesions, thus delaying tumourigenesis. The levels of p53 in this instance may not be high enough to drive the regulation feedback loop via the MDM2-P2 promoter. Particularly since a p53 deficiency in conjunction with a deficiency of the P1 promoter on the $Apc^{Min/+}$ model reversed the phenotype observed, it could point to a p53-related phenomenon. Thus it would be interesting to determine p53, MDM2, $p19^{ARF}$ levels at a pre-neoplastic stage could support or disprove this hypothesis. Conversely, in the heterozygous P2-mutant mouse, an acceleration in tumourigenesis may mimic what was

observed when p53 was spontaneously lost in th Eμ-MYC model (Eischen et al., 1999). These two hypotheses focus on p53 largely mediating the differential effects of the promoters in this lymphoma model.

At clinical endpoint, the disease distribution is generally unchanged in both the P1 and P2 cohorts. The CD45R (B220) stain and flow cytometry analysis showed that the majority of the tumours found were B-cell tumours. Interestingly, two P1-HOM tumours in the immunohistochemistry and flow cytometry analysis were not phenotyped as B-cell lymphomas. It has been shown that T-cell tumours can arise in some Eμ-MYC mice when accompanied by a mutation in *Pim-1* (Moroy et al., 1991). Interestingly, in collaboration with the Sansom lab, I have phenotyped the thymic lymphomas observed in $Apc^{Min/+}$ P1-HOM mice and shown them to be T-cell in origin. In addition to the lymphoma model, two liver carcinogenesis models on a P1-null and P2-mutant background are currently being investigated. A few P1-null nice in both the liver models have presented with thymic lymphomas. It would be interesting to see if the thymic lymphomas from P1-HOM mice are also T-cell tumours, by analysing for CD3/CD4/CD8 expression using immunohistochemistry or flow cytometry. This alludes to a potential mechanism whereby the loss of the P1 promoter is selecting for an expansion of T-cells. How, or why, this is achieved is currently unknown.

As MDM2 is tightly involved with p53, a protein central to apoptosis, the apoptotic milieu was also explored. Perhaps it was not surprising that were no differences were observed in the levels of cleaved caspase-3 positive cells in endpoint tumours as the apoptotic machinery is disabled in the Eμ-MYC model (Eischen et al., 2001a). MYC is known to have both proliferative and apoptotic functions. It has previously been shown that MYC induced proliferation contributed to lymphomagenesis rather than reduced apoptosis (Hsu et al., 1995a). Furthermore, in double BCL-2 and MYC knockouts on an Eμ-MYC background, tumourigenesis was also driven by proliferation (Strasser et al., 1990, Hsu et al., 1995b). Furthermore, a loss of function in pro-apoptotic mediators p53 and $p14^{ARF}$ are shown to cooperate with the overexpression of MYC, reiterating that apoptosis is likely to be defective for tumourigenesis to occur (Vecchio et al., 2020). The results in this chapter have shown that apoptosis does not seem to be affected although this was quite a superficial analysis and it may be interesting to see what is happening particularly at early

stages of disease progression where others have shown that MYC-induced apoptosis can be circumvented (Hsu et al., 1995b, Strasser et al., 1990). Assessment of early and endpoint tumours for p53 and proliferation markers such as Ki-67 would be important. Additional targets such of MDM2 in regards to proliferation could also be explored. Foxo3, a known tumour suppressor downstream of the Ras pathway, is ubiquitinated and subsequently degraded resulting in enhanced proliferation and oncogenic signalling during tumourigenesis (Yang et al., 2008). These experiments could elucidate and confirm that proliferation is vital in the context of MDM2 and lymphomagenesis.

The P1 and P2 promoters represent two aspects of MDM2 – the constitutive functions and a stress response respectively. The lymphoma model represented a genetic induced tumourigenesis model. To further understand the role of the promoters in another context, two additional stress and carcinogenic-induced liver cancer models are currently being used (unpublished, data not shown). The diethynitrosamine (DEN)-ALIOS diet induced hepatocellular carcinoma (HCC) model and streptozotocin (STZ) – high fat diet (HFD) liver model for both the P1 and P2 experimental arms are currently being carried out to assess whether a stress induced model yields different results to a genetic model. Although preliminary, there have been instances, a minority, where the P1 null mice have developed T-cell thymic lymphomas in both models, which is highly unusual (unpublished data). This mimics what was seen with the $Apc^{Min/+}$ model, highlighting a predisposition to lymphomas, likely to be T-cell expansion, when the constitutive P1 promoter is removed.

The analysis of the MDM2 isoforms on an Eμ-MYC model have indicated that the P1 and P2 MDM2 promoters may be behaving in different ways. The study so far has not provided any mechanistic insight into what is occurring in the lymphoma or intestinal models. Dissecting the mechanism is important to shed light onto how the isoform encoded by the basal P1 promoter is potentially oncogenic whilst the isoform encoded as a result of the p53-inducible (P2) promoter protects against tumour development, at least on an MYC-driven B-cell tumour model. Examining p53, MDM2 and $p14^{ARF}$ levels by immunohistochemistry, RNAscope and PCR would determine whether p53-dependent or p53-independent functions are responsible for the different phenotypes observed from the P1 and P2 promoters in the Eμ-MYC model. Additionally, to determine if p53 is

functional, downstream targets such as p21 and PUMA can be assessed. Preliminary analysis on the thymic lymphoma samples of the *Apc*$^{Mlin/+}$ P1-HOM mice showed variable levels of p53, however all were negative for p21 (data not shown). This indicates that p53 is not functional. Furthermore, utilising qPCR techniques can shed light on the mutational status of p53. Whether this is similar in the Eμ-MYC model remains to be seen.

There are other studies that have investigated the role of the different MDM2 promoters. Experimental studies in adult human astrocytic tumours, reveal that the P1 promoter was found to drive the amplification of *MDM2*, which is correlated with a subset of malignant astrocytic tumours (Dimitriadi et al., 2008, Louis et al., 2007). What remains to be assessed is what the expression levels of each of the P1- and P2- driven *MDM2* transcripts are in the models described herein and whether there is compensation when one or other promoter is lost. If P1-driven transcripts are associated with a more aggressive tumour type, this would provide a basis for exploring the promoters as a potential alternative therapeutic MDM2 targets. Work from the Lozano group have studied the P2 isoform in more detail, predominately focusing on the stress induced pathway in acute radiation studies (Pant et al., 2013, Pant et al., 2019).

These experiments demonstrate the protective effects of the mutant P2 promoter through elevated p53 levels in the gastrointestinal system when exposed to radiation (Pant et al., 2019). Additionally, the elevated DNA damage response from irradiation in the P2-mutant mouse was also shown to sensitise hematopoietic stem cells to death (Pant et al., 2013). These studies allude to a difference in the way the P2-mutant responds in an acute external damage inducing setting and in a long-term genetic tumour setting. As the P1-knockout model is novel, no comparisons have been made in acute irradiation studies thus far. This is currently an ongoing project in collaboration with the Sansom and Boyd labs exploring the contribution of these p53-dependent and p53-independent MDM2 isoforms in tumourigenesis.

Thus far, there has been a lot of emphasis on the p53-related mechanisms and functions in regards the phenotypes observed in the MDM2 P1-null and P2-mutant Eμ-MYC model. The p53-independent functions of MDM2 are also important in tumourigenesis which could be important in the MDM2 P1-knockout and P2-

mutant models (Ganguli and Wasylyk, 2003, Manfredi, 2010, Bohlman and Manfredi, 2014). For example, MDM2 is known to target E-Cadherin for degradation, promoting tumour cells to become more invasive and motile (Yang et al., 2006). MDM2 can also promote tumour growth by disrupting cell cycle control through retinoblastoma protein (pRB) and E2F (Xiao et al., 1995). Specific to the P1 MDM2 promoter, the phosphatase and tensin homolog (PTEN), has been shown to regulate the transcription of MDM2 via the p1 promoter (Chang et al., 2004). The tumour suppressor PTEN has been shown to inhibit the formation of T-cell lymphomas in mice (Liu et al., 2010). This study offers a rationale to investigate the PTEN-MDM2 axis in the P1-null and P2-mutant models as the emergence of T-cell lymphomas was observed.

Additionally, given the emergence of T-cell lymphomas in the *Apc*$^{Min/+}$ model, as well as in the DEN-HCC and STZ liver carcinoma models, utilising a genetic T-cell lymphoma mouse model, such as the cutaneous T-cell lymphoma model or peripheral T-cell lymphoma model, or even a xenograft model of human cutaneous T-cell lymphomas could be more suitable. Additional experiments that could take this project further include transplantation of Eμ-MYC P1-null or P2-mutant tumour cells into syngeneic mice to assess parameters of survival and death. This could provide insight into the roles of the MDM2 promoters in tumour initiation and tumour growth. Furthermore, there have been studies that demonstrate an interaction between NFκB and MDM2 (Thomasova et al., 2012). NFκB was shown to induce MDM2 in order to stimulate T-cell activation and proliferation (Busuttil et al., 2010). It would be a key pathway to investigate in the MDM2 promoter studies. This could provide insight into the T-cell expansion observed in the *Apc*$^{Min/+}$, DEN-HCC or STZ liver models then crossing these model systems onto NFκB knockout mice would be highly informative.

Another aspect that would be interesting to explore is the metabolic functions of MDM2 and how these interact with the metabolic reprogramming abilities of MYC in tumourigenesis (Camarda et al., 2017, Sabnis et al., 2017). A plethora of studies in the past 10 years have revealed a role for MDM2 in serine metabolism, redox homeostasis, as well as the ability to regulate mitochondria and promote the invasiveness of cancer cells (Riscal et al., 2016, Arena et al., 2018). Metabolic reprogramming has been observed in lymphomas (Ricci and Chiche, 2018, Eberlin et al., 2014, Dang, 1999). Thus it would be highly interesting to

investigate how the two promoters drive the metabolic functions of MDM2 in lymphoma, but also the intestinal and liver carcinogenesis models.

6.3.1 Possible explanations for phenotypes observed in the different MDM2 isoform models

In the P1-null mouse, the P2 promoter functions are intact, therefore MDM2 is responsive to p53 and able to downregulate p53 levels if required. In the P2-mutant mouse, this feedback loop is abrogated and only the constitutive/basal P1 promoter is functional. The heterozygous and homozygous loss of the P1 promoter delayed tumourigenesis, whilst the heterozygous loss of the P2 promoter accelerated tumourigenesis in the Eμ-MYC model. An overexpression of MDM2 itself leads to accelerated tumourigenesis (Eischen et al., 1999). This implies that MDM2 is tumour suppressive in this context, similar to what was observed in the P2-mutant Eμ-MYC model. Regardless of which isoform is abrogated, MDM2 is still produced. This then raises the question of whether there are compensatory mechanisms between the two promoters. Although transcripts from the P1 promoter are less efficiently translated, MDM2 transcribed from the P1 promoter would still be able to regulate p53, however, arguably less efficiently (Landers et al., 1997). Furthermore, when looking at compensatory mechanisms, the MDM4/MDMX proteins must also be considered. These proteins can heterodimerise with MDM2 to carry out its function but also regulate p53 on its own (Marine and Jochemsen, 2016). Cancer cells have also been shown to upregulate MDMX in order to eliminate p53 apoptotic functions (Riemenschneider et al., 1999).

Similarly, the localisation of the MDM2 protein itself is important to its functions. There are several models regarding MDM2 localisation and function. For example, MDM2 is largely found in the nucleus and is thought to shuttle p53 in and out of the nucleus for degradation (Tao and Levine, 1999), whereas ubiquitination of Foxo3 takes place in the cytoplasm (Fu et al., 2009). Perhaps the localisation of MDM2 is affected when the promoters are disrupted. Furthermore, there has been evidence regarding splice variants of MDM2 in relation to poorer patient prognosis and advance cancer including ovary and brain cancers (Sigalas et al., 1996, Matsumoto et al., 1998). Whilst the role of

MDM2 in tumourigenesis has been investigated, the potential difference seen here with the different isoforms requires further exploration (Figure 6-13).

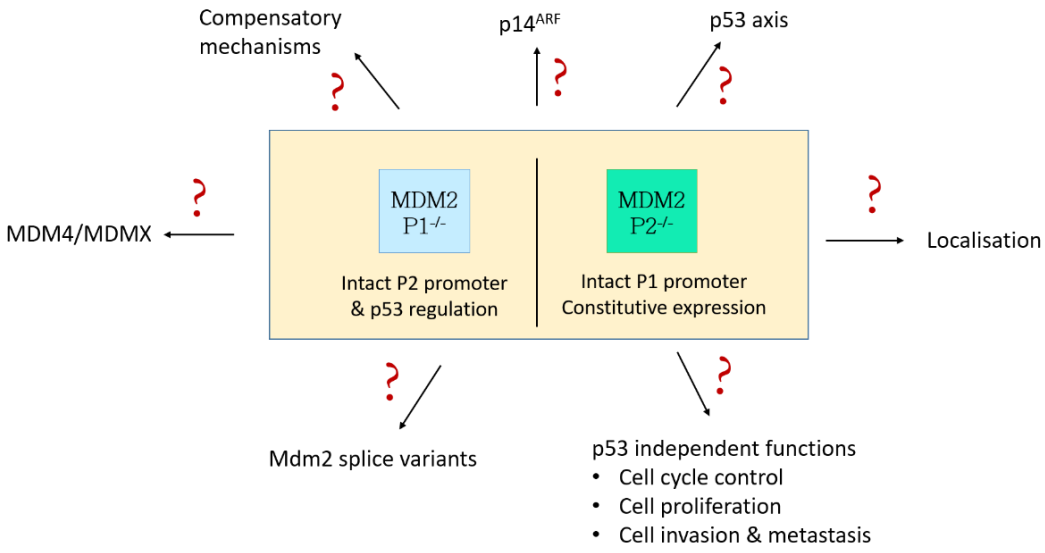

Figure 6-13 Schematic representation of potential mechanisms to explain the phenotypes observed when each of the *Mdm2* promoters are silenced. The mechanism behind the observed phenotypes are currently unknown. Here outlines potential mechanisms that could explain what is occurring and could be explored in the future.

7 Final discussions and future work

7.1 Apoptosis in thymic homeostasis

Apoptotic membrane blebbing is a hallmark characteristic of an apoptotic cell that has been very well studied (Elmore, 2007, Zhang et al., 2018, Häcker, 2000). During apoptosis, the cleavage of the ROCK1 protein by caspase-3 propagates the phosphorylation of downstream targets, including actin and myosin, to cause apoptotic membrane blebs (Coleman et al., 2001, Sebbagh et al., 2001, Leverrier and Ridley, 2001a). The driver of apoptotic membrane blebbing is known, however, dissecting the purpose of this morphological feature has only recently been investigated using an *in vivo* model (Olson lab, unpublished data). Exploring the role of ROCK1-mediated apoptotic membrane blebbing has been achieved through utilising the non-cleavable ROCK1 (ROCK1nc) model. In this particular mouse model, genetic modifications through amino substitution at the caspase-3 cleavage site of ROCK1 results in a caspase-resistant ROCK1 and defective apoptotic membrane blebbing. The first part of this thesis addresses the role of apoptotic membrane blebbing in thymic development and apoptotic cell clearance. The role of apoptotic membrane blebbing studied in the thymus because of the high apoptotic activity in this organ due to selection processes during T-cell development. Results shown here were unexpected, as the ROCK1nc mutation did not alter the physical, architectural and cellular parameters of the thymus.

This was particularly surprising as one would have thought that defective apoptotic membrane blebbing would cause disturbances in some aspects of thymic development or homeostatic functions. It could be that apoptotic membrane blebbing is redundant in the thymus as a failsafe mechanism, to ensure that an inflammatory response due to impaired blebbing would not occur. This could likely be the case as a reduction in a variety of cytokine levels from 10 week old ROCK1nc mice was observed previously (Julian, 2015). One hypothesis could be that due to the disruption in apoptotic membrane blebbing, the ROCK1nc mice are able to tolerate low levels of inflammation from the constant exposure of damage associated molecular patterns. The mice might adjust their responses to deal with this. The lower cytokine levels observed

previously and responses observed in the adoptive transfer experiments in the ROCK1nc mice shown here support this notion.

Although membrane blebbing is a feature of apoptotic cells, not all cells undergo apoptotic membrane blebbing (Atencia et al., 2000, Julian and Olson, 2014). Blebbing itself is not only confined to apoptotic morphology, but also seen during migration of both normal and tumour cells (Fackler and Grosse, 2008). Three parameters that are likely to dictate whether cells bleb during migration are a disrupted actin cortex, high levels of linker molecules and high intracellular pressure (Paluch and Raz, 2013). These parameters could also impact on apoptotic blebbing and should be studied in thymocytes and compared with cells known to efficiently bleb (e.g. hepatocytes and mouse embryonic fibroblasts) (Julian, 2015, Naylor, 2019). Other studies using scanning electron microscopy (SEM) have shown that thymocytes do produce membrane blebs and bodies *in vivo*; for example after irradiation in rats (Ohyama et al., 1985, Atkin-Smith and Poon, 2017). SEM images from *in vivo* irradiated or dexamethasone treated thymi would help clarify observations made with *in vitro* SEM images, similar to what was done by Ohyama and colleagues. Furthermore, Jurkat cells, a human T- lymphocyte cell line, have also been shown to bleb during apoptosis (Tixeira et al., 2020). Thymocytes are small in size with the majority of its composition being the nucleus (Cano RLE, 2013). It could be that the low amount of cytoplasm found in these cells means that thymocytes bleb less, or more subtly, and capturing images at the right time is critical. Regardless, the results shown here argue that ROCK1-mediated apoptotic membrane blebbing is likely to be dispensable in the thymus. This could actually be beneficial as aberrant immune responses and disruption to thymic homeostasis would likely disturb T-cell development.

Proliferative and apoptotic signals are highly important in the thymus, governing the T-cell development process. What was observed here was not the first time where perturbations in the apoptotic cascade generally does not cause detriments in the thymus. The balance between the pro- and anti- apoptotic BCL-2 proteins are an important aspect in determining the fate of a thymocyte. The expression of anti- apoptotic BCL-2 in murine thymocytes confers protection against dexamethasone induced apoptosis, whilst the expression of the pro-apoptotic BAX results in an acceleration of cell death post dexamethasone

treatment (Sentman et al., 1991, Strasser et al., 1991, Brady et al., 1996, Williams et al., 1998). Interestingly, although in BCL-2 knockout mice greater apoptosis in the thymus was observed in older mice, earlier studies utilising an overexpression of the *Bcl-2* gene in the thymus showed an enhanced ability to withstand negative selection (Veis et al., 1993, Strasser et al., 1991). Higher levels of self-reactive T-cells were observed in the thymus with an overexpression of BCL-2, however, no major alterations were seen in the T-cell populations, thymic cellularity and involution rate (Strasser et al., 1991).

Another study utilising a slightly different model of BCL-2 overexpression in cortical thymocytes, did observe a higher level of mature $CD3^+$ T-cells in the thymus, as well as the lymph node and spleen (Sentman et al., 1991). Despite this increase, negative selection still occurred and no other phenotypes were observed (Sentman et al., 1991). Similar to BCL-2, p53 is a central protein to the apoptotic cascade. In a p53 knockout model, higher levels of memory T-cells were observed which aided in anti-viral responses (Grayson et al., 2001). Mice with p53 deficiencies exhibit normal T-cell expansion and development, although are more prone to developing T-cell thymic lymphomas (Donehower et al., 1992, Haines et al., 2006, Lozano, 2010). The general lack of autoimmunity, with no overt phenotype in aged mice in the BCL-2 overexpression and p53 knockout models is consistent with what the Olson lab has previously observed in the ROCK1nc model (Julian, 2015). These previous studies in conjunction with what was shown here could highlight the potential of the thymus to tolerate deviations in the apoptotic cascade itself, as well as any changes in apoptotic morphology.

7.2 Apoptosis and tumourigenesis

The role of ROCK1-mediated apoptotic membrane blebbing was also interrogated in a variety of tumour models. The ROCK1nc mutation presented with contrasting effects in different tumour models. Previous results in the Olson lab showed a trend for an extension in survival for the mice in the Eμ-MYC model of B-cell lymphoma, which was accompanied by an inflammatory population of macrophages (Julian, 2015, Naylor, 2019). In addition to the Eμ-MYC model, the ROCK1nc mutation also reduced tumour burden as a result of defective apoptotic membrane blebbing in the DEN-induced HCC model, a phenotype that

was further recapitulated with the use of Fasudil, a ROCK inhibitor (Julian, 2015, Naylor, 2019). This was in contrast to what was initially hypothesised, as disruptions in apoptotic morphology were thought to promote tumourigenesis. Instead this supported the premise that defective apoptotic blebbing would cause an immune response. To the contrary, accelerated tumourigenesis was seen here in lung adenocarcinoma models with ROCK1nc mutant mice which was not due to an altered immune response. It is interesting that the ROCK1nc mutation had opposite effects in the HCC model and the KMA lung model. It could be due to the nature of the models, where the HCC model is induced by carcinogens and the lung adenocarcinoma driven by conditional oncogenic expression. Investigating the differences between the models as well as what pathways and oncogenic parameters are involved would be highly informative. This would provide useful evidence to inform the potential use of ROCK inhibitors appropriately.

The role of apoptosis itself in tumourigenesis is multifaceted. One of the features of cancer is the ability to resist cell death (Fernald and Kurokawa, 2013). Conventional wisdom is that deactivating pro-apoptotic proteins or upregulation of anti-apoptotic proteins would facilitate tumourigenesis. However, in reality it is not so straightforward. Interestingly, mice without the pro-apoptotic proteins BAX and BAK do not develop any more spontaneous tumours than wild-type mice (Lindsten and Thompson, 2006). Another apoptotic ligand, CD95, was shown to be important in facilitating tumourigenesis *in vivo*, which is in contrast to what is observed in patients with an autoimmune disease where a loss in CD95 leads to the development of lymphomas (Chen et al., 2010, Ramenghi et al., 2000). Furthermore, a loss of CD95 function on a CD2-*Myc* T-cell lymphoma model did not show any differences lymphomagenesis (Cameron et al., 2000). This shows that context is highly important when considering the relationship between apoptosis and tumourigenesis.

7.2.1 Final conclusions

The results and observations discussed here suggests that the apoptotic morphology affects tumourigenesis to a greater extent than homeostasis itself. Possibly, the ability of the thymus to tolerate any deviations in the apoptotic cascade and apoptotic morphology is beneficial to maintain efficient T-cell

development and maintain a low immunogenic milieu. Compensatory mechanisms could be relied upon to maintain tissue homeostasis. During tumourigenesis however, the impact of genetic mutations or environmental stresses are enough to uncover a role for apoptotic membrane blebbing. The context of the tumour setting is important as certain cancers could benefit from a ROCK inhibitor treatment, such as HCC and B-cell lymphomas. This may not be the case for lung adenocarcinomas based on the data from the ROCK1nc model alone. However, as the ROCK inhibitor affects all functions of ROCK, this needs to be investigated further. Additional investigations into ROCK1-mediated apoptotic membrane blebbing during tumourigenesis will provide further insights into the role of apoptotic morphology in cancer, and aid in governing whether ROCK inhibitors are suitable for the treatment of cancer.

7.3 The different MDM2 P1 and P2 promoters in lymphomagenesis

The MDM2-p53 axis has been well studied and deemed important in lymphomagenesis. The protein MYC can interact with the $p14^{ARF}$-MDM2-p53 axis when MYC is exerting its pro-apoptotic functions (Zindy et al., 1998). There is a selective pressure for loss of p53 or $p14^{ARF}$ function by deletion or mutations when MYC is overexpressed (Eischen et al., 2001b). The loss of either of these two tumour suppressor proteins significantly accelerates tumourigenesis in the Eμ-MYC model (Eischen et al., 1999, Schmitt et al., 1999, Hsu et al., 1995a, Jacobs et al., 1999). MDM2 itself has been shown to be overexpressed in both human and in models of lymphoma (Wang et al., 2008). Interestingly, heterozygous loss of *Mdm2* leads to reduced lymphoma development through enhanced tumour cell apoptosis driven by p53 in the Eμ-MYC model (Alt et al., 2003, Eischen et al., 2004). Surprisingly, despite the loss of an allele, there was still an overexpression of MDM2 proteins observed in the lymphomas, regardless of whether p53 or $p14^{ARF}$ was expressed (Alt et al., 2003, Eischen et al., 2004). Although the role of MDM2 in lymphoma has been explored, it is less known what the role of the two MDM2 promoters are in tumourigenesis itself, particularly in *in vivo* settings.

The results shown here with the heterozygous loss of the P1 promoter seems to have a similar phenotype to the heterozygous loss of *Mdm2* observed in earlier

studies by Alt *et.al* and Eischen *et.al*. Therefore, it would be interesting to interrogate both $p14^{ARF}$ and p53 levels and functionality, as no differences were observed in apoptotic levels in endpoint tumours. In the P1-knockout model, the functional P2 promoter is still capable of being responsive to p53. It is very likely that what is observed in the P1 knockout model recapitulates the earlier studies by Alt *et.al* and Eischen *et.al*. In contrast, the P2-mutant model is not able to respond to p53. The accelerated lymphomagenesis observed in the P2-mutant model, could allude to the oncogenic potential of the protein driven by the P1 promoter or perhaps the selective pressure of tumour cells to lose p53 due to a disruption in the feedback loop. Conversely, studies in the Sansom lab found that in $Apc^{Min/+}$ mice mutant for the P2 promoter did not alter tumour related survival. Interestingly however, $Apc^{Min/+}$ mice null for the P1 promoter saw a delay in intestinal tumourigenesis, but an emergence of thymic lymphomas (unpublished data). These observations from the intestinal model would suggest the opposite, that MDM2 driven under the control of the P2 promoter may be more oncogenic.

The unusual emergence of thymic lymphomas was observed in 3 different cancer models in which the P1-null isoform was studied. However, this phenomenon is not observed when P1-null mice are aged in the absence of a confounding event. Evidence suggests that deletion of the P1 promoter somehow signals the expansion of lymphocytes only when accompanied by oncogenic or carcinogenic events. In the intestinal model, thymic lymphomas from P1-null mice were shown to be T-cell lymphomas (unpublished data). It is highly probable that the thymic lymphomas from the two mice in the P1-null Eμ-MYC cohort and P1-null HCC mice would be T-cells. Perhaps there is a P2-driven MDM2 involvement the expansion of T-cells. An interesting protein that could be involved is MYC. The MYC protein has been shown to interact with p53, as well as mediate downstream effects in the $Apc^{Min/+}$ model (Liu et al., 2017, Sansom et al., 2007). One hypothesis is that there could be an involvement of MYC in the expansion of T-cells, when the P1 promoter is removed. These speculations would need to be investigated further by exploring the cell types in the thymic lymphomas and the level of MYC expression in the various P1-null and P2-mutant models. These results show that the MDM2 promoters likely contribute to tumourigenesis in different ways. How this is achieved, is yet to be explored.

7.3.1 Final conclusions

The use of *in vivo* models to dissect the roles of both the P1 and P2 promoters of MDM2 is novel. Given that the promoters are regulated by different factors, it is important to understand how each promoter contributes to tumourigenesis. The results shown here and additional ongoing experimental studies suggest that the P1 and P2 promoters do not contribute to tumourigenesis in the same manner. These studies will allow for a better understanding of MDM2 functions, but also perhaps provide an alternative therapeutic strategy for cancers with aberrations in the p53-MDM2 signalling axis.

List of Reference

ABDELWAHID, E., PELLINIEMI, L. J. & JOKINEN, E. 2002. Cell death and differentiation in the development of the endocardial cushion of the embryonic heart. *Microscopy Research and Technique,* 58**,** 395-403.

ABE, H., KAMAI, T., TSUJII, T., NAKAMURA, F., MASHIDORI, T., MIZUNO, T., TANAKA, M., TATSUMIYA, K., FURUYA, N., MASUDA, A., YAMANISHI, T. & YOSHIDA, K. 2008. Possible role of the RhoC/ROCK pathway in progression of clear cell renal cell carcinoma. *Biomed Res,* 29**,** 155-61.

ABE, K. & ITO, T. 1970. Fine structure of small lymphocytes in the thymus of the mouse: Qualitative and quantitative analysis by electron microscopy. *Zeitschrift für Zellforschung und Mikroskopische Anatomie,* 110**,** 321-335.

ADAMS, J. M. & CORY, S. 2007. The Bcl-2 apoptotic switch in cancer development and therapy. *Oncogene,* 26**,** 1324-37.

ADAMS, J. M., HARRIS, A. W., PINKERT, C. A., CORCORAN, L. M., ALEXANDER, W. S., CORY, S., PALMITER, R. D. & BRINSTER, R. L. 1985. The c-myc oncogene driven by immunoglobulin enhancers induces lymphoid malignancy in transgenic mice. *Nature,* 318**,** 533-538.

AHMED, S. A. & SRIRANGANATHAN, N. 1994. Differential effects of dexamethasone on the thymus and spleen: alterations in programmed cell death, lymphocyte subsets and activation of T cells. *Immunopharmacology,* 28**,** 55-66.

AIHARA, M., DOBASHI, K., IIZUKA, K., NAKAZAWA, T. & MORI, M. 2003. Comparison of effects of Y-27632 and Isoproterenol on release of cytokines from human peripheral T cells. *Int Immunopharmacol,* 3**,** 1619-25.

ALT, J. R., GREINER, T. C., CLEVELAND, J. L. & EISCHEN, C. M. 2003. Mdm2 haplo-insufficiency profoundly inhibits Myc-induced lymphomagenesis. *The EMBO Journal,* 22**,** 1442-1450.

AMANO, M., ITO, M., KIMURA, K., FUKATA, Y., CHIHARA, K., NAKANO, T., MATSUURA, Y. & KAIBUCHI, K. 1996. Phosphorylation and activation of myosin by Rho-associated kinase (Rho-kinase). *J Biol Chem,* 271**,** 20246-9.

AMANO, M., NAKAYAMA, M. & KAIBUCHI, K. 2010. Rho-kinase/ROCK: A key regulator of the cytoskeleton and cell polarity. *Cytoskeleton (Hoboken),* 67**,** 545-54.

APPELLA, E. & ANDERSON, C. W. 2001. Post-translational modifications and activation of p53 by genotoxic stresses. *Eur J Biochem,* 268**,** 2764-72.

ARAKI, S., EITEL, J. A., BATUELLO, C. N., BIJANGI-VISHEHSARAEI, K., XIE, X. J., DANIELPOUR, D., POLLOK, K. E., BOOTHMAN, D. A. & MAYO, L. D. 2010. TGF-beta1-induced expression of human Mdm2 correlates with late-stage metastatic breast cancer. *J Clin Invest,* 120**,** 290-302.

ARAKI, S., ITO, M., KUREISHI, Y., FENG, J., MACHIDA, H., ISAKA, N., AMANO, M., KAIBUCHI, K., HARTSHORNE, D. & NAKANO, T. 2001. Arachidonic acid-induced Ca2+ sensitization of smooth muscle contraction through activation of Rho-kinase. *Pflügers Archiv : European journal of physiology,* 441**,** 596-603.

ARANDJELOVIC, S. & RAVICHANDRAN, K. S. 2015. Phagocytosis of apoptotic cells in homeostasis. *Nature immunology,* 16**,** 907-917.

ARENA, G., CISSÉ, M. Y., PYRDZIAK, S., CHATRE, L., RISCAL, R., FUENTES, M., ARNOLD, J. J., KASTNER, M., GAYTE, L., BERTRAND-GADAY, C., NAY, K., ANGEBAULT-PROUTEAU, C., MURRAY, K., CHABI, B., KOECHLIN-RAMONATXO, C., ORSETTI, B., VINCENT, C., CASAS, F., MARINE, J.-C.,

ETIENNE-MANNEVILLE, S., BERNEX, F., LOMBÈS, A., CAMERON, C. E., DUBOUCHAUD, H., RICCHETTI, M., LINARES, L. K. & LE CAM, L. 2018. Mitochondrial MDM2 Regulates Respiratory Complex I Activity Independently of p53. *Molecular Cell,* 69**,** 594-609.e8.

ASANO, T., IKEGAKI, I., SATOH, S., SUZUKI, Y., SHIBUYA, M., TAKAYASU, M. & HIDAKA, H. 1987. Mechanism of action of a novel antivasospasm drug, HA1077. *J Pharmacol Exp Ther,* 241**,** 1033-40.

ASHCROFT, M., KUBBUTAT, M. H. & VOUSDEN, K. H. 1999. Regulation of p53 function and stability by phosphorylation. *Mol Cell Biol,* 19**,** 1751-8.

ASHCROFT, M., TAYA, Y. & VOUSDEN, K. H. 2000. Stress signals utilize multiple pathways to stabilize p53. *Mol Cell Biol,* 20**,** 3224-33.

ASHWELL, J. D., LU, F. W. & VACCHIO, M. S. 2000. Glucocorticoids in T cell development and function*. *Annu Rev Immunol,* 18**,** 309-45.

ATENCIA, R., ASUMENDI, A. & GARCÍA-SANZ, M. 2000. Role of cytoskeleton in apoptosis. *Vitamins & Hormones*. Academic Press.

ATKIN-SMITH, G. K. & POON, I. K. H. 2017. Disassembly of the Dying: Mechanisms and Functions. *Trends in Cell Biology,* 27**,** 151-162.

AUBREY, B. J., STRASSER, A. & KELLY, G. L. 2016. Tumor-Suppressor Functions of the TP53 Pathway. *Cold Spring Harb Perspect Med,* 6.

AVERILL, F., ALBERTSON, T. E., BARATZ, D. M., CHAUDHARY, S., MOBIN, S., O'BRIEN, T., SCHOLAND, M. B., WHELAN, T. P. M., POYUROVSKY, M., SCHUELLER, O., RYAN, J. & GIBSON, K. F. 2018. A Phase 2 Trial of KD025 to Assess Efficacy, Safety and Tolerability in Patients with Idiopathic Pulmonary Fibrosis. *C97. DIFFUSE PARENCHYMAL LUNG DISEASES: EVALUATION, OUTCOMES, AND TRIALS*. American Thoracic Society.

AWASAKI, T., TATSUMI, R., TAKAHASHI, K., ARAI, K., NAKANISHI, Y., UEDA, R. & ITO, K. 2006. Essential role of the apoptotic cell engulfment genes draper and ced-6 in programmed axon pruning during Drosophila metamorphosis. *Neuron,* 50**,** 855-67.

BAGGER, F. O., KINALIS, S. & RAPIN, N. 2018. BloodSpot: a database of healthy and malignant haematopoiesis updated with purified and single cell mRNA sequencing profiles. *Nucleic Acids Research,* 47**,** D881-D885.

BAMBERGER, C. M., SCHULTE, H. M. & CHROUSOS, G. P. 1996. Molecular determinants of glucocorticoid receptor function and tissue sensitivity to glucocorticoids. *Endocr Rev,* 17**,** 245-61.

BARAK, Y., GOTTLIEB, E., JUVEN-GERSHON, T. & OREN, M. 1994. Regulation of mdm2 expression by p53: alternative promoters produce transcripts with nonidentical translation potential. *Genes Dev,* 8**,** 1739-49.

BARBOZA, J. A., LIU, G., JU, Z., EL-NAGGAR, A. K. & LOZANO, G. 2006. p21 delays tumor onset by preservation of chromosomal stability. *Proc Natl Acad Sci U S A,* 103**,** 19842-7.

BARTON, G. M., BEERS, C., DEROOS, P., EASTMAN, S. R., GOMEZ, M. E., FORBUSH, K. A. & RUDENSKY, A. Y. 2002. Positive selection of self-MHC-reactive T cells by individual peptide–MHC class II complexes. *Proceedings of the National Academy of Sciences,* 99**,** 6937.

BENSAAD, K., TSURUTA, A., SELAK, M. A., VIDAL, M. N., NAKANO, K., BARTRONS, R., GOTTLIEB, E. & VOUSDEN, K. H. 2006. TIGAR, a p53-inducible regulator of glycolysis and apoptosis. *Cell,* 126**,** 107-20.

BEREITER-HAHN, J., LÜCK, M., MIEBACH, T., STELZER, H. K. & VÖTH, M. 1990. Spreading of trypsinized cells: cytoskeletal dynamics and energy requirements. *J Cell Sci,* 96 (Pt 1)**,** 171-88.

BERGSMEDH, A., SZELES, A., HENRIKSSON, M., BRATT, A., FOLKMAN, M. J., SPETZ, A. L. & HOLMGREN, L. 2001. Horizontal transfer of oncogenes by uptake of apoptotic bodies. *Proc Natl Acad Sci U S A,* 98**,** 6407-11.

BERKERS, C. R., MADDOCKS, O. D., CHEUNG, E. C., MOR, I. & VOUSDEN, K. H. 2013. Metabolic regulation by p53 family members. *Cell Metab,* 18**,** 617-33.

BEVAN, M. J. 1997. In Thymic Selection, Peptide Diversity Gives and Takes Away. *Immunity,* 7**,** 175-178.

BIALIK, S., DASARI, S. K. & KIMCHI, A. 2018. Autophagy-dependent cell death – where, how and why a cell eats itself to death. *Journal of Cell Science,* 131**,** jcs215152.

BIANCONI, E., PIOVESAN, A., FACCHIN, F., BERAUDI, A., CASADEI, R., FRABETTI, F., VITALE, L., PELLERI, M. C., TASSANI, S., PIVA, F., PEREZ-AMODIO, S., STRIPPOLI, P. & CANAIDER, S. 2013. An estimation of the number of cells in the human body. *Annals of Human Biology,* 40**,** 463-471.

BISWAS, P. S., GUPTA, S., CHANG, E., SONG, L., STIRZAKER, R. A., LIAO, J. K., BHAGAT, G. & PERNIS, A. B. 2010. Phosphorylation of IRF4 by ROCK2 regulates IL-17 and IL-21 production and the development of autoimmunity in mice. *J Clin Invest,* 120**,** 3280-95.

BITEAU, B., HOCHMUTH, C. E. & JASPER, H. 2011. Maintaining tissue homeostasis: dynamic control of somatic stem cell activity. *Cell Stem Cell,* 9**,** 402-11.

BLANPAIN, C., HORSLEY, V. & FUCHS, E. 2007. Epithelial stem cells: turning over new leaves. *Cell,* 128**,** 445-58.

BLASER, H., REICHMAN-FRIED, M., CASTANON, I., DUMSTREI, K., MARLOW, FLORENCE L., KAWAKAMI, K., SOLNICA-KREZEL, L., HEISENBERG, C.-P. & RAZ, E. 2006. Migration of Zebrafish Primordial Germ Cells: A Role for Myosin Contraction and Cytoplasmic Flow. *Developmental Cell,* 11**,** 613-627.

BLUMENSTEIN, L. & AHMADIAN, M. R. 2004. Models of the cooperative mechanism for Rho effector recognition: implications for RhoA-mediated effector activation. *J Biol Chem,* 279**,** 53419-26.

BOECKLER, F. M., JOERGER, A. C., JAGGI, G., RUTHERFORD, T. J., VEPRINTSEV, D. B. & FERSHT, A. R. 2008. Targeted rescue of a destabilized mutant of p53 by an in silico screened drug. *Proc Natl Acad Sci U S A,* 105**,** 10360-5.

BOHLMAN, S. & MANFREDI, J. J. 2014. p53-independent effects of Mdm2. *Subcell Biochem,* 85**,** 235-46.

BOMMER, G. T., GERIN, I., FENG, Y., KACZOROWSKI, A. J., KUICK, R., LOVE, R. E., ZHAI, Y., GIORDANO, T. J., QIN, Z. S., MOORE, B. B., MACDOUGALD, O. A., CHO, K. R. & FEARON, E. R. 2007. p53-mediated activation of miRNA34 candidate tumor-suppressor genes. *Curr Biol,* 17**,** 1298-307.

BONDANZA, A., ZIMMERMANN, V. S., ROVERE-QUERINI, P., TURNAY, J., DUMITRIU, I. E., STACH, C. M., VOLL, R. E., GAIPL, U. S., BERTLING, W., POSCHL, E., KALDEN, J. R., MANFREDI, A. A. & HERRMANN, M. 2004. Inhibition of phosphatidylserine recognition heightens the immunogenicity of irradiated lymphoma cells in vivo. *J Exp Med,* 200**,** 1157-65.

BONFOCO, E., STUART, P. M., BRUNNER, T., LIN, T., GRIFFITH, T. S., GAO, Y., NAKAJIMA, H., HENKART, P. A., FERGUSON, T. A. & GREEN, D. R. 1998. Inducible nonlymphoid expression of Fas ligand is responsible for superantigen-induced peripheral deletion of T cells. *Immunity,* 9**,** 711-20.

BOTTO, M., DELL'AGNOLA, C., BYGRAVE, A. E., THOMPSON, E. M., COOK, H. T., PETRY, F., LOOS, M., PANDOLFI, P. P. & WALPORT, M. J. 1998.

Homozygous C1q deficiency causes glomerulonephritis associated with multiple apoptotic bodies. *Nat Genet,* 19**,** 56-9.
BOUAOUN, L., SONKIN, D., ARDIN, M., HOLLSTEIN, M., BYRNES, G., ZAVADIL, J. & OLIVIER, M. 2016. TP53 Variations in Human Cancers: New Lessons from the IARC TP53 Database and Genomics Data. *Hum Mutat,* 37**,** 865-76.
BOYD, S. D., TSAI, K. Y. & JACKS, T. 2000. An intact HDM2 RING-finger domain is required for nuclear exclusion of p53. *Nat Cell Biol,* 2**,** 563-8.
BRADY, C. A. & ATTARDI, L. D. 2010. p53 at a glance. *Journal of Cell Science,* 123**,** 2527.
BRADY, C. A., JIANG, D., MELLO, S. S., JOHNSON, T. M., JARVIS, L. A., KOZAK, M. M., KENZELMANN BROZ, D., BASAK, S., PARK, E. J., MCLAUGHLIN, M. E., KARNEZIS, A. N. & ATTARDI, L. D. 2011. Distinct p53 transcriptional programs dictate acute DNA-damage responses and tumor suppression. *Cell,* 145**,** 571-83.
BRADY, H. J., SALOMONS, G. S., BOBELDIJK, R. C. & BERNS, A. J. 1996. T cells from baxalpha transgenic mice show accelerated apoptosis in response to stimuli but do not show restored DNA damage-induced cell death in the absence of p53. *Embo j,* 15**,** 1221-30.
BRUGAROLAS, J., CHANDRASEKARAN, C., GORDON, J. I., BEACH, D., JACKS, T. & HANNON, G. J. 1995. Radiation-induced cell cycle arrest compromised by p21 deficiency. *Nature,* 377**,** 552-7.
BRUNET, C., GUNBY, R., BENSON, R., HICKMAN, J., WATSON, A. & BRADY, G. 1998. Brunet CL, Gunby RH, Benson RSP, Hickman JA, Watson AJM and Brady GCommitment to cell death measured by loss of clonogenicity is separable from the appearance of apoptotic markers. Cell Death Differ. 5: 107-115. *Cell death and differentiation,* 5**,** 107-15.
BURNS, M. B., TEMIZ, N. A. & HARRIS, R. S. 2013. Evidence for APOBEC3B mutagenesis in multiple human cancers. *Nat Genet,* 45**,** 977-83.
BUSUTTIL, V., DROIN, N., MCCORMICK, L., BERNASSOLA, F., CANDI, E., MELINO, G. & GREEN, D. R. 2010. NF-kappaB inhibits T-cell activation-induced, p73-dependent cell death by induction of MDM2. *Proc Natl Acad Sci U S A,* 107**,** 18061-6.
CAHILLY-SNYDER, L., YANG-FENG, T., FRANCKE, U. & GEORGE, D. L. 1987. Molecular analysis and chromosomal mapping of amplified genes isolated from a transformed mouse 3T3 cell line. *Somat Cell Mol Genet,* 13**,** 235-44.
CALLIS, J. 2014. The ubiquitination machinery of the ubiquitin system. *Arabidopsis Book,* 12**,** e0174.
CAMARDA, R., WILLIAMS, J. & GOGA, A. 2017. In vivo Reprogramming of Cancer Metabolism by MYC. *Frontiers in Cell and Developmental Biology,* 5.
CAMERON, E. R., MORTON, J., JOHNSTON, C. J., IRVINE, J., BELL, M., ONIONS, D. E., NEIL, J. C., CAMPBELL, M. & BLYTH, K. 2000. Fas-independent apoptosis in T-cell tumours induced by the CD2-myc transgene. *Cell Death & Differentiation,* 7**,** 80-88.
CAMPBELL, K. J., DHAYADE, S., FERRARI, N., SIMS, A. H., JOHNSON, E., MASON, S. M., DICKSON, A., RYAN, K. M., KALNA, G., EDWARDS, J., TAIT, S. W. G. & BLYTH, K. 2018. MCL-1 is a prognostic indicator and drug target in breast cancer. *Cell Death & Disease,* 9**,** 19.
CAMPBELL, K. J. & TAIT, S. W. G. 2018. Targeting BCL-2 regulated apoptosis in cancer. *Open Biol,* 8.

CANO RLE, L. H. 2013. Introduction to T and B lymphocytes. *In:* ANAYA JM, S. Y., ROJAS-VILLARRAGA A, ET. AL. (ed.) *Autoimmunity: From Bench to Bedside*. El Rosario University Press.

CARON, E. & HALL, A. 1998. Identification of two distinct mechanisms of phagocytosis controlled by different Rho GTPases. *Science,* 282**,** 1717-21.

CASTRO, D. J., MAURER, J., HEBBARD, L. & OSHIMA, R. G. 2013. ROCK1 inhibition promotes the self-renewal of a novel mouse mammary cancer stem cell. *Stem Cells,* 31**,** 12-22.

CATTORETTI, G., RILKE, F., ANDREOLA, S., D'AMATO, L. & DELIA, D. 1988. P53 expression in breast cancer. *Int J Cancer,* 41**,** 178-83.

CECCONI, F., ALVAREZ-BOLADO, G., MEYER, B. I., ROTH, K. A. & GRUSS, P. 1998. Apaf1 (CED-4 homolog) regulates programmed cell death in mammalian development. *Cell,* 94**,** 727-37.

CERRETTI, D. P., KOZLOSKY, C. J., MOSLEY, B., NELSON, N., VAN NESS, K., GREENSTREET, T. A., MARCH, C. J., KRONHEIM, S. R., DRUCK, T., CANNIZZARO, L. A. & ET AL. 1992. Molecular cloning of the interleukin-1 beta converting enzyme. *Science,* 256**,** 97-100.

CHANG, C. J., FREEMAN, D. J. & WU, H. 2004. PTEN regulates Mdm2 expression through the P1 promoter. *J Biol Chem,* 279**,** 29841-8.

CHANG, D. W., XING, Z., CAPACIO, V. L., PETER, M. E. & YANG, X. 2003. Interdimer processing mechanism of procaspase-8 activation. *EMBO J,* 22**,** 4132-42.

CHANG, J., XIE, M., SHAH, V. R., SCHNEIDER, M. D., ENTMAN, M. L., WEI, L. & SCHWARTZ, R. J. 2006. Activation of Rho-associated coiled-coil protein kinase 1 (ROCK-1) by caspase-3 cleavage plays an essential role in cardiac myocyte apoptosis. *Proceedings of the National Academy of Sciences,* 103**,** 14495-14500.

CHANG, J. R., GHAFOURI, M., MUKERJEE, R., BAGASHEV, A., CHABRASHVILI, T. & SAWAYA, B. E. 2012. Role of p53 in neurodegenerative diseases. *Neurodegener Dis,* 9**,** 68-80.

CHAO, C., HERR, D., CHUN, J. & XU, Y. 2006. Ser18 and 23 phosphorylation is required for p53-dependent apoptosis and tumor suppression. *EMBO J,* 25**,** 2615-22.

CHAO, M. P., JAISWAL, S., WEISSMAN-TSUKAMOTO, R., ALIZADEH, A. A., GENTLES, A. J., VOLKMER, J., WEISKOPF, K., WILLINGHAM, S. B., RAVEH, T., PARK, C. Y., MAJETI, R. & WEISSMAN, I. L. 2010. Calreticulin is the dominant pro-phagocytic signal on multiple human cancers and is counterbalanced by CD47. *Sci Transl Med,* 2**,** 63ra94.

CHARRAS, G. & PALUCH, E. 2008. Blebs lead the way: how to migrate without lamellipodia. *Nature Reviews Molecular Cell Biology,* 9**,** 730-736.

CHEKENI, F. B., ELLIOTT, M. R., SANDILOS, J. K., WALK, S. F., KINCHEN, J. M., LAZAROWSKI, E. R., ARMSTRONG, A. J., PENUELA, S., LAIRD, D. W., SALVESEN, G. S., ISAKSON, B. E., BAYLISS, D. A. & RAVICHANDRAN, K. S. 2010. Pannexin 1 channels mediate 'find-me' signal release and membrane permeability during apoptosis. *Nature,* 467**,** 863-7.

CHEN, L., PARK, S. M., TUMANOV, A. V., HAU, A., SAWADA, K., FEIG, C., TURNER, J. R., FU, Y. X., ROMERO, I. L., LENGYEL, E. & PETER, M. E. 2010. CD95 promotes tumour growth. *Nature,* 465**,** 492-6.

CHEN, L., WILLIS, S. N., WEI, A., SMITH, B. J., FLETCHER, J. I., HINDS, M. G., COLMAN, P. M., DAY, C. L., ADAMS, J. M. & HUANG, D. C. 2005. Differential targeting of prosurvival Bcl-2 proteins by their BH3-only ligands allows complementary apoptotic function. *Mol Cell,* 17**,** 393-403.

CHEN, W., WANG, H.-G., SRINIVASULA, S. M., ALNEMRI, E. S. & COOPER, N. R. 1999. B Cell Apoptosis Triggered by Antigen Receptor Ligation Proceeds Via a Novel Caspase-Dependent Pathway. *The Journal of Immunology,* 163**,** 2483.

CHENG, C. I., CHEN, P. H., LIN, Y. C. & KAO, Y. H. 2015. High glucose activates Raw264.7 macrophages through RhoA kinase-mediated signaling pathway. *Cell Signal,* 27**,** 283-92.

CHEOK, C. F. & LANE, D. P. 2017. Exploiting the p53 Pathway for Therapy. *Cold Spring Harb Perspect Med,* 7.

CHEVRIER, V., PIEL, M., COLLOMB, N., SAOUDI, Y., FRANK, R., PAINTRAND, M., NARUMIYA, S., BORNENS, M. & JOB, D. 2002. The Rho-associated protein kinase p160ROCK is required for centrosome positioning. *J Cell Biol,* 157**,** 807-17.

CHIPUK, J. E., BOUCHIER-HAYES, L. & GREEN, D. R. 2006. Mitochondrial outer membrane permeabilization during apoptosis: the innocent bystander scenario. *Cell Death & Differentiation,* 13**,** 1396-1402.

CHIPUK, J. E., BOUCHIER-HAYES, L., KUWANA, T., NEWMEYER, D. D. & GREEN, D. R. 2005. PUMA Couples the Nuclear and Cytoplasmic Proapoptotic Function of p53. *Science,* 309**,** 1732.

CHIPUK, J. E. & GREEN, D. R. 2005. Do inducers of apoptosis trigger caspase-independent cell death? *Nature Reviews Molecular Cell Biology,* 6**,** 268-275.

CHUANG, H. H., LIANG, S. W., CHANG, Z. F. & LEE, H. H. 2013. Ser1333 phosphorylation indicates ROCKI activation. *J Biomed Sci,* 20**,** 83.

CIFONE, M. G., MIGLIORATI, G., PARRONI, R., MARCHETTI, C., MILLIMAGGI, D., SANTONI, A. & RICCARDI, C. 1999. Dexamethasone-Induced Thymocyte Apoptosis: Apoptotic Signal Involves the Sequential Activation of Phosphoinositide-Specific Phospholipase C, Acidic Sphingomyelinase, and Caspases. *Blood,* 93**,** 2282-2296.

CLORE, G. M., ERNST, J., CLUBB, R., OMICHINSKI, J. G., KENNEDY, W. M., SAKAGUCHI, K., APPELLA, E. & GRONENBORN, A. M. 1995. Refined solution structure of the oligomerization domain of the tumour suppressor p53. *Nat Struct Biol,* 2**,** 321-33.

COELHO, M. A., DE CARNE TRECESSON, S., RANA, S., ZECCHIN, D., MOORE, C., MOLINA-ARCAS, M., EAST, P., SPENCER-DENE, B., NYE, E., BARNOUIN, K., SNIJDERS, A. P., LAI, W. S., BLACKSHEAR, P. J. & DOWNWARD, J. 2017. Oncogenic RAS Signaling Promotes Tumor Immunoresistance by Stabilizing PD-L1 mRNA. *Immunity,* 47**,** 1083-1099 e6.

COLEMAN, M. L., SAHAI, E. A., YEO, M., BOSCH, M., DEWAR, A. & OLSON, M. F. 2001. Membrane blebbing during apoptosis results from caspase-mediated activation of ROCK I. *Nature Cell Biology,* 3**,** 339-345.

COMMUNAL, C., SUMANDEA, M., DE TOMBE, P., NARULA, J., SOLARO, R. J. & HAJJAR, R. J. 2002. Functional consequences of caspase activation in cardiac myocytes. *Proc Natl Acad Sci U S A,* 99**,** 6252-6.

CONSORTIUM, A. P. G. 2017. AACR Project GENIE: Powering Precision Medicine through an International Consortium. *Cancer Discov,* 7**,** 818-831.

COUCOUVANIS, E. & MARTIN, G. R. 1995. Signals for death and survival: a two-step mechanism for cavitation in the vertebrate embryo. *Cell,* 83**,** 279-87.

CRAWFORD, L. V., PIM, D. C. & LAMB, P. 1984. The cellular protein p53 in human tumours. *Mol Biol Med,* 2**,** 261-72.

CROFT, D. R., COLEMAN, M. L., LI, S., ROBERTSON, D., SULLIVAN, T., STEWART, C. L. & OLSON, M. F. 2005. Actin-myosin–based contraction is responsible

for apoptotic nuclear disintegration. *Journal of Cell Biology,* 168**,** 245-255.
CROFT, D. R. & OLSON, M. F. 2006. The Rho GTPase Effector ROCK Regulates Cyclin A, Cyclin D1, and p27^{Kip1} Levels by Distinct Mechanisms. *Molecular and Cellular Biology,* 26**,** 4612.
CROFT, D. R., SAHAI, E., MAVRIA, G., LI, S., TSAI, J., LEE, W. M., MARSHALL, C. J. & OLSON, M. F. 2004. Conditional ROCK activation in vivo induces tumor cell dissemination and angiogenesis. *Cancer Res,* 64**,** 8994-9001.
CRUK. 2017. *Cancer Research UK Lung Cancer Statistics* [Online]. Available: https://www.cancerresearchuk.org/health-professional/cancer-statistics/statistics-by-cancer-type/lung-cancer#heading-One [Accessed 14 July 2020].
CUMMINS, J. M. & VOGELSTEIN, B. 2004. HAUSP is required for p53 destabilization. *Cell Cycle,* 3**,** 689-92.
D'ARCY, M. S. 2019. Cell death: a review of the major forms of apoptosis, necrosis and autophagy. *Cell Biology International,* 43**,** 582-592.
DANG, C. V. 1999. c-Myc Target Genes Involved in Cell Growth, Apoptosis, and Metabolism. *Molecular and Cellular Biology,* 19**,** 1.
DANKORT, D., FILENOVA, E., COLLADO, M., SERRANO, M., JONES, K. & MCMAHON, M. 2007. A new mouse model to explore the initiation, progression, and therapy of BRAFV600E-induced lung tumors. *Genes Dev,* 21**,** 379-84.
DE ROZIERES, S., MAYA, R., OREN, M. & LOZANO, G. 2000. The loss of mdm2 induces p53-mediated apoptosis. *Oncogene,* 19**,** 1691-7.
DE TOLEDO, M., ANGUILLE, C., ROGER, L., ROUX, P. & GADEA, G. 2012. Cooperative anti-invasive effect of Cdc42/Rac1 activation and ROCK inhibition in SW620 colorectal cancer cells with elevated blebbing activity. *PLoS One,* 7**,** e48344.
DEVARAJAN, E., SAHIN, A. A., CHEN, J. S., KRISHNAMURTHY, R. R., AGGARWAL, N., BRUN, A. M., SAPINO, A., ZHANG, F., SHARMA, D., YANG, X. H., TORA, A. D. & MEHTA, K. 2002. Down-regulation of caspase 3 in breast cancer: a possible mechanism for chemoresistance. *Oncogene,* 21**,** 8843-51.
DEVITT, A. & MARSHALL, L. J. 2011. The innate immune system and the clearance of apoptotic cells. *J Leukoc Biol,* 90**,** 447-57.
DIEUDÉ, M., BELL, C., TURGEON, J., BEILLEVAIRE, D., POMERLEAU, L., YANG, B., HAMELIN, K., QI, S., PALLET, N., BÉLAND, C., DHAHRI, W., CAILHIER, J. F., ROUSSEAU, M., DUCHEZ, A. C., LÉVESQUE, T., LAU, A., RONDEAU, C., GINGRAS, D., MURUVE, D., RIVARD, A., CARDINAL, H., PERREAULT, C., DESJARDINS, M., BOILARD, É., THIBAULT, P. & HÉBERT, M. J. 2015. The 20S proteasome core, active within apoptotic exosome-like vesicles, induces autoantibody production and accelerates rejection. *Sci Transl Med,* 7**,** 318ra200.
DIMITRIADI, M., POULOGIANNIS, G., LIU, L., BÄCKLUND, L. M., PEARSON, D. M., ICHIMURA, K. & COLLINS, V. P. 2008. p53-independent mechanisms regulate the P2-MDM2 promoter in adult astrocytic tumours. *British Journal of Cancer,* 99**,** 1144-1152.
DIXON, S. J., LEMBERG, K. M., LAMPRECHT, M. R., SKOUTA, R., ZAITSEV, E. M., GLEASON, C. E., PATEL, D. N., BAUER, A. J., CANTLEY, A. M., YANG, W. S., MORRISON, B., 3RD & STOCKWELL, B. R. 2012. Ferroptosis: an iron-dependent form of nonapoptotic cell death. *Cell,* 149**,** 1060-72.
DONEHOWER, L. A., HARVEY, M., SLAGLE, B. L., MCARTHUR, M. J., MONTGOMERY, C. A., JR., BUTEL, J. S. & BRADLEY, A. 1992. Mice

deficient for p53 are developmentally normal but susceptible to spontaneous tumours. *Nature,* 356**,** 215-21.
DORAN, A. C., YURDAGUL, A., JR. & TABAS, I. 2020. Efferocytosis in health and disease. *Nat Rev Immunol,* 20**,** 254-267.
DORNAN, D., WERTZ, I., SHIMIZU, H., ARNOTT, D., FRANTZ, G. D., DOWD, P., O'ROURKE, K., KOEPPEN, H. & DIXIT, V. M. 2004. The ubiquitin ligase COP1 is a critical negative regulator of p53. *Nature,* 429**,** 86-92.
DOWNWARD, J. 2003. Targeting RAS signalling pathways in cancer therapy. *Nat Rev Cancer,* 3**,** 11-22.
DUKE, R. C., CHERVENAK, R. & COHEN, J. J. 1983. Endogenous endonuclease-induced DNA fragmentation: an early event in cell-mediated cytolysis. *Proc Natl Acad Sci U S A,* 80**,** 6361-5.
DUPAGE, M., DOOLEY, A. L. & JACKS, T. 2009. Conditional mouse lung cancer models using adenoviral or lentiviral delivery of Cre recombinase. *Nature Protocols,* 4**,** 1064-1072.
DUYCKAERTS, C., DELATOUR, B. & POTIER, M. C. 2009. Classification and basic pathology of Alzheimer disease. *Acta Neuropathol,* 118**,** 5-36.
DVORSKY, R., BLUMENSTEIN, L., VETTER, I. R. & AHMADIAN, M. R. 2004. Structural insights into the interaction of ROCKI with the switch regions of RhoA. *J Biol Chem,* 279**,** 7098-104.
EBERLIN, L. S., GABAY, M., FAN, A. C., GOUW, A. M., TIBSHIRANI, R. J., FELSHER, D. W. & ZARE, R. N. 2014. Alteration of the lipid profile in lymphomas induced by MYC overexpression. *Proceedings of the National Academy of Sciences,* 111**,** 10450.
EDWARDS, S. W., DEROUET, M., HOWSE, M. & MOOTS, R. J. 2004. Regulation of neutrophil apoptosis by Mcl-1. *Biochem Soc Trans,* 32**,** 489-92.
EISCHEN, C. M., ALT, J. R. & WANG, P. 2004. Loss of one allele of ARF rescues Mdm2 haploinsufficiency effects on apoptosis and lymphoma development. *Oncogene,* 23**,** 8931-8940.
EISCHEN, C. M., ROUSSEL, M. F., KORSMEYER, S. J. & CLEVELAND, J. L. 2001a. Bax loss impairs Myc-induced apoptosis and circumvents the selection of p53 mutations during Myc-mediated lymphomagenesis. *Mol Cell Biol,* 21**,** 7653-62.
EISCHEN, C. M., WEBER, J. D., ROUSSEL, M. F., SHERR, C. J. & CLEVELAND, J. L. 1999. Disruption of the ARF-Mdm2-p53 tumor suppressor pathway in Myc-induced lymphomagenesis. *Genes & development,* 13**,** 2658-2669.
EISCHEN, C. M., WOO, D., ROUSSEL, M. F. & CLEVELAND, J. L. 2001b. Apoptosis Triggered by Myc-Induced Suppression of Bcl-X_L or Bcl-2 Is Bypassed during Lymphomagenesis. *Molecular and Cellular Biology,* 21**,** 5063.
EL-DEIRY, W. S., KERN, S. E., PIETENPOL, J. A., KINZLER, K. W. & VOGELSTEIN, B. 1992. Definition of a consensus binding site for p53. *Nature Genetics,* 1**,** 45-49.
EL-SERAG, H. B. & RUDOLPH, K. L. 2007. Hepatocellular carcinoma: epidemiology and molecular carcinogenesis. *Gastroenterology,* 132**,** 2557-76.
ELLIOTT, M. R., CHEKENI, F. B., TRAMPONT, P. C., LAZAROWSKI, E. R., KADL, A., WALK, S. F., PARK, D., WOODSON, R. I., OSTANKOVICH, M., SHARMA, P., LYSIAK, J. J., HARDEN, T. K., LEITINGER, N. & RAVICHANDRAN, K. S. 2009. Nucleotides released by apoptotic cells act as a find-me signal to promote phagocytic clearance. *Nature,* 461**,** 282-6.

ELLIOTT, M. R. & RAVICHANDRAN, K. S. 2010. Clearance of apoptotic cells: implications in health and disease. *The Journal of Cell Biology,* 189, 1059-1070.

ELMORE, S. 2007. Apoptosis: a review of programmed cell death. *Toxicol Pathol,* 35, 495-516.

ENARI, M., SAKAHIRA, H., YOKOYAMA, H., OKAWA, K., IWAMATSU, A. & NAGATA, S. 1998. A caspase-activated DNase that degrades DNA during apoptosis, and its inhibitor ICAD. *Nature,* 391, 43-50.

ERWIG, L. P., MCPHILIPS, K. A., WYNES, M. W., IVETIC, A., RIDLEY, A. J. & HENSON, P. M. 2006. Differential regulation of phagosome maturation in macrophages and dendritic cells mediated by Rho GTPases and ezrin-radixin-moesin (ERM) proteins. *Proc Natl Acad Sci U S A,* 103, 12825-30.

ETIENNE-MANNEVILLE, S. & HALL, A. 2002. Rho GTPases in cell biology. *Nature,* 420, 629-35.

EVANS, S. C., VISWANATHAN, M., GRIER, J. D., NARAYANA, M., EL-NAGGAR, A. K. & LOZANO, G. 2001. An alternatively spliced HDM2 product increases p53 activity by inhibiting HDM2. *Oncogene,* 20, 4041-9.

FACKLER, O. T. & GROSSE, R. 2008. Cell motility through plasma membrane blebbing. *The Journal of cell biology,* 181, 879-884.

FADEEL, B. 2004. Plasma membrane alterations during apoptosis: role in corpse clearance. *Antioxid Redox Signal,* 6, 269-75.

FADOK, V. A., VOELKER, D. R., CAMPBELL, P. A., COHEN, J. J., BRATTON, D. L. & HENSON, P. M. 1992. Exposure of phosphatidylserine on the surface of apoptotic lymphocytes triggers specific recognition and removal by macrophages. *J Immunol,* 148, 2207-16.

FAKHARZADEH, S. S., TRUSKO, S. P. & GEORGE, D. L. 1991. Tumorigenic potential associated with enhanced expression of a gene that is amplified in a mouse tumor cell line. *EMBO J,* 10, 1565-9.

FANG, S., JENSEN, J. P., LUDWIG, R. L., VOUSDEN, K. H. & WEISSMAN, A. M. 2000. Mdm2 is a RING finger-dependent ubiquitin protein ligase for itself and p53. *J Biol Chem,* 275, 8945-51.

FAVALORO, B., ALLOCATI, N., GRAZIANO, V., DI ILIO, C. & DE LAURENZI, V. 2012. Role of apoptosis in disease. *Aging,* 4, 330-349.

FEIG, C. & PETER, M. E. 2007. How apoptosis got the immune system in shape. *Eur J Immunol,* 37 Suppl 1, S61-70.

FENG, J., ITO, M., ICHIKAWA, K., ISAKA, N., NISHIKAWA, M., HARTSHORNE, D. J. & NAKANO, T. 1999. Inhibitory phosphorylation site for Rho-associated kinase on smooth muscle myosin phosphatase. *J Biol Chem,* 274, 37385-90.

FENG, X., DENG, T., ZHANG, Y., SU, S., WEI, C. & HAN, D. 2011. Lipopolysaccharide inhibits macrophage phagocytosis of apoptotic neutrophils by regulating the production of tumour necrosis factor α and growth arrest-specific gene 6. *Immunology,* 132, 287-295.

FENG, Y., LOGRASSO, P. V., DEFERT, O. & LI, R. 2016. Rho Kinase (ROCK) Inhibitors and Their Therapeutic Potential. *J Med Chem,* 59, 2269-300.

FERNALD, K. & KUROKAWA, M. 2013. Evading apoptosis in cancer. *Trends Cell Biol,* 23, 620-33.

FERRER, I., ZUGAZAGOITIA, J., HERBERTZ, S., JOHN, W., PAZ-ARES, L. & SCHMID-BINDERT, G. 2018. KRAS-Mutant non-small cell lung cancer: From biology to therapy. *Lung Cancer,* 124, 53-64.

FINCH, A., PRESCOTT, J., SHCHORS, K., HUNT, A., SOUCEK, L., DANSEN, T. B., SWIGART, L. B. & EVAN, G. I. 2006. Bcl-xL gain of function and p19 ARF

loss of function cooperate oncogenically with Myc in vivo by distinct mechanisms. *Cancer Cell,* 10**,** 113-20.

FINLAY, C. A., HINDS, P. W. & LEVINE, A. J. 1989. The p53 proto-oncogene can act as a suppressor of transformation. *Cell,* 57**,** 1083-93.

FINNEMANN, S. C., BONILHA, V. L., MARMORSTEIN, A. D. & RODRIGUEZ-BOULAN, E. 1997. Phagocytosis of rod outer segments by retinal pigment epithelial cells requires alpha(v)beta5 integrin for binding but not for internalization. *Proc Natl Acad Sci U S A,* 94**,** 12932-7.

FISHKIND, D. J., CAO, L. G. & WANG, Y. L. 1991. Microinjection of the catalytic fragment of myosin light chain kinase into dividing cells: effects on mitosis and cytokinesis. *Journal of Cell Biology,* 114**,** 967-975.

FORD, C. A., PETROVA, S., POUND, J. D., VOSS, J. J., MELVILLE, L., PATERSON, M., FARNWORTH, S. L., GALLIMORE, A. M., CUFF, S., WHEADON, H., DOBBIN, E., OGDEN, C. A., DUMITRIU, I. E., DUNBAR, D. R., MURRAY, P. G., RUCKERL, D., ALLEN, J. E., HUME, D. A., VAN ROOIJEN, N., GOODLAD, J. R., FREEMAN, T. C. & GREGORY, C. D. 2015. Oncogenic properties of apoptotic tumor cells in aggressive B cell lymphoma. *Curr Biol,* 25**,** 577-88.

FOX, S., LEITCH, A. E., DUFFIN, R., HASLETT, C. & ROSSI, A. G. 2010. Neutrophil apoptosis: relevance to the innate immune response and inflammatory disease. *J Innate Immun,* 2**,** 216-27.

FRANCOZ, S., FROMENT, P., BOGAERTS, S., DE CLERCQ, S., MAETENS, M., DOUMONT, G., BELLEFROID, E. & MARINE, J. C. 2006. Mdm4 and Mdm2 cooperate to inhibit p53 activity in proliferating and quiescent cells in vivo. *Proc Natl Acad Sci U S A,* 103**,** 3232-7.

FRIDMAN, J. S. & LOWE, S. W. 2003. Control of apoptosis by p53. *Oncogene,* 22**,** 9030-9040.

FRIEDL, P. & WOLF, K. 2003. Tumour-cell invasion and migration: diversity and escape mechanisms. *Nature Reviews Cancer,* 3**,** 362-374.

FRIESEN, C., FULDA, S. & DEBATIN, K. M. 1997. Deficient activation of the CD95 (APO-1/Fas) system in drug-resistant cells. *Leukemia,* 11**,** 1833-41.

FRISCH, S. M. & FRANCIS, H. 1994. Disruption of epithelial cell-matrix interactions induces apoptosis. *J Cell Biol,* 124**,** 619-26.

FU, W., MA, Q., CHEN, L., LI, P., ZHANG, M., RAMAMOORTHY, S., NAWAZ, Z., SHIMOJIMA, T., WANG, H., YANG, Y., SHEN, Z., ZHANG, Y., ZHANG, X., NICOSIA, S. V., ZHANG, Y., PLEDGER, J. W., CHEN, J. & BAI, W. 2009. MDM2 acts downstream of p53 as an E3 ligase to promote FOXO ubiquitination and degradation. *The Journal of biological chemistry,* 284**,** 13987-14000.

FU, X., GONG, M. C., JIA, T., SOMLYO, A. V. & SOMLYO, A. P. 1998. The effects of the Rho-kinase inhibitor Y-27632 on arachidonic acid-, GTPγS-, and phorbol ester-induced Ca2+-sensitization of smooth muscle. *FEBS Letters,* 440**,** 183-187.

FUKATA, Y., KIMURA, K., OSHIRO, N., SAYA, H., MATSUURA, Y. & KAIBUCHI, K. 1998. Association of the myosin-binding subunit of myosin phosphatase and moesin: dual regulation of moesin phosphorylation by Rho-associated kinase and myosin phosphatase. *J Cell Biol,* 141**,** 409-18.

FUKUSHIMA, M., NAKAMUTA, M., KOHJIMA, M., KOTOH, K., ENJOJI, M., KOBAYASHI, N. & NAWATA, H. 2005. Fasudil hydrochloride hydrate, a Rho-kinase (ROCK) inhibitor, suppresses collagen production and enhances collagenase activity in hepatic stellate cells. *Liver Int,* 25**,** 829-38.

FULDA, S. & DEBATIN, K. M. 2006. Extrinsic versus intrinsic apoptosis pathways in anticancer chemotherapy. *Oncogene,* 25**,** 4798-811.

FULDA, S., LOS, M., FRIESEN, C. & DEBATIN, K. M. 1998. Chemosensitivity of solid tumor cells in vitro is related to activation of the CD95 system. *Int J Cancer,* 76**,** 105-14.

GAGGIOLI, C., HOOPER, S., HIDALGO-CARCEDO, C., GROSSE, R., MARSHALL, J. F., HARRINGTON, K. & SAHAI, E. 2007. Fibroblast-led collective invasion of carcinoma cells with differing roles for RhoGTPases in leading and following cells. *Nat Cell Biol,* 9**,** 1392-400.

GAJEWSKI, T. F., SCHREIBER, H. & FU, Y.-X. 2013. Innate and adaptive immune cells in the tumor microenvironment. *Nature immunology,* 14**,** 1014-1022.

GALLUZZI, L., VITALE, I., AARONSON, S. A., ABRAMS, J. M., ADAM, D., AGOSTINIS, P., ALNEMRI, E. S., ALTUCCI, L., AMELIO, I., ANDREWS, D. W., ANNICCHIARICO-PETRUZZELLI, M., ANTONOV, A. V., ARAMA, E., BAEHRECKE, E. H., BARLEV, N. A., BAZAN, N. G., BERNASSOLA, F., BERTRAND, M. J. M., BIANCHI, K., BLAGOSKLONNY, M. V., BLOMGREN, K., BORNER, C., BOYA, P., BRENNER, C., CAMPANELLA, M., CANDI, E., CARMONA-GUTIERREZ, D., CECCONI, F., CHAN, F. K. M., CHANDEL, N. S., CHENG, E. H., CHIPUK, J. E., CIDLOWSKI, J. A., CIECHANOVER, A., COHEN, G. M., CONRAD, M., CUBILLOS-RUIZ, J. R., CZABOTAR, P. E., D'ANGIOLELLA, V., DAWSON, T. M., DAWSON, V. L., DE LAURENZI, V., DE MARIA, R., DEBATIN, K.-M., DEBERARDINIS, R. J., DESHMUKH, M., DI DANIELE, N., DI VIRGILIO, F., DIXIT, V. M., DIXON, S. J., DUCKETT, C. S., DYNLACHT, B. D., EL-DEIRY, W. S., ELROD, J. W., FIMIA, G. M., FULDA, S., GARCÍA-SÁEZ, A. J., GARG, A. D., GARRIDO, C., GAVATHIOTIS, E., GOLSTEIN, P., GOTTLIEB, E., GREEN, D. R., GREENE, L. A., GRONEMEYER, H., GROSS, A., HAJNOCZKY, G., HARDWICK, J. M., HARRIS, I. S., HENGARTNER, M. O., HETZ, C., ICHIJO, H., JÄÄTTELÄ, M., JOSEPH, B., JOST, P. J., JUIN, P. P., KAISER, W. J., KARIN, M., KAUFMANN, T., KEPP, O., KIMCHI, A., KITSIS, R. N., KLIONSKY, D. J., KNIGHT, R. A., KUMAR, S., LEE, S. W., LEMASTERS, J. J., LEVINE, B., LINKERMANN, A., LIPTON, S. A., LOCKSHIN, R. A., LÓPEZ-OTÍN, C., LOWE, S. W., LUEDDE, T., LUGLI, E., MACFARLANE, M., MADEO, F., MALEWICZ, M., MALORNI, W., MANIC, G., et al. 2018. Molecular mechanisms of cell death: recommendations of the Nomenclature Committee on Cell Death 2018. *Cell Death & Differentiation,* 25**,** 486-541.

GAMBLIN, T. C., CHEN, F., ZAMBRANO, A., ABRAHA, A., LAGALWAR, S., GUILLOZET, A. L., LU, M., FU, Y., GARCIA-SIERRA, F., LAPOINTE, N., MILLER, R., BERRY, R. W., BINDER, L. I. & CRYNS, V. L. 2003. Caspase cleavage of tau: linking amyloid and neurofibrillary tangles in Alzheimer's disease. *Proc Natl Acad Sci U S A,* 100**,** 10032-7.

GANGULI, G. & WASYLYK, B. 2003. p53-independent functions of MDM2. *Mol Cancer Res,* 1**,** 1027-35.

GARDAI, S. J., MCPHILLIPS, K. A., FRASCH, S. C., JANSSEN, W. J., STAREFELDT, A., MURPHY-ULLRICH, J. E., BRATTON, D. L., OLDENBORG, P. A., MICHALAK, M. & HENSON, P. M. 2005. Cell-surface calreticulin initiates clearance of viable or apoptotic cells through trans-activation of LRP on the phagocyte. *Cell,* 123**,** 321-34.

GARG, A. D., DUDEK-PERIC, A. M., ROMANO, E. & AGOSTINIS, P. 2015. Immunogenic cell death. *Int J Dev Biol,* 59**,** 131-40.

GE, Q. & ZHAO, Y. 2013. Evolution of thymus organogenesis. *Dev Comp Immunol,* 39**,** 85-90.

GERMAIN, R. N. 2002. T-cell development and the CD4-CD8 lineage decision. *Nat Rev Immunol,* 2, 309-22.

GIL, J. & PETERS, G. 2006. Regulation of the INK4b-ARF-INK4a tumour suppressor locus: all for one or one for all. *Nat Rev Mol Cell Biol,* 7, 667-77.

GLASSER, S. W., KORFHAGEN, T. R., WERT, S. E., BRUNO, M. D., MCWILLIAMS, K. M., VORBROKER, D. K. & WHITSETT, J. A. 1991. Genetic element from human surfactant protein SP-C gene confers bronchiolar-alveolar cell specificity in transgenic mice. *Am J Physiol,* 261, L349-56.

GLYN, M. C., LAWRENSON, J. G. & WARD, B. J. 2003. A Rho-associated kinase mitigates reperfusion-induced change in the shape of cardiac capillary endothelial cells in situ. *Cardiovasc Res,* 57, 195-206.

GODFREY, D. I., KENNEDY, J., SUDA, T. & ZLOTNIK, A. 1993. A developmental pathway involving four phenotypically and functionally distinct subsets of CD3-CD4-CD8- triple-negative adult mouse thymocytes defined by CD44 and CD25 expression. *J Immunol,* 150, 4244-52.

GONG, H., ZHOU, L., KHELFAT, L., QIU, G., WANG, Y., MAO, K. & CHEN, W. 2019. Rho-Associated Protein Kinase (ROCK) Promotes Proliferation and Migration of PC-3 and DU145 Prostate Cancer Cells by Targeting LIM Kinase 1 (LIMK1) and Matrix Metalloproteinase-2 (MMP-2). *Med Sci Monit,* 25, 3090-3099.

GORDON, J. & MANLEY, N. R. 2011. Mechanisms of thymus organogenesis and morphogenesis. *Development,* 138, 3865-78.

GRABOW, S., DELBRIDGE, ALEX R. D., AUBREY, BRANDON J., VANDENBERG, CASSANDRA J. & STRASSER, A. 2016. Loss of a Single Mcl-1 Allele Inhibits MYC-Driven Lymphomagenesis by Sensitizing Pro-B Cells to Apoptosis. *Cell Reports,* 14, 2337-2347.

GRAYSON, J. M., LANIER, J. G., ALTMAN, J. D. & AHMED, R. 2001. The role of p53 in regulating antiviral T cell responses. *J Immunol,* 167, 1333-7.

GRAZIANO, S. L., GAMBLE, G. P., NEWMAN, N. B., ABBOTT, L. Z., ROONEY, M., MOOKHERJEE, S., LAMB, M. L., KOHMAN, L. J. & POIESZ, B. J. 1999. Prognostic significance of K-ras codon 12 mutations in patients with resected stage I and II non-small-cell lung cancer. *J Clin Oncol,* 17, 668-75.

GREEN, D. R. & EVAN, G. I. 2002. A matter of life and death. *Cancer Cell,* 1, 19-30.

GREEN, D. R. & LLAMBI, F. 2015. Cell Death Signaling. *Cold Spring Harb Perspect Biol,* 7.

GREEN, D. R., OGUIN, T. H. & MARTINEZ, J. 2016. The clearance of dying cells: table for two. *Cell Death Differ,* 23, 915-26.

GREENMAN, C., STEPHENS, P., SMITH, R., DALGLIESH, G. L., HUNTER, C., BIGNELL, G., DAVIES, H., TEAGUE, J., BUTLER, A., STEVENS, C., EDKINS, S., O'MEARA, S., VASTRIK, I., SCHMIDT, E. E., AVIS, T., BARTHORPE, S., BHAMRA, G., BUCK, G., CHOUDHURY, B., CLEMENTS, J., COLE, J., DICKS, E., FORBES, S., GRAY, K., HALLIDAY, K., HARRISON, R., HILLS, K., HINTON, J., JENKINSON, A., JONES, D., MENZIES, A., MIRONENKO, T., PERRY, J., RAINE, K., RICHARDSON, D., SHEPHERD, R., SMALL, A., TOFTS, C., VARIAN, J., WEBB, T., WEST, S., WIDAA, S., YATES, A., CAHILL, D. P., LOUIS, D. N., GOLDSTRAW, P., NICHOLSON, A. G., BRASSEUR, F., LOOIJENGA, L., WEBER, B. L., CHIEW, Y. E., DEFAZIO, A., GREAVES, M. F., GREEN, A. R., CAMPBELL, P., BIRNEY, E., EASTON, D. F., CHENEVIX-TRENCH, G., TAN, M. H., KHOO, S. K., TEH, B. T., YUEN, S. T., LEUNG, S.

Y., WOOSTER, R., FUTREAL, P. A. & STRATTON, M. R. 2007. Patterns of somatic mutation in human cancer genomes. *Nature,* 446**,** 153-8.

GREGORY, C. D. & DEVITT, A. 2004. The macrophage and the apoptotic cell: an innate immune interaction viewed simplistically? *Immunology,* 113**,** 1-14.

GREGORY, C. D., FORD, C. A. & VOSS, J. J. 2016. Microenvironmental Effects of Cell Death in Malignant Disease. *Adv Exp Med Biol,* 930**,** 51-88.

GREGORY, C. D. & PATERSON, M. 2018. An apoptosis-driven 'onco-regenerative niche': roles of tumour-associated macrophages and extracellular vesicles. *Philosophical Transactions of the Royal Society B: Biological Sciences,* 373**,** 20170003.

GROCHOLA, L. F., TAUBERT, H., GREITHER, T., BHANOT, U., UDELNOW, A. & WÜRL, P. 2011. Elevated transcript levels from the MDM2 P1 promoter and low p53 transcript levels are associated with poor prognosis in human pancreatic ductal adenocarcinoma. *Pancreas,* 40**,** 265-70.

GU, W., SHI, X.-L. & ROEDER, R. G. 1997. Synergistic activation of transcription by CBP and p53. *Nature,* 387**,** 819-823.

GUALBERTO, A., ALDAPE, K., KOZAKIEWICZ, K. & TLSTY, T. D. 1998. An oncogenic form of p53 confers a dominant, gain-of-function phenotype that disrupts spindle checkpoint control. *Proc Natl Acad Sci U S A,* 95**,** 5166-71.

GUAN, R., XU, X., CHEN, M., HU, H., GE, H., WEN, S., ZHOU, S. & PI, R. 2013. Advances in the studies of roles of Rho/Rho-kinase in diseases and the development of its inhibitors. *Eur J Med Chem,* 70**,** 613-22.

GUDE, D. R., ALVAREZ, S. E., PAUGH, S. W., MITRA, P., YU, J., GRIFFITHS, R., BARBOUR, S. E., MILSTIEN, S. & SPIEGEL, S. 2008. Apoptosis induces expression of sphingosine kinase 1 to release sphingosine-1-phosphate as a "come-and-get-me" signal. *FASEB J,* 22**,** 2629-38.

HÄCKER, G. 2000. The morphology of apoptosis. *Cell and Tissue Research,* 301**,** 5-17.

HAGA, R. B. & RIDLEY, A. J. 2016. Rho GTPases: Regulation and roles in cancer cell biology. *Small GTPases,* 7**,** 207-221.

HAINES, B. B., RYU, C. J., CHANG, S., PROTOPOPOV, A., LUCH, A., KANG, Y. H., DRAGANOV, D. D., FRAGOSO, M. F., PAIK, S. G., HONG, H. J., DEPINHO, R. A. & CHEN, J. 2006. Block of T cell development in P53-deficient mice accelerates development of lymphomas with characteristic RAG-dependent cytogenetic alterations. *Cancer Cell,* 9**,** 109-120.

HAKEM, R., HAKEM, A., DUNCAN, G. S., HENDERSON, J. T., WOO, M., SOENGAS, M. S., ELIA, A., DE LA POMPA, J. L., KAGI, D., KHOO, W., POTTER, J., YOSHIDA, R., KAUFMAN, S. A., LOWE, S. W., PENNINGER, J. M. & MAK, T. W. 1998. Differential requirement for caspase 9 in apoptotic pathways in vivo. *Cell,* 94**,** 339-52.

HANAHAN, D. & WEINBERG, R. A. 2011. Hallmarks of cancer: the next generation. *Cell,* 144**,** 646-74.

HANAYAMA, R., TANAKA, M., MIWA, K., SHINOHARA, A., IWAMATSU, A. & NAGATA, S. 2002. Identification of a factor that links apoptotic cells to phagocytes. *Nature,* 417**,** 182-7.

HANAYAMA, R., TANAKA, M., MIYASAKA, K., AOZASA, K., KOIKE, M., UCHIYAMA, Y. & NAGATA, S. 2004. Autoimmune disease and impaired uptake of apoptotic cells in MFG-E8-deficient mice. *Science,* 304**,** 1147-50.

HANKINS, H. M., BALDRIDGE, R. D., XU, P. & GRAHAM, T. R. 2015. Role of flippases, scramblases and transfer proteins in phosphatidylserine subcellular distribution. *Traffic,* 16**,** 35-47.

HARRIS, A. W., PINKERT, C. A., CRAWFORD, M., LANGDON, W. Y., BRINSTER, R. L. & ADAMS, J. M. 1988. The E mu-myc transgenic mouse. A model for high-incidence spontaneous lymphoma and leukemia of early B cells. *Journal of Experimental Medicine,* 167**,** 353-371.

HARRIS, R. S., BISHOP, K. N., SHEEHY, A. M., CRAIG, H. M., PETERSEN-MAHRT, S. K., WATT, I. N., NEUBERGER, M. S. & MALIM, M. H. 2003. DNA deamination mediates innate immunity to retroviral infection. *Cell,* 113**,** 803-9.

HARTLEY, S. B., COOKE, M. P., FULCHER, D. A., HARRIS, A. W., CORY, S., BASTEN, A. & GOODNOW, C. C. 1993. Elimination of self-reactive B lymphocytes proceeds in two stages: arrested development and cell death. *Cell,* 72**,** 325-35.

HARTMANN, S., RIDLEY, A. J. & LUTZ, S. 2015. The Function of Rho-Associated Kinases ROCK1 and ROCK2 in the Pathogenesis of Cardiovascular Disease. *Front Pharmacol,* 6**,** 276.

HASEGAWA, H. & MATSUMOTO, T. 2018. Mechanisms of Tolerance Induction by Dendritic Cells In Vivo. *Frontiers in Immunology,* 9.

HAUPT, S., BERGER, M., GOLDBERG, Z. & HAUPT, Y. 2003. Apoptosis - the p53 network. *Journal of Cell Science,* 116**,** 4077.

HAUPT, S., MEJÍA-HERNÁNDEZ, J. O., VIJAYAKUMARAN, R., KEAM, S. P. & HAUPT, Y. 2019. The long and the short of it: the MDM4 tail so far. *Journal of Molecular Cell Biology,* 11**,** 231-244.

HAUPT, Y., MAYA, R., KAZAZ, A. & OREN, M. 1997. Mdm2 promotes the rapid degradation of p53. *Nature,* 387**,** 296-9.

HEASMAN, S. J. & RIDLEY, A. J. 2010. Multiple roles for RhoA during T cell transendothelial migration. *Small GTPases,* 1**,** 174-179.

HELFER, B., BOSWELL, B. C., FINLAY, D., CIPRES, A., VUORI, K., BONG KANG, T., WALLACH, D., DORFLEUTNER, A., LAHTI, J. M., FLYNN, D. C. & FRISCH, S. M. 2006. Caspase-8 promotes cell motility and calpain activity under nonapoptotic conditions. *Cancer Res,* 66**,** 4273-8.

HENDERSON, S. & FENTON, T. 2015. APOBEC3 genes: retroviral restriction factors to cancer drivers. *Trends in Molecular Medicine,* 21**,** 274-284.

HENNIGHAUSEN, L. & ROBINSON, G. W. 2005. Information networks in the mammary gland. *Nat Rev Mol Cell Biol,* 6**,** 715-25.

HENSON, P. M. 2017. Cell Removal: Efferocytosis. *Annu Rev Cell Dev Biol,* 33**,** 127-144.

HENSON, P. M. & HUME, D. A. 2006. Apoptotic cell removal in development and tissue homeostasis. *Trends Immunol,* 27**,** 244-50.

HERNANDEZ-MARTINEZ, R. & COVARRUBIAS, L. 2011. Interdigital cell death function and regulation: new insights on an old programmed cell death model. *Dev Growth Differ,* 53**,** 245-58.

HERRMANN, M., VOLL, R. E., ZOLLER, O. M., HAGENHOFER, M., PONNER, B. B. & KALDEN, J. R. 1998. Impaired phagocytosis of apoptotic cell material by monocyte-derived macrophages from patients with systemic lupus erythematosus. *Arthritis Rheum,* 41**,** 1241-50.

HOCHREITER-HUFFORD, A. & RAVICHANDRAN, K. S. 2013. Clearing the dead: apoptotic cell sensing, recognition, engulfment, and digestion. *Cold Spring Harb Perspect Biol,* 5**,** a008748.

HOCK, A. K., CHEUNG, E. C., HUMPTON, T. J., MONTEVERDE, T., PAULUS-HOCK, V., LEE, P., MCGHEE, E., SCOPELLITI, A., MURPHY, D. J., STRATHDEE, D., BLYTH, K. & VOUSDEN, K. H. 2017. Development of an inducible mouse

model of iRFP713 to track recombinase activity and tumour development in vivo. *Scientific Reports,* 7**,** 1837.

HODGE, S., HODGE, G., SCICCHITANO, R., REYNOLDS, P. N. & HOLMES, M. 2003. Alveolar macrophages from subjects with chronic obstructive pulmonary disease are deficient in their ability to phagocytose apoptotic airway epithelial cells. *Immunol Cell Biol,* 81**,** 289-96.

HOLLSTEIN, M., RICE, K., GREENBLATT, M. S., SOUSSI, T., FUCHS, R., SORLIE, T., HOVIG, E., SMITH-SORENSEN, B., MONTESANO, R. & HARRIS, C. C. 1994. Database of p53 gene somatic mutations in human tumors and cell lines. *Nucleic Acids Res,* 22**,** 3551-5.

HOLMGREN, L., SZELES, A., RAJNAVOLGYI, E., FOLKMAN, J., KLEIN, G., ERNBERG, I. & FALK, K. I. 1999. Horizontal transfer of DNA by the uptake of apoptotic bodies. *Blood,* 93**,** 3956-63.

HONDA, R., TANAKA, H. & YASUDA, H. 1997. Oncoprotein MDM2 is a ubiquitin ligase E3 for tumor suppressor p53. *FEBS Lett,* 420**,** 25-7.

HONDA, R. & YASUDA, H. 2000. Activity of MDM2, a ubiquitin ligase, toward p53 or itself is dependent on the RING finger domain of the ligase. *Oncogene,* 19**,** 1473-1476.

HOU, H., SUN, D. & ZHANG, X. 2019. The role of MDM2 amplification and overexpression in therapeutic resistance of malignant tumors. *Cancer Cell International,* 19**,** 216.

HOUDEBINE, L.-M. 2014. 17 - Design of Vectors for Optimizing Transgene Expression. *In:* PINKERT, C. A. (ed.) *Transgenic Animal Technology (Third Edition)*. London: Elsevier.

HOWARD, K. J., HOLLEY, S. J., YAMAMOTO, K. R. & DISTELHORST, C. W. 1990. Mapping the HSP90 binding region of the glucocorticoid receptor. *J Biol Chem,* 265**,** 11928-35.

HSU, B., MARIN, M. C., EL-NAGGAR, A. K., STEPHENS, L. C., BRISBAY, S. & MCDONNELL, T. J. 1995a. Evidence that c-myc mediated apoptosis does not require wild-type p53 during lymphomagenesis. *Oncogene,* 11**,** 175-9.

HSU, B., MARIN, M. C. & MCDONNELL, T. J. 1995b. Cell death regulation during multistep lymphomagenesis. *Cancer Lett,* 94**,** 17-23.

HSU, H., XIONG, J. & GOEDDEL, D. V. 1995c. The TNF receptor 1-associated protein TRADD signals cell death and NF-kappa B activation. *Cell,* 81**,** 495-504.

HU, C., ZHOU, H., LIU, Y., HUANG, J., LIU, W., ZHANG, Q., TANG, Q., SHENG, F., LI, G. & ZHANG, R. 2019. ROCK1 promotes migration and invasion of non-small-cell lung cancer cells through the PTEN/PI3K/FAK pathway. *International journal of oncology,* 55**,** 833-844.

HU, Q., PENG, J., LIU, W., HE, X., CUI, L., CHEN, X., YANG, M., LIU, H., LIU, S. & WANG, H. 2014. Elevated cleaved caspase-3 is associated with shortened overall survival in several cancer types. *International journal of clinical and experimental pathology,* 7**,** 5057-5070.

HUANG, K., ZHANG, J., O'NEILL, K. L., GURUMURTHY, C. B., QUADROS, R. M., TU, Y. & LUO, X. 2016. Cleavage by Caspase 8 and Mitochondrial Membrane Association Activate the BH3-only Protein Bid during TRAIL-induced Apoptosis. *J Biol Chem,* 291**,** 11843-51.

HUESMANN, M., SCOTT, B., KISIELOW, P. & VON BOEHMER, H. 1991. Kinetics and efficacy of positive selection in the thymus of normal and T cell receptor transgenic mice. *Cell,* 66**,** 533-540.

HUSSAIN, S. P. & HARRIS, C. C. 1998. Molecular epidemiology of human cancer: contribution of mutation spectra studies of tumor suppressor genes. *Cancer Res,* 58**,** 4023-37.

HUYNH, M. L., MALCOLM, K. C., KOTARU, C., TILSTRA, J. A., WESTCOTT, J. Y., FADOK, V. A. & WENZEL, S. E. 2005. Defective apoptotic cell phagocytosis attenuates prostaglandin E2 and 15-hydroxyeicosatetraenoic acid in severe asthma alveolar macrophages. *Am J Respir Crit Care Med,* 172**,** 972-9.

ICHIM, G., LOPEZ, J., AHMED, S. U., MUTHALAGU, N., GIAMPAZOLIAS, E., DELGADO, M. E., HALLER, M., RILEY, J. S., MASON, S. M., ATHINEOS, D., PARSONS, M. J., VAN DE KOOIJ, B., BOUCHIER-HAYES, L., CHALMERS, A. J., ROOSWINKEL, R. W., OBERST, A., BLYTH, K., REHM, M., MURPHY, D. J. & TAIT, S. W. G. 2015. Limited mitochondrial permeabilization causes DNA damage and genomic instability in the absence of cell death. *Mol Cell,* 57**,** 860-872.

ICHIM, G. & TAIT, S. W. G. 2016. A fate worse than death: apoptosis as an oncogenic process. *Nature Reviews Cancer,* 16**,** 539-548.

IIZUKA, M., KIMURA, K., WANG, S., KATO, K., AMANO, M., KAIBUCHI, K. & MIZOGUCHI, A. 2012. Distinct distribution and localization of Rho-kinase in mouse epithelial, muscle and neural tissues. *Cell Struct Funct,* 37**,** 155-75.

INA, K., ITOH, J., FUKUSHIMA, K., KUSUGAMI, K., YAMAGUCHI, T., KYOKANE, K., IMADA, A., BINION, D. G., MUSSO, A., WEST, G. A., DOBREA, G. M., MCCORMICK, T. S., LAPETINA, E. G., LEVINE, A. D., OTTAWAY, C. A. & FIOCCHI, C. 1999. Resistance of Crohn's disease T cells to multiple apoptotic signals is associated with a Bcl-2/Bax mucosal imbalance. *J Immunol,* 163**,** 1081-90.

INADA, H., TOGASHI, H., NAKAMURA, Y., KAIBUCHI, K., NAGATA, K. & INAGAKI, M. 1999. Balance between activities of Rho kinase and type 1 protein phosphatase modulates turnover of phosphorylation and dynamics of desmin/vimentin filaments. *J Biol Chem,* 274**,** 34932-9.

ISCHENKO, I., ZHI, J., HAYMAN, M. J. & PETRENKO, O. 2017. KRAS-dependent suppression of MYC enhances the sensitivity of cancer cells to cytotoxic agents. *Oncotarget,* 8**,** 17995-18009.

ISHIKURA, K., YAMADA, N., ITO, M., OTA, S., NAKAMURA, M., ISAKA, N. & NAKANO, T. 2006. Beneficial acute effects of rho-kinase inhibitor in patients with pulmonary arterial hypertension. *Circ J,* 70**,** 174-8.

ISHIUCHI, T. & TAKEICHI, M. 2011. Willin and Par3 cooperatively regulate epithelial apical constriction through aPKC-mediated ROCK phosphorylation. *Nat Cell Biol,* 13**,** 860-6.

ISHIZAKI, T., MAEKAWA, M., FUJISAWA, K., OKAWA, K., IWAMATSU, A., FUJITA, A., WATANABE, N., SAITO, Y., KAKIZUKA, A., MORII, N. & NARUMIYA, S. 1996. The small GTP-binding protein Rho binds to and activates a 160 kDa Ser/Thr protein kinase homologous to myotonic dystrophy kinase. *EMBO J,* 15**,** 1885-93.

ISHIZAKI, Y., JACOBSON, M. D. & RAFF, M. C. 1998. A role for caspases in lens fiber differentiation. *J Cell Biol,* 140**,** 153-8.

IWAKAWA, R., KOHNO, T., KATO, M., SHIRAISHI, K., TSUTA, K., NOGUCHI, M., OGAWA, S. & YOKOTA, J. 2011. MYC amplification as a prognostic marker of early-stage lung adenocarcinoma identified by whole genome copy number analysis. *Clin Cancer Res,* 17**,** 1481-9.

IWAKUMA, T. & LOZANO, G. 2003. MDM2, An Introduction. *Molecular Cancer Research,* 1, 993.

JAALOUK, D. E. & LAMMERDING, J. 2009. Mechanotransduction gone awry. *Nat Rev Mol Cell Biol,* 10, 63-73.

JACKSON, E. L., WILLIS, N., MERCER, K., BRONSON, R. T., CROWLEY, D., MONTOYA, R., JACKS, T. & TUVESON, D. A. 2001. Analysis of lung tumor initiation and progression using conditional expression of oncogenic K-ras. *Genes & development,* 15, 3243-3248.

JACOBI, A. M. & DIAMOND, B. 2005. Balancing diversity and tolerance: lessons from patients with systemic lupus erythematosus. *J Exp Med,* 202, 341-4.

JACOBS, J. J. L., SCHEIJEN, B., VONCKEN, J.-W., KIEBOOM, K., BERNS, A. & VAN LOHUIZEN, M. 1999. Bmi-1 collaborates with c-Myc in tumorigenesis by inhibiting c-Myc-induced apoptosis via INK4a/ARF. *Genes & Development,* 13, 2678-2690.

JACOBS, M., HAYAKAWA, K., SWENSON, L., BELLON, S., FLEMING, M., TASLIMI, P. & DORAN, J. 2006. The structure of dimeric ROCK I reveals the mechanism for ligand selectivity. *J Biol Chem,* 281, 260-8.

JAISWAL, S., JAMIESON, C. H., PANG, W. W., PARK, C. Y., CHAO, M. P., MAJETI, R., TRAVER, D., VAN ROOIJEN, N. & WEISSMAN, I. L. 2009. CD47 is upregulated on circulating hematopoietic stem cells and leukemia cells to avoid phagocytosis. *Cell,* 138, 271-85.

JANEWAY, C. A., JR. 2001. How the immune system protects the host from infection. *Microbes Infect,* 3, 1167-71.

JEFFERS, J. R., PARGANAS, E., LEE, Y., YANG, C., WANG, J., BRENNAN, J., MACLEAN, K. H., HAN, J., CHITTENDEN, T., IHLE, J. N., MCKINNON, P. J., CLEVELAND, J. L. & ZAMBETTI, G. P. 2003. Puma is an essential mediator of p53-dependent and -independent apoptotic pathways. *Cancer Cell,* 4, 321-8.

JENNE, C. N., LIAO, S. & SINGH, B. 2018. Neutrophils: multitasking first responders of immunity and tissue homeostasis. *Cell Tissue Res,* 371, 395-397.

JIN, X., TURCOTT, E., ENGLEHARDT, S., MIZE, G. J. & MORRIS, D. R. 2003. The two upstream open reading frames of oncogene mdm2 have different translational regulatory properties. *J Biol Chem,* 278, 25716-21.

JINESH, G. G., CHOI, W., SHAH, J. B., LEE, E. K., WILLIS, D. L. & KAMAT, A. M. 2013. Blebbishields, the emergency program for cancer stem cells: sphere formation and tumorigenesis after apoptosis. *Cell Death & Differentiation,* 20, 382-395.

JOERGER, A. C. & FERSHT, A. R. 2008. Structural Biology of the Tumor Suppressor p53. *Annual Review of Biochemistry,* 77, 557-582.

JONES, S. N., ANSARI-LARI, M. A., HANCOCK, A. R., JONES, W. J., GIBBS, R. A., DONEHOWER, L. A. & BRADLEY, A. 1996. Genomic organization of the mouse double minute 2 gene. *Gene,* 175, 209-13.

JONES, S. N., HANCOCK, A. R., VOGEL, H., DONEHOWER, L. A. & BRADLEY, A. 1998. Overexpression of Mdm2 in mice reveals a p53-independent role for Mdm2 in tumorigenesis. *Proceedings of the National Academy of Sciences,* 95, 15608.

JONES, S. N., ROE, A. E., DONEHOWER, L. A. & BRADLEY, A. 1995. Rescue of embryonic lethality in Mdm2-deficient mice by absence of p53. *Nature,* 378, 206-8.

JULIAN, L. 2015. *Investigating the role of caspase cleavage of ROCK1 in tissue homeostasis and tumour development*. University of Glasgow.

JULIAN, L. & OLSON, M. F. 2014. Rho-associated coiled-coil containing kinases (ROCK). *Small GTPases,* 5**,** e29846.

JULIAN, L. & OLSON, M. F. 2015. Apoptotic membrane dynamics in health and disease. *Cell Health and Cytoskeleton,* 7**,** 133-142.

JUVEN, T., BARAK, Y., ZAUBERMAN, A., GEORGE, D. L. & OREN, M. 1993. Wild type p53 can mediate sequence-specific transactivation of an internal promoter within the mdm2 gene. *Oncogene,* 8**,** 3411-6.

KALE, J., OSTERLUND, E. J. & ANDREWS, D. W. 2018. BCL-2 family proteins: changing partners in the dance towards death. *Cell Death Differ,* 25**,** 65-80.

KAMAI, T., TSUJII, T., ARAI, K., TAKAGI, K., ASAMI, H., ITO, Y. & OSHIMA, H. 2003. Significant association of Rho/ROCK pathway with invasion and metastasis of bladder cancer. *Clin Cancer Res,* 9**,** 2632-41.

KAMIJO, T., WEBER, J. D., ZAMBETTI, G., ZINDY, F., ROUSSEL, M. F. & SHERR, C. J. 1998. Functional and physical interactions of the ARF tumor suppressor with p53 and Mdm2. *Proc Natl Acad Sci U S A,* 95**,** 8292-7.

KANG, J. H., JIANG, Y., TOITA, R., OISHI, J., KAWAMURA, K., HAN, A., MORI, T., NIIDOME, T., ISHIDA, M., TATEMATSU, K., TANIZAWA, K. & KATAYAMA, Y. 2007. Phosphorylation of Rho-associated kinase (Rho-kinase/ROCK/ROK) substrates by protein kinases A and C. *Biochimie,* 89**,** 39-47.

KARNI-SCHMIDT, O., LOKSHIN, M. & PRIVES, C. 2016. The Roles of MDM2 and MDMX in Cancer. *Annu Rev Pathol,* 11**,** 617-44.

KASTENHUBER, E. R. & LOWE, S. W. 2017. Putting p53 in Context. *Cell,* 170**,** 1062-1078.

KATOH, K., KANO, Y., AMANO, M., ONISHI, H., KAIBUCHI, K. & FUJIWARA, K. 2001. Rho-kinase--mediated contraction of isolated stress fibers. *J Cell Biol,* 153**,** 569-84.

KAWABATA, S., USUKURA, J., MORONE, N., ITO, M., IWAMATSU, A., KAIBUCHI, K. & AMANO, M. 2004. Interaction of Rho-kinase with myosin II at stress fibres. *Genes Cells,* 9**,** 653-60.

KE, F. F. S., VANYAI, H. K., COWAN, A. D., DELBRIDGE, A. R. D., WHITEHEAD, L., GRABOW, S., CZABOTAR, P. E., VOSS, A. K. & STRASSER, A. 2018. Embryogenesis and Adult Life in the Absence of Intrinsic Apoptosis Effectors BAX, BAK, and BOK. *Cell,* 173**,** 1217-1230 e17.

KELLER, U., HUBER, J., NILSSON, J. A., FALLAHI, M., HALL, M. A., PESCHEL, C. & CLEVELAND, J. L. 2010. Myc suppression of Nfkb2 accelerates lymphomagenesis. *BMC Cancer,* 10**,** 348.

KELLY, P. N., PUTHALAKATH, H., ADAMS, J. M. & STRASSER, A. 2007. Endogenous bcl-2 is not required for the development of Eμ-myc–induced B-cell lymphoma. *Blood,* 109**,** 4907-4913.

KERR, J. F., WYLLIE, A. H. & CURRIE, A. R. 1972. Apoptosis: a basic biological phenomenon with wide-ranging implications in tissue kinetics. *Br J Cancer,* 26**,** 239-57.

KHAN, N., GOWTHAMAN, U., PAHARI, S. & AGREWALA, J. N. 2012. Manipulation of costimulatory molecules by intracellular pathogens: veni, vidi, vici!! *PLoS Pathog,* 8**,** e1002676.

KHAN, Z. S., SANTOS, J. M., VAZ, N. G. & HUSSAIN, F. 2019. Enhanced blebbing as a marker for metastatic prostate cancer. *Biomicrofluidics,* 13**,** 034110.

KIM, H. H. & AYATA, C. 2017. Chapter 54 - Rho-Associated Kinases in Cerebrovascular Disease. *In:* CAPLAN, L. R., BILLER, J., LEARY, M. C., LO, E. H., THOMAS, A. J., YENARI, M. & ZHANG, J. H. (eds.) *Primer on Cerebrovascular Diseases (Second Edition).* San Diego: Academic Press.

KIM, S. Y., KIM, S., BAE, D. J., PARK, S. Y., LEE, G. Y., PARK, G. M. & KIM, I. S. 2017. Coordinated balance of Rac1 and RhoA plays key roles in determining phagocytic appetite. *PLoS One,* 12**,** e0174603.

KISCHKEL, F. C., HELLBARDT, S., BEHRMANN, I., GERMER, M., PAWLITA, M., KRAMMER, P. H. & PETER, M. E. 1995. Cytotoxicity-dependent APO-1 (Fas/CD95)-associated proteins form a death-inducing signaling complex (DISC) with the receptor. *The EMBO journal,* 14**,** 5579-5588.

KISHI, T., HIROOKA, Y., MASUMOTO, A., ITO, K., KIMURA, Y., INOKUCHI, K., TAGAWA, T., SHIMOKAWA, H., TAKESHITA, A. & SUNAGAWA, K. 2005. Rho-kinase inhibitor improves increased vascular resistance and impaired vasodilation of the forearm in patients with heart failure. *Circulation,* 111**,** 2741-7.

KISIELOW, P., TEH, H. S., BLÜTHMANN, H. & VON BOEHMER, H. 1988. Positive selection of antigen-specific T cells in thymus by restricting MHC molecules. *Nature,* 335**,** 730-733.

KLEIN, L., KYEWSKI, B., ALLEN, P. M. & HOGQUIST, K. A. 2014. Positive and negative selection of the T cell repertoire: what thymocytes see (and don't see). *Nat Rev Immunol,* 14**,** 377-91.

KO, A., HAN, S. Y. & SONG, J. 2018. Regulatory Network of ARF in Cancer Development. *Mol Cells,* 41**,** 381-389.

KO, L. J. & PRIVES, C. 1996. p53: puzzle and paradigm. *Genes Dev,* 10**,** 1054-72.

KOBAYASHI, M., AZUMA, E., IDO, M., HIRAYAMA, M., JIANG, Q., IWAMOTO, S., KUMAMOTO, T., YAMAMOTO, H., SAKURAI, M. & KOMADA, Y. 2001. A pivotal role of Rho GTPase in the regulation of morphology and function of dendritic cells. *J Immunol,* 167**,** 3585-91.

KOFLER, R. 2000. The molecular basis of glucocorticoid-induced apoptosis of lymphoblastic leukemia cells. *Histochem Cell Biol,* 114**,** 1-7.

KOMANDER, D., GARG, R., WAN, P. T., RIDLEY, A. J. & BARFORD, D. 2008. Mechanism of multi-site phosphorylation from a ROCK-I:RhoE complex structure. *EMBO J,* 27**,** 3175-85.

KONKEL, J. E., JIN, W., ABBATIELLO, B., GRAINGER, J. R. & CHEN, W. 2014. Thymocyte apoptosis drives the intrathymic generation of regulatory T cells. *Proceedings of the National Academy of Sciences,* 111**,** E465.

KORTLEVER, R. M., SODIR, N. M., WILSON, C. H., BURKHART, D. L., PELLEGRINET, L., BROWN SWIGART, L., LITTLEWOOD, T. D. & EVAN, G. I. 2017. Myc Cooperates with Ras by Programming Inflammation and Immune Suppression. *Cell,* 171**,** 1301-1315.e14.

KOSAKO, H., GOTO, H., YANAGIDA, M., MATSUZAWA, K., FUJITA, M., TOMONO, Y., OKIGAKI, T., ODAI, H., KAIBUCHI, K. & INAGAKI, M. 1999. Specific accumulation of Rho-associated kinase at the cleavage furrow during cytokinesis: cleavage furrow-specific phosphorylation of intermediate filaments. *Oncogene,* 18**,** 2783-8.

KOSAKO, H., YOSHIDA, T., MATSUMURA, F., ISHIZAKI, T., NARUMIYA, S. & INAGAKI, M. 2000. Rho-kinase/ROCK is involved in cytokinesis through the phosphorylation of myosin light chain and not ezrin/radixin/moesin proteins at the cleavage furrow. *Oncogene,* 19**,** 6059-64.

KROEMER, G., GALLUZZI, L. & BRENNER, C. 2007. Mitochondrial membrane permeabilization in cell death. *Physiol Rev,* 87**,** 99-163.

KROEMER, G., GALLUZZI, L., KEPP, O. & ZITVOGEL, L. 2013. Immunogenic cell death in cancer therapy. *Annu Rev Immunol,* 31**,** 51-72.

KRUSE, J. P. & GU, W. 2008. SnapShot: p53 posttranslational modifications. *Cell,* 133**,** 930-30 e1.

KRUSE, J. P. & GU, W. 2009. Modes of p53 regulation. *Cell,* 137**,** 609-22.
KRUSPIG, B., MONTEVERDE, T., NEIDLER, S., HOCK, A., KERR, E., NIXON, C., CLARK, W., HEDLEY, A., LAING, S., COFFELT, S. B., LE QUESNE, J., DICK, C., VOUSDEN, K. H., MARTINS, C. P. & MURPHY, D. J. 2018. The ERBB network facilitates KRAS-driven lung tumorigenesis. *Science Translational Medicine,* 10**,** eaao2565.
KUBBUTAT, M. H., JONES, S. N. & VOUSDEN, K. H. 1997. Regulation of p53 stability by Mdm2. *Nature,* 387**,** 299-303.
KUMAR, R., MATEO, J., SMITH, A. D., KHAN, K. H., RUDDLE, R., SWALES, K. E., DECORDOVA, S., BACKHOLER, Z., JONES, P., TRAN, C., SEERAMREDDI, S., MCLEOD, R., YAP, T. A., RAYNAUD, F. I., GARRETT, M. D. & BANERJI, U. 2014. First-in-human, first-in-class phase 1 study of a novel oral multi-AGC kinase inhibitor AT13148 in patients (pts) with advanced solid tumors. *Journal of Clinical Oncology,* 32**,** 2554-2554.
KUMPER, S., MARDAKHEH, F. K., MCCARTHY, A., YEO, M., STAMP, G. W., PAUL, A., WORBOYS, J., SADOK, A., JORGENSEN, C., GUICHARD, S. & MARSHALL, C. J. 2016. Rho-associated kinase (ROCK) function is essential for cell cycle progression, senescence and tumorigenesis. *Elife,* 5**,** e12994.
KURD, N. & ROBEY, E. A. 2016. T-cell selection in the thymus: a spatial and temporal perspective. *Immunol Rev,* 271**,** 114-26.
KUSSIE, P. H., GORINA, S., MARECHAL, V., ELENBAAS, B., MOREAU, J., LEVINE, A. J. & PAVLETICH, N. P. 1996. Structure of the MDM2 Oncoprotein Bound to the p53 Tumor Suppressor Transactivation Domain. *Science,* 274**,** 948.
KUWANA, T., BOUCHIER-HAYES, L., CHIPUK, J. E., BONZON, C., SULLIVAN, B. A., GREEN, D. R. & NEWMEYER, D. D. 2005. BH3 domains of BH3-only proteins differentially regulate Bax-mediated mitochondrial membrane permeabilization both directly and indirectly. *Mol Cell,* 17**,** 525-35.
KWON, M.-C. & BERNS, A. 2013. Mouse models for lung cancer. *Molecular Oncology,* 7**,** 165-177.
LACASSE, E. C., MAHONEY, D. J., CHEUNG, H. H., PLENCHETTE, S., BAIRD, S. & KORNELUK, R. G. 2008. IAP-targeted therapies for cancer. *Oncogene,* 27**,** 6252-75.
LAHAV, G., ROSENFELD, N., SIGAL, A., GEVA-ZATORSKY, N., LEVINE, A. J., ELOWITZ, M. B. & ALON, U. 2004. Dynamics of the p53-Mdm2 feedback loop in individual cells. *Nature Genetics,* 36**,** 147-150.
LAMHAMEDI-CHERRADI, S. E., ZHENG, S. J., MAGUSCHAK, K. A., PESCHON, J. & CHEN, Y. H. 2003. Defective thymocyte apoptosis and accelerated autoimmune diseases in TRAIL-/- mice. *Nat Immunol,* 4**,** 255-60.
LANDERS, J. E., CASSEL, S. L. & GEORGE, D. L. 1997. Translational enhancement of mdm2 oncogene expression in human tumor cells containing a stabilized wild-type p53 protein. *Cancer Res,* 57**,** 3562-8.
LANE, D. P. 1992. Cancer. p53, guardian of the genome. *Nature,* 358**,** 15-6.
LANE, D. P. & CRAWFORD, L. V. 1979. T antigen is bound to a host protein in SV40-transformed cells. *Nature,* 278**,** 261-3.
LANE, J., MARTIN, T. A., WATKINS, G., MANSEL, R. E. & JIANG, W. G. 2008. The expression and prognostic value of ROCK I and ROCK II and their role in human breast cancer. *Int J Oncol,* 33**,** 585-93.
LANE, J. D., ALLAN, V. J. & WOODMAN, P. G. 2005. Active relocation of chromatin and endoplasmic reticulum into blebs in late apoptotic cells. *Journal of Cell Science,* 118**,** 4059.
LEE, J. H., ZHENG, Y., VON BORNSTADT, D., WEI, Y., BALCIOGLU, A., DANESHMAND, A., YALCIN, N., YU, E., HERISSON, F., ATALAY, Y. B., KIM,

M. H., AHN, Y. J., BALKAYA, M., SWEETNAM, P., SCHUELLER, O., POYUROVSKY, M. V., KIM, H. H., LO, E. H., FURIE, K. L. & AYATA, C. 2014. Selective ROCK2 Inhibition In Focal Cerebral Ischemia. *Ann Clin Transl Neurol,* 1, 2-14.

LENARDO, M. J. 1991. Interleukin-2 programs mouse alpha beta T lymphocytes for apoptosis. *Nature,* 353, 858-61.

LENG, R. P., LIN, Y., MA, W., WU, H., LEMMERS, B., CHUNG, S., PARANT, J. M., LOZANO, G., HAKEM, R. & BENCHIMOL, S. 2003. Pirh2, a p53-induced ubiquitin-protein ligase, promotes p53 degradation. *Cell,* 112, 779-91.

LEONARD, B., HART, S. N., BURNS, M. B., CARPENTER, M. A., TEMIZ, N. A., RATHORE, A., VOGEL, R. I., NIKAS, J. B., LAW, E. K., BROWN, W. L., LI, Y., ZHANG, Y., MAURER, M. J., OBERG, A. L., CUNNINGHAM, J. M., SHRIDHAR, V., BELL, D. A., APRIL, C., BENTLEY, D., BIBIKOVA, M., CHEETHAM, R. K., FAN, J. B., GROCOCK, R., HUMPHRAY, S., KINGSBURY, Z., PEDEN, J., CHIEN, J., SWISHER, E. M., HARTMANN, L. C., KALLI, K. R., GOODE, E. L., SICOTTE, H., KAUFMANN, S. H. & HARRIS, R. S. 2013. APOBEC3B upregulation and genomic mutation patterns in serous ovarian carcinoma. *Cancer Res,* 73, 7222-31.

LEONCINI, L., DEL VECCHIO, M. T., MEGHA, T., BARBINI, P., GALIENI, P., PILERI, S., SABATTINI, E., GHERLINZONI, F., TOSI, P., KRAFT, R. & ET AL. 1993. Correlations between apoptotic and proliferative indices in malignant non-Hodgkin's lymphomas. *Am J Pathol,* 142, 755-63.

LETAI, A., BASSIK, M. C., WALENSKY, L. D., SORCINELLI, M. D., WEILER, S. & KORSMEYER, S. J. 2002. Distinct BH3 domains either sensitize or activate mitochondrial apoptosis, serving as prototype cancer therapeutics. *Cancer Cell,* 2, 183-92.

LEUNG, T., CHEN, X. Q., MANSER, E. & LIM, L. 1996. The p160 RhoA-binding kinase ROK alpha is a member of a kinase family and is involved in the reorganization of the cytoskeleton. *Mol Cell Biol,* 16, 5313-27.

LEUNG, T., MANSER, E., TAN, L. & LIM, L. 1995. A novel serine/threonine kinase binding the Ras-related RhoA GTPase which translocates the kinase to peripheral membranes. *J Biol Chem,* 270, 29051-4.

LEVERRIER, Y. & RIDLEY, A. J. 2001a. Apoptosis: caspases orchestrate the ROCK `n' bleb. *Nature Cell Biology,* 3, E91-E92.

LEVERRIER, Y. & RIDLEY, A. J. 2001b. Requirement for Rho GTPases and PI 3-kinases during apoptotic cell phagocytosis by macrophages. *Curr Biol,* 11, 195-9.

LI, J., BRIEHER, W. M., SCIMONE, M. L., KANG, S. J., ZHU, H., YIN, H., VON ANDRIAN, U. H., MITCHISON, T. & YUAN, J. 2007. Caspase-11 regulates cell migration by promoting Aip1-Cofilin-mediated actin depolymerization. *Nat Cell Biol,* 9, 276-86.

LI, M., BROOKS, C. L., WU-BAER, F., CHEN, D., BAER, R. & GU, W. 2003. Mono- versus polyubiquitination: differential control of p53 fate by Mdm2. *Science,* 302, 1972-5.

LI, T., KON, N., JIANG, L., TAN, M., LUDWIG, T., ZHAO, Y., BAER, R. & GU, W. 2012. Tumor suppression in the absence of p53-mediated cell-cycle arrest, apoptosis, and senescence. *Cell,* 149, 1269-83.

LINARES, L. K., HENGSTERMANN, A., CIECHANOVER, A., MULLER, S. & SCHEFFNER, M. 2003. HdmX stimulates Hdm2-mediated ubiquitination and degradation of p53. *Proc Natl Acad Sci U S A,* 100, 12009-14.

LINDSTEN, T. & THOMPSON, C. B. 2006. Cell death in the absence of Bax and Bak. *Cell Death Differ,* 13, 1272-6.

LING, B. & WEI-GUO, Z. 2006. p53: Structure, Function and Therapeutic Applications. *Journal of Cancer Molecules,* 2.

LINNOILA, R. I., MULSHINE, J. L., STEINBERG, S. M. & GAZDAR, A. F. 1992. Expression of surfactant-associated protein in non-small-cell lung cancer: a discriminant between biologic subsets. *J Natl Cancer Inst Monogr,* 61-6.

LIU, S., TACKMANN, N. R., YANG, J. & ZHANG, Y. 2017. Disruption of the RP-MDM2-p53 pathway accelerates APC loss-induced colorectal tumorigenesis. *Oncogene,* 36**,** 1374-1383.

LIU, X., CHOY, E., HORNICEK, F. J., YANG, S., YANG, C., HARMON, D., MANKIN, H. & DUAN, Z. 2011. ROCK1 as a potential therapeutic target in osteosarcoma. *J Orthop Res,* 29**,** 1259-66.

LIU, X., KARNELL, J. L., YIN, B., ZHANG, R., ZHANG, J., LI, P., CHOI, Y., MALTZMAN, J. S., PEAR, W. S., BASSING, C. H. & TURKA, L. A. 2010. Distinct roles for PTEN in prevention of T cell lymphoma and autoimmunity in mice. *The Journal of clinical investigation,* 120**,** 2497-2507.

LIU, X., YU, X., ZACK, D. J., ZHU, H. & QIAN, J. 2008. TiGER: a database for tissue-specific gene expression and regulation. *BMC Bioinformatics,* 9**,** 271.

LIU, X., ZHANG, Z., RUAN, J., PAN, Y., MAGUPALLI, V. G., WU, H. & LIEBERMAN, J. 2016a. Inflammasome-activated gasdermin D causes pyroptosis by forming membrane pores. *Nature,* 535**,** 153-8.

LIU, Y. & LEVINE, B. 2015. Autosis and autophagic cell death: the dark side of autophagy. *Cell Death Differ,* 22**,** 367-76.

LIU, Y., MINZE, L. J., MUMMA, L., LI, X. C., GHOBRIAL, R. M. & KLOC, M. 2016b. Mouse macrophage polarity and ROCK1 activity depend on RhoA and non-apoptotic Caspase 3. *Exp Cell Res,* 341**,** 225-36.

LIU, Y. J., DE BOUTEILLER, O. & FUGIER-VIVIER, I. 1997. Mechanisms of selection and differentiation in germinal centers. *Curr Opin Immunol,* 9**,** 256-62.

LIU, Y. J., JOSHUA, D. E., WILLIAMS, G. T., SMITH, C. A., GORDON, J. & MACLENNAN, I. C. 1989. Mechanism of antigen-driven selection in germinal centres. *Nature,* 342**,** 929-31.

LIU, Z.-G. & JIAO, D. 2019. Necroptosis, tumor necrosis and tumorigenesis. *Cell stress,* 4**,** 1-8.

LOCHHEAD, P. A., WICKMAN, G., MEZNA, M. & OLSON, M. F. 2010. Activating ROCK1 somatic mutations in human cancer. *Oncogene,* 29**,** 2591-8.

LOCKSLEY, R. M., KILLEEN, N. & LENARDO, M. J. 2001. The TNF and TNF receptor superfamilies: integrating mammalian biology. *Cell,* 104**,** 487-501.

LOPES, R. B., GANGESWARAN, R., MCNEISH, I. A., WANG, Y. & LEMOINE, N. R. 2007. Expression of the IAP protein family is dysregulated in pancreatic cancer cells and is important for resistance to chemotherapy. *Int J Cancer,* 120**,** 2344-52.

LOUIS, D. N., OHGAKI, H., WIESTLER, O. D., CAVENEE, W. K., BURGER, P. C., JOUVET, A., SCHEITHAUER, B. W. & KLEIHUES, P. 2007. The 2007 WHO classification of tumours of the central nervous system. *Acta Neuropathol,* 114**,** 97-109.

LOWERY, D. M., CLAUSER, K. R., HJERRILD, M., LIM, D., ALEXANDER, J., KISHI, K., ONG, S. E., GAMMELTOFT, S., CARR, S. A. & YAFFE, M. B. 2007. Proteomic screen defines the Polo-box domain interactome and identifies Rock2 as a Plk1 substrate. *EMBO J,* 26**,** 2262-73.

LOZANO, G. 2010. Mouse models of p53 functions. *Cold Spring Harbor perspectives in biology,* 2**,** a001115-a001115.

LOZANO, M. F. R. A. G. 2012. The Many Faces of MDM2 Binding Partners. *Genes and Cancer,* 3**,** 226 –239.

LU, H. & LEVINE, A. J. 1995. Human TAFII31 protein is a transcriptional coactivator of the p53 protein. *Proceedings of the National Academy of Sciences,* 92**,** 5154.

LU, H., OUYANG, W. & HUANG, C. 2006. Inflammation, a key event in cancer development. *Mol Cancer Res,* 4**,** 221-33.

LU, X., MA, O., NGUYEN, T. A., JONES, S. N., OREN, M. & DONEHOWER, L. A. 2007. The Wip1 Phosphatase acts as a gatekeeper in the p53-Mdm2 autoregulatory loop. *Cancer Cell,* 12**,** 342-54.

LUO, C. & SHEN, J. 2017. Adducin in tumorigenesis and metastasis. *Oncotarget,* 8**,** 48453-48459.

LV, Z., BIAN, Z., SHI, L., NIU, S., HA, B., TREMBLAY, A., LI, L., ZHANG, X., PALUSZYNSKI, J., LIU, M., ZEN, K. & LIU, Y. 2015. Loss of Cell Surface CD47 Clustering Formation and Binding Avidity to SIRPalpha Facilitate Apoptotic Cell Clearance by Macrophages. *J Immunol,* 195**,** 661-71.

MA, W., WONG, C. C., TUNG, E. K., WONG, C. M. & NG, I. O. 2013. RhoE is frequently down-regulated in hepatocellular carcinoma (HCC) and suppresses HCC invasion through antagonizing the Rho/Rho-kinase/myosin phosphatase target pathway. *Hepatology,* 57**,** 152-61.

MA, Z., KANAI, M., KAWAMURA, K., KAIBUCHI, K., YE, K. & FUKASAWA, K. 2006. Interaction between ROCK II and nucleophosmin/B23 in the regulation of centrosome duplication. *Mol Cell Biol,* 26**,** 9016-34.

MAEKAWA, M., ISHIZAKI, T., BOKU, S., WATANABE, N., FUJITA, A., IWAMATSU, A., OBINATA, T., OHASHI, K., MIZUNO, K. & NARUMIYA, S. 1999. Signaling from Rho to the actin cytoskeleton through protein kinases ROCK and LIM-kinase. *Science,* 285**,** 895-8.

MALAGOBADAN, S. & NAGOOR, N. H. 2019. Anoikis. *In:* BOFFETTA, P. & HAINAUT, P. (eds.) *Encyclopedia of Cancer (Third Edition)*. Oxford: Academic Press.

MALKIN, D., LI, F. P., STRONG, L. C., FRAUMENI, J. F., JR., NELSON, C. E., KIM, D. H., KASSEL, J., GRYKA, M. A., BISCHOFF, F. Z., TAINSKY, M. A. & ET AL. 1990. Germ line p53 mutations in a familial syndrome of breast cancer, sarcomas, and other neoplasms. *Science,* 250**,** 1233-8.

MANFREDI, J. J. 2010. The Mdm2–p53 relationship evolves: Mdm2 swings both ways as an oncogene and a tumor suppressor. *Genes & Development,* 24**,** 1580-1589.

MANGEAT, B., TURELLI, P., CARON, G., FRIEDLI, M., PERRIN, L. & TRONO, D. 2003. Broad antiretroviral defence by human APOBEC3G through lethal editing of nascent reverse transcripts. *Nature,* 424**,** 99-103.

MANTOVANI, F., COLLAVIN, L. & DEL SAL, G. 2019. Mutant p53 as a guardian of the cancer cell. *Cell Death Differ,* 26**,** 199-212.

MANZ, D. H., BLANCHETTE, N. L., PAUL, B. T., TORTI, F. M. & TORTI, S. V. 2016. Iron and cancer: recent insights. *Annals of the New York Academy of Sciences,* 1368**,** 149-161.

MARCHETTI, M. C., DI MARCO, B., CIFONE, G., MIGLIORATI, G. & RICCARDI, C. 2003. Dexamethasone-induced apoptosis of thymocytes: role of glucocorticoid receptor–associated Src kinase and caspase-8 activation. *Blood,* 101**,** 585-593.

MARINCOLA, F. M., JAFFEE, E. M., HICKLIN, D. J. & FERRONE, S. 2000. Escape of human solid tumors from T-cell recognition: molecular mechanisms and functional significance. *Adv Immunol,* 74**,** 181-273.

MARINE, J.-C. & JOCHEMSEN, A. G. 2016. MDMX (MDM4), a Promising Target for p53 Reactivation Therapy and Beyond. *Cold Spring Harbor perspectives in medicine,* 6**,** a026237.

MARSDEN, V. S., O'CONNOR, L., O'REILLY, L. A., SILKE, J., METCALF, D., EKERT, P. G., HUANG, D. C., CECCONI, F., KUIDA, K., TOMASELLI, K. J., ROY, S., NICHOLSON, D. W., VAUX, D. L., BOUILLET, P., ADAMS, J. M. & STRASSER, A. 2002. Apoptosis initiated by Bcl-2-regulated caspase activation independently of the cytochrome c/Apaf-1/caspase-9 apoptosome. *Nature,* 419**,** 634-7.

MARSHALL, J. S., WARRINGTON, R., WATSON, W. & KIM, H. L. 2018. An introduction to immunology and immunopathology. *Allergy, Asthma & Clinical Immunology,* 14**,** 49.

MARTINEZ, J., ALMENDINGER, J., OBERST, A., NESS, R., DILLON, C. P., FITZGERALD, P., HENGARTNER, M. O. & GREEN, D. R. 2011. Microtubule-associated protein 1 light chain 3 alpha (LC3)-associated phagocytosis is required for the efficient clearance of dead cells. *Proceedings of the National Academy of Sciences,* 108**,** 17396.

MARTINON, F., BURNS, K. & TSCHOPP, J. 2002. The inflammasome: a molecular platform triggering activation of inflammatory caspases and processing of proIL-beta. *Mol Cell,* 10**,** 417-26.

MARTINS, V. C., BUSCH, K., JURAEVA, D., BLUM, C., LUDWIG, C., RASCHE, V., LASITSCHKA, F., MASTITSKY, S. E., BRORS, B., HIELSCHER, T., FEHLING, H. J. & RODEWALD, H. R. 2014. Cell competition is a tumour suppressor mechanism in the thymus. *Nature,* 509**,** 465-70.

MASSÓ-VALLÉS, D., BEAULIEU, M.-E. & SOUCEK, L. 2020. MYC, MYCL, and MYCN as therapeutic targets in lung cancer. *Expert Opinion on Therapeutic Targets,* 24**,** 101-114.

MATSUI, T., AMANO, M., YAMAMOTO, T., CHIHARA, K., NAKAFUKU, M., ITO, M., NAKANO, T., OKAWA, K., IWAMATSU, A. & KAIBUCHI, K. 1996. Rho-associated kinase, a novel serine/threonine kinase, as a putative target for small GTP binding protein Rho. *EMBO J,* 15**,** 2208-16.

MATSUI, T., MAEDA, M., DOI, Y., YONEMURA, S., AMANO, M., KAIBUCHI, K., TSUKITA, S. & TSUKITA, S. 1998. Rho-kinase phosphorylates COOH-terminal threonines of ezrin/radixin/moesin (ERM) proteins and regulates their head-to-tail association. *J Cell Biol,* 140**,** 647-57.

MATSUMOTO, R., TADA, M., NOZAKI, M., ZHANG, C.-L., SAWAMURA, Y. & ABE, H. 1998. Short Alternative Splice Transcripts of the mdm2 Oncogene Correlate to Malignancy in Human Astrocytic Neoplasms. *Cancer Research,* 58**,** 609.

MATSUMURA, F. 2005. Regulation of myosin II during cytokinesis in higher eukaryotes. *Trends Cell Biol,* 15**,** 371-7.

MATZINGER, P. & GUERDER, S. 1989. Does T-cell tolerance require a dedicated antigen-presenting cell? *Nature,* 338**,** 74-6.

MAYA, R., BALASS, M., KIM, S. T., SHKEDY, D., LEAL, J. F., SHIFMAN, O., MOAS, M., BUSCHMANN, T., RONAI, Z., SHILOH, Y., KASTAN, M. B., KATZIR, E. & OREN, M. 2001. ATM-dependent phosphorylation of Mdm2 on serine 395: role in p53 activation by DNA damage. *Genes Dev,* 15**,** 1067-77.

MCDONNELL, T. J., MONTES DE OCA LUNA, R., CHO, S., AMELSE, L. L., CHAVEZ-REYES, A. & LOZANO, G. 1999. Loss of one but not two mdm2 null alleles alters the tumour spectrum in p53 null mice. *J Pathol,* 188**,** 322-8.

MCILWAIN, D. R., BERGER, T. & MAK, T. W. 2013. Caspase functions in cell death and disease. *Cold Spring Harb Perspect Biol,* 5**,** a008656.

MCPHEE, D., PYE, J. & SHORTMAN, K. 1979. The differentiation of T lymphocytes. V. Evidence for intrathymic death of most thymocytes. *Thymus,* 1**,** 151-62.

MCPHILLIPS, K., JANSSEN, W. J., GHOSH, M., BYRNE, A., GARDAI, S., REMIGIO, L., BRATTON, D. L., KANG, J. L. & HENSON, P. 2007. TNF-alpha inhibits macrophage clearance of apoptotic cells via cytosolic phospholipase A2 and oxidant-dependent mechanisms. *J Immunol,* 178**,** 8117-26.

MEDINA, C. B. & RAVICHANDRAN, K. S. 2016. Do not let death do us part: 'find-me' signals in communication between dying cells and the phagocytes. *Cell Death Differ,* 23**,** 979-89.

MEIER, P., FINCH, A. & EVAN, G. 2000. Apoptosis in development. *Nature,* 407**,** 796-801.

MENDOZA, M., MANDANI, G. & MOMAND, J. 2014. The MDM2 gene family. *Biomol Concepts,* 5**,** 9-19.

MERKENSCHLAGER, M., GRAF, D., LOVATT, M., BOMMHARDT, U., ZAMOYSKA, R. & FISHER, A. G. 1997. How many thymocytes audition for selection? *J Exp Med,* 186**,** 1149-58.

MERLO, L. M. F. & MANDIK-NAYAK, L. 2013. Chapter 3 - Adaptive Immunity: B Cells and Antibodies. *In:* PRENDERGAST, G. C. & JAFFEE, E. M. (eds.) *Cancer Immunotherapy (Second Edition)*. San Diego: Academic Press.

MIAO, E. A., RAJAN, J. V. & ADEREM, A. 2011. Caspase-1-induced pyroptotic cell death. *Immunol Rev,* 243**,** 206-14.

MICHALAK, E. M., VILLUNGER, A., ADAMS, J. M. & STRASSER, A. 2008. In several cell types tumour suppressor p53 induces apoptosis largely via Puma but Noxa can contribute. *Cell Death Differ,* 15**,** 1019-29.

MIGLIORINI, D., LAZZERINI DENCHI, E., DANOVI, D., JOCHEMSEN, A., CAPILLO, M., GOBBI, A., HELIN, K., PELICCI, P. G. & MARINE, J. C. 2002. Mdm4 (Mdmx) regulates p53-induced growth arrest and neuronal cell death during early embryonic mouse development. *Mol Cell Biol,* 22**,** 5527-38.

MIKHUTKINA, S. V., SALMINA, A. B., SYCHEV, A. V., USPENSKAYA, Y. A., TRUFANOVA, L. V., TAKSANOVA, E. I. & OLOVYANNIKOVA, R. Y. 2004. Blebbing of thymocyte plasma membrane and apoptosis are related to impairment of capacitance Ca2+ entry into cells. *Bull Exp Biol Med,* 137**,** 551-5.

MILLS, J. C., STONE, N. L., ERHARDT, J. & PITTMAN, R. N. 1998. Apoptotic membrane blebbing is regulated by myosin light chain phosphorylation. *J Cell Biol,* 140**,** 627-36.

MOGI, M. & TOGARI, A. 2003. Activation of caspases is required for osteoblastic differentiation. *J Biol Chem,* 278**,** 47477-82.

MOMAND, J., JUNG, D., WILCZYNSKI, S. & NILAND, J. 1998. The MDM2 gene amplification database. *Nucleic Acids Res,* 26**,** 3453-9.

MONTEFUSCO, M. C., MERLO, K., BRYAN, C. D., SURKS, H. K., REIS, S. E., MENDELSOHN, M. E. & HUGGINS, G. S. 2010. Little ROCK is a ROCK1 pseudogene expressed in human smooth muscle cells. *BMC Genet,* 11**,** 22.

MONTES DE OCA LUNA, R., WAGNER, D. S. & LOZANO, G. 1995. Rescue of early embryonic lethality in mdm2-deficient mice by deletion of p53. *Nature,* 378**,** 203-6.

MOREAUX, J., VEYRUNE, J. L., REME, T., DE VOS, J. & KLEIN, B. 2008. CD200: a putative therapeutic target in cancer. *Biochem Biophys Res Commun,* 366**,** 117-22.

MORENO, E. 2014. Cancer: Darwinian tumour suppression. *Nature,* 509**,** 435-6.

MORGAN-FISHER, M., WEWER, U. M. & YONEDA, A. 2013. Regulation of ROCK activity in cancer. *J Histochem Cytochem,* 61**,** 185-98.

MORIYAMA, K., IIDA, K. & YAHARA, I. 1996. Phosphorylation of Ser-3 of cofilin regulates its essential function on actin. *Genes Cells,* 1**,** 73-86.

MOROY, T., VERBEEK, S., MA, A., ACHACOSO, P., BERNS, A. & ALT, F. 1991. E mu N- and E mu L-myc cooperate with E mu pim-1 to generate lymphoid tumors at high frequency in double-transgenic mice. *Oncogene,* 6**,** 1941-8.

MOSS, D. K., BETIN, V. M., MALESINSKI, S. D. & LANE, J. D. 2006. A novel role for microtubules in apoptotic chromatin dynamics and cellular fragmentation. *J Cell Sci,* 119**,** 2362-74.

MOULDING, D. A., AKGUL, C., DEROUET, M., WHITE, M. R. & EDWARDS, S. W. 2001. BCL-2 family expression in human neutrophils during delayed and accelerated apoptosis. *J Leukoc Biol,* 70**,** 783-92.

MURPHY, D. J., JUNTTILA, M. R., POUYET, L., KARNEZIS, A., SHCHORS, K., BUI, D. A., BROWN-SWIGART, L., JOHNSON, L. & EVAN, G. I. 2008. Distinct thresholds govern Myc's biological output in vivo. *Cancer cell,* 14**,** 447-457.

MURPHY, K. L., DENNIS, A. P. & ROSEN, J. M. 2000. A gain of function p53 mutant promotes both genomic instability and cell survival in a novel p53-null mammary epithelial cell model. *FASEB J,* 14**,** 2291-302.

MURRAY, J. M., KAUFMANN, G. R., HODGKIN, P. D., LEWIN, S. R., KELLEHER, A. D., DAVENPORT, M. P. & ZAUNDERS, J. J. 2003. Naive T cells are maintained by thymic output in early ages but by proliferation without phenotypic change after age twenty. *Immunol Cell Biol,* 81**,** 487-95.

MUZIO, M., STOCKWELL, B. R., STENNICKE, H. R., SALVESEN, G. S. & DIXIT, V. M. 1998. An induced proximity model for caspase-8 activation. *J Biol Chem,* 273**,** 2926-30.

NAG, S., QIN, J., SRIVENUGOPAL, K. S., WANG, M. & ZHANG, R. 2013. The MDM2-p53 pathway revisited. *J Biomed Res,* 27**,** 254-71.

NAKAGAWA, A., SHIRATSUCHI, A., TSUDA, K. & NAKANISHI, Y. 2005. In vivo analysis of phagocytosis of apoptotic cells by testicular Sertoli cells. *Mol Reprod Dev,* 71**,** 166-77.

NAKAGAWA, O., FUJISAWA, K., ISHIZAKI, T., SAITO, Y., NAKAO, K. & NARUMIYA, S. 1996. ROCK-I and ROCK-II, two isoforms of Rho-associated coiled-coil forming protein serine/threonine kinase in mice. *FEBS Lett,* 392**,** 189-93.

NAKAJIMA, Y.-I. & KURANAGA, E. 2017. Caspase-dependent non-apoptotic processes in development. *Cell Death & Differentiation,* 24**,** 1422-1430.

NAKAMURA, S., ROTH, J. A. & MUKHOPADHYAY, T. 2000. Multiple lysine mutations in the C-terminal domain of p53 interfere with MDM2-dependent protein degradation and ubiquitination. *Mol Cell Biol,* 20**,** 9391-8.

NAKANISHI, Y., NAGAOSA, K. & SHIRATSUCHI, A. 2011. Phagocytic removal of cells that have become unwanted: Implications for animal development and tissue homeostasis. *Development, Growth & Differentiation,* 53**,** 149-160.

NAKAYA, M., TANAKA, M., OKABE, Y., HANAYAMA, R. & NAGATA, S. 2006. Opposite effects of rho family GTPases on engulfment of apoptotic cells by macrophages. *J Biol Chem,* 281**,** 8836-42.

NAM, G.-H., LEE, E. J., KIM, Y. K., HONG, Y., CHOI, Y., RYU, M.-J., WOO, J., CHO, Y., AHN, D. J., YANG, Y., KWON, I.-C., PARK, S.-Y. & KIM, I.-S. 2018. Combined Rho-kinase inhibition and immunogenic cell death triggers and propagates immunity against cancer. *Nature communications,* 9**,** 2165-2165.

NAPIREI, M., KARSUNKY, H., ZEVNIK, B., STEPHAN, H., MANNHERZ, H. G. & MOROY, T. 2000. Features of systemic lupus erythematosus in Dnase1-deficient mice. *Nat Genet,* 25**,** 177-81.

NATKANSKI, E., LEE, W. Y., MISTRY, B., CASAL, A., MOLLOY, J. E. & TOLAR, P. 2013. B cells use mechanical energy to discriminate antigen affinities. *Science,* 340**,** 1587-90.

NAYLOR, G. 2019. *The role of apoptotic cell morphology in anti-tumour immunity* PhD in Cancer Sciences, University of Glasgow.

NEIDLER, S. 2015. *Identification of tumour progression genes in a mouse model for non-small cell lung cancer*. University of Glasgow.

NEIDLER, S., KRUSPIG, B., HEWIT, K., MONTEVERDE, T., GYURASZOVA, K., BRAUN, A., CLARK, W., JAMES, D., HEDLEY, A., NIESWANDT, B., SHANKS, E., DICK, C. & MURPHY, D. J. 2019. Identification of a Clinically Relevant Signature for Early Progression in KRAS-Driven Lung Adenocarcinoma. *Cancers,* 11**,** 600.

NEMES, Z., JR., FRIIS, R. R., AESCHLIMANN, D., SAURER, S., PAULSSON, M. & FESUS, L. 1996. Expression and activation of tissue transglutaminase in apoptotic cells of involuting rodent mammary tissue. *Eur J Cell Biol,* 70**,** 125-33.

NETWORK., C. G. A. R. 2014. Comprehensive molecular profiling of lung adenocarcinoma. *Nature,* 511**,** 543-50.

NEWTON, K., HARRIS, A. W., BATH, M. L., SMITH, K. G. & STRASSER, A. 1998. A dominant interfering mutant of FADD/MORT1 enhances deletion of autoreactive thymocytes and inhibits proliferation of mature T lymphocytes. *EMBO J,* 17**,** 706-18.

NICHOLSON, L. B. 2016. The immune system. *Essays Biochem,* 60**,** 275-301.

NOHRIA, A., GRUNERT, M. E., RIKITAKE, Y., NOMA, K., PRSIC, A., GANZ, P., LIAO, J. K. & CREAGER, M. A. 2006. Rho kinase inhibition improves endothelial function in human subjects with coronary artery disease. *Circ Res,* 99**,** 1426-32.

NUTT, S. L. & HUNTINGTON, N. D. 2019. 17 - Cytotoxic T Lymphocytes and Natural Killer Cells. *In:* RICH, R. R., FLEISHER, T. A., SHEARER, W. T., SCHROEDER, H. W., FREW, A. J. & WEYAND, C. M. (eds.) *Clinical Immunology (Fifth Edition)*. London: Content Repository Only!

O'HAGAN, R. C. & HEYER, J. 2011. KRAS Mouse Models: Modeling Cancer Harboring KRAS Mutations. *Genes & cancer,* 2**,** 335-343.

OHASHI, K., NAGATA, K., MAEKAWA, M., ISHIZAKI, T., NARUMIYA, S. & MIZUNO, K. 2000. Rho-associated kinase ROCK activates LIM-kinase 1 by phosphorylation at threonine 508 within the activation loop. *J Biol Chem,* 275**,** 3577-82.

OHSAKO, S., HARA, M., HARIGAI, M., FUKASAWA, C., KRAJEWSKI, S., REED, J. C. & KASHIWAZAKI, S. 1997. The Bcl-2/Bax ratio of lymphocytes from human systemic lupus erythematosus patients. *Japanese Journal of Rheumatology,* 7**,** 305-313.

OHYAMA, H., YAMADA, T., OHKAWA, A. & WATANABE, I. 1985. Radiation-induced formation of apoptotic bodies in rat thymus. *Radiat Res,* 101**,** 123-30.

OLAZABAL, I. M., CARON, E., MAY, R. C., SCHILLING, K., KNECHT, D. A. & MACHESKY, L. M. 2002. Rho-kinase and myosin-II control phagocytic cup formation during CR, but not FcgammaR, phagocytosis. *Curr Biol,* 12**,** 1413-18.

OLINER, J. D., KINZLER, K. W., MELTZER, P. S., GEORGE, D. L. & VOGELSTEIN, B. 1992. Amplification of a gene encoding a p53-associated protein in human sarcomas. *Nature,* 358**,** 80-3.

OLINER, J. D., SAIKI, A. Y. & CAENEPEEL, S. 2016. The Role of MDM2 Amplification and Overexpression in Tumorigenesis. *Cold Spring Harb Perspect Med,* 6.

OLSON, D. C., MARECHAL, V., MOMAND, J., CHEN, J., ROMOCKI, C. & LEVINE, A. J. 1993. Identification and characterization of multiple mdm-2 proteins and mdm-2-p53 protein complexes. *Oncogene,* 8**,** 2353-60.

OLSON, M. F. 2008. Applications for ROCK kinase inhibition. *Curr Opin Cell Biol,* 20**,** 242-8.

OREN, M. & ROTTER, V. 2010. Mutant p53 gain-of-function in cancer. *Cold Spring Harb Perspect Biol,* 2**,** a001107.

OZAKI, T. & NAKAGAWARA, A. 2011. Role of p53 in Cell Death and Human Cancers. *Cancers (Basel),* 3**,** 994-1013.

PACAUD, P. & LOIRAND, G. 2010. Rho kinase inhibitors for pulmonary hypertension: waiting for clinical evidence. *European Respiratory Journal,* 36**,** 709.

PACE, K. E., LEE, C., STEWART, P. L. & BAUM, L. G. 1999. Restricted receptor segregation into membrane microdomains occurs on human T cells during apoptosis induced by galectin-1. *J Immunol,* 163**,** 3801-11.

PALMER, S., ALBERGANTE, L., BLACKBURN, C. C. & NEWMAN, T. J. 2018. Thymic involution and rising disease incidence with age. *Proceedings of the National Academy of Sciences,* 115**,** 1883.

PALUCH, E. K. & RAZ, E. 2013. The role and regulation of blebs in cell migration. *Current opinion in cell biology,* 25**,** 582-590.

PAN, P., SHEN, M., YU, H., LI, Y., LI, D. & HOU, T. 2013. Advances in the development of Rho-associated protein kinase (ROCK) inhibitors. *Drug Discovery Today,* 18**,** 1323-1333.

PANARETAKIS, T., KEPP, O., BROCKMEIER, U., TESNIERE, A., BJORKLUND, A. C., CHAPMAN, D. C., DURCHSCHLAG, M., JOZA, N., PIERRON, G., VAN ENDERT, P., YUAN, J., ZITVOGEL, L., MADEO, F., WILLIAMS, D. B. & KROEMER, G. 2009. Mechanisms of pre-apoptotic calreticulin exposure in immunogenic cell death. *EMBO J,* 28**,** 578-90.

PANT, V., XIONG, S., JACKSON, J. G., POST, S. M., ABBAS, H. A., QUINTÁS-CARDAMA, A., HAMIR, A. N. & LOZANO, G. 2013. The p53-Mdm2 feedback loop protects against DNA damage by inhibiting p53 activity but is dispensable for p53 stability, development, and longevity. *Genes Dev,* 27**,** 1857-67.

PANT, V., XIONG, S., WASYLISHEN, A. R., LARSSON, C. A., ARYAL, N. K., CHAU, G., TAILOR, R. C. & LOZANO, G. 2019. Transient enhancement of p53 activity protects from radiation-induced gastrointestinal toxicity. *Proceedings of the National Academy of Sciences,* 116**,** 17429-17437.

PARANT, J., CHAVEZ-REYES, A., LITTLE, N. A., YAN, W., REINKE, V., JOCHEMSEN, A. G. & LOZANO, G. 2001. Rescue of embryonic lethality in Mdm4-null mice by loss of Trp53 suggests a nonoverlapping pathway with MDM2 to regulate p53. *Nat Genet,* 29**,** 92-5.

PARDAL, R., CLARKE, M. F. & MORRISON, S. J. 2003. Applying the principles of stem-cell biology to cancer. *Nat Rev Cancer,* 3**,** 895-902.

PAWELETZ, C. P., ORNSTEIN, D. K., ROTH, M. J., BICHSEL, V. E., GILLESPIE, J. W., CALVERT, V. S., VOCKE, C. D., HEWITT, S. M., DURAY, P. H., HERRING, J., WANG, Q. H., HU, N., LINEHAN, W. M., TAYLOR, P. R., LIOTTA, L. A., EMMERT-BUCK, M. R. & PETRICOIN, E. F., 3RD 2000. Loss of annexin 1 correlates with early onset of tumorigenesis in esophageal and prostate carcinoma. *Cancer Res,* 60**,** 6293-7.

PEARCE, L. R., KOMANDER, D. & ALESSI, D. R. 2010. The nuts and bolts of AGC protein kinases. *Nat Rev Mol Cell Biol,* 11**,** 9-22.

PELLEGRINI, M., BELZ, G., BOUILLET, P. & STRASSER, A. 2003. Shutdown of an acute T cell immune response to viral infection is mediated by the proapoptotic Bcl-2 homology 3-only protein Bim. *Proc Natl Acad Sci U S A,* 100**,** 14175-80.

PELLETTIERI, J. & SANCHEZ ALVARADO, A. 2007. Cell turnover and adult tissue homeostasis: from humans to planarians. *Annu Rev Genet,* 41**,** 83-105.

PELOSI, M., MARAMPON, F., ZANI, B. M., PRUDENTE, S., PERLAS, E., CAPUTO, V., CIANETTI, L., BERNO, V., NARUMIYA, S., KANG, S. W., MUSARO, A. & ROSENTHAL, N. 2007. ROCK2 and its alternatively spliced isoform ROCK2m positively control the maturation of the myogenic program. *Mol Cell Biol,* 27**,** 6163-76.

PENG, Y., LATCHMAN, Y. & ELKON, K. B. 2009. Ly6C(low) monocytes differentiate into dendritic cells and cross-tolerize T cells through PDL-1. *Journal of immunology (Baltimore, Md. : 1950),* 182**,** 2777-2785.

PERNIS, A. B., RICKER, E., WENG, C. H., ROZO, C. & YI, W. 2016. Rho Kinases in Autoimmune Diseases. *Annu Rev Med,* 67**,** 355-74.

PERRI, F., PISCONTI, S. & DELLA VITTORIA SCARPATI, G. 2016. P53 mutations and cancer: a tight linkage. *Ann Transl Med,* 4**,** 522.

PERRY, M. E., MENDRYSA, S. M., SAUCEDO, L. J., TANNOUS, P. & HOLUBAR, M. 2000. p76(MDM2) inhibits the ability of p90(MDM2) to destabilize p53. *J Biol Chem,* 275**,** 5733-8.

PERRY, M. E., PIETTE, J., ZAWADZKI, J. A., HARVEY, D. & LEVINE, A. J. 1993. The mdm-2 gene is induced in response to UV light in a p53-dependent manner. *Proc Natl Acad Sci U S A,* 90**,** 11623-7.

PETER, C., WAIBEL, M., RADU, C. G., YANG, L. V., WITTE, O. N., SCHULZE-OSTHOFF, K., WESSELBORG, S. & LAUBER, K. 2008. Migration to apoptotic "find-me" signals is mediated via the phagocyte receptor G2A. *J Biol Chem,* 283**,** 5296-305.

PETITJEAN, A., MATHE, E., KATO, S., ISHIOKA, C., TAVTIGIAN, S. V., HAINAUT, P. & OLIVIER, M. 2007. Impact of mutant p53 functional properties on TP53 mutation patterns and tumor phenotype: lessons from recent developments in the IARC TP53 database. *Human Mutation,* 28**,** 622-629.

PHILIP, M., ROWLEY, D. A. & SCHREIBER, H. 2004. Inflammation as a tumor promoter in cancer induction. *Semin Cancer Biol,* 14**,** 433-9.

PIDO-LOPEZ, J., IMAMI, N. & ASPINALL, R. 2001. Both age and gender affect thymic output: more recent thymic migrants in females than males as they age. *Clinical and experimental immunology,* 125**,** 409-413.

PIEPER, K., GRIMBACHER, B. & EIBEL, H. 2013. B-cell biology and development. *Journal of Allergy and Clinical Immunology,* 131**,** 959-971.

PINNER, S. & SAHAI, E. 2008. PDK1 regulates cancer cell motility by antagonising inhibition of ROCK1 by RhoE. *Nat Cell Biol,* 10**,** 127-37.

PLATT, N., SUZUKI, H., KODAMA, T. & GORDON, S. 2000. Apoptotic thymocyte clearance in scavenger receptor class A-deficient mice is apparently normal. *J Immunol,* 164**,** 4861-7.

POLLARD, T. D. & BORISY, G. G. 2003. Cellular motility driven by assembly and disassembly of actin filaments. *Cell,* 112**,** 453-65.

POMERANTZ, J., SCHREIBER-AGUS, N., LIEGEOIS, N. J., SILVERMAN, A., ALLAND, L., CHIN, L., POTES, J., CHEN, K., ORLOW, I., LEE, H. W., CORDON-CARDO, C. & DEPINHO, R. A. 1998. The Ink4a tumor suppressor gene product, p19Arf, interacts with MDM2 and neutralizes MDM2's inhibition of p53. *Cell,* 92**,** 713-23.

POON, I. K., LUCAS, C. D., ROSSI, A. G. & RAVICHANDRAN, K. S. 2014. Apoptotic cell clearance: basic biology and therapeutic potential. *Nat Rev Immunol,* 14**,** 166-80.

PRAME KUMAR, K., NICHOLLS, A. J. & WONG, C. H. Y. 2018. Partners in crime: neutrophils and monocytes/macrophages in inflammation and disease. *Cell and tissue research,* 371**,** 551-565.

RAFFO, A. J., PERLMAN, H., CHEN, M. W., DAY, M. L., STREITMAN, J. S. & BUTTYAN, R. 1995. Overexpression of bcl-2 protects prostate cancer cells from apoptosis in vitro and confers resistance to androgen depletion in vivo. *Cancer Res,* 55**,** 4438-45.

RAJPUT, A., KANG, T. B., BOGDANOV, K., KIM, J. C., BEN-MOSHE, T., KOVALENKO, A. & WALLACH, D. 2011. Anti-inflammatory functions of caspase-8. *Adv Exp Med Biol,* 691**,** 253-60.

RAMENGHI, U., BONISSONI, S., MIGLIARETTI, G., DEFRANCO, S., BOTTAREL, F., GAMBARUTO, C., DIFRANCO, D., PRIORI, R., CONTI, F., DIANZANI, I., VALESINI, G., MERLETTI, F. & DIANZANI, U. 2000. Deficiency of the Fas apoptosis pathway without Fas gene mutations is a familial trait predisposing to development of autoimmune diseases and cancer. *Blood,* 95**,** 3176-82.

RANA, M. K. & WORTHYLAKE, R. A. 2012. Novel mechanism for negatively regulating Rho-kinase (ROCK) signaling through Coronin1B protein in neuregulin 1 (NRG-1)-induced tumor cell motility. *J Biol Chem,* 287**,** 21836-45.

RAPOPORT, B. L. & ANDERSON, R. 2019. Realizing the Clinical Potential of Immunogenic Cell Death in Cancer Chemotherapy and Radiotherapy. *Int J Mol Sci,* 20.

RAPP, U. R., KORN, C., CETECI, F., KARREMAN, C., LUETKENHAUS, K., SERAFIN, V., ZANUCCO, E., CASTRO, I. & POTAPENKO, T. 2009. MYC is a metastasis gene for non-small-cell lung cancer. *PLoS One,* 4**,** e6029.

RATH, N., MUNRO, J., CUTIONGCO, M. F., JAGIEŁŁO, A., GADEGAARD, N., MCGARRY, L., UNBEKANDT, M., MICHALOPOULOU, E., KAMPHORST, J. J., SUMPTON, D., MACKAY, G., VENNIN, C., PAJIC, M., TIMPSON, P. & OLSON, M. F. 2018. Rho Kinase Inhibition by AT13148 Blocks Pancreatic Ductal Adenocarcinoma Invasion and Tumor Growth. *Cancer Research,* 78**,** 3321.

RAUTOU, P. E., VION, A. C., AMABILE, N., CHIRONI, G., SIMON, A., TEDGUI, A. & BOULANGER, C. M. 2011. Microparticles, vascular function, and atherothrombosis. *Circ Res,* 109**,** 593-606.

RAVICHANDRAN, K. S. 2003. "Recruitment signals" from apoptotic cells: invitation to a quiet meal. *Cell,* 113**,** 817-20.

RAYBURN, E., ZHANG, R., HE, J. & WANG, H. 2005. MDM2 and human malignancies: expression, clinical pathology, prognostic markers, and implications for chemotherapy. *Curr Cancer Drug Targets,* 5**,** 27-41.

RICCI, J.-E. & CHICHE, J. 2018. Metabolic Reprogramming of Non-Hodgkin's B-Cell Lymphomas and Potential Therapeutic Strategies. *Frontiers in Oncology,* 8.

RICCI, J. E., MUNOZ-PINEDO, C., FITZGERALD, P., BAILLY-MAITRE, B., PERKINS, G. A., YADAVA, N., SCHEFFLER, I. E., ELLISMAN, M. H. & GREEN, D. R. 2004. Disruption of mitochondrial function during apoptosis is mediated by caspase cleavage of the p75 subunit of complex I of the electron transport chain. *Cell,* 117, 773-86.

RICCI, J. E., WATERHOUSE, N. & GREEN, D. R. 2003. Mitochondrial functions during cell death, a complex (I–V) dilemma. *Cell Death & Differentiation,* 10, 488-492.

RICH, T., ALLEN, R. L. & WYLLIE, A. H. 2000. Defying death after DNA damage. *Nature,* 407, 777-83.

RIEDL, J., FLYNN, K. C., RADUCANU, A., GÄRTNER, F., BECK, G., BÖSL, M., BRADKE, F., MASSBERG, S., ASZODI, A., SIXT, M. & WEDLICH-SÖLDNER, R. 2010. Lifeact mice for studying F-actin dynamics. *Nat Methods,* 7, 168-9.

RIEDL, S. J. & SHI, Y. 2004. Molecular mechanisms of caspase regulation during apoptosis. *Nat Rev Mol Cell Biol,* 5, 897-907.

RIEMENSCHNEIDER, M. J., BÜSCHGES, R., WOLTER, M., REIFENBERGER, J., BOSTRÖM, J., KRAUS, J. A., SCHLEGEL, U. & REIFENBERGER, G. 1999. Amplification and overexpression of the MDM4 (MDMX) gene from 1q32 in a subset of malignant gliomas without TP53 mutation or MDM2 amplification. *Cancer Res,* 59, 6091-6.

RIENTO, K., GUASCH, R. M., GARG, R., JIN, B. & RIDLEY, A. J. 2003. RhoE binds to ROCK I and inhibits downstream signaling. *Mol Cell Biol,* 23, 4219-29.

RIKITAKE, Y., KIM, H. H., HUANG, Z., SETO, M., YANO, K., ASANO, T., MOSKOWITZ, M. A. & LIAO, J. K. 2005. Inhibition of Rho kinase (ROCK) leads to increased cerebral blood flow and stroke protection. *Stroke,* 36, 2251-7.

RILEY, M. F. & LOZANO, G. 2012. The Many Faces of MDM2 Binding Partners. *Genes Cancer,* 3, 226-39.

RISCAL, R., LE CAM, L. & LINARES, L. K. 2016. Chromatin-bound MDM2, a new player in metabolism. *Molecular & cellular oncology,* 3, e1210560-e1210560.

ROBERTS, A. W., DAVIDS, M. S., PAGEL, J. M., KAHL, B. S., PUVVADA, S. D., GERECITANO, J. F., KIPPS, T. J., ANDERSON, M. A., BROWN, J. R., GRESSICK, L., WONG, S., DUNBAR, M., ZHU, M., DESAI, M. B., CERRI, E., HEITNER ENSCHEDE, S., HUMERICKHOUSE, R. A., WIERDA, W. G. & SEYMOUR, J. F. 2016. Targeting BCL2 with Venetoclax in Relapsed Chronic Lymphocytic Leukemia. *N Engl J Med,* 374, 311-22.

ROBERTS, S. A., STERLING, J., THOMPSON, C., HARRIS, S., MAV, D., SHAH, R., KLIMCZAK, L. J., KRYUKOV, G. V., MALC, E., MIECZKOWSKI, P. A., RESNICK, M. A. & GORDENIN, D. A. 2012. Clustered mutations in yeast and in human cancers can arise from damaged long single-strand DNA regions. *Mol Cell,* 46, 424-35.

ROBEY, E. & FOWLKES, B. J. 1994. Selective events in T cell development. *Annu Rev Immunol,* 12, 675-705.

ROCK, K. L. & KONO, H. 2008. The inflammatory response to cell death. *Annual review of pathology,* 3, 99-126.

RODRIGUEZ, M. S., DESTERRO, J. M., LAIN, S., LANE, D. P. & HAY, R. T. 2000. Multiple C-terminal lysine residues target p53 for ubiquitin-proteasome-mediated degradation. *Mol Cell Biol,* 20, 8458-67.

ROHN, T. T. 2010. The role of caspases in Alzheimer's disease; potential novel therapeutic opportunities. *Apoptosis,* 15, 1403-9.

RONCHETTI, A., ROVERE, P., IEZZI, G., GALATI, G., HELTAI, S., PROTTI, M. P., GARANCINI, M. P., MANFREDI, A. A., RUGARLI, C. & BELLONE, M. 1999. Immunogenicity of apoptotic cells in vivo: role of antigen load, antigen-presenting cells, and cytokines. *J Immunol,* 163, 130-6.

ROTH, J. A., NGUYEN, D., LAWRENCE, D. D., KEMP, B. L., CARRASCO, C. H., FERSON, D. Z., HONG, W. K., KOMAKI, R., LEE, J. J., NESBITT, J. C., PISTERS, K. M., PUTNAM, J. B., SCHEA, R., SHIN, D. M., WALSH, G. L., DOLORMENTE, M. M., HAN, C. I., MARTIN, F. D., YEN, N., XU, K., STEPHENS, L. C., MCDONNELL, T. J., MUKHOPADHYAY, T. & CAI, D. 1996. Retrovirus-mediated wild-type p53 gene transfer to tumors of patients with lung cancer. *Nat Med,* 2, 985-91.

RUSSELL, D. M., DEMBIC, Z., MORAHAN, G., MILLER, J. F., BURKI, K. & NEMAZEE, D. 1991. Peripheral deletion of self-reactive B cells. *Nature,* 354, 308-11.

RYTER, S. W. & CHOI, A. M. K. 2014. Cell Death and Repair in Lung Disease. *In:* MCMANUS, L. M. & MITCHELL, R. N. (eds.) *Pathobiology of Human Disease*. San Diego: Academic Press.

SABNIS, H. S., SOMASAGARA, R. R. & BUNTING, K. D. 2017. Targeting MYC Dependence by Metabolic Inhibitors in Cancer. *Genes,* 8, 114.

SADOK, A. & MARSHALL, C. J. 2014. Rho GTPases: masters of cell migration. *Small GTPases,* 5, e29710.

SADOK, A., MCCARTHY, A., CALDWELL, J., COLLINS, I., GARRETT, M. D., YEO, M., HOOPER, S., SAHAI, E., KUEMPER, S., MARDAKHEH, F. K. & MARSHALL, C. J. 2015. Rho kinase inhibitors block melanoma cell migration and inhibit metastasis. *Cancer Res,* 75, 2272-84.

SAHAI, E., ISHIZAKI, T., NARUMIYA, S. & TREISMAN, R. 1999. Transformation mediated by RhoA requires activity of ROCK kinases. *Curr Biol,* 9, 136-45.

SAKAGUCHI, K., HERRERA, J. E., SAITO, S., MIKI, T., BUSTIN, M., VASSILEV, A., ANDERSON, C. W. & APPELLA, E. 1998. DNA damage activates p53 through a phosphorylation-acetylation cascade. *Genes Dev,* 12, 2831-41.

SAKAGUCHI, K., SAKAMOTO, H., XIE, D., ERICKSON, J. W., LEWIS, M. S., ANDERSON, C. W. & APPELLA, E. 1997. Effect of Phosphorylation on Tetramerization of the Tumor Suppressor Protein p53. *Journal of Protein Chemistry,* 16, 553-556.

SAMEJIMA, K., TONE, S. & EARNSHAW, W. C. 2001. CAD/DFF40 nuclease is dispensable for high molecular weight DNA cleavage and stage I chromatin condensation in apoptosis. *J Biol Chem,* 276, 45427-32.

SAMUEL, M. S. & OLSON, M. F. 2010. Dying alone: a tale of rho. *Cell Stem Cell,* 7, 135-6.

SANSOM, O. J., MENIEL, V. S., MUNCAN, V., PHESSE, T. J., WILKINS, J. A., REED, K. R., VASS, J. K., ATHINEOS, D., CLEVERS, H. & CLARKE, A. R. 2007. Myc deletion rescues Apc deficiency in the small intestine. *Nature,* 446, 676-679.

SASAKI, Y., SUZUKI, M. & HIDAKA, H. 2002. The novel and specific Rho-kinase inhibitor (S)-(+)-2-methyl-1-[(4-methyl-5-isoquinoline)sulfonyl]-homopiperazine as a probing molecule for Rho-kinase-involved pathway. *Pharmacol Ther,* 93, 225-32.

SCAFFIDI, C., SCHMITZ, I., KRAMMER, P. H. & PETER, M. E. 1999. The role of c-FLIP in modulation of CD95-induced apoptosis. *J Biol Chem,* 274, 1541-8.

SCHILLER, H. B. & FASSLER, R. 2013. Mechanosensitivity and compositional dynamics of cell-matrix adhesions. *EMBO Rep,* 14, 509-19.

SCHMIDT, S., RAINER, J., PLONER, C., PRESUL, E., RIML, S. & KOFLER, R. 2004. Glucocorticoid-induced apoptosis and glucocorticoid resistance: molecular mechanisms and clinical relevance. *Cell Death Differ,* 11 Suppl 1, S45-55.

SCHMITT, C. A. & LOWE, S. W. 2002. Apoptosis and chemoresistance in transgenic cancer models. *J Mol Med (Berl),* 80, 137-46.

SCHMITT, C. A., MCCURRACH, M. E., DE STANCHINA, E., WALLACE-BRODEUR, R. R. & LOWE, S. W. 1999. INK4a/ARF mutations accelerate lymphomagenesis and promote chemoresistance by disabling p53. *Genes Dev,* 13, 2670-7.

SCHOFIELD, A. V. & BERNARD, O. 2013. Rho-associated coiled-coil kinase (ROCK) signaling and disease. *Crit Rev Biochem Mol Biol,* 48, 301-16.

SCHON, O., FRIEDLER, A., BYCROFT, M., FREUND, S. M. V. & FERSHT, A. R. 2002. Molecular Mechanism of the Interaction between MDM2 and p53. *Journal of Molecular Biology,* 323, 491-501.

SCHRIJVERS, D. M., DE MEYER, G. R., KOCKX, M. M., HERMAN, A. G. & MARTINET, W. 2005. Phagocytosis of apoptotic cells by macrophages is impaired in atherosclerosis. *Arterioscler Thromb Vasc Biol,* 25, 1256-61.

SCHWARTZENBERG-BAR-YOSEPH, F., ARMONI, M. & KARNIELI, E. 2004. The tumor suppressor p53 down-regulates glucose transporters GLUT1 and GLUT4 gene expression. *Cancer Res,* 64, 2627-33.

SEBBAGH, M., HAMELIN, J., BERTOGLIO, J., SOLARY, E. & BREARD, J. 2005. Direct cleavage of ROCK II by granzyme B induces target cell membrane blebbing in a caspase-independent manner. *J Exp Med,* 201, 465-71.

SEBBAGH, M., RENVOIZE, C., HAMELIN, J., RICHE, N., BERTOGLIO, J. & BREARD, J. 2001. Caspase-3-mediated cleavage of ROCK I induces MLC phosphorylation and apoptotic membrane blebbing. *Nat Cell Biol,* 3, 346-52.

SENGUPTA, S. & HARRIS, C. C. 2005. p53: traffic cop at the crossroads of DNA repair and recombination. *Nature Reviews Molecular Cell Biology,* 6, 44-55.

SENTMAN, C. L., SHUTTER, J. R., HOCKENBERY, D., KANAGAWA, O. & KORSMEYER, S. J. 1991. bcl-2 inhibits multiple forms of apoptosis but not negative selection in thymocytes. *Cell,* 67, 879-88.

SENTURK, E. & MANFREDI, J. J. 2012. Mdm2 and tumorigenesis: evolving theories and unsolved mysteries. *Genes Cancer,* 3, 192-8.

SEO, A. N., YANG, J. M., KIM, H., JHEON, S., KIM, K., LEE, C. T., JIN, Y., YUN, S., CHUNG, J. H. & PAIK, J. H. 2014. Clinicopathologic and prognostic significance of c-MYC copy number gain in lung adenocarcinomas. *Br J Cancer,* 110, 2688-99.

SHALINI, S., DORSTYN, L., DAWAR, S. & KUMAR, S. 2015. Old, new and emerging functions of caspases. *Cell death and differentiation,* 22, 526-539.

SHAMAS-DIN, A., KALE, J., LEBER, B. & ANDREWS, D. W. 2013. Mechanisms of action of Bcl-2 family proteins. *Cold Spring Harb Perspect Biol,* 5, a008714.

SHANLEY, D. P., AW, D., MANLEY, N. R. & PALMER, D. B. 2009. An evolutionary perspective on the mechanisms of immunosenescence. *Trends in Immunology,* 30, 374-381.

SHARPLESS, N. E. & DEPINHO, R. A. 2004. Telomeres, stem cells, senescence, and cancer. *J Clin Invest,* 113, 160-8.

SHCHORS, K., SHCHORS, E., ROSTKER, F., LAWLOR, E. R., BROWN-SWIGART, L. & EVAN, G. I. 2006. The Myc-dependent angiogenic switch in tumors is mediated by interleukin 1beta. *Genes Dev,* 20, 2527-38.

SHEN, X. G., WANG, C., LI, Y., WANG, L., ZHOU, B., XU, B., JIANG, X., ZHOU, Z. G. & SUN, X. F. 2010. Downregulation of caspase-9 is a frequent event in patients with stage II colorectal cancer and correlates with poor clinical outcome. *Colorectal Dis,* 12**,** 1213-8.

SHERR, C. J., BERTWISTLE, D., W, D. E. N. B., KUO, M. L., SUGIMOTO, M., TAGO, K., WILLIAMS, R. T., ZINDY, F. & ROUSSEL, M. F. 2005. p53-Dependent and -independent functions of the Arf tumor suppressor. *Cold Spring Harb Symp Quant Biol,* 70**,** 129-37.

SHI, J., ZHANG, L. & WEI, L. 2011. Rho-kinase in development and heart failure: insights from genetic models. *Pediatr Cardiol,* 32**,** 297-304.

SHI, Y., GLYNN, J. M., GUILBERT, L. J., COTTER, T. G., BISSONNETTE, R. P. & GREEN, D. R. 1992. Role for c-myc in activation-induced apoptotic cell death in T cell hybridomas. *Science,* 257**,** 212-4.

SHIBUYA, M., SUZUKI, Y., SUGITA, K., SAITO, I., SASAKI, T., TAKAKURA, K., NAGATA, I., KIKUCHI, H., TAKEMAE, T., HIDAKA, H. & ET AL. 1992. Effect of AT877 on cerebral vasospasm after aneurysmal subarachnoid hemorrhage. Results of a prospective placebo-controlled double-blind trial. *J Neurosurg,* 76**,** 571-7.

SHIMIZU, T., IHARA, K., MAESAKI, R., AMANO, M., KAIBUCHI, K. & HAKOSHIMA, T. 2003. Parallel coiled-coil association of the RhoA-binding domain in Rho-kinase. *J Biol Chem,* 278**,** 46046-51.

SHIMIZU, Y., THUMKEO, D., KEEL, J., ISHIZAKI, T., OSHIMA, H., OSHIMA, M., NODA, Y., MATSUMURA, F., TAKETO, M. M. & NARUMIYA, S. 2005. ROCK-I regulates closure of the eyelids and ventral body wall by inducing assembly of actomyosin bundles. *J Cell Biol,* 168**,** 941-53.

SHIRAO, S., KASHIWAGI, S., SATO, M., MIWA, S., NAKAO, F., KUROKAWA, T., TODOROKI-IKEDA, N., MOGAMI, K., MIZUKAMI, Y., KURIYAMA, S., HAZE, K., SUZUKI, M. & KOBAYASHI, S. 2002. Sphingosylphosphorylcholine Is a Novel Messenger for Rho-Kinase–Mediated Ca²⁺ Sensitization in the Bovine Cerebral Artery. *Circulation Research,* 91**,** 112-119.

SHORTMAN, K., EGERTON, M., SPANGRUDE, G. J. & SCOLLAY, R. 1990. The generation and fate of thymocytes. *Seminars in immunology,* 2**,** 3-12.

SIEGHART, W., LOSERT, D., STROMMER, S., CEJKA, D., SCHMID, K., RASOUL-ROCKENSCHAUB, S., BODINGBAUER, M., CREVENNA, R., MONIA, B. P., PECK-RADOSAVLJEVIC, M. & WACHECK, V. 2006. Mcl-1 overexpression in hepatocellular carcinoma: a potential target for antisense therapy. *J Hepatol,* 44**,** 151-7.

SIGALAS, I., CALVERT, A. H., ANDERSON, J. J., NEAL, D. E. & LUNEC, J. 1996. Alternatively spliced mdm2 transcripts with loss of p53 binding domain sequences: Transforming ability and frequent detection in human cancer. *Nature Medicine,* 2**,** 912-917.

SINGH, R., LETAI, A. & SAROSIEK, K. 2019. Regulation of apoptosis in health and disease: the balancing act of BCL-2 family proteins. *Nat Rev Mol Cell Biol,* 20**,** 175-193.

SINNING, J. M., LOSCH, J., WALENTA, K., BOHM, M., NICKENIG, G. & WERNER, N. 2011. Circulating CD31+/Annexin V+ microparticles correlate with cardiovascular outcomes. *Eur Heart J,* 32**,** 2034-41.

SLACK, A., CHEN, Z., TONELLI, R., PULE, M., HUNT, L., PESSION, A. & SHOHET, J. M. 2005. The p53 regulatory gene MDM2 is a direct transcriptional target of MYCN in neuroblastoma. *Proc Natl Acad Sci U S A,* 102**,** 731-6.

SLY, L. M., HINGLEY-WILSON, S. M., REINER, N. E. & MCMASTER, W. R. 2003. Survival of Mycobacterium tuberculosis in host macrophages involves resistance to apoptosis dependent upon induction of antiapoptotic Bcl-2 family member Mcl-1. *J Immunol,* 170, 430-7.

SMITH, L. K. & CIDLOWSKI, J. A. 2010. Glucocorticoid-induced apoptosis of healthy and malignant lymphocytes. *Progress in brain research,* 182, 1-30.

SORDET, O., RÉBÉ, C., PLENCHETTE, S., ZERMATI, Y., HERMINE, O., VAINCHENKER, W., GARRIDO, C., SOLARY, E. & DUBREZ-DALOZ, L. 2002. Specific involvement of caspases in the differentiation of monocytes into macrophages. *Blood,* 100, 4446-53.

SPITS, H. 2002. Development of alphabeta T cells in the human thymus. *Nat Rev Immunol,* 2, 760-72.

STOMMEL, J. M., MARCHENKO, N. D., JIMENEZ, G. S., MOLL, U. M., HOPE, T. J. & WAHL, G. M. 1999. A leucine-rich nuclear export signal in the p53 tetramerization domain: regulation of subcellular localization and p53 activity by NES masking. *EMBO J,* 18, 1660-72.

STRASSER, A., HARRIS, A. W., BATH, M. L. & CORY, S. 1990. Novel primitive lymphoid tumours induced in transgenic mice by cooperation between myc and bcl-2. *Nature,* 348, 331-333.

STRASSER, A., HARRIS, A. W. & CORY, S. 1991. bcl-2 transgene inhibits T cell death and perturbs thymic self-censorship. *Cell,* 67, 889-99.

STROEKEN, P. J., ALVAREZ, B., VAN RHEENEN, J., WIJNANDS, Y. M., GEERTS, D., JALINK, K. & ROOS, E. 2006. Integrin cytoplasmic domain-associated protein-1 (ICAP-1) interacts with the ROCK-I kinase at the plasma membrane. *J Cell Physiol,* 208, 620-8.

SUZUKI, K. & MATSUBARA, H. 2011. Recent Advances in p53 Research and Cancer Treatment. *Journal of Biomedicine and Biotechnology,* 2011, 978312.

SWANTON, C., MCGRANAHAN, N., STARRETT, G. J. & HARRIS, R. S. 2015. APOBEC Enzymes: Mutagenic Fuel for Cancer Evolution and Heterogeneity. *Cancer Discov,* 5, 704-12.

SYKES, S. M., MELLERT, H. S., HOLBERT, M. A., LI, K., MARMORSTEIN, R., LANE, W. S. & MCMAHON, S. B. 2006. Acetylation of the p53 DNA-binding domain regulates apoptosis induction. *Mol Cell,* 24, 841-51.

TAKAMURA, M., SAKAMOTO, M., GENDA, T., ICHIDA, T., ASAKURA, H. & HIROHASHI, S. 2001. Inhibition of intrahepatic metastasis of human hepatocellular carcinoma by Rho-associated protein kinase inhibitor Y-27632. *Hepatology,* 33, 577-81.

TAKEDA, N., KONDO, M., ITO, S., ITO, Y., SHIMOKATA, K. & KUME, H. 2006. Role of RhoA inactivation in reduced cell proliferation of human airway smooth muscle by simvastatin. *Am J Respir Cell Mol Biol,* 35, 722-9.

TAMURA, M., NAKAO, H., YOSHIZAKI, H., SHIRATSUCHI, M., SHIGYO, H., YAMADA, H., OZAWA, T., TOTSUKA, J. & HIDAKA, H. 2005. Development of specific Rho-kinase inhibitors and their clinical application. *Biochim Biophys Acta,* 1754, 245-52.

TANAKA, T., NISHIMURA, D., WU, R. C., AMANO, M., ISO, T., KEDES, L., NISHIDA, H., KAIBUCHI, K. & HAMAMORI, Y. 2006. Nuclear Rho kinase, ROCK2, targets p300 acetyltransferase. *J Biol Chem,* 281, 15320-9.

TANG, J., QU, L. K., ZHANG, J., WANG, W., MICHAELSON, J. S., DEGENHARDT, Y. Y., EL-DEIRY, W. S. & YANG, X. 2006. Critical role for Daxx in regulating Mdm2. *Nat Cell Biol,* 8, 855-62.

TANIMURA, S., OHTSUKA, S., MITSUI, K., SHIROUZU, K., YOSHIMURA, A. & OHTSUBO, M. 1999. MDM2 interacts with MDMX through their RING finger domains. *FEBS Lett,* 447**,** 5-9.

TAO, W. & LEVINE, A. J. 1999. Nucleocytoplasmic shuttling of oncoprotein Hdm2 is required for Hdm2-mediated degradation of p53. *Proc Natl Acad Sci U S A,* 96**,** 3077-80.

TAYLOR, R. C., CULLEN, S. P. & MARTIN, S. J. 2008. Apoptosis: controlled demolition at the cellular level. *Nat Rev Mol Cell Biol,* 9**,** 231-41.

THARAUX, P. L., BUKOSKI, R. C., ROCHA, P. N., CROWLEY, S. D., RUIZ, P., NATARAJ, C., HOWELL, D. N., KAIBUCHI, K., SPURNEY, R. F. & COFFMAN, T. M. 2003. Rho kinase promotes alloimmune responses by regulating the proliferation and structure of T cells. *J Immunol,* 171**,** 96-105.

THIEDE, B., TREUMANN, A., KRETSCHMER, A., SÖHLKE, J. & RUDEL, T. 2005. Shotgun proteome analysis of protein cleavage in apoptotic cells. *PROTEOMICS,* 5**,** 2123-2130.

THOMASOVA, D., MULAY, S. R., BRUNS, H. & ANDERS, H.-J. 2012. p53-independent roles of MDM2 in NF-κB signaling: implications for cancer therapy, wound healing, and autoimmune diseases. *Neoplasia (New York, N.Y.),* 14**,** 1097-1101.

THORNBERRY, N. A., BULL, H. G., CALAYCAY, J. R., CHAPMAN, K. T., HOWARD, A. D., KOSTURA, M. J., MILLER, D. K., MOLINEAUX, S. M., WEIDNER, J. R., AUNINS, J. & ET AL. 1992. A novel heterodimeric cysteine protease is required for interleukin-1 beta processing in monocytes. *Nature,* 356**,** 768-74.

THUMKEO, D., KEEL, J., ISHIZAKI, T., HIROSE, M., NONOMURA, K., OSHIMA, H., OSHIMA, M., TAKETO, M. M. & NARUMIYA, S. 2003. Targeted disruption of the mouse rho-associated kinase 2 gene results in intrauterine growth retardation and fetal death. *Mol Cell Biol,* 23**,** 5043-55.

THUT, C. J., GOODRICH, J. A. & TJIAN, R. 1997. Repression of p53-mediated transcription by MDM2: a dual mechanism. *Genes Dev,* 11**,** 1974-86.

TIDOW, H., MELERO, R., MYLONAS, E., FREUND, S. M. V., GROSSMANN, J. G., CARAZO, J. M., SVERGUN, D. I., VALLE, M. & FERSHT, A. R. 2007. Quaternary structures of tumor suppressor p53 and a specific p53–DNA complex. *Proceedings of the National Academy of Sciences,* 104**,** 12324.

TISO, M., GANGEMI, R., BARGELLESI SEVERI, A., PIZZOLITTO, S., FABBI, M. & RISSO, A. 1995. Spontaneous apoptosis in human thymocytes. *The American journal of pathology,* 147**,** 434-444.

TIXEIRA, R., PHAN, T. K., CARUSO, S., SHI, B., ATKIN-SMITH, G. K., NEDEVA, C., CHOW, J. D. Y., PUTHALAKATH, H., HULETT, M. D., HEROLD, M. J. & POON, I. K. H. 2020. ROCK1 but not LIMK1 or PAK2 is a key regulator of apoptotic membrane blebbing and cell disassembly. *Cell Death & Differentiation,* 27**,** 102-116.

TOJKANDER, S., GATEVA, G. & LAPPALAINEN, P. 2012. Actin stress fibers – assembly, dynamics and biological roles. *Journal of Cell Science,* 125**,** 1855.

TOLEDO, F. & WAHL, G. M. 2007. MDM2 and MDM4: p53 regulators as targets in anticancer therapy. *Int J Biochem Cell Biol,* 39**,** 1476-82.

TOPPER, M. J., VAZ, M., CHIAPPINELLI, K. B., DESTEFANO SHIELDS, C. E., NIKNAFS, N., YEN, R. C., WENZEL, A., HICKS, J., BALLEW, M., STONE, M., TRAN, P. T., ZAHNOW, C. A., HELLMANN, M. D., ANAGNOSTOU, V., STRISSEL, P. L., STRICK, R., VELCULESCU, V. E. & BAYLIN, S. B. 2017.

Epigenetic Therapy Ties MYC Depletion to Reversing Immune Evasion and Treating Lung Cancer. *Cell,* 171, 1284-1300 e21.

TOSELLO-TRAMPONT, A. C., NAKADA-TSUKUI, K. & RAVICHANDRAN, K. S. 2003. Engulfment of apoptotic cells is negatively regulated by Rho-mediated signaling. *J Biol Chem,* 278, 49911-9.

TROTTA, R., VIGNUDELLI, T., CANDINI, O., INTINE, R. V., PECORARI, L., GUERZONI, C., SANTILLI, G., BYROM, M. W., GOLDONI, S., FORD, L. P., CALIGIURI, M. A., MARAIA, R. J., PERROTTI, D. & CALABRETTA, B. 2003. BCR/ABL activates mdm2 mRNA translation via the La antigen. *Cancer Cell,* 3, 145-60.

TRUEBESTEIN, L., ELSNER, D. J., FUCHS, E. & LEONARD, T. A. 2015. A molecular ruler regulates cytoskeletal remodelling by the Rho kinases. *Nat Commun,* 6, 10029.

TRUMAN, L. A., FORD, C. A., PASIKOWSKA, M., POUND, J. D., WILKINSON, S. J., DUMITRIU, I. E., MELVILLE, L., MELROSE, L. A., OGDEN, C. A., NIBBS, R., GRAHAM, G., COMBADIERE, C. & GREGORY, C. D. 2008. CX3CL1/fractalkine is released from apoptotic lymphocytes to stimulate macrophage chemotaxis. *Blood,* 112, 5026-36.

TRUONG, A. H., CERVI, D., LEE, J. & BEN-DAVID, Y. 2005. Direct transcriptional regulation of MDM2 by Fli-1. *Oncogene,* 24, 962-9.

UCKER, D. S. & LEVINE, J. S. 2018. Exploitation of Apoptotic Regulation in Cancer. *Frontiers in immunology,* 9, 241-241.

UEHATA, M., ISHIZAKI, T., SATOH, H., ONO, T., KAWAHARA, T., MORISHITA, T., TAMAKAWA, H., YAMAGAMI, K., INUI, J., MAEKAWA, M. & NARUMIYA, S. 1997. Calcium sensitization of smooth muscle mediated by a Rho-associated protein kinase in hypertension. *Nature,* 389, 990-4.

UENO, T., SAITO, F., GRAY, D. H. D., KUSE, S., HIESHIMA, K., NAKANO, H., KAKIUCHI, T., LIPP, M., BOYD, R. L. & TAKAHAMA, Y. 2004. CCR7 Signals Are Essential for Cortex–Medulla Migration of Developing Thymocytes. *The Journal of Experimental Medicine,* 200, 493-505.

ULDRIJAN, S., PANNEKOEK, W.-J. & VOUSDEN, K. H. 2007. An essential function of the extreme C-terminus of MDM2 can be provided by MDMX. *The EMBO Journal,* 26, 102-112.

UTSUGI, T., SCHROIT, A. J., CONNOR, J., BUCANA, C. D. & FIDLER, I. J. 1991. Elevated expression of phosphatidylserine in the outer membrane leaflet of human tumor cells and recognition by activated human blood monocytes. *Cancer Res,* 51, 3062-6.

VAN DE MARK, D., KONG, D., LONCAREK, J. & STEARNS, T. 2015. MDM1 is a microtubule-binding protein that negatively regulates centriole duplication. *Mol Biol Cell,* 26, 3788-802.

VAN ZANDWIJK, N., MOOI, W. J. & RODENHUIS, S. 1995. Prognostic factors in NSCLC. Recent experiences. *Lung Cancer,* 12 Suppl 1, S27-33.

VANDENABEELE, P., VANDECASTEELE, K., BACHERT, C., KRYSKO, O. & KRYSKO, D. V. 2016. Immunogenic Apoptotic Cell Death and Anticancer Immunity. *Adv Exp Med Biol,* 930, 133-49.

VANDIVIER, R. W., FADOK, V. A., OGDEN, C. A., HOFFMANN, P. R., BRAIN, J. D., ACCURSO, F. J., FISHER, J. H., GREENE, K. E. & HENSON, P. M. 2002. Impaired clearance of apoptotic cells from cystic fibrosis airways. *Chest,* 121, 89S.

VANLANGENAKKER, N., VANDEN BERGHE, T. & VANDENABEELE, P. 2012. Many stimuli pull the necrotic trigger, an overview. *Cell death and differentiation,* 19, 75-86.

VASSILEV, L. T., VU, B. T., GRAVES, B., CARVAJAL, D., PODLASKI, F., FILIPOVIC, Z., KONG, N., KAMMLOTT, U., LUKACS, C., KLEIN, C., FOTOUHI, N. & LIU, E. A. 2004. In vivo activation of the p53 pathway by small-molecule antagonists of MDM2. *Science,* 303**,** 844-8.

VECCHIO, E., FIUME, G., CORRENTI, S., ROMANO, S., IACCINO, E., MIMMI, S., MAISANO, D., NISTICÒ, N. & QUINTO, I. 2020. Insights about MYC and Apoptosis in B-Lymphomagenesis: An Update from Murine Models. *International journal of molecular sciences,* 21**,** 4265.

VEIS, D. J., SORENSON, C. M., SHUTTER, J. R. & KORSMEYER, S. J. 1993. Bcl-2-deficient mice demonstrate fulminant lymphoid apoptosis, polycystic kidneys, and hypopigmented hair. *Cell,* 75**,** 229-40.

VEPRINTSEV, D. B., FREUND, S. M. V., ANDREEVA, A., RUTLEDGE, S. E., TIDOW, H., CAÑADILLAS, J. M. P., BLAIR, C. M. & FERSHT, A. R. 2006. Core domain interactions in full-length p53 in solution. *Proceedings of the National Academy of Sciences,* 103**,** 2115.

VICENTE-MANZANARES, M., CABRERO, J. R., REY, M., PEREZ-MARTINEZ, M., URSA, A., ITOH, K. & SANCHEZ-MADRID, F. 2002. A role for the Rho-p160 Rho coiled-coil kinase axis in the chemokine stromal cell-derived factor-1alpha-induced lymphocyte actomyosin and microtubular organization and chemotaxis. *J Immunol,* 168**,** 400-10.

VILLUNGER, A., MICHALAK, E. M., COULTAS, L., MULLAUER, F., BOCK, G., AUSSERLECHNER, M. J., ADAMS, J. M. & STRASSER, A. 2003. p53- and drug-induced apoptotic responses mediated by BH3-only proteins puma and noxa. *Science,* 302**,** 1036-8.

VOGELSTEIN, B., LANE, D. & LEVINE, A. J. 2000. Surfing the p53 network. *Nature,* 408**,** 307-10.

VOGELSTEIN, B., PAPADOPOULOS, N., VELCULESCU, V. E., ZHOU, S., DIAZ, L. A., JR. & KINZLER, K. W. 2013. Cancer genome landscapes. *Science,* 339**,** 1546-58.

VON BOEHMER, H., TEH, H. S. & KISIELOW, P. 1989. The thymus selects the useful, neglects the useless and destroys the harmful. *Immunol Today,* 10**,** 57-61.

VOUSDEN, K. H. & LANE, D. P. 2007. p53 in health and disease. *Nat Rev Mol Cell Biol,* 8**,** 275-83.

VOUSDEN, K. H. & RYAN, K. M. 2009. p53 and metabolism. *Nat Rev Cancer,* 9**,** 691-700.

WADE, M., LI, Y.-C. & WAHL, G. M. 2013. MDM2, MDMX and p53 in oncogenesis and cancer therapy. *Nature Reviews Cancer,* 13**,** 83-96.

WAJANT, H. 2002. The Fas Signaling Pathway: More Than a Paradigm. *Science,* 296**,** 1635.

WANG, P., LUSHNIKOVA, T., ODVODY, J., GREINER, T. C., JONES, S. N. & EISCHEN, C. M. 2008. Elevated Mdm2 expression induces chromosomal instability and confers a survival and growth advantage to B cells. *Oncogene,* 27**,** 1590-1598.

WANG, X., TAPLICK, J., GEVA, N. & OREN, M. 2004. Inhibition of p53 degradation by Mdm2 acetylation. *FEBS Lett,* 561**,** 195-201.

WANG, Y., ZHENG, X. R., RIDDICK, N., BRYDEN, M., BAUR, W., ZHANG, X. & SURKS, H. K. 2009. ROCK isoform regulation of myosin phosphatase and contractility in vascular smooth muscle cells. *Circ Res,* 104**,** 531-40.

WARD, Y., YAP, S. F., RAVICHANDRAN, V., MATSUMURA, F., ITO, M., SPINELLI, B. & KELLY, K. 2002. The GTP binding proteins Gem and Rad are negative regulators of the Rho-Rho kinase pathway. *J Cell Biol,* 157**,** 291-302.

WATANABE, T., ICHIKAWA, A., SAITO, H. & HOTTA, T. 1996. Overexpression of the MDM2 Oncogene in Leukemia and Lymphoma. *Leukemia & Lymphoma,* 21, 391-397.

WEBER, J. D., KUO, M. L., BOTHNER, B., DIGIAMMARINO, E. L., KRIWACKI, R. W., ROUSSEL, M. F. & SHERR, C. J. 2000. Cooperative signals governing ARF-mdm2 interaction and nucleolar localization of the complex. *Mol Cell Biol,* 20, 2517-28.

WEERASINGHE, P. & BUJA, L. M. 2012. Oncosis: an important non-apoptotic mode of cell death. *Exp Mol Pathol,* 93, 302-8.

WEIL, M., JACOBSON, M. D. & RAFF, M. C. 1997. Is programmed cell death required for neural tube closure? *Curr Biol,* 7, 281-4.

WEN, W., LIU, W., YAN, J. & ZHANG, M. 2008. Structure basis and unconventional lipid membrane binding properties of the PH-C1 tandem of rho kinases. *J Biol Chem,* 283, 26263-73.

WICKMAN, G., JULIAN, L. & OLSON, M. F. 2012. How apoptotic cells aid in the removal of their own cold dead bodies. *Cell Death Differ,* 19, 735-42.

WICKMAN, G. R., JULIAN, L., MARDILOVICH, K., SCHUMACHER, S., MUNRO, J., RATH, N., ZANDER, S. A., MLECZAK, A., SUMPTON, D., MORRICE, N., BIENVENUT, W. V. & OLSON, M. F. 2013. Blebs produced by actin-myosin contraction during apoptosis release damage-associated molecular pattern proteins before secondary necrosis occurs. *Cell Death Differ,* 20, 1293-305.

WIJEYESAKERE, S. J., BEDI, S. K., HUYNH, D. & RAGHAVAN, M. 2016. The C-Terminal Acidic Region of Calreticulin Mediates Phosphatidylserine Binding and Apoptotic Cell Phagocytosis. *J Immunol,* 196, 3896-3909.

WILDA, M., BRUCH, J., HARDER, L., RAWER, D., REITER, A., BORKHARDT, A. & WOESSMANN, W. 2004. Inactivation of the ARF–MDM-2–p53 pathway in sporadic Burkitt's lymphoma in children. *Leukemia,* 18, 584-588.

WILLIAMS, O., NORTON, T., HALLIGEY, M., KIOUSSIS, D. & BRADY, H. J. 1998. The action of Bax and bcl-2 on T cell selection. *The Journal of experimental medicine,* 188, 1125-1133.

WILLIS, A., JUNG, E. J., WAKEFIELD, T. & CHEN, X. 2004. Mutant p53 exerts a dominant negative effect by preventing wild-type p53 from binding to the promoter of its target genes. *Oncogene,* 23, 2330-2338.

WOEHLECKE, H., POHL, A., ALDER-BAERENS, N., LAGE, H. & HERRMANN, A. 2003. Enhanced exposure of phosphatidylserine in human gastric carcinoma cells overexpressing the half-size ABC transporter BCRP (ABCG2). *Biochem J,* 376, 489-95.

WOLFER, A., WITTNER, B. S., IRIMIA, D., FLAVIN, R. J., LUPIEN, M., GUNAWARDANE, R. N., MEYER, C. A., LIGHTCAP, E. S., TAMAYO, P., MESIROV, J. P., LIU, X. S., SHIODA, T., TONER, M., LODA, M., BROWN, M., BRUGGE, J. S. & RAMASWAMY, S. 2010. MYC regulation of a "poor-prognosis" metastatic cancer cell state. *Proc Natl Acad Sci U S A,* 107, 3698-703.

WONG, C. C., WONG, C. M., TUNG, E. K., MAN, K. & NG, I. O. 2009. Rho-kinase 2 is frequently overexpressed in hepatocellular carcinoma and involved in tumor invasion. *Hepatology,* 49, 1583-94.

WONG, R. S. 2011. Apoptosis in cancer: from pathogenesis to treatment. *J Exp Clin Cancer Res,* 30, 87.

WOOLLEY, K. L., GIBSON, P. G., CARTY, K., WILSON, A. J., TWADDELL, S. H. & WOOLLEY, M. J. 1996. Eosinophil apoptosis and the resolution of airway inflammation in asthma. *Am J Respir Crit Care Med,* 154, 237-43.

WYLLIE, A. H., KERR, J. F. & CURRIE, A. R. 1980. Cell death: the significance of apoptosis. *Int Rev Cytol,* 68, 251-306.

XIAO, Z. X., CHEN, J., LEVINE, A. J., MODJTAHEDI, N., XING, J., SELLERS, W. R. & LIVINGSTON, D. M. 1995. Interaction between the retinoblastoma protein and the oncoprotein MDM2. *Nature,* 375, 694-8.

YAMAGUCHI, H., KASA, M., AMANO, M., KAIBUCHI, K. & HAKOSHIMA, T. 2006. Molecular mechanism for the regulation of rho-kinase by dimerization and its inhibition by fasudil. *Structure,* 14, 589-600.

YAMANAKA, S., BALESTRA, M. E., FERRELL, L. D., FAN, J., ARNOLD, K. S., TAYLOR, S., TAYLOR, J. M. & INNERARITY, T. L. 1995. Apolipoprotein B mRNA-editing protein induces hepatocellular carcinoma and dysplasia in transgenic animals. *Proc Natl Acad Sci U S A,* 92, 8483-7.

YAN, S., HE, F., GAO, B., WU, H., LI, M., HUANG, L., LIANG, J., WU, Q. & LI, Y. 2016. Increased APOBEC3B Predicts Worse Outcomes in Lung Cancer: A Comprehensive Retrospective Study. *Journal of Cancer,* 7, 618-625.

YAN, X. X., NAJBAUER, J., WOO, C. C., DASHTIPOUR, K., RIBAK, C. E. & LEON, M. 2001. Expression of active caspase-3 in mitotic and postmitotic cells of the rat forebrain. *J Comp Neurol,* 433, 4-22.

YANG, J. Y., ZONG, C. S., XIA, W., WEI, Y., ALI-SEYED, M., LI, Z., BROGLIO, K., BERRY, D. A. & HUNG, M. C. 2006. MDM2 promotes cell motility and invasiveness by regulating E-cadherin degradation. *Mol Cell Biol,* 26, 7269-82.

YANG, J. Y., ZONG, C. S., XIA, W., YAMAGUCHI, H., DING, Q., XIE, X., LANG, J. Y., LAI, C. C., CHANG, C. J., HUANG, W. C., HUANG, H., KUO, H. P., LEE, D. F., LI, L. Y., LIEN, H. C., CHENG, X., CHANG, K. J., HSIAO, C. D., TSAI, F. J., TSAI, C. H., SAHIN, A. A., MULLER, W. J., MILLS, G. B., YU, D., HORTOBAGYI, G. N. & HUNG, M. C. 2008. ERK promotes tumorigenesis by inhibiting FOXO3a via MDM2-mediated degradation. *Nat Cell Biol,* 10, 138-48.

YANG, S. & KIM, H.-M. 2012. The RhoA-ROCK-PTEN pathway as a molecular switch for anchorage dependent cell behavior. *Biomaterials,* 33, 2902-2915.

YANG, Y. & YU, X. 2003. Regulation of apoptosis: the ubiquitous way. *FASEB J,* 17, 790-9.

YAP, T. A., WALTON, M. I., GRIMSHAW, K. M., TE POELE, R. H., EVE, P. D., VALENTI, M. R., DE HAVEN BRANDON, A. K., MARTINS, V., ZETTERLUND, A., HEATON, S. P., HEINZMANN, K., JONES, P. S., FELTELL, R. E., REULE, M., WOODHEAD, S. J., DAVIES, T. G., LYONS, J. F., RAYNAUD, F. I., ECCLES, S. A., WORKMAN, P., THOMPSON, N. T. & GARRETT, M. D. 2012. AT13148 Is a Novel, Oral Multi-AGC Kinase Inhibitor with Potent Pharmacodynamic and Antitumor Activity. *Clinical Cancer Research,* 18, 3912.

YING, H., BIROC, S. L., LI, W. W., ALICKE, B., XUAN, J. A., PAGILA, R., OHASHI, Y., OKADA, T., KAMATA, Y. & DINTER, H. 2006. The Rho kinase inhibitor fasudil inhibits tumor progression in human and rat tumor models. *Mol Cancer Ther,* 5, 2158-64.

YONEDA, A., MULTHAUPT, H. A. & COUCHMAN, J. R. 2005. The Rho kinases I and II regulate different aspects of myosin II activity. *J Cell Biol,* 170, 443-53.

YONISH-ROUACH, E., RESNITZKY, D., LOTEM, J., SACHS, L., KIMCHI, A. & OREN, M. 1991. Wild-type p53 induces apoptosis of myeloid leukaemic cells that is inhibited by interleukin-6. *Nature,* 352, 345-7.

ZAKERI, Z., QUAGLINO, D. & AHUJA, H. S. 1994. Apoptotic cell death in the mouse limb and its suppression in the hammertoe mutant. *Dev Biol,* 165**,** 294-7.

ZANIN-ZHOROV, A., WEISS, J. M., NYUYDZEFE, M. S., CHEN, W., SCHER, J. U., MO, R., DEPOIL, D., RAO, N., LIU, B., WEI, J., LUCAS, S., KOSLOW, M., ROCHE, M., SCHUELLER, O., WEISS, S., POYUROVSKY, M. V., TONRA, J., HIPPEN, K. L., DUSTIN, M. L., BLAZAR, B. R., LIU, C. J. & WAKSAL, S. D. 2014. Selective oral ROCK2 inhibitor down-regulates IL-21 and IL-17 secretion in human T cells via STAT3-dependent mechanism. *Proc Natl Acad Sci U S A,* 111**,** 16814-9.

ZANIN-ZHOROV, A., WEISS, J. M., TRZECIAK, A., CHEN, W., ZHANG, J., NYUYDZEFE, M. S., ARENCIBIA, C., POLIMERA, S., SCHUELLER, O., FUENTES-DUCULAN, J., BONIFACIO, K. M., KUNJRAVIA, N., CUETO, I., SOUNG, J., FLEISCHMANN, R. M., KIVITZ, A., LEBWOHL, M., NUNEZ, M., WOODSON, J., SMITH, S. L., WEST, R. F., BERGER, M., KRUEGER, J. G., RYAN, J. L. & WAKSAL, S. D. 2017. Cutting Edge: Selective Oral ROCK2 Inhibitor Reduces Clinical Scores in Patients with Psoriasis Vulgaris and Normalizes Skin Pathology via Concurrent Regulation of IL-17 and IL-10. *J Immunol,* 198**,** 3809-3814.

ZAUBERMAN, A., FLUSBERG, D., HAUPT, Y., BARAK, Y. & OREN, M. 1995. A functional p53-responsive intronic promoter is contained within the human mdm2 gene. *Nucleic Acids Res,* 23**,** 2584-92.

ZHANG, J., XU, X. & LIU, Y. 2004. Activation-induced cell death in T cells and autoimmunity. *Cell Mol Immunol,* 1**,** 186-92.

ZHANG, S., TANG, Q., XU, F., XUE, Y., ZHEN, Z., DENG, Y., LIU, M., CHEN, J., LIU, S., QIU, M., LIAO, Z., LI, Z., LUO, D., SHI, F., ZHENG, Y. & BI, F. 2009. RhoA Regulates G₁-S Progression of Gastric Cancer Cells by Modulation of Multiple INK4 Family Tumor Suppressors. *Molecular Cancer Research,* 7**,** 570.

ZHANG, Y., CHEN, X., GUEYDAN, C. & HAN, J. 2018. Plasma membrane changes during programmed cell deaths. *Cell Res,* 28**,** 9-21.

ZHAO, Z. & RIVKEES, S. A. 2003. Rho-associated kinases play an essential role in cardiac morphogenesis and cardiomyocyte proliferation. *Dev Dyn,* 226**,** 24-32.

ZHENG, T. S., HUNOT, S., KUIDA, K. & FLAVELL, R. A. 1999. Caspase knockouts: matters of life and death. *Cell Death Differ,* 6**,** 1043-53.

ZHOU, J., WANG, G., CHEN, Y., WANG, H., HUA, Y. & CAI, Z. 2019. Immunogenic cell death in cancer therapy: Present and emerging inducers. *J Cell Mol Med,* 23**,** 4854-4865.

ZINDY, F., EISCHEN, C. M., RANDLE, D. H., KAMIJO, T., CLEVELAND, J. L., SHERR, C. J. & ROUSSEL, M. F. 1998. Myc signaling via the ARF tumor suppressor regulates p53-dependent apoptosis and immortalization. *Genes & development,* 12**,** 2424-2433.

ZÚÑIGA-PFLÜCKER, J. C. 2004. T-cell development made simple. *Nature Reviews Immunology,* 4**,** 67-72.